## Title

The Photochemistry of [8]-Pyridinophane N-Oxide and Characterization of Prodiginine–microRNA Binding Interactions



## Author

Hurlow, Evan

## Publication Date

2022

Peer reviewed|Thesis/dissertation

UNIVERSITY OF CALIFORNIA

Los Angeles

# The Photochemistry of [8]-Pyridinophane *N*-Oxide

and

# Characterization of Prodiginine–microRNA Binding Interactions

A dissertation submitted in partial satisfaction of the

requirements for the degree Doctor of Philosophy in Chemistry

by

Evan Hurlow

2022

ABSTRACT OF THE DISSERTATION

The Photochemistry of [8]-Pyridinophane *N*-Oxide

and

Characterization of Prodiginine–microRNA Binding Interactions

by

Evan Hurlow

Doctor of Philosophy in Chemistry

University of California, Los Angeles, 2022

Professor Patrick G. Harran, Chair

Chapter one details my work associated with the photorearrangement of [8]-pyridinophane *N*-oxide and its application in to an eight-step asymmetric synthesis of (+)-marineosin A. The route proceeds by condensing fragments of reversed polarity relative to conventional prodiginine constructions. The resultant unstable chromophore is disrupted by a unique cycloisomerization promoted at a tailored manganese surface providing a premarineosin and subsequently marineosin A in a particularly concise manner. A pyridinophane *N*-oxide photorearrangement in flow and structural isomers of premarineosin are discussed, as is the

reassignment of marineosin stereochemistry. The route gives access to the natural product as well as diastereomers, congeners and analogs that are currently inaccessible by other means. Following completion of this route, I began studying the mechanism of the pyridinophane *N*-oxide photorearrangement using time course studies with support from DFT calculations. Based on the data and the isolation of two previously unknown heterocyclophanes, I outlined a unified mechanistic scheme that explains competing processes under varying photochemical conditions.

Chapter two describes my work characterizing of prodiginine–microRNA binding interactions. I developed a fluorescence-based binding assay to determine the binding strength of prodiginines to an oncogenic microRNA precursor. After identifying the small molecule's binding site, I fused it to a readily crystallizable riboswitch with the aim of obtaining a co-crystal structure. I also explored several other crystallization constructs and developed a structure-affinity relationship by synthesizing and assaying novel prodiginine compounds. From this I identified a lead compound which is one of the strongest microRNA binders discovered to date.

The dissertation of Evan Hurlow is approved.

Feng Guo

Michael E. Jung

Ohyun Kwon

Patrick G. Harran, Committee Chair

University of California, Los Angeles

2022

To Mom, Dad, Rose, and Toni

and The Color Orange

TABLE OF CONTENTS

List of Figures and Tables

**Figures**

**Tables**

List of Abbreviations

| | |
|---|---|
| Ac | acetyl |
| anh. | anhydrous |
| APT | attached proton test |
| aq. | aqueous |
| cod | cyclooctadiene |
| cps | counts per seconds |
| DCM | dichloromethane |
| DFT | density-functional theory |
| DI | de-ionized |
| DME | 1,2-dimethoxy ethane |
| DMSO | dimethyl sulfoxide |
| DNA | deoxyribonucleic acid |
| dppp | diphenylphosphino propane |
| dr, d.r. | diastereomeric ratio |
| EDTA | ethylenediaminetetraacetic acid |
| ee, e.e. | enantiomeric excess |
| EI | electron impact |
| ESI | electro-spray ionization |
| Et | ethyl |
| FCC | flash column chromatography |
| FEP | fluorinated ethylene-propylene |
| GC | gas chromatography |
| h | hour |
| HEPES | 4-(2-hydroxyethyl)-1-piperazineethanesulfonic acid |
| HPLC | high-performance liquid chromatography |
| HRMS | high-resolution mass spectrum/spectrometry |
| ID | inner diameter |

| | |
|---|---|
| IEF-PCM | integral equation formalism-polarizable continuum method |
| IVT | *in vitro* transcription |
| $K_d$ | dissociation constant |
| LC | liquid chromatography |
| LDA | lithium diisopropylamide |
| M.P. | melting point |
| mCPBA | meta-chloroperoxybenzoic acid |
| Me | methyl |
| mRNA | messenger ribonucleic acid |
| miRNA, miR | micro ribonucleic acid |
| MPD | 2-methyl-2,4-pentanediol |
| MS | mass spectrometer/spectrometry/spectrum |
| Ms | methanesulfonyl |
| NCI | National Cancer Institute |
| nd, n.d. | not determined |
| *n*-mer | (in the context of this document) an oligoribonucleotide *n* residues long |
| NMR | nuclear magnetic resonance |
| nOe | nuclear Overhauser effect |
| NOESY | nuclear Overhauser effect spectroscopy |
| OD | outer diameter |
| ORTEP | Oak Ridge thermal ellipsoid plot |
| PCR | polymerase chain reaction |
| Ph | phenyl |
| pre-miR | precursor micro ribonucleic acid |
| pri-miR | primary micro ribonucleic acid |
| PTLC | preparative thin-layer chromatography |
| RNA | ribonucleic acid |
| RT, rt, r.t. | room temperature |

| | |
|---|---|
| SI | supplemental information |
| TD-DFT | time-dependent density-functional theory |
| TEA | triethylamine |
| temp. | temperature |
| Tf | trifluoromethane sulfonyl |
| TFA | trifluoroacetic acid |
| THF | tetrahydrofuran |
| TLC | thin layer chromatography |
| TS | transition state |
| Ts | 4-toluenesulfonyl |
| UCLA | University of California, Los Angeles |
| UV-Vis | ultraviolet-visual |
| UV-Vis-NIR | ultraviolet-visual-near-infrared |
| WT | wild-type |

ACKNOWLEDGEMENTS

I would like to acknowledge the people with whom I co-authored the two publications adapted in this document. Each person was instrumental to the success of these projects and I am proud to have worked alongside them.

Zhengao Feng was the mastermind of the marineosin A total synthesis described in Chapter 1.1, and was an important mentor to me. His efficiency, fortitude, and attention to detail enabled completion of the route and were an immense source of inspiration during my first two years in the lab. I am a better chemist for having worked alongside him and I aspire to achieve a similar level of competency he displayed *en route* to marineosin A. Tyler K. Allred also played a crucial role in this paper. His tremendous knowledge of chemical reactions was the source of many creative experiments, and his Woodwardian grit became evident to me when he ran 12 large-scale batch photolyses within 4 days to fill-out an optimization table. (It took me two weeks to purify and quantify the aftermath!)

Janice B. Lin and Selbi Nuryyeva were instrumental in forging our understanding of the photorearrangement's mechanism, and they were a pleasure to interact with. Prof. Houk provided fundamental insight critical to our mechanistic investigation. Morris J. Dweck not only helped develop the GC/MS method critical to the project, but also provided me the moral support to push this project over the finish line. Truly, Morris' impact on the members of Harran lab cannot be understated. As the *de facto* lab manager, he has lent his time to every ongoing project, whether it's offering troubleshooting suggestions, keeping the glassware clean and organized

(especially the Quarks), or just making you laugh when you're feeling overwhelmed. He is the glue that holds us together and he is a friend of unparalleled loyalty.

Prof. Harran was key not only to the above projects, but to my development as a scientist. Throughout my graduate career he pushed me to reach for the higher bar, and I am much the better for it. He allowed me to pursue my interests in the lab, and helped me return to the most productive path when I stepped astray. Thank you, Dr. Harran, I am the scientist I am today because of you.

Prof. Feng Guo was absolutely critical to the work described in Chapter 2. I began an internship in his lab at the close of my third year with essentially no knowledge of molecular biology. Feng was patient and generous with his time, even teaching me basic lab techniques himself. I am sincerely grateful to have had him as a mentor. I had the pleasure of mentoring Olivia Henshaw during my time in Feng's lab, and she is responsible for the beautiful binding curves in Section 2.6. She is sharp-witted and determined, and has a brilliant career ahead of her. I am grateful to the other members of Feng's lab: Grant Shoffner, Yan Li, Christen Tai, and Julia Chen. They were all wonderful to work alongside and taught me many things.

The past and present members of Harran were the best lab mates I could have asked for—Hui Ding, Emily Murzinski, Luke Sisto, Liubo Li, Salvador Bernardino, Anton El Khoury, Ishika Saha, Angel Mendoza, Gilbert Walker, Jackie Bustamante, Gabby Cooper, Emma Greene, Alek Lotuzas, Kyle Nagasawa, and all others mentioned previously—you were the people who I celebrated with, commiserated with, and just-got-through-the-day with. You have all made an enormous impact

on me and are my dearest friends. I wish you all success and thank you from the bottom of my heart!

Mom, Dad, and Rose (and Pico and Fabio)—my family—gave me unwavering support through the ups and downs of grad school. I love you so much and am eternally grateful to you! Toni, my love, you have supported and encouraged me since the day we met. The impact you've made on my life is immense, and I love you with all of my heart and soul!

**Evan Hurlow** *Curriculum Vitae*

## Education

B.Sc., Chemistry ---------- *2017*
*University of Utah, Salt Lake City, UT*

## Experience

Graduate Student Researcher ---------- *2017 – 2022*
*UCLA*
*PI: Prof. Patrick Harran*
*Collaborators: Prof. Kendall Houk (UCLA), Prof. Feng Guo (UCLA)*

**1. Synthesis of complex prodiginine natural products and analogs.**

- Aided development of the total synthesis of marineosin A via material synthesis and step optimization.

**2. Optimization and mechanistic investigation of macrocyclic pyridine *N*-oxide photorearrangement.**

- Optimized flow-photolytic production of a key acylpyrrolophane in the synthesis of marineosin A.
- Elucidated the photorearrangement mechanism of pyridinophane *N*-oxides to acylpyrrolophanes using GC/MS time course experiments in collaboration with computational chemists.
- Discovered and characterized novel macrobicyclic intermediates in the rearrangement of pyridinophane *N*-oxides.

**3. Medicinal chemistry and structural biology of small-molecule–RNA interactions.**

- Studied and quantified the interaction of prodiginine compounds with oncogenic microRNA.
- Synthesized modular RNA scaffolds for small molecule co-crystallization studies.
- Developed a general method for RNA–small molecule crystallography.
- Synthesized prodiginine congeners to establish a microRNA structure-affinity relationship.

Undergraduate Researcher ---------- *2015 – 2017*
*University of Utah*
*PI: Prof. Jon Rainier*

- Synthesized novel quinone–amino acid conjugates used to disrupt pathogenic protein aggregates associated with ocular degeneration.

Laboratory Technician ---------- *2013 – 2015*
*SymbioCellTech, LLC., Salt Lake City, Utah*

- Performed upkeep of diabetic and immunocompromised rodent colonies.
- Maintained dog mesenchymal stem cells and characterized their re-differentiation capacities.

**Publications**

- **Hurlow, E. E.**; Lin, J. B.; Dweck, M. J.; Nuryyeva, S.; Feng, Z.; Allred, T. K.; Houk, K. N.; Harran, P. G. Photorearrangement of [8]-2,6-Pyridinophane N-Oxide. *J. Am. Chem. Soc.* **2020,** *142* (49), 20717-20724.

- Feng, Z.; Allred, T. K.; **Hurlow, E. E.**; Harran, P. G. Anomalous Chromophore Disruption Enables an Eight-Step Synthesis and Stereochemical Reassignment of (+)-Marineosin A. *J. Am. Chem. Soc.* **2019,** *141* (6), 2274-2278.

**Awards & Fellowships**

- UCLA Chemistry & Biochemistry Saul and Sylvia Winstein Dissertation Award ---------- *2022*
- UCLA Chemistry & Biochemistry Excellence in Research Award ---------- *2021*
- NIH Chemistry–Biology Interface Training Fellowship ---------- *2019 – 2021*
- Crocker Science House Scholar ---------- *2016 – 2017*
- Ronald and Eileen Ragsdale Scholarship ---------- *2016 – 2017*
- ACS DOC Summer Undergraduate Research Fellowship ---------- *2016*
- Mack Thomas Rozelle Memorial Scholarship ---------- *2015 – 2016*
- James M. Sugihara Student Award ---------- *2015 – 2016*

**Teaching**

Teaching Assistant ---------- *Fall 2021*
*Organic Reactions and Pharmaceuticals*

Teaching Assistant ---------- *Fall 2021*
*Strategy and Design in Organic Synthesis (Graduate Course)*

Teaching Assistant ---------- *Fall 2021*
*Organic Chemistry Lab II*

Teaching Assistant ---------- *Summer 2021*
*General and Organic Chemistry Lab II*

Teaching Assistant ---------- *2017 – 2018*
*Organic Chemistry Lab I*

Supplemental Instructor ---------- *2016 – 2017*
*Organic Chemistry 1 & 2*

**Selected Presentations**

- **Hurlow, E. E.**, Lin, J. B., Nuryyeva, S., Dweck, M. J., Henshaw, O. G., Houk, K. N., Guo, F., Harran, P. G. Prodiginines in Two Parts: An Unusual Photorearrangement en route to Marineosin A and Scaffold-Assisted Co-Crystallization of RNA-Binding Molecules American Chemical Society Division of Organic Chemistry Graduate Research Symposium, November 2021. *Invited Presentation*.

# Chapter One

*The Photochemistry of [8]-Pyridinophane N-Oxide.*

## 1.1 Introduction

Heterocyclic *N*-oxides exhibit diverse photochemistry, undergoing a wide variety of transformation when irradiated.[1-3] Despite being one of the simplest in this class of compounds, pyridine *N*-oxide (**1**) exhibits exceptionally diverse rearrangements. The photochemistry of pyridine *N*-oxide was first investigated in the 1950s;[4-5] these studies probed electronic structure of the molecule and described its photodeoxygenation. In 1966, Streith and Sigwalt described the photorearrangement of pyridine *N*-oxides to 2-formylpyrroles (Scheme 1.1.1).[6] Drawing an analogy to nitrone photochemistry,[7] they postulated an oxaziridine as the first ground state intermediate. Subsequent norcaradiene-type electrocyclic ring expansion was thought to generate a 1,2-oxazepine en route to the formylpyrrole. The same group later discovered that performing the photolyses in aqueous $CuSO_4$ solutions markedly improved yields of formylpyrroles.[8] This efficient procedure was scalable[9-11] and minimized tar formation typical of metal-free variants. The authors suggested a nitrene intermediate derived from the 1,2-oxazepine could be stabilized by metal complexation, allowing electrocyclic ring closure to proceed more efficiently. Additional support for a nitrene intermediate came from flash photolysis studies. Lohse and coworkers observed that irradiation of pyridine was insensitive to base concentration and dissolved oxygen.[12] Reactivity of an unknown intermediate (lifetime in $H_2O$ ~63 ms) towards amines was inconsistent with ground state chemistry of oxazepines and oxaziridines and product formation was thought too slow to involve an excited state. Instead they postulated the

intermediate to be a vinyl nitrene, deprotonation of which was the source of nitrile. It is notable that tars formed in many pyridine *N*-oxide photolyses contain the nitrile functional group.[12]

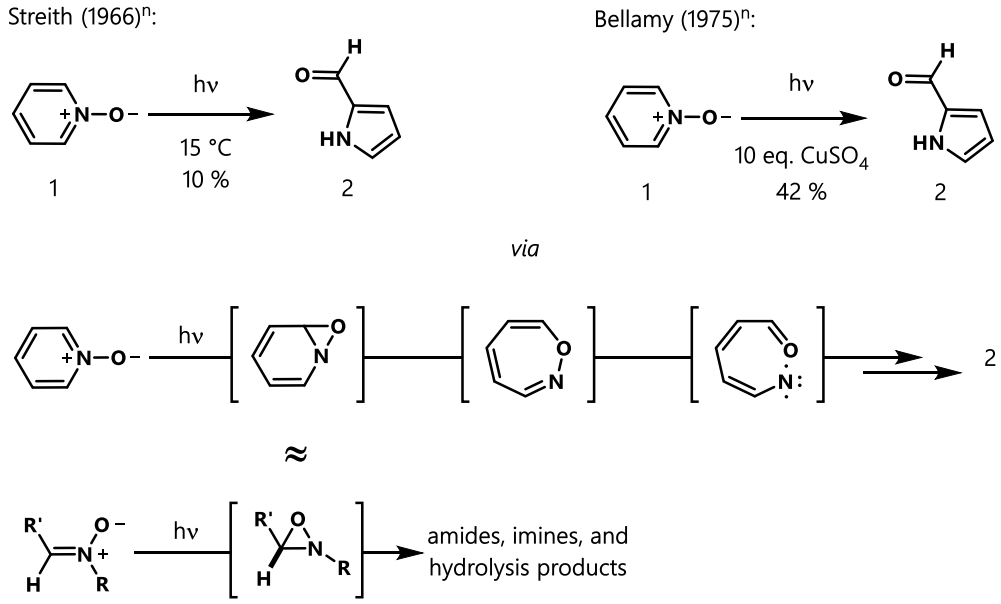


**Figure 1.1.1** Photorearrangement of pyridine *N*-oxides was proposed to proceed through an oxaziridine intermediate analogous to that produced by irradiation of nitrones.

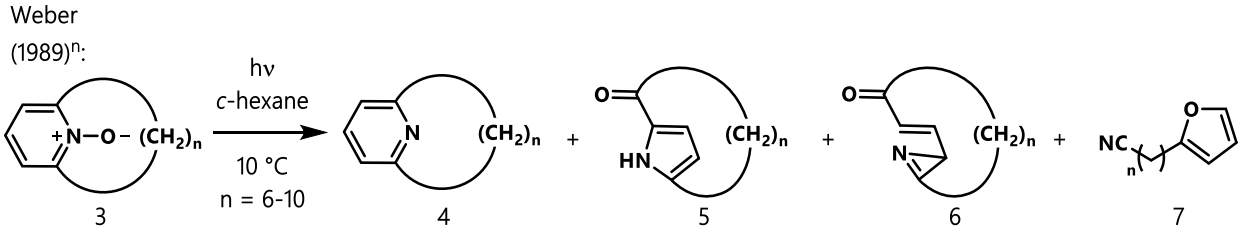


| *n* | Time (h) | % Yield | | | | |
|---|---|---|---|---|---|---|
| | | **4** | **5** | **7** | **8** | **4** (recovered) |
| 6 | 3 | 1.0 | 0.4 | — | 4.2 | — |
| 7 | 5 | 4.6 | 1.3 | 4.0 | 0.7 | 20.0 |
| 8 | 5 | 5.3 | 0.6 | 5.2 | — | 25.0 |
| 9 | 15 | — | 1.7 | 1.0 | — | 9.4 |
| 10 | 20 | 5.8 | 11.9 | 0.4 | 3.1 | 7.6 |

**Table 1.1.1.** Results from Weber's study of pyridinophane photorearrangement.

In 1989, Weber reported syntheses of pyridine *N*-oxides with carbons 2 and 6 bridged by hydrocarbon chains of varying length.[13] Photolyses of these materials gave mixtures containing ketopyrrolophanes, macrocyclic azirenes, and furanylalkyl nitriles. Based on Streith and Sigwalt's mechanistic framework, Weber proposed that excitation of the *N*-oxide generated oxaziridines **I** (Scheme 1.1.2). Valence bond isomerism analogous to norcaradiene-type walking rearrangements[14] was thought to interconvert oxaziridines **i** and epoxides **ii**, from which both 1,2- and 1,3-oxazepine intermediates could derive via electrocyclic ring expansions. The latter could fragment to furanylalkyl nitriles **7** while the former would proceed to nitrenes **v**. Azirenes **6** and ketopyrrolophanes **5** were seen as competing products of 1,3- and 1,5-electrocyclic ring closures

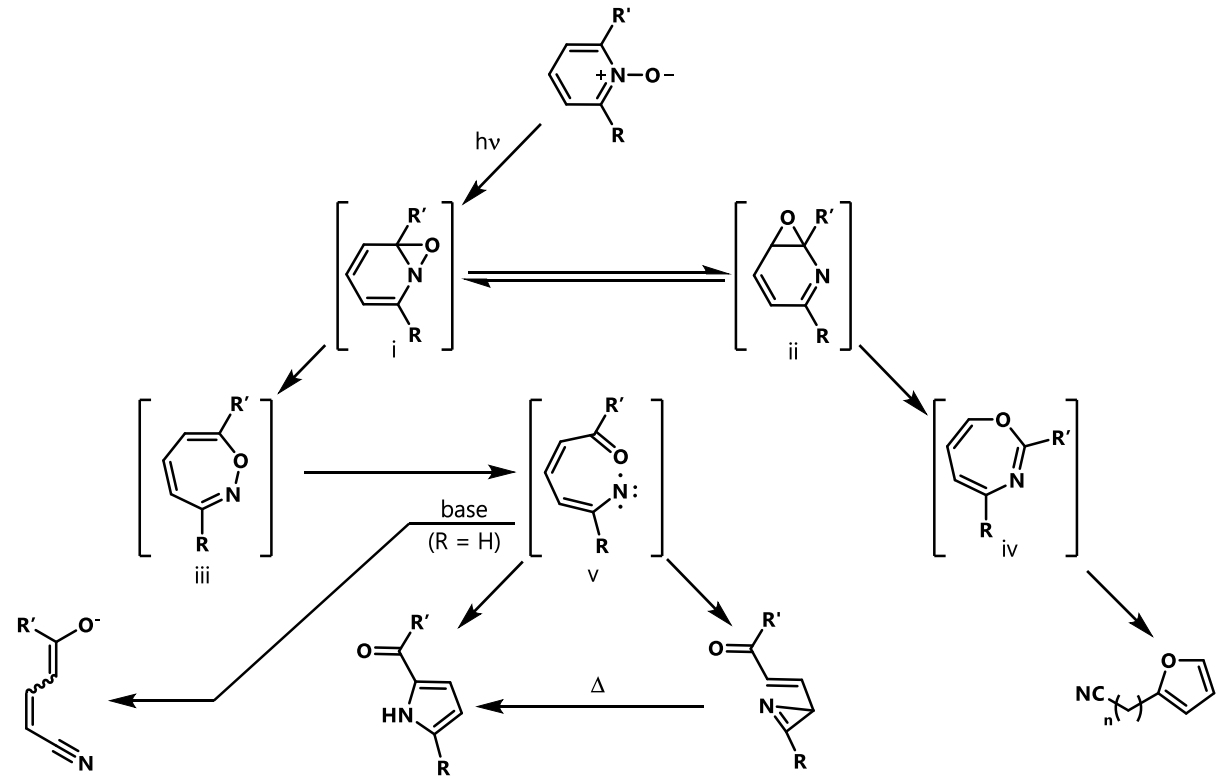


**Figure 1.1.2** The mechanistic framework for pyridine *N*-oxide photorearrangement prior to this work**.**

within **v**. In Weber's report, the amount of azirene formed was directly correlated with ansa bridge size and isolated azirenes could be independently converted to keto pyrrolophanes by thermolysis. Photolysis of azirenes was reported to give intractable mixtures.

We became interested in the photochemistry of pyridinophane *N*-oxides when we recognized that Marineosin A, and anti-cancer natural product of interest to our lab, could be derived from ketopyrrolophane (**5**, n=8) in a straightforward sequence. In this chapter, section 1.2 describes how we optimized the photorearrangement of [8]-2,6-pyridinophane *N*-oxide and applied it to the total synthesis of Marineosin A. Section 1.3 describes our mechanistic investigation of this rearrangement, and section 1.4 discusses efforts toward an alternative route to the desired ketopyrrolophane.

## 1.2 Anomalous Chromophore Disruption Enables an Eight-Step Synthesis and Stereochemical Reassignment of (+)-Marineosin A.

The prodiginine alkaloids have fascinated chemists for decades. These bacterial lipochromophores possess a range of biological activities[15] and synthetic variants have advanced to clinical trials as cancer therapy.[16,17] The ansa-bridged members of the family (e.g. **11**, Scheme 1.2.1) have been coveted synthetic targets.[18] Structures of this kind are biosynthesized from acyclic hydrocarbon precursors, wherein a non-heme iron oxygenase catalyzes dehydrogenative macrocyclization via a mechanism reminiscent of p450 hydroxylations.[19]

In 2008, the discovery of marineosins A and B (Scheme 1.2.1) revealed a new variant of this chemistry.[20] Marineosins harbor oxygenation in their aliphatic domain, and it is integrated into a

spiroiminal motif interrupting the typical prodiginine chromophore. Reynolds *et al.* subsequently studied the marineosin (*mar*) gene cluster from *Streptomyces* sp. CNQ-617, an operon homologous to the *red* gene cluster in *S. coelicolor* that produces streptorubin B (**11**).[21-22] They

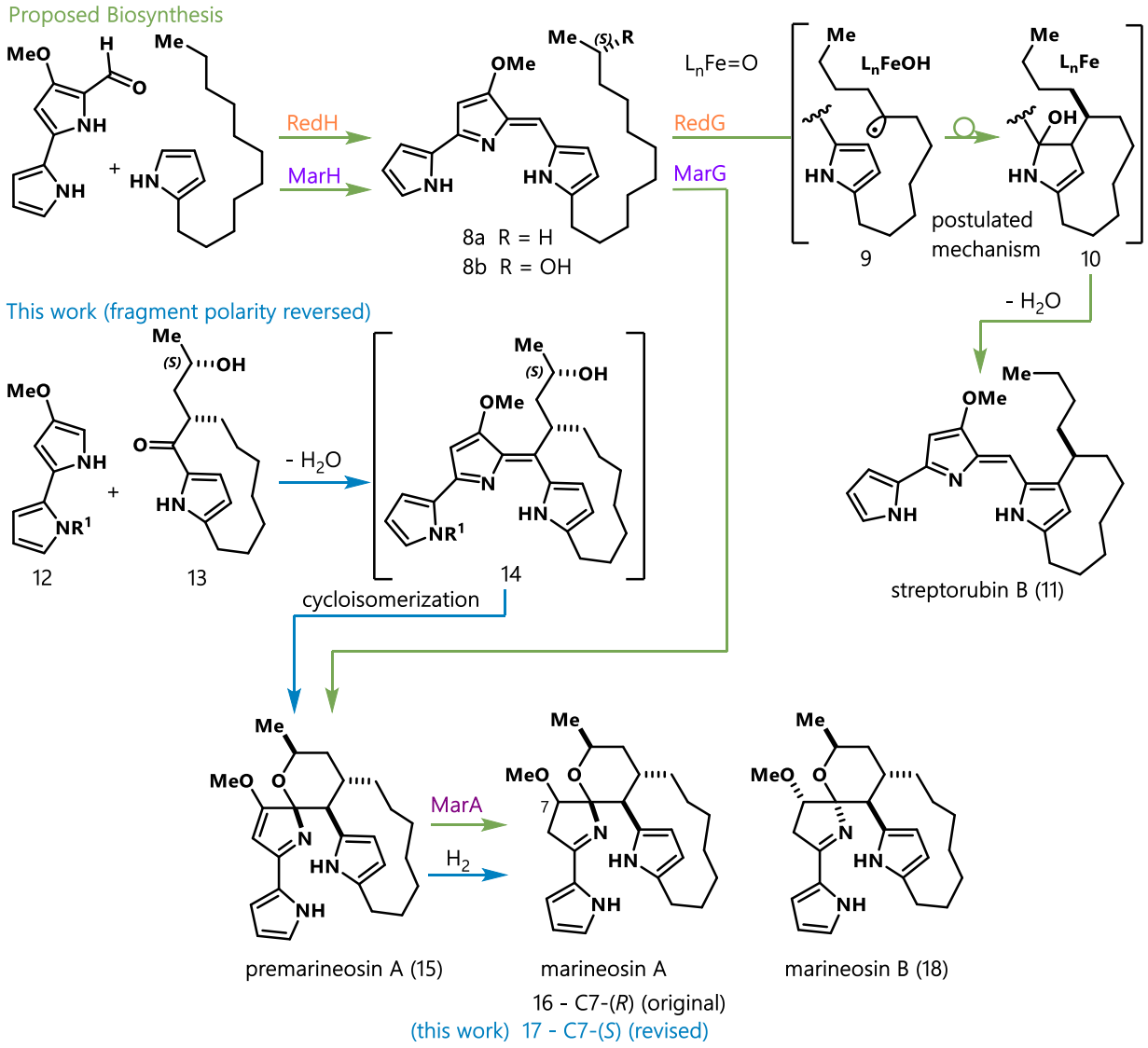


**Figure 1.2.1** Marineosins are oxygenated, spirocyclic ansa-bridged prodiginines.

found spiroiminal formation is coupled with macrocyclization during the MarG catalyzed conversion of (*S*)-23-hydroxyundecylprodiginine (**8b**) into premarineosin (assigned as **15**). Similar to proposals for **11**, the result was rationalized in terms of regio-controlled alkyl radical addition

to the chromophore.[23] Yet the fate of the presumed cyclized radical was less clear. Was it oxidized to afford **15** directly, or oxygenated to form a hemi-aminal analogous to **10**? Alternatively, could prodiginine **14** be an intermediate and proceed non-enzymatically to **15**? While replicating actions of MarG was likely not feasible, we felt insight into these questions could be achieved with a synthesis that passed through **14**, wherein methods to 'bleach' that chromophore by internal hydroalkoxylation could be examined.

The novel structure of marineosins and the selective cellular cytotoxicity attributed to **16**[20] drew attention. The Lindsley, Snider, and Shi laboratories each developed synthetic routes to marineosin substructures.[24-29] In fact, Shi's experiments culminated in a 19-step synthesis of **16+**.[29] The identity of synthetic **16** was confirmed by crystallography, but its spectroscopic data differed from that reported for the natural product. Evaluation of Shi's data, relative to that published by Fenical,[20] suggested the discrepancy was subtle and likely an issue of relative stereochemistry rather than composition or connectivity (*vide infra*).

To assemble chromophore **14**, wherein only one of two bonds formed by MarG was present, we choose to reverse the polarity of fragments joined during prodiginine biosyntheses (Figure 1.2.1) and previous laboratory preparations.[15,18,23] In our case the prodiginine would derive from condensation of a nucleophilic bispyrrole (**12**) with ketopyrrolophane **13**. The latter was seen as the product of alkylating pyrrolophane **24** (Figure 1.2.2) with propylene oxide.

Weber *et al.* had isolated trace amounts (0.6% yield) of compound **24** during the UV photolysis of pyridinophane *N*-oxide **22**.[13] Because **22** could be prepared readily from commercial 2,6-dichloropyridine and 1,8-dibromoctane,[30] we sought to optimize its photorearrangement. We

observed a solvent effect, with ethers being superior to the originally reported hydrocarbon (see Table 1.5.2). THF at -78˚C provided the best result (19% isolated yield of **24**). It had been reported that inclusion of aq. $CuSO_4$ in the photolysis of substituted pyridine *N*-oxides markedly increased

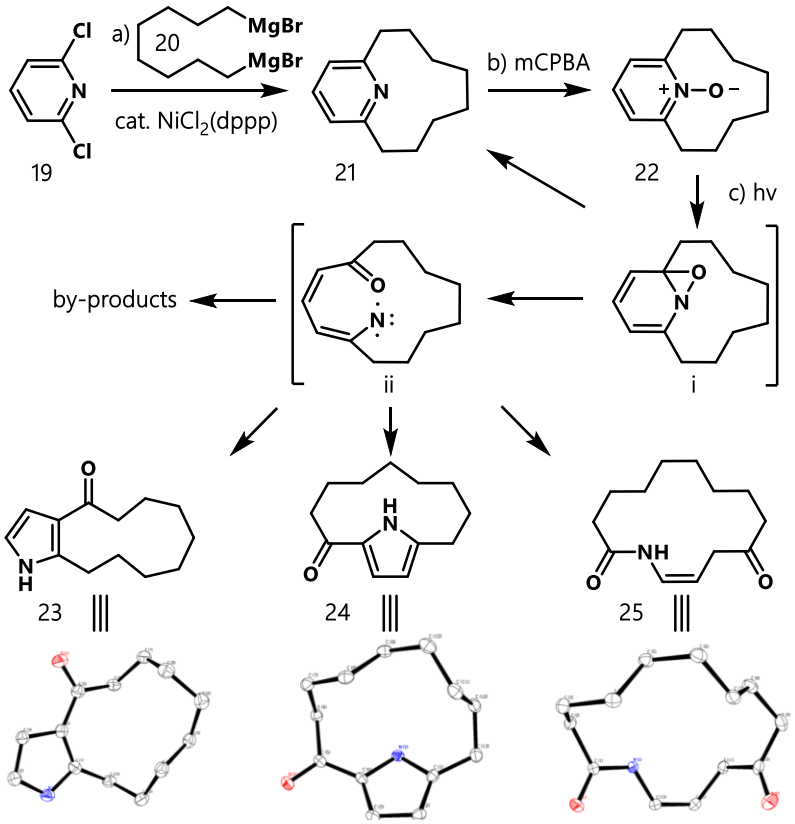


**Figure 1.2.2** Photochemical synthesis of ketopyrrolophane **24**. Reagents and conditions: a) **19** (1 eq.), 13 (1 eq.), 0.8 mol% $NiCl_2$(dppp) $Et_2O$, 10 °C, 6 h, 50%; b) mCPBA (1.5 eq.), $CHCl_3$, rt, 48 h, 82%; c) hv (254 nm), THF (0.01 M), -78 °C in flow, residence time = 2 min. **21** (15%), **23** (5%), **24** (25%) and **25** (18%). See also Table 1.5.2. X-ray structures are drawn in ORTEP format (50% probability thermal ellipsoids). H atoms removed for clarity.

the yield of incipient 2-formylpyrroles.[8] This was explained by Cu(II) stabilizing a postulated nitrene intermediate analogous to **ii**. However, irradiating **22** in aq. $CuSO_4$ provided **24** in only 4% yield. Photolysis of an isolated $Cu(NO_3)_2$· [**22**]$_2$ complex as well as solutions of **22** containing $Rh_2(TFA)_4$

gave similarly low yields. In all instances, irradiation of **22** produced significant amounts of deoxygenation product **21**, along with newly identified macrocycles **23** and **25**. Moreover**,** control experiments established **24** was photolabile and degraded during the timeframe of the batch process. We therefore adopted a flow technique wherein a cold THF solution (-78 ˚C, 0.01 M) of **22** circumscribed a jacketed mercury lamp in small-bore FEP tubing. In that case an exposure time of only 2 minutes afforded **24** in yields (25%) exceeding our best batch reaction while minimizing formation of **23** (Figure 1.2.2). Photolysis in flow greatly increased throughput and allowed grams of pure **24** to be isolated in short order.

| Entry | Solvent | Temp (°C) | % Yield | | | |
|---|---|---|---|---|---|---|
| | | | **21** | **23** | **24** | **25** |
| 1 | *c*-hexane | r.t. | 17 | 3 | 3 | 4 |
| 2 | DME | r.t. | 12 | 6 | 4 | 10 |
| 3 | EtOH | r.t. | 7 | 3 | 6 | 7 |
| 4 | MeCN | r.t. | 8 | 4 | 5 | 7 |
| 5 | THF | r.t. | 11 | 9 | 7 | 14 |
| 6 | THF | -40 | 19 | 5 | 18 | 12 |
| 7 | THF | -78 | 10 | 2 | 19 | 10 |
| 8 | DME | -30 | 14 | 5 | 10 | 15 |
| 9a | water | r.t. | nd | nd | 4 | nd |
| 10b | EtOH | r.t. | nd | nd | 7 | nd |
| 11c | THF | r.t. | nd | nd | trace | nd |
| 12d | THF | -75 | 9 | 3 | 19 | 17 |
| 13e | THF | -75 | 15 | 5 | 25 | 18 |

**Table 1.2.1** Optimization of the photo-induced rearrangement. [a]10 eq. $CuSO_4$ were added. [b]The $Cu(NO_3)_2$ bis-adduct of **22** was used. [c]$Rh_2TFA_4$ was added, complete decomposition of **22** was observed. [d]Experiment performed in flow format (residence time = 2 min) with one layer of FEP tubing around the immersion well. [e]Experiment performed in flow format with three layers of FEP tubing around the immersion well (residence time = 5 min). nd = not determined.

Deprotonation of **24** with 3.1 eq. LDA in rigorously anhydrous, deoxygenated THF at 0˚C, followed by addition of (*S*)-propylene oxide and $AlMe_3$ gave alkylation products **13** in 71% yield (dr = 2:1). The two isomers of **13** were separable by chromatography, although they would readily equilibrate under mildly acidic conditions (to the same 2:1 ratio observed in crude reaction mixtures, see SI), presumably via their enol tautomer.

When ketones **13** and bipyrrole **27**[31] were dissolved in anhydrous MeOH and treated with HCl, the solution turned deep red within seconds. This was consistent with condensation product **28** (Figure 1.2.3) being formed. However, after 30 min, predominantly starting materials were recovered following aqueous workup. Despite repeated attempts, target **28** could not be isolated from the reaction. Prodiginines bearing a hydrogen at C9 (e.g. **11**) are isolable species,[32] but branched ansa bridge connectivity at C9 appeared to destabilize the system. Condensation product **28** hydrolyzed readily and, standing in MeOH, it would degrade via an unusual sigmatropic rearrangement of the 2-hydroxypropyl branch onto the C ring pyrrole.[33] To stabilize the molecule in situ, we quenched the condensation reaction with dry NaOMe. This gave novel structural variants of premarineosin (namely **29**, dr 1:1) in good yield. These tetrahydrofurans derive from the chromophore in **28** being internally disrupted at C9, the same position attacked by water during hydrolysis (as depicted). Compounds **29** were air-sensitive, but sufficiently stable to be purified by rapid chromatography.

The question became: how do we ring-expand **29** in route to hydropyran **15**? The sulfonamide in **29** was cleaved using $Mg^0$ in MeOH and the unstable product (**30**) was oxidized with $MnO_2$.[27] This cleanly transformed the bipyrrole into oxo derivative **31** (Figure 1.2.4), wherein C8 was now a potentially electrophilic site. The intent was to activate the pyrrolinone π system to

induce the conjugated C9-O bond to migrate to C8. Unfortunately, **31** degraded in the presence of Brønsted and Lewis acids. Its precursor **30** was also unstable to acid, but in that case exposure to dry HCl in MeOH reformed a prodiginine chromophore via ring-opening of the tetrahydrofuran ring. It was thought $MnO_2$ might oxygenate that product (i.e. **32**) in a manner analogous to **31**, wherein a 6-exo trig cyclization of the tethered alcohol could ensue. Compound **32** was highly

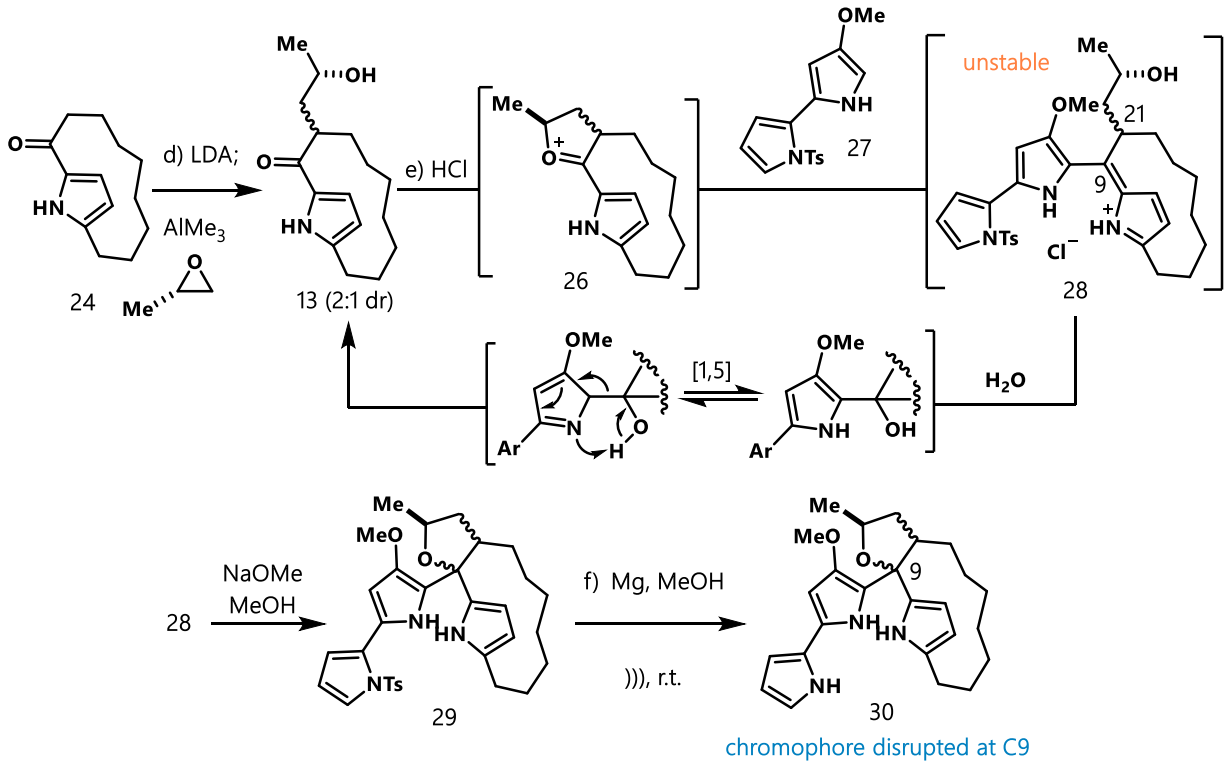


**Figure 1.2.3** Rapid synthesis of 'iso'-premarineosins. Reagents and conditions: d) LDA (3.1 eq.), 0 °C, 1 h; (S)-propylene oxide (5 eq.), $AlMe_3$ (1.1 eq.), -78 °C to rt, 12h, 72%, dr=2:1; e) **13** (1 eq.), **27** (1 eq.), 1.5 eq. HCl (1M in MeOH), $Na_2SO_4$, toluene, 0 °C, 30 min; 1M NaOMe, MeOH, 58%, dr=1:1. f) 5 eq $Mg^0$, MeOH (0.1M), 30 min, rt, 90%.

unstable and its handling was minimized to avoid the aforementioned sigmatropic rearrangement.[30] When freshly prepared **32** was stirred with commercial $MnO_2$ in acetone, workup gave pyrrolinones **31**, along with lesser amounts of hydrolysis products **13**. Notably, we also

isolated trace amounts (~1%) of a new, pale-yellow isomer of **32**. This substance was not an oxidation product, and it had spectral data consistent with a premarineosin. But its $^{1}$H NMR spectrum was slightly different from that reported for premarineosin A.[22] Gratifyingly, hydrogenating the sample over Pd/$BaSO_4$ gave a molecule (**17**, see Figure 1.2.5) whose spectroscopic data was identical to that reported for natural marineosin A.[20]

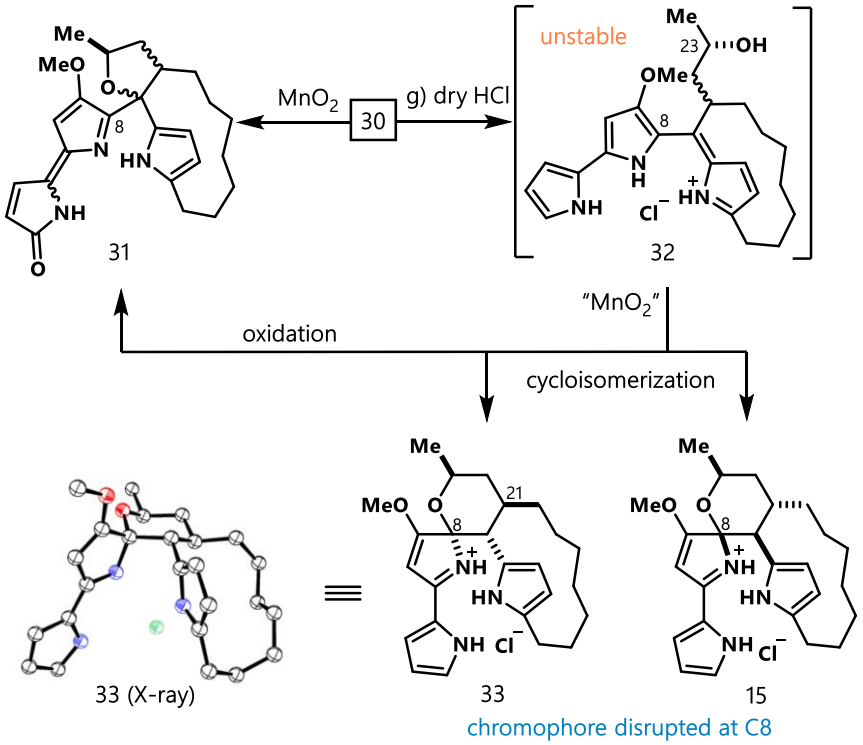


**Figure 1.2.4** Competing cycloisomerization at a $MnO_2$ surface. Reagents and conditions: g) 3.0 eq. HCl in MeOH; acidic $MnO_2$ powder (see SI, ~80 eq.), $MgSO_4$, acetone, rt, 5 min, 6% of **15** and 6% of **33** (overall from **29**).

With this exciting result, we were eager to refine the sequence. Suspended manganese oxide was required for the cycloisomerization, although the nature of the surface promoting its non-oxidative chemistry was unclear. Certain forms of $MnO_2$ were known to promote hydration of nitriles,[34] but the analogy was tenuous. Other nitrile hydration catalysts caused no isomerization

of **32**. On the other hand, when preparing $MnO_2$ in-house ($KMnO_4$ + $MnSO_4$), samples that were relatively poor oxidants (see Table 1.5.3) retained an ability to hydrate p-$MeOC_6H_4CN$ in dry organic solvent, presumably by delivering adsorbed water. These same samples mediated cyclization in our system. Best results were achieved using carefully dried, 'acidic' $MnO_2$[35] wherein isomerization products derived from both diastereomers of **32** (namely **15** and **33**, dr = 1:1, Figure 1.2.4) formed within minutes at 25˚C and were isolated in 12% combined yield. Relative to the behavior of **28**, whose chromophore readily accepted nucleophiles at C9 (Figure 1.2.3), the formation of **33** and **15** from **32** was an anomaly, wherein the chromophore was disrupted at C8 via a non-oxidative addition of the C23 alcohol under ostensibly oxidative conditions.

Each C21 epimer of **32** appeared to convert to a single cycloisomerization product. The structure of **33** was secured by crystallography. The structure of **15** was assigned by inference, with the pyrrolophane emanating from the pyran ring as equatorial substituents and the C-N bond of the spiroiminal oriented axial. These designations were fully consistent with extensive NMR analyses (see SI). Our revised structure of marineosin A (**17**) results from hydrogenating the vinylogous imidate in **15** from its less hindered face (Figure 1.2.5, dr >19:1). NOESY correlations between C25 protons and C11H/C12H firmly supported this designation, whereas the original C7 assignment[20] based on an nOe signal between C7H and C9H was ambiguous. The distance between C7H and C9H is similar in both C7 epimers of the structure.

To date, the minor, less biologically active marineosin B isomer has not been observed in our experiments. Data is consistent with marineosin B being the C8 epimer of **17** (namely **18**). It may arise via equilibration of the spirocycle, precedent for which exists in Snider's model studies.[27]

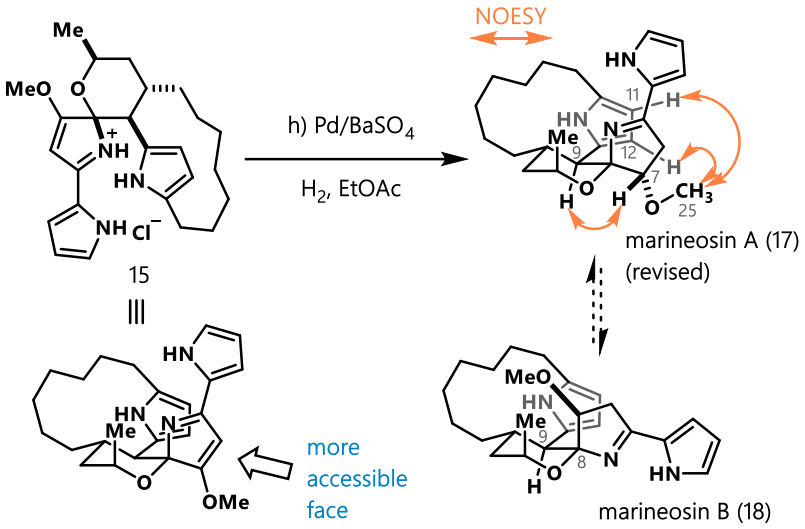


**Figure 1.2.5.** Vinylogous imidate hydrogenation.

In conclusion, we have developed an eight-step asymmetric synthesis of marineosin A and reassigned its stereochemistry.[36] The route exploits a photorearrangement in flow followed by a ketopyrrolophane/bipyrrole condensation to build the first peripherally functionalized, C-9 linked ansa-bridged prodiginine. The high reactivity of this molecule led to the discovery of "isopremarineosins", a novel manganese surface-mediated cycloisomerization and an atypical [1,7] sigmatropic carbon shift. The chemistry offers means to prepare a new class of bridged prodiginines with previously inaccessible substitution patterns. Studies along those lines are ongoing, as are attempts to further understand the key isomerization, improve yields and to probe the antimalarial, immunosuppressive, and antineoplastic properties of these structures in detail.

## 1.3 Photorearrangement of [8]-Pyridinophane *N*-Oxide.

Our interest in the photochemistry of pyridinophane *N*-oxide **22** persisted following completion of Marineosin A. We had isolated two novel side products, macrolactam **25** and fused

bicyclic pyrrole **23**, but were unable to rationalize their formation within the existing mechanistic framework. If we could understand how these compounds formed and eliminate or minimize those pathways, we could further optimize the yield of **5**. To achieve this, we employed analytical GC/MS time series experiments and collaborated with the Houk group to study the mechanism using DFT. Herein is described our work to this end.

To begin, we probed relative energies of postulated photolytic intermediates in Figure 1.1.2 using density functional theory (DFT). We included electronic energies, appropriate in describing electronic excitations, and free energies, appropriate for energetics on the ground state. The calculations supported a pathway from **22** to **24** and **37** *via* common intermediate nitrene **36**. As shown in Figure 1.3.1, the first excited state of *N*-oxide **22** relaxes to a geometry with increased C-O bonding and passes through a funnel onto the ground state surface of oxaziridine **34**. Cleavage of the C-N bond (**34→35 TS**, via electrocyclic ring expansion) in **34** is calculated to proceed with a low barrier of 4.5 kcal/mol to generate 1,2-oxazepine **35**. Photoexcitation of **35** (vide infra) would then lead to lengthening of its N-O bond and the formation of nitrene **36**. Both singlet and triplet states of **36** were probed, and the triplet state was calculated to be significantly more stable. Triplet nitrene **36** is a key intermediate in the overall photorearrangement.

Figure 1.3.2 depicts the pathway for conversion of **36** to azirene **37** and ketopyrrolophane **24**. The c*is* geometric isomer of **37** is calculated to be 1.2 kcal/mol higher in energy than its *trans* counterpart and has not been observed experimentally. Thus, *trans*-**37** is referred to simply as **37** from here on. Reversion of **37** to **36** is unfavorable, as cleavage of the newly formed C-N bond would require temperatures of ~200 °C.[43,44] Triplet **36** could also electrocyclize to 2*H*-pyrrole **38.**

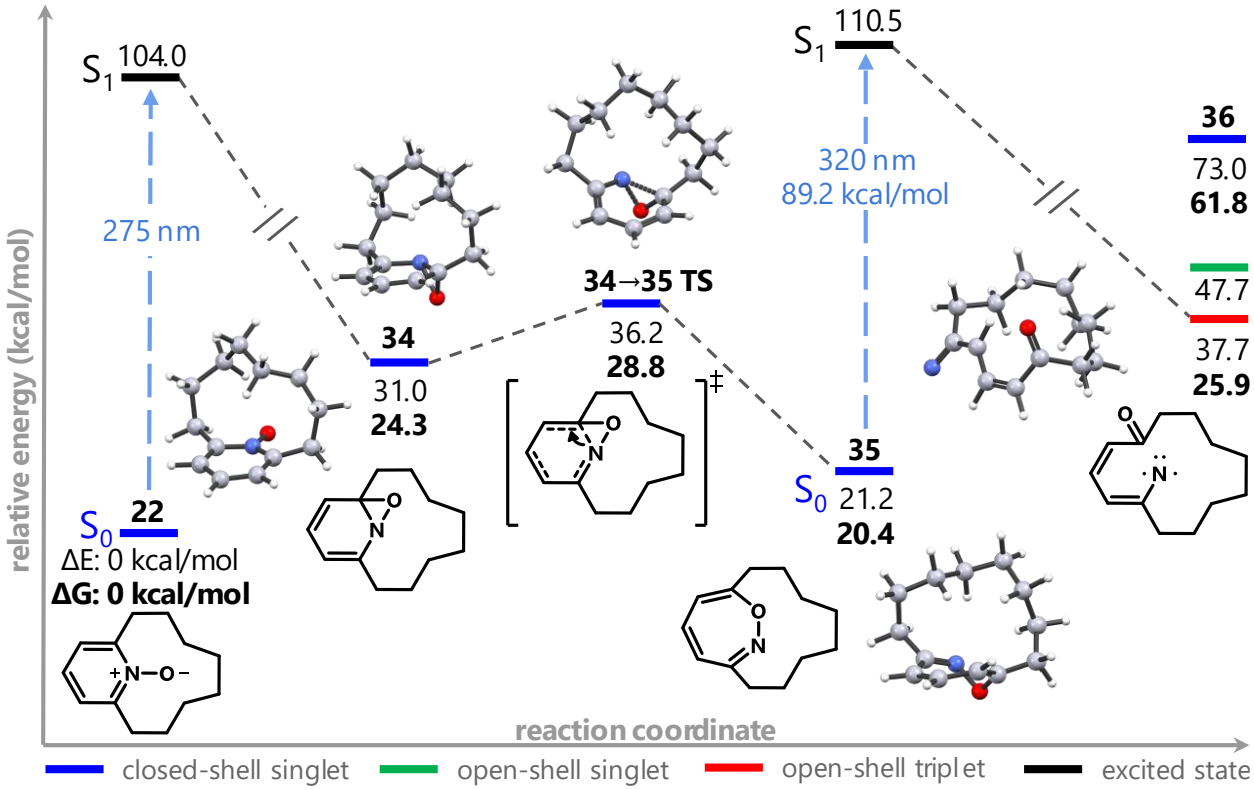


**Figure 1.3.1.** Calculated energies for proposed intermediates en route to nitrene **36**. Unless indicated otherwise, all geometries were optimized using B3LYP/6-31G(d) in the gas phase as a closed shell singlet.[37-40] **36** was optimized as an open shell triplet using UB3LYP/6-31G(d) in the gas phase. Subsequent single-point energy calculations on each of the optimized structures were performed using (U)M06-2X/6-311+G(d,p) with the polarizable continuum model IEF-PCM for solvation by cyclohexane as either a closed shell singlet (blue) or open-shell triplet (red).[41] For **22** and **35**, a TD-DFT energy calculation was used to compute its lowest energy excitation using M06-2X/6-311+G(d,p) with the same solvation model as single-point calculations (black). Images of optimized structures were generated with Mercury 4.3.1.[42]

Isomerization of **38** to its 1H form **24** may occur via thermal 1,5 hydrogen shift (activation barrier = 19 kcal/mol) or via bimolecular proton transfers.

Regarding the origin of fused bicyclic pyrrole **23**, Padwa had reported that photolysis of vinyl azirenes of type **39** gave 3-formylpyrroles,[43] with subsequent mechanistic studies implicating

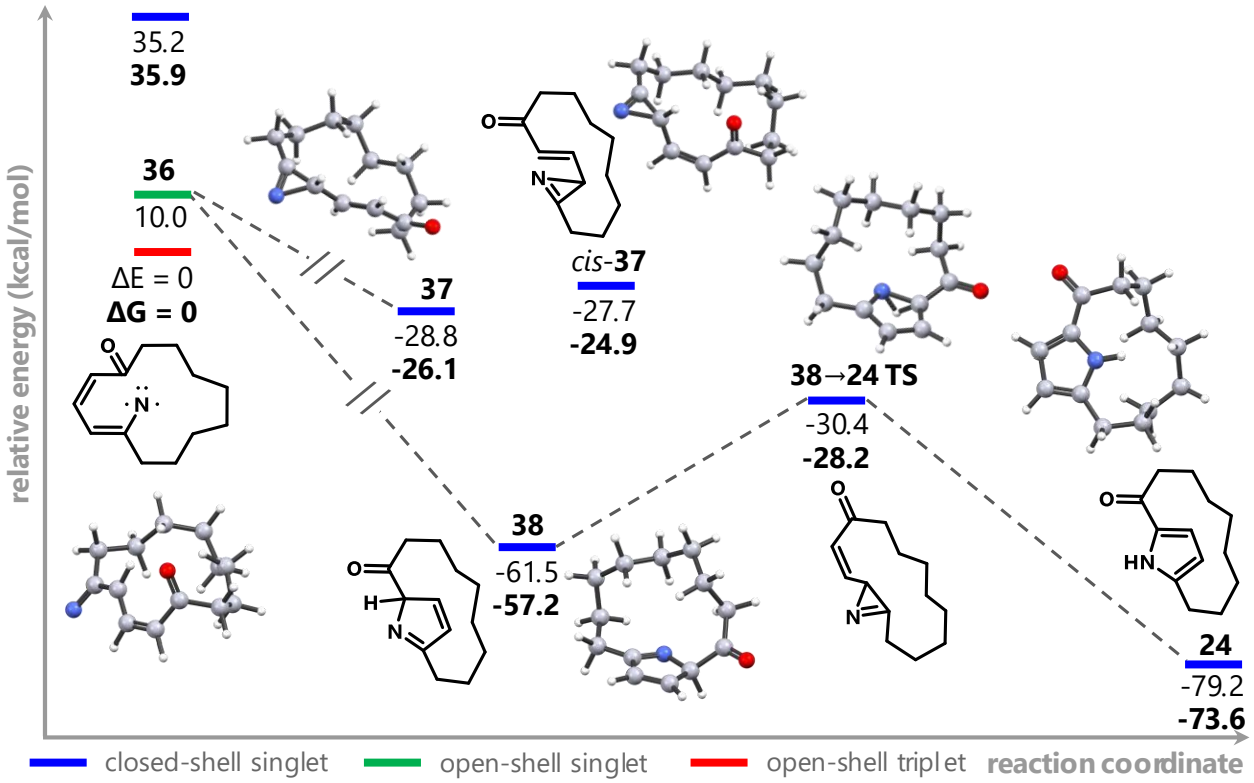


**Figure 1.3.2** Calculated relative energies of intermediates in the formation of acylpyrrolophane **24** from nitrene **36**. See Figure 1.3.1 for computational details.

a nitrile ylide intermediate (e.g. **40**[45], Figure 1.3.3, inset). Though these findings seemed at odds with Weber's account of unproductive azirine photolysis, DFT calculations suggested this to be a feasible pathway to **23**. As depicted in Figure 1.3.3, photoexcitation of **37** could cleave the azirene C-C bond to generate nitrile ylide **42**. Ring closure in **42** to afford 2H pyrrole **43** is calculated to be facile (**42→43 TS**), whereupon prototropy in **43** would generate fused bicyclic 1H-pyrrole **23**.

The above calculations provided a framework to design new experiments. If keto pyrrole **23** derived from photorearrangement of azirene **37**, blocking that process could be useful. We simulated the UV-Vis spectrum of **37** (TD-DFT) and compared it to experimental spectra for *N*-oxide **22** and pyrrolophane **24**. All three absorbed maximally near 280 nm. However, the spectrum

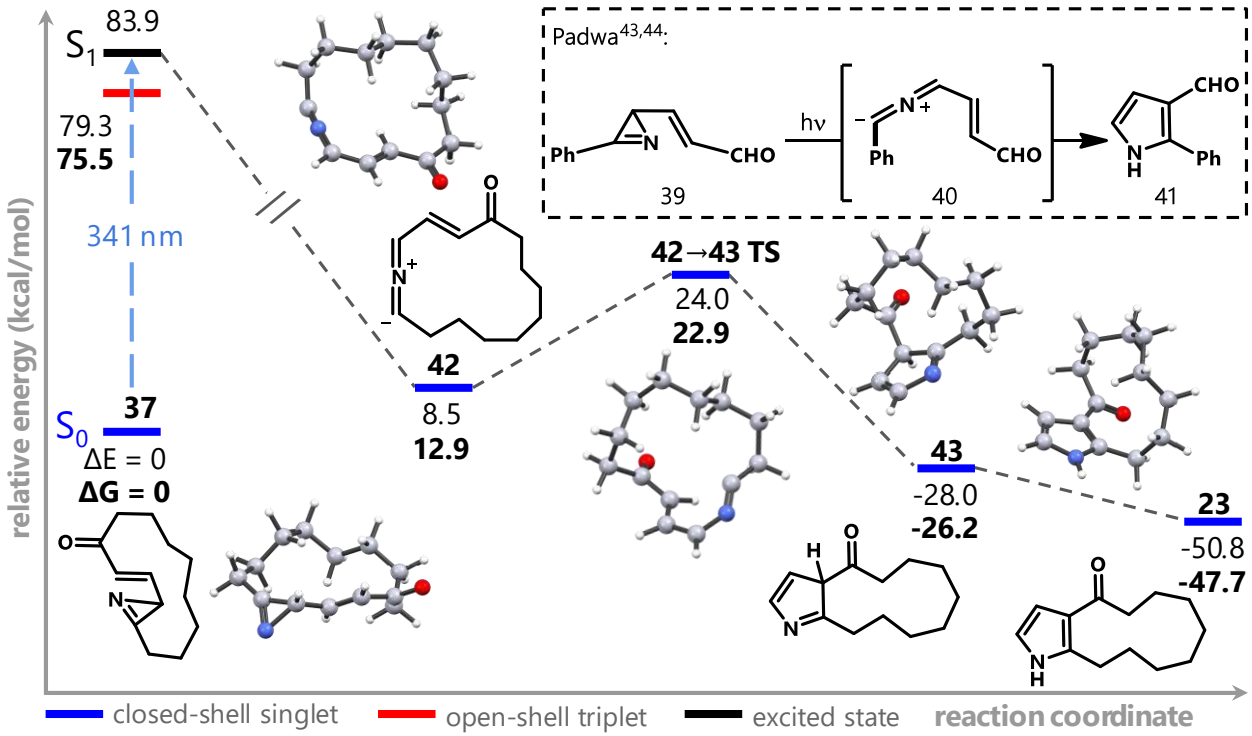


**Figure 1.3.3** Photoexcitation of vinyl azirene **37** is thought to generate nitrile ylide **21** *en route* to bicyclic pyrrole **7**. Precedent for this proposal is found in Padwa's synthesis of formyl pyrroles from vinyl azirenes (inset). See Figure 1.3.1 for computational details.

of **22** showed a second absorbance maxima near 235 nm. We speculated that selective irradiation in that region might allow the photorearrangement of **22** to proceed to **24** while minimizing secondary photochemistry of azirene **37**. In that case **37** would accumulate in the reaction, allowing it to be isolated and subsequently converted to **24** by thermolysis.[13]

We considered laser excitation and the use of band pass filters to achieve selective excitation at 235 nm, but neither was practical in our experimental format. Fortunately, published spectra of vinamidinium perchlorate (**44a**) suggested it could serve as a solution filter with transmissive character in the region around 240 nm.[46] Both the perchlorate and

hexafluorophosphate salts of compound **44** were readily synthesized and isolated as light yellow crystals.[47]

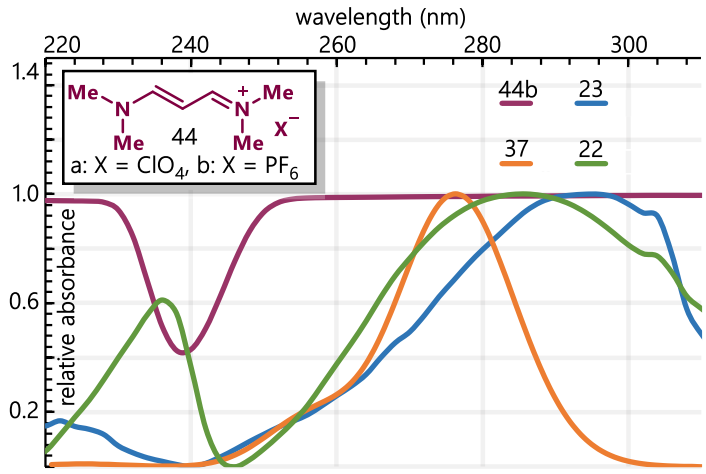


**Figure 1.3.4** Overlay of UV-vis spectra of **44b** (15 mM 70% aq. ethylene glycol), pyrrolophane **24** (0.1 mM THF), *N*-oxide **22** (0.005 mM THF), and the simulated spectrum of azirene **37** (computed using TD-B3LYP/-@31+G(d,p)/IEFPCMcyclohexane).

Screening counter ion, solvent, and concentration revealed that a 15 mM solution of hexafluorophosphate salt **44b** in 70% aqueous ethylene glycol possessed a UV spectrum aligned with our needs. To filter light in our flow apparatus, the glycol solution of **44b** was pumped through the inner lamp-jacket of the Hanovia apparatus (see SI for details) from an external reservoir pre-cooled to -78 ˚C. Control experiments showed the filter solution lost transmittance in the 240 nm region within 1 hour, necessitating its replacement every 45 minutes. Even in that case, however, product mixtures from solution filtered photolyses were little changed relative to those run in Pyrex. Because the experiments were premised on the simulated UV-Vis spectrum of azirene **37** being accurate and the absence of overlapping absorption from other intermediates, we were hesitant to interpret the results.

Instead, to test the validity of Figure 1.3.3, we sought to isolate **37**, which Weber had characterized previously. Analytical GC/MS was used to monitor products formed in the photolysis of **22** over time. This was best achieved by sampling solutions of **22** (10 mM in THF) during irradiation at ambient temperature in a Rayonet carousel. Preparative-scale batch reactions require several hours to complete. The GC/MS trace after 1 hour was surprising (Figure 1.3.5a). While expected products **45**, **24**, and **23** were present, lactam **25** was absent, and the major products were three unknown molecules. The mass spectrum of each unknown showed a parent ion with m/z = 205, indicating they were isomers of starting material **22**. Sampling the photolysis every 15 minutes and plotting relative peak areas versus time showed that unknowns **I**-**III** predominated at early time points (Figure 1.3.5b). The concentration of **II** plateaued at 45 min and remained stable thereafter, whereas amounts of **I** and **III** decreased significantly. The concentration of target pyrrolophane **24** continued to increase after starting material **22** was consumed, indicating it derived from either **I** or **III**. The time course experiment was repeated in 1:1 DME:$H_2O$ solvent. This resulted in rapid consumption of **22** (<1 h) and a correspondingly fast appearance of **I**, yet neither **II** nor **III** were detected (Figure 1.3.5c). In the context of prior observations, this pointed towards **I** as the source of pyrrolophane **24**.

To verify this hypothesis, it was necessary to isolate and photolyze **I**. This substance was acid-labile and unstable to chromatography. However, we were able to enrich crude samples in the molecule. Pyridinophane **22** was photolyzed for 1 hour in 1:1 DME:$H_2O$ (wherein **II** and **III** were not formed) and the reaction mixture was extracted with ethyl acetate. Concentration of the organic layer provided a residue that was triturated with hexanes to leave behind insoluble pyrroles **24** and **23**. The resultant hexanes solution contained ~75% **I** (GC/MS). $^{13}C$ NMR analysis

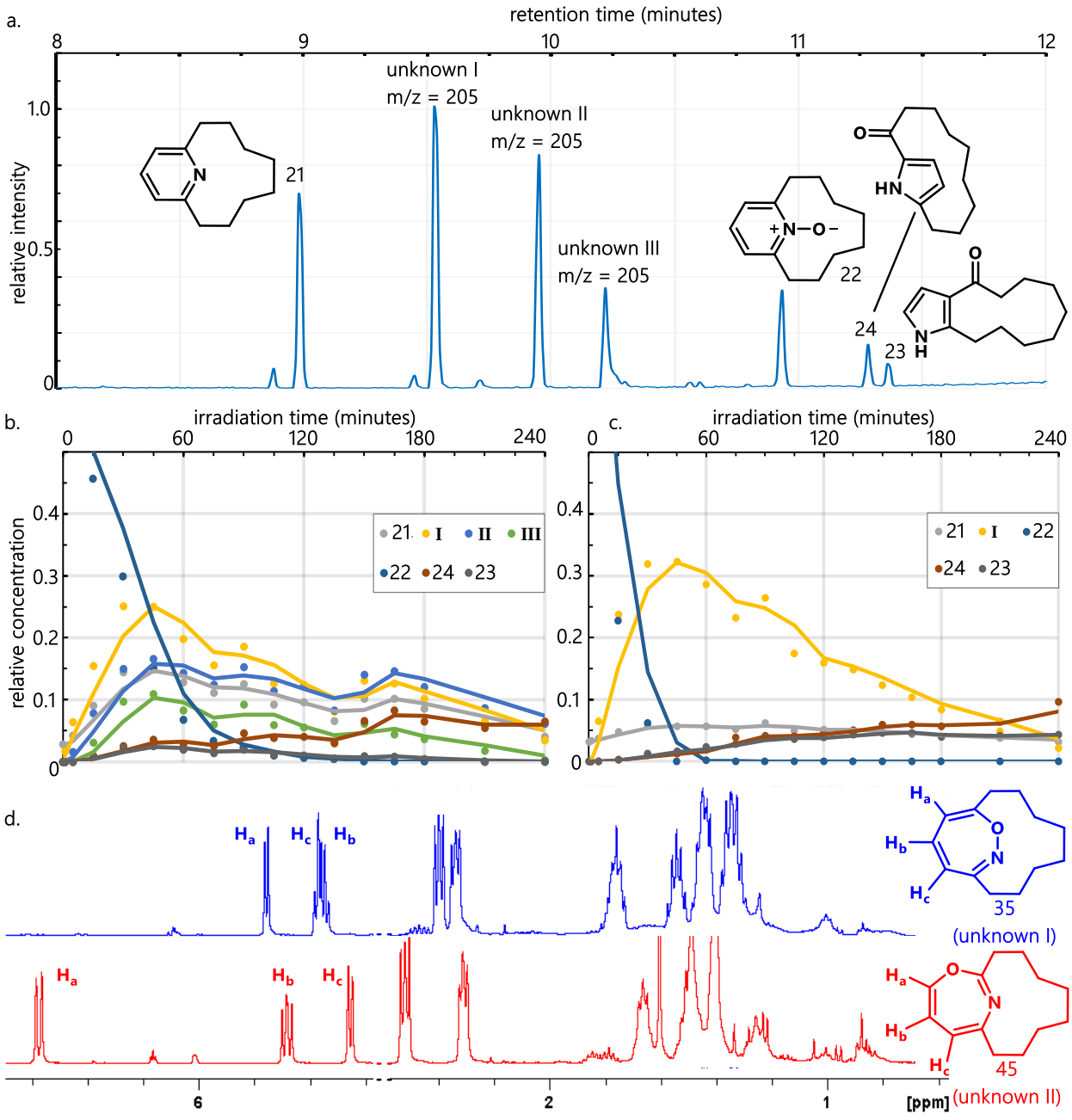


**Figure 1.3.5** a. Analytical gas chromatograph of crude mixture derived from batch photolysis of **4** (254 nm, 0.01 M THF, rt) after 60 minutes. b. Relative concentrations of species in panel a plotted vs time during photolysis of **22** (254 nm, 0.01 M THF, rt). For details see SI. c. Same as panel b except photolysis reaction solvent was 1:1 DME:$H_2O$. Trend lines are two-period moving averages. d. $^1H$ NMR spectra ($CDCl_3$, 400 MHz) of isolated unknowns I and II from panel a, eventually assigned as structures **35** and **45**, respectively.

indicated the main component of the mixture had an intact ansa bridge and the three vinylic resonances observed by $^1$H NMR were consistent with 1,2–oxazepinophane **35** (Figure 1.3.5d). To our knowledge, this was the first direct evidence for a 1,2-oxazepine intermediate in the photorearrangement of pyridine *N*-oxides.[48] Moreover, structure **35** is the first 1,2-oxazepine isolated lacking electron withdrawing substitution.[49] Re-photolyzing **35** in DME:$H_2O$ resulted in its conversion to keto pyrrolophane **24** and unknown **II**, confirming **35** as an intermediate in the photolysis of **22**. This is supported by several additional experiments: Irradiation of a 0.1 M THF solution of **22** produced a dark orange mixture in which **35** accumulated quickly, but **24** and **II** were produced in trace quantities (Figure 1.5.6). Strongly absorbing orange tars likely slowed photoreaction of **35**. Similar results were observed when the photolysis was carried out using a 312 nm light source, a wavelength at which **35** has minimal absorbance (Figure 1.5.8). The instability of **35** accounts for it not being observed in prior studies.[13]

GC/MS analysis of an optimized flow photolysis reaction showed substantial production of **II** (Scheme 1.5.5). **II** proved to be quite sensitive, but careful chromatography using dry, triethylamine-neutralized silica gel afforded small quantities of the compound (~85% purity by GC/MS). Its $^1$H NMR spectrum was similar to that obtained for 1,2-oxazepine **35**, but a downfield resonance was indicative of a vinyl ether, suggesting **II** to be 1,3-oxazepinophane **45** (Figure 1.3.5d). Precedent for this assignment was found in prior photolyses of pyridine *N*-oxides bearing one or more phenyl substituents, which were reported to afford the corresponding 1,3-oxazepins in high yields.[50] Photolysis of **45** did not lead to discernible products, only slow decomposition (Figure 1.5.9). This result was consistent with the reported photostability of 1,3-oxazepin-2,4-dicarbonitrile.[51] To our knowledge, **45** represents the first 1,3-oxazepinophane and indeed the

first 1,3-oxazepine to be isolated without the aid of aryl and cyano substitutions.[52] Unknown **III**, despite numerous attempts, has yet to be isolated. Merely concentrating crude solutions containing **III** resulted in its degradation.

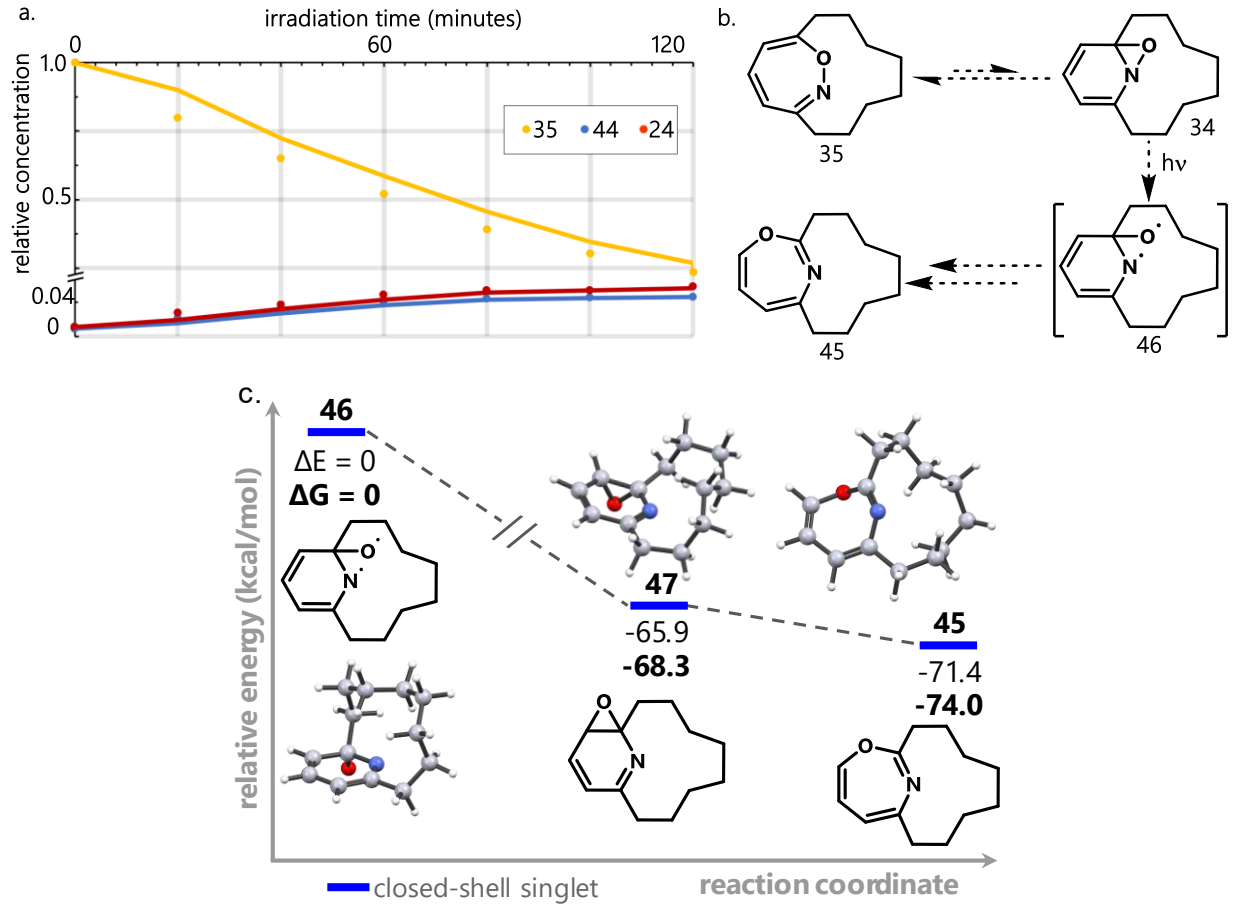


**Figure 1.3.6** a. Time dependent concentrations of major species observed during the photolysis (254 nm, 0.01 M THF, rt) of isolated **35**. b. a possible path to **45** during the photolysis of **35** c. If formed, calculations indicate aminyl diyl **46** could proceed readily to **45** by way of intermediate epoxypyridine **47**. See Figure 1.3.1 and SI for computational details.

Mechanistically, it is not clear how the excited state of **35** leads to **45** in addition to products **23**-**24**. One possibility is that a ground state equilibrium between **35** and its electrocyclized counterpart **34** (calculated to be ~1000:1 at 25˚C) is perturbed towards **34** in the excited state, such that N-O bond homolysis to afford aminyl diyl **46** (Figure 1.3.6a.) becomes

competitive with nitrene formation. If so, calculations predict cyclization to epoxypyridine **47** and subsequent electrocyclic ring-opening to **45** to be facile (Figure 1.3.6c).

In the photolysis of **35**, azirene **37** was isolated alongside **45**. Interestingly, **37** co-eluted with macrolactam **25** during silica gel chromatography, despite the two having significantly different $R_f$ values on TLC. A 2D-TLC experiment was performed, drying the plate between runs. In that case, the spot for **37** cleanly converted into the spot for **25**. GC/MS analyses of samples of **37** that had been adsorbed onto silica gel and allowed to stand at ambient atmosphere overnight also showed full conversion of **37** into **25** (Figure 1.3.7a.). Calculations depicted in Figure 1.3.7b indicate hydration of **37** and ring opening of the resulting hemiaminal **48** should be facile. We conclude that macrolactam **25** is not a primary photoproduct. It forms only through hydrolysis of residual azirine **37** during chromatographic purification of crude reaction mixtures.

When protected from hydrolysis, **37** was found to convert to fused bicyclic pyrrole **23** within minutes of exposure to 254 nm light (Figure 1.3.7d), confirming the prediction outlined in Figure 1.3.3. Continued irradiation resulted in near-complete degradation of **23** within an additional 45 minutes. Such photoinstability is perhaps why this molecule escaped Weber's careful analyses, as their irradiations were conducted over a period of hours. Additionally, we obtained a UV-Vis spectrum of **37** (Scheme 1.5.13). Although our calculations accurately predicted its absorbance maxima at 269 nm, they markedly overestimated absorbance at 235 nm (see SI for additional discussion). This likely contributed to ineffectual attempts at solution filtering described earlier.

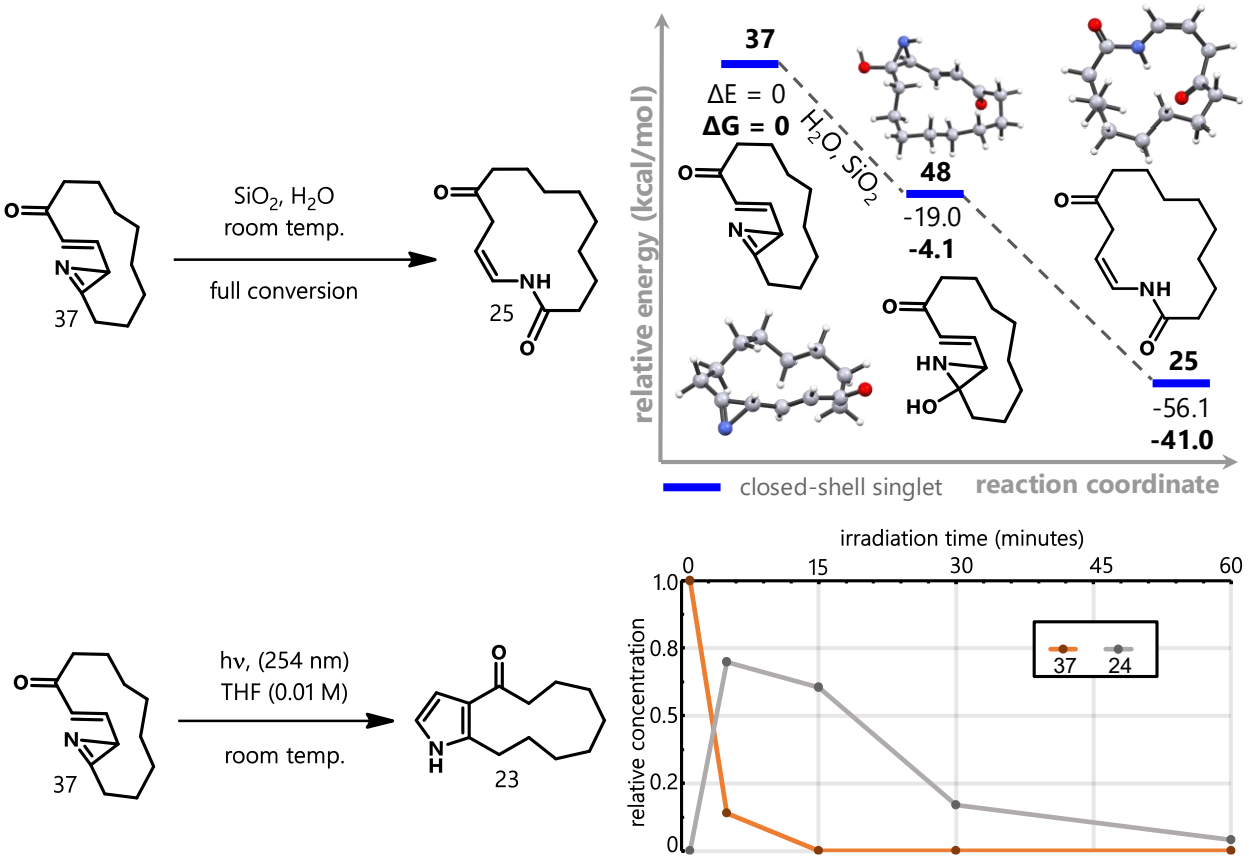


**Scheme 1.3.7** a. Azirene **37** hydrolyzes to lactam **25** during silica gel chromatography (see Figure 1.5.10) and b. computations indicate the process is energetically favorable. See Scheme 1.3.1 and SI for computational details. c. GC/MS analysis reveals that photolysis of **37** (254 nm, 0.01 M THF, rt) forms bicyclic pyrrole **23** and that **23** is unstable to the reaction conditions.

On a related note,[13] we did not detect formation of furanonitrile **7** (Table 1.1.1, n = 8) in any photolysis. This was consistent with Weber's findings, wherein furanonitriles (postulated to be derived from 1,3-oxazepine intermediates) were detected only in photorearrangement of the shortest and longest ansa bridge lengths examined (Table 1.1.1 2, n = 6, 4.2%; n = 7, 0.7%; n = 10, 3.1%). Lastly, we speculate reduction of **34** is the source of pyridinophane **21**. **21** is observed in all photoreactions of **22**. However, we have not yet identified the species that is concomitantly oxidized.[53]

The photorearrangement of [8]-2,6-pyridinophane *N*-oxide has been studied using a combination of experiments and calculations. Weber had originally isolated 0.6% yield of ketopyrrolophane **24** from the reaction. We modified the photoreaction solvent and temperature and adapted the reaction to a flow format to maximize pyrrolophane formation. The yield of product **24** increased 40-fold under those conditions, but previously undetected byproducts were formed. Density functional theory was used to calculate energies of putative oxaziridine, oxazepine, and nitrene intermediates consistent with early mechanistic studies of pyridine *N*-oxide photorearrangements. By carefully analyzing the time course of batch photoreactions using analytical GC/MS, we were able to show that ansa-bridged 1,2- and 1,3-oxazepins were isolable species that formed rapidly in the reaction. Control experiments established that both pyrrolophane **24** and bicyclic pyrrole **23** in our optimized photoreaction were actually derived from secondary photoexcitation of 1,2-oxazepine **35**. We speculate that the excited state of **35** diverges to either nitrene or walking-type rearrangement pathways leading to **24** and azirene **37** or 1,3-oxazepinophane **45**, respectively. We isolated trace amounts of macrocyclic vinyl azirene **37** first identified by Weber and showed it converted to **23** within minutes upon UV irradiation at room temperature. The data show that the formation of **24** is the result of two successive photoexcitations starting from **22**, wherein the second photoexcitation is the origin of competing pathways that result in multiple end products. This suggests that optimizing the photosynthesis of 1,2-oxazepine **35** may be the most the effective means to access **24** on scale, wherein a nonphotochemical method to rearrange **35** would be required.

## 1.4 Efforts Toward an Alternative Ketopyrrolophane Synthesis.

As shown in Figure 1.3.5, photoirradiation of **22** in 1:1 DME:$H_2O$ produces substantial quantities of 1,2-oxazepinophane **35** within the span of an hour. I optimized the reaction to consistently produce **35** in high yield and purity (Figure 1.4.1), as I sought to find an efficient, non-photochemical method to isomerize it to **24**. Isoxazoles have been reported to isomerize to azirines and pyrroles following treatment with low-valent transition metals,[54] and I hypothesized that **35** may react in a similar manner.

Initial experiments showed that while Rh and Ir complexes afforded no reactivity, $PtCl_2$ and $PtCl_4$ afforded minor amounts of azirine **37** by GC/MS. Although no **24** was produced, Weber had found that **37** could be efficiently converted to **24** by reflux in cyclohexane, so a method to prepare **37** could suffice. Expanding on this, I tested soluble group 10 complexes under the same conditions. $PtCl_2(PhCN)_2$ and $PdCl_2(PPh_3)_2$ gave low conversion and only trace **37**, and, though $NiCl_2(PPh_3)_2$ produced some **37**, its yield was inferior to $PtCl_2$. Returning to the initial hit, I found that increasing the $PtCl_2$ loading increased yield of **37**, and that $PtCl_4$ was also competent at promoting the rearrangement. At this point it was necessary to determine if the observed reactivity was the result of Brønsted acid contamination of the Lewis acidity of Pt, as the formation of a Pt(IV) nitrenoid is improbable due to reduced backbonding capacity of the electron-deficient metal. Treating **35** with 0.1 eq. of HCl resulted in rapid side-product formation, but 0.1 eq. $Zn(OTf)_2$ promoted rearrangement to the azirine and minor amounts of ketopyrrolophane **24** (Figure 1.4.2). Both products were isolated from these conditions and verified by GC/MS and NMR. Increasing $Zn(OTf)_2$ loading resulted in degradation and minimal product formation, as did performing the

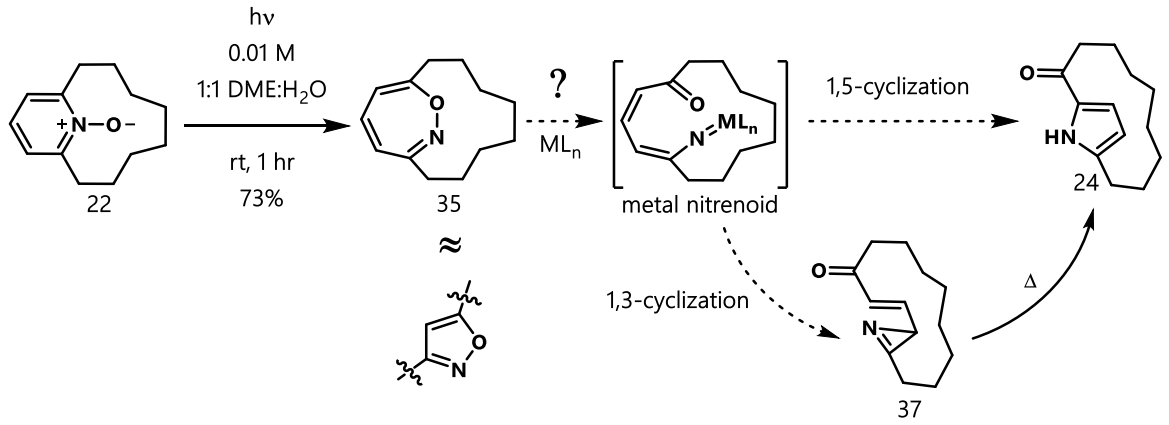


**Figure 1.4.1** A non-photochemical synthesis of **24** from **35** might proceed through a metal nitrenoid intermediate.

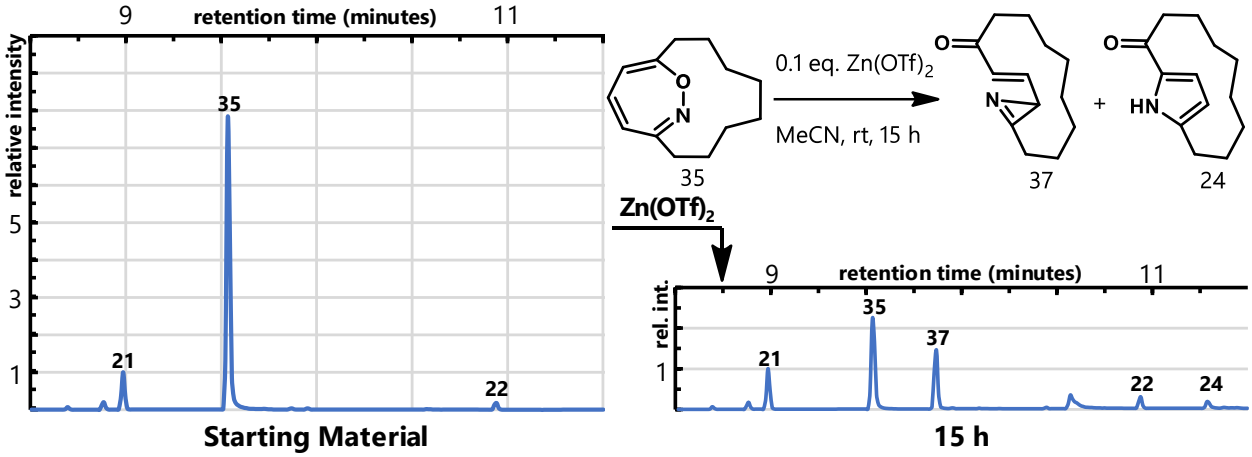


**Figure 1.4.2** $Zn(OTf)_2$ promotes rearrangement of **35** to both **37** and **24**.

reaction with water as a co-solvent. Other metal triflates, including Sc(III), In(III), La(III), and Yb(III) all caused decomposition. Performing the reaction with 0.1 eq. anhydrous $Cu(OTf)_2$ under argon resulted in no rearrangement. However, when the reaction was subsequently stirred under air, substantial conversion to **37** occurred. Future experiments will need to determine if oxygen or water in the air promote this reaction, and whether or not this same effect can be observed in with $Zn(OTf)_2$. Although there is not enough information to postulate a mechanism, it is unlikely

that Zn(II) is promoting nitrene formation. Instead, it is likely acting as a Lewis acid of generating trace quantities of Brønsted acid This sequence has the potential to produce substantial quantities of **24** when scaled-up and optimized.

| Entry | Additive | Eq. Additive | Solvent | Time (h) | Conversion | Yield of **37** |
|---|---|---|---|---|---|---|
| 1 | $[RhClcod]_2$ | 0.1 | PhMe | 20 | 19% | tr |
| 2 | $RuCl_2cod$ | 0.1 | PhMe | 20 | 29% | tr |
| 3 | $PtCl_2$ | 0.1 | PhMe | 20 | 72% | 5% |
| 4 | $PtCl_2(PhCN)_2$ | 0.1 | $CH_2Cl_2$ | 24 | tr | tr |
| 5 | $PdCl_2(PPh_3)_2$ | 0.1 | $CH_2Cl_2$ | 24 | 23% | tr |
| 6 | $NiCl_2(PPh_3)_2$ | 0.1 | $CH_2Cl_2$ | 20 | 58% | 3% |
| 7 | $PtCl_2$ | 0.2 | PhMe | 18 | 55% | 11% |
| 8 | $PtCl_2$ | 1.0 | PhMe | 21 | 80% | 16% |
| 9 | $PtCl_2$ | 1.0 | $CH_2Cl_2$ | 21 | 52% | 3% |
| 10 | $PtCl_4$ | 1.0 | PhMe | 2 | 100% | 36% |
| 11 | HCl | 0.1 | PhMe | 0.25 | 98% | 6% |
| 12 | $Zn(OTf)_2$ | 0.1 | MeCN | 22 | 96% | 92%[a] |
| 13 | $Zn(OTf)_2$ | 1.0 | MeCN | 17 | 100% | 4% |
| 14 | $Zn(OTf)_2$ | 0.1 | 1:1 DME:$H_2O$ | 17 | 100% | 2% |
| 15 | $Sc(OTf)_3$ | 0.1 | MeCN | 20 | 100% | tr |
| 16 | $In(OTf)_3$ | 0.1 | MeCN | 20 | 100% | tr |
| 17 | $La(OTf)_3$ | 0.1 | MeCN | 21 | 90% | tr |
| 18 | $Yb(OTf)_3$ | 0.1 | MeCN | 21 | 61% | tr |
| 19[b] | $Cu(OTf)_2$ | 0.1 | MeCN | 20 | 100% | 8% |

**Table 1.4.1** Conditions screened for rearrangement of **35**. All reactions were performed at 0.05 mmol scale (0.05 mM) under inert atmosphere unless otherwise noted. Chromatograms are available in the SI. [a]Percent conversion for entry 12 is approximate as the peak corresponding to **37** was atypically broad, potentially due to decomposition during analysis. [b]Experiment was conducted in two stages. 21 h under standard conditions, followed by 20 h under air. Yields given are after air exposure. See SI for details.

## 1.5 Supporting Information

*NMR spectra of published compounds are omitted for conciseness. They may be found in their corresponding publication.*

### 1.5.1 Supporting Information for Section 1.2

Unless otherwise specified, reactions were performed in flame-dried glassware under an atmosphere of argon. Reagents were purchased from commercial vendors and used as received unless otherwise stated. Tetrahydrofuran (THF), diethyl ether ($Et_2O$), acetonitrile ($CH_3CN$) and toluene (PhMe) were passed through a Glass Contour solvent drying system. Methanol (MeOH) was distilled from $Mg(OMe)_2$, which was generated by refluxing methanol over magnesium turnings until all the turnings had converted into a white precipitate. The distilled MeOH was stored in a flame-dried flask over activated 3Å molecular sieves under argon. Magnesium turnings were polished by sequential rinsing with aqueous 1M HCl, absolute ethanol, and $Et_2O$. The washed turnings were placed under vacuum for several hours then stored under an atmosphere of argon.

Yields refer to chromatographically and spectroscopically ($^1$H NMR) homogeneous materials, unless otherwise stated. Thin-layer chromatography (TLC) was conducted on precoated plates (Sorbent Technologies, silica gel 60 PF254, 0.25 mm) visualized with UV 254 nm. For acid-sensitive compounds, TLC plates were neutralized with TEA/Hexane (1%) before use. Column chromatography was performed on silica gel 60 (SiliCycle, 240−400 mesh). For acid-sensitive compounds, silica gel was premixed with TEA/Hexane (1%) before being loaded into the column. Purification of **15** and **33** was performed using an Agilent 1200 HPLC system equipped with G1361A preparative pumps, a G1314A autosampler, a G1314A VWD, a G1364B automated fraction

collector, and a Waters Sunfire C18 column (5 μm, 19 mm × 250 mm), unless otherwise noted. Analytical HPLC was performed using the same system, but with a G1312A binary pump. Mass spectra were recorded using an Agilent 6130 LC/MS system equipped with an ESI source. High resolution mass spectra were recorded using Thermo Fisher Scientific Exactive Plus with IonSense ID-CUBE DART source and Orbitrap analyzer. NMR spectra were recorded on Bruker Avance spectrometers (400/100 MHz and 500/125 MHz).

Batch photoreactions were carried out in either a standard Ace Glass immersion well photoreactor or an Ace Glass low temperature immersion well photoreactor using a Hanovia 450W mercury arc lamp. Photoreactions were also examined in a Rayonet photoreactor with a 254 and 300 nm bulb set using quartz test tubes. For setup of photoreaction in flow format, 1/16" ID x 1/8" OD x 1/32" Wall Versilon™ FEP Tubing was coiled around an Ace Glass 7858 triple-walled quartz immersion well in either one or three layers. The reaction solution was propelled by a peristaltic pump (Binaca model 1001) through the FEP tubing under irradiation by a Hanovia 450W mercury arc lamp.

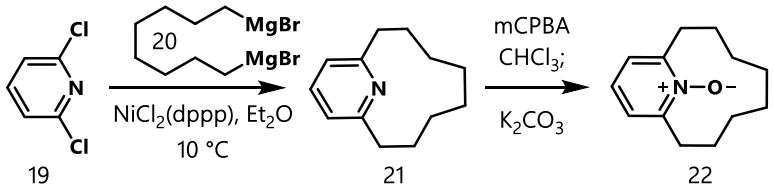


| Entry | Concentration (M) | Temperature (°C) | Grignard reagent addition time (h) | yield |
|---|---|---|---|---|
| 1 | 0.4 | 30 | 2 | 27% |
| 2 | 0.4 | 10 | 2 | 36% |
| 3 | 0.4 | -10 | 2 | 5% |
| 4 | 0.1 | 10 | 2 | 43% |
| 5 | 0.1 | 10 | 6 | 50% |

**Table 1.5.1**. Optimization for the synthesis of pyridinophane **22**.

[8]-(2,6)-pyridinophane (**21**)

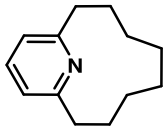


To a flame-dried 500 mL 3-neck round bottom flask, equipped with an addition funnel, condenser, and stir bar, were added polished magnesium tunings (4.86 g, 0.2 mol, 2.0 eq.) and a single iodine crystal in anhydrous $Et_2O$ (200 ml) under Ar. With vigorous stirring, from the addition funnel was added 1,8-dibromooctane (1 mL). The mixture was heated using a heat gun until the brown color dissipated. The remaining 1,8-dibromooctane (27.6 g in total, 0.1 mol, 1.0 eq.) was added dropwise into the flask at a rate such that the solution was maintained at a gentle reflux. After addition was complete, the addition funnel was rinsed with anhydrous diethyl ether (10 mL) into the reaction mixture. The resulting mixture was refluxed for another hour. (When stirring was

stopped, the mixture separated into two layers; the top a translucent light gray and the bottom a viscous, opaque gray).

During the reflux, to a separate flame-dried 2 L 3-necked round bottom flask equipped with a thermometer was added 2,6-dichloropyridine **19** (14.8 g, 0.1 mol, 1.0 eq.) and $NiCl_2$(dppp) (0.43 g, 0.75 mmol, 0.8 mol %) in anhydrous $Et_2O$ (1 L) under Ar. The mixture was cooled in an ice-water batch to 10 °C, followed by addition of the newly formed di-Grignard solution in $Et_2O$ via syringe pump over 6 h. During the addition, the reaction solution was kept at 10 °C with vigorous stirring. When TLC monitoring (5% EtOAc/Hexane) confirmed that **19** was fully consumed, the reaction mixture was carefully poured into ice water then filtered through celite. The organic layer was separated and the aqueous layer was extracted with EtOAc (100 mL X 3). The organic layers were combined, washed with brine, dried over $Na_2SO_4$, filtered, and concentrated to an orange oil. The resulting 23 g of crude product was dry-loaded onto silica gel (30 g) and purified by flash column chromatography (EtOAc in Hexane: 3%) to yield compound **21** (9.48 g, 50 mmol, 50%) as a colorless oil. $^1$H-NMR (400 MHz, $CDCl_3$) δ 7.46 (t, *J* = 7.6 Hz, 1H), 6.89 (d, *J* = 7.6 Hz, 2H), 2.84 (t, *J* = 6.38 Hz, 4H), 1.83 – 1.77 (m, 4H), 1.42 – 1.36 (m, 4H), 1.06 – 0.98 (m, 4H); $^{13}$C-NMR (100 MHz, $CDCl_3$) δ 160.6, 136.6, 120.0, 35.7, 26.3, 25.1, 23.2; HRMS (EI) calculated for $C_{13}H_{20}N$ $[M+H]^+$: 190.1590, found 190.1583.

[8]-(2,6)-pyridinophane *N*-oxide (**22**)

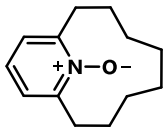

To a stirred solution of **21** (34.4 g, 182 mmol, 1.0 eq.) in $CHCl_3$ (182 mL) in a 3 L flask submerged in a room temperature water bath was added mCPBA (62.8 g, 75% purity, 273 mmol, 1.5 eq.) in several portions. After 30 min, the reaction turned too thick to stir and another 100 mL of $CHCl_3$ was added. The resulting mixture was then stirred at r.t. for 16 h, and then diluted with $CHCl_3$ (2 L), followed by addition of $K_2CO_3$. The resulting white slurry was stirred at r.t. for 2 h then mixed with celite (200 g) and filtered through a layer of celite. The filter cake was rinsed with $CHCl_3$ until no product could be detected by TLC. The filtrate was then concentrated and purified by flash column chromatography (EtOAc in Hexane:10%-40%) to yield compound **22** (30.6 g, 149 mmol, 82%) as pale yellow crystalline solid, and recovered compound **21** (2.64 g, 14 mmol, 8%). $^1$H-NMR (400 MHz, $CDCl_3$) δ 7.46 (t, *J* = 7.6 Hz, 1H), 6.89 (d, *J* = 7.6 Hz, 2H), 2.84 (t, *J* = 6.38 Hz, 4H), 1.82 – 1.76 (m, 4H), 1.42 – 1.36 (m, 4H), 1.04 – 0.98 (m, 4H); $^{13}$C-NMR (100 MHz, $CDCl_3$) δ 160.6, 136.6, 120.0, 35.7, 26.3, 25.1, 23.2; HRMS (EI) calculated for $C_{13}H_{20}NO$ $[M + H]^+$: 206.1539, found 206.1534.

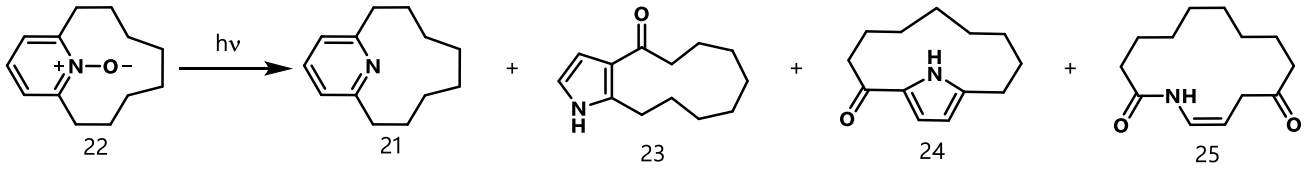


| .Entry | Solvent | Temp (°C) | % Yield | | | |
|---|---|---|---|---|---|---|
| | | | **21** | **23** | **24** | **25** |
| 1 | *c*-hexane | r.t. | 17 | 3 | 3 | 4 |
| 2 | DME | r.t. | 12 | 6 | 4 | 10 |
| 3 | EtOH | r.t. | 7 | 3 | 6 | 7 |
| 4 | MeCN | r.t. | 8 | 4 | 5 | 7 |
| 5 | THF | r.t. | 11 | 9 | 7 | 14 |
| 6 | THF | -40 | 19 | 5 | 18 | 12 |
| 7 | THF | -78 | 10 | 2 | 19 | 10 |
| 8 | DME | -30 | 14 | 5 | 10 | 15 |
| 9[a] | water | r.t. | nd | nd | 4 | nd |
| 10[b] | EtOH | r.t. | nd | nd | 7 | nd |
| 11[c] | THF | r.t. | nd | nd | trace | nd |
| 12[d] | THF | -75 | 9 | 3 | 19 | 17 |
| **13[e]** | **THF** | **-75** | **15** | **5** | **25** | **18** |

**Table 1.5.2**. Optimization of the photo-induced rearrangement. [a] 10 eq. $CuSO_4$ were added. [b] The $Cu(NO_3)_2$ bis-adduct of **22** was used. [c] $Rh_2TFA_4$ was added, complete decomposition of **22** was observed. [d] Experiment performed in flow format (residence time = 2 min) with one layer of FEP tubing around the immersion well. [e] Experiment performed in flow format with three layers of FEP tubing around the immersion well (residence time = 5 min). nd = not determined.

Batch Irradiation Conditions (Table S2, entry 6):

A 1 L immersion well photoreactor was charged with a solution of **22** (3.9 g, 19.18 mmol) in THF (1 L, 0.02M). The solution was cooled to -40 °C and then irradiated with a 450 W Hanovia Mercury Arc lamp for 3h with stirring. The mixture was monitored by $^{1}$H-NMR spectrum analysis of aliquots. The lamp was removed and the mixture was warmed to room temperature and concentrated. The residue was then purified by flash column chromatography (EtOAc in Hexane: 10% - 20% - 22% - 30% - 40%).

Flow Irradiation Conditions (Table S2, entry 13):

A quartz immersion well wrapped with 3 layers of FEP tubing was placed in a dewar and cooled to -75 °C with isopropanol and dry ice. The solution of **22** (6.32 g, 30.8 mmol) in anhydrous THF (0.01 M) was pumped through the FEP tubing with a residence time of 5 minutes. The resulting light-yellow solution was concentrated, purified by flash column chromatography (EtOAc in Hexane: 10% - 20% - 22% - 30% - 40%). This resulted in **23** (292 mg, 1.42 mmol, 5%), **24** (1.56 g, 7.6 mmol, 25%), **25** (1.185 g, 5.3 mmol, 18%) and **21** (866 mg, 4.6 mmol, 15%).

5,6,7,8,9,10,11,12-octahydrocycloundeca[*b*]pyrrol-4(1*H*)-one (**23**)

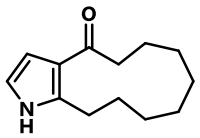

White solid. M.P.: 154 °C. $^{1}$H-NMR (500 MHz, $CDCl_3$) δ 8.14 (s, 1H), 6.63 (t, *J* = 2.7 Hz, 1H), 6.44 (t, *J* = 2.9 Hz, 1H), 3.09 (t, *J* = 6.35 Hz, 1H), 2.68 (t, *J* = 6.35 Hz, 1H), 1.75 (p, *J* = 6.2 Hz, 2H), 1.64 – 1.58 (m, 2H), 1.37 (p, *J* = 6.1 Hz, 2H), 1.23 (tt, *J* = 8.9, 4.6 Hz, 2H), 1.12 (ddt, *J* = 10.3, 7.7, 4.6 Hz, 2H), 1.09 – 1.01 (m, 2H); $^{13}$C-NMR (126 MHz, $CDCl_3$) δ 202.3, 136.9, 124.3, 116.6, 110.1, 41.7, 28.1, 27.8, 25.4, 25.1, 24.6, 24.5, 22.8; HRMS (EI) calculated for $C_{13}H_{20}NO$ $[M + H]^+$: 206.1545, found 206.1532.

1*[1]H*-1(2,5)-pyrrolacyclodecaphan-2-one (**24**)

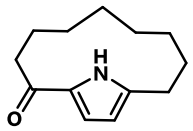

white solid. M.P.: 198 °C. $^{1}$H-NMR (500 MHz, $CDCl_3$) δ 8.73 (s, 1H), 6.98 (t, *J* = 3.2 Hz, 1H), 6.09 (t, *J* = 3.2 Hz, 1H), 2.78 – 2.73 (m, 2H), 2.68 (t, *J* = 6.3 Hz, 2H), 1.79 (m, 4H), 1.60 – 1.49 (m, 2H), 1.37 (p, *J* = 6.0 Hz, 2H), 1.21 (p, *J* = 6.9 Hz, 2H), 1.08 (ddt, *J* = 12.3, 8.9, 5.4 Hz, 2H); $^{13}$C-NMR (125 MHz, $CDCl_3$): 190.3, 137.9, 132.3, 115.9, 111.5, 36.1, 27.0, 26.7, 26.2, 23.5, 23.4, 23.3, 21.7; HRMS (EI) calculated for $C_{13}H_{20}NO$ $[M + H]^+$: 206.1545, found 206.1533.

(*Z*)-azacyclotetradec-13-ene-2,11-dione (**25**)

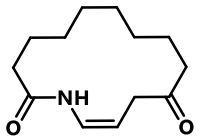


White solid. M.P.: 119 °C. $^{1}$H-NMR (500 MHz, $CDCl_3$) δ 7.63 (d, *J* = 10.1 Hz, 1H), 6.90 (ddt, *J* = 10.4, 9.0, 1.3 Hz, 1H), 4.80 (q, *J* = 7.7 Hz, 1H), 3.15 (dd, *J* = 7.7, 1.2 Hz, 2H), 2.45 (t, *J* = 6.7 Hz, 2H), 2.36 – 2.33 (m, 2H), 1.69 – 1.61 (m, 4H), 1.35 (tt, *J* = 7.1, 3.0 Hz, 4H), 1.27 (q, *J* = 7.3 Hz, 2H), 1.17 (dq, *J* = 8.4, 6.5 Hz, 2H); $^{13}$C-NMR (126 MHz, $CDCl_3$) δ 210.7, 170.9, 125.4, 101.0, 41.9, 40.7, 36.0, 26.8, 26.0, 25.3, 25.3, 24.3, 23.3; HRMS (EI) calculated for $C_{13}H_{21}NO_2$ $[M + H]^+$: 224.1651, found 224.1637.

**Figure 1.5.1.** Setup of flow chemistry for photolysis.

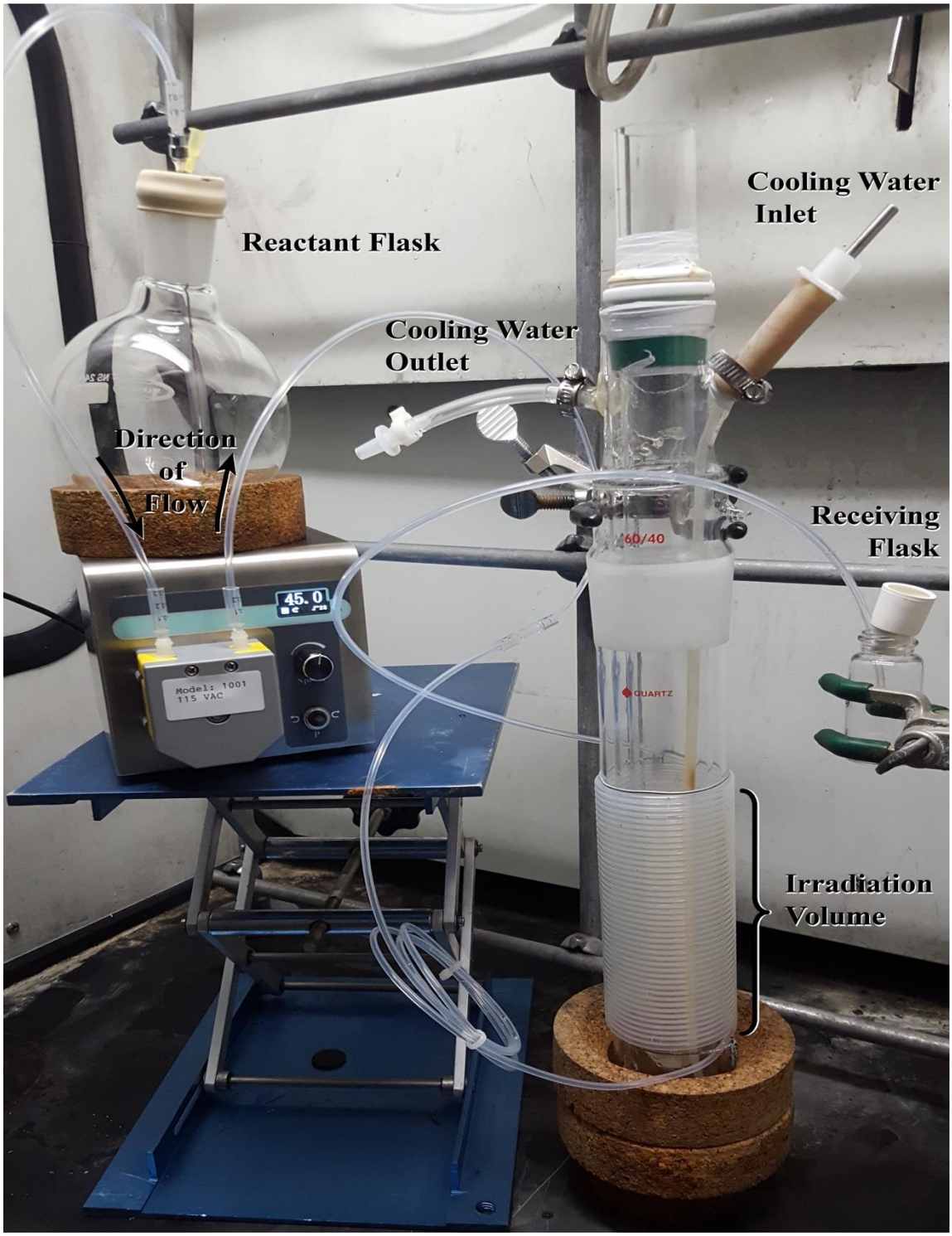

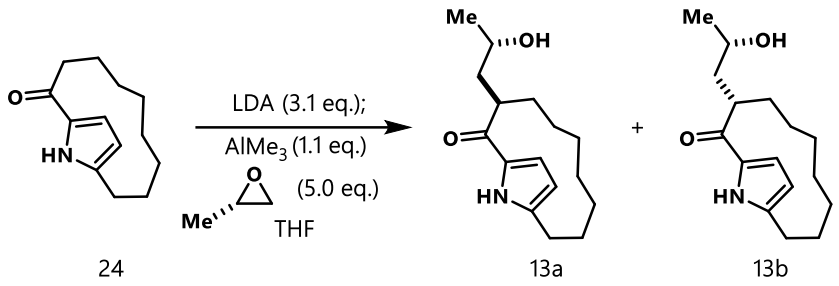


24 13a 13b

To a flame-dried 3-neck 100 mL round bottom flask, equipped with a low-temperature thermometer and a stir bar, was added anhydrous THF (10 mL) and *i*$Pr_2NH$ (0.9 mL, 6.2 mmol, 3.2 eq.) at r.t., and then cooled to -78 °C with an acetone-dry ice bath, followed by addition of n-BuLi (2.5 M in hexane, 2.5 mL, 6.2 mmol, 3.1 eq.). After addition, the resulting colorless solution was stirred for 10 min at -78 °C, then warmed up to 0 °C in ice-water bath. The solution of **24** (410 mg, 2 mmol, 1.0 eq.) in anhydrous THF (30 mL) was added into the formed LDA solution via syringe pump over 3 h while maintaining the LDA solution at 0 °C. The resulting light-yellow solution was stirred for another 30 min at 0 °C, then cooled to -78 °C with an acetone-dry ice bath. (*S*)-Propylene oxide (0.7 mL, 10 mmol, 5.0 eq.) was added, followed by $AlMe_3$ solution (2.0 M in hexane, 1.1 mL, 2.2 mmol, 1.1 eq.). The reaction mixture was stirred at -78 °C for another 30 min, and then slowly warmed up to r.t. over 1 h, then allowed to stir at r.t. overnight. TLC monitoring showed products were the major spots. To quench the reaction, the mixture was carefully added into a stirred solution of potassium sodium tartrate and ice, then extracted with EtOAc (50 mL x 3). The organic layers were combined, washed with brine, dried over $Na_2SO_4$, filtered, concentrated, and purified by flash column chromatography using TEA neutralized silica gel (EtOAc in Hexane: 25% - 30% - 35% - 40%). The mixture of **13a** and **13b** (374 mg, 4.95 mmol, 71%, d.r. = 2:1) was obtained as a light-yellow semisolid. **24** (60 mg, 15%) was also recovered. Two

isomers **13a** and **13b** could be separated via flash column chromatography on TEA-neutralized silica gel (EtOAc in Hexane: 30% - 35%)

(*R*)-3-((*S*)-2-hydroxypropyl)-11*H*-1(2,5)-pyrrolacyclodecaphan-2-one (**13a**)

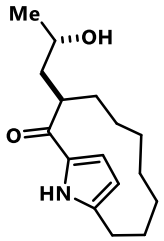


$^{1}$H-NMR (500 MHz, $C_6D_6$) δ 9.14 (s, 1H), 7.25 (t, *J* = 3.0 Hz, 1H), 5.94 (t, *J* = 3.0 Hz, 1H), 3.81 – 3.79 (m, 1H), 3.47 – 3.43 (m, 1H), 2.45 – 2.40 (m, 1H), 2.38 – 2.35 (m, 1H), 2.23 – 2.16 (m, 1H), 1.77 – 1.75 (m, 1H), 1.65 – 1.60 (m, 1H), 1.51 – 1.49 (m, 1H), 1.40-1.03 (m, 7H), 1.00 (d, *J* = 6.2 Hz, 3H), 0.98 – 0.75 (m, 4H); $^{13}$C-NMR (125 MHz, $C_6D_6$) δ 192.0, 137.9, 134.3, 115.9, 111.6, 66.4, 42.1, 41.1, 35.7, 27.2, 26.9, 24.9, 24.4, 24.1, 24.0, 22.3; HRMS (EI) calculated for $C_{16}H_{25}NO_2$ $[M]^+$: 263.1885, found: 263.1844

(*S*)-3-((*S*)-2-hydroxypropyl)-11*H*-1(2,5)-pyrrolacyclodecaphan-2-one (**13b**)

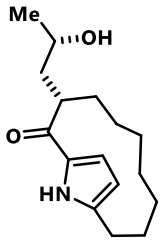


$^{1}$H-NMR (500 MHz, $C_6D_6$) δ 9.23 (s, 1H), 7,22 (dd, *J* = 2.7, 3.7 Hz, 1H), 5.94 (t, *J* = 2.7 Hz, 1H), 3.70 – 3.80 (m, 1H), 3.25 – 3.32 (m,1H), 2.49 (td, *J* = 3.9, 15.5 Hz, 1H), 2.15 – 2.32 (m, 3H), 1.63 – 1.72 (m, 1H), 1.50 – 1.61 (m, 2H), 1.40 – 1.11 (m, 5H), 1.09 (d, *J* = 6.2 Hz, 3H), 0.99 – 0.80 (m, 5H); $^{13}$C-NMR (125 MHz, $C_6D_6$) δ 193.0, 138.1, 133.8, 116.2, 111.6, 67.0, 41.52, 41.50, 35.2, 27.2, 27.0, 24.5, 24.3, 24.1, 24.0, 22.5; HRMS (EI) calculated for $C_{16}H_{25}NO_2$ $[M]^+$: 263.1885, found: 263.1838

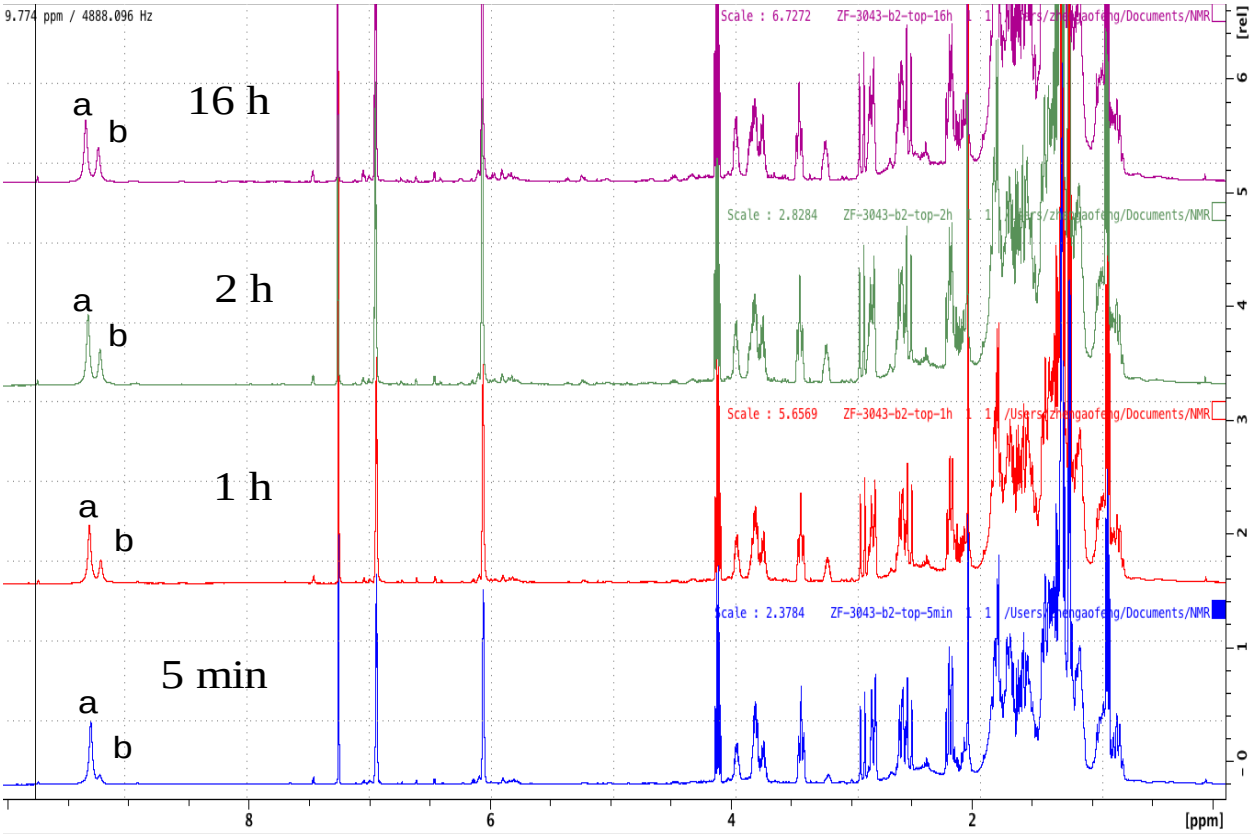


**Figure 1.5.2.** Equilibrium of compound **13** isomers in wet $CDCl_3$**.**

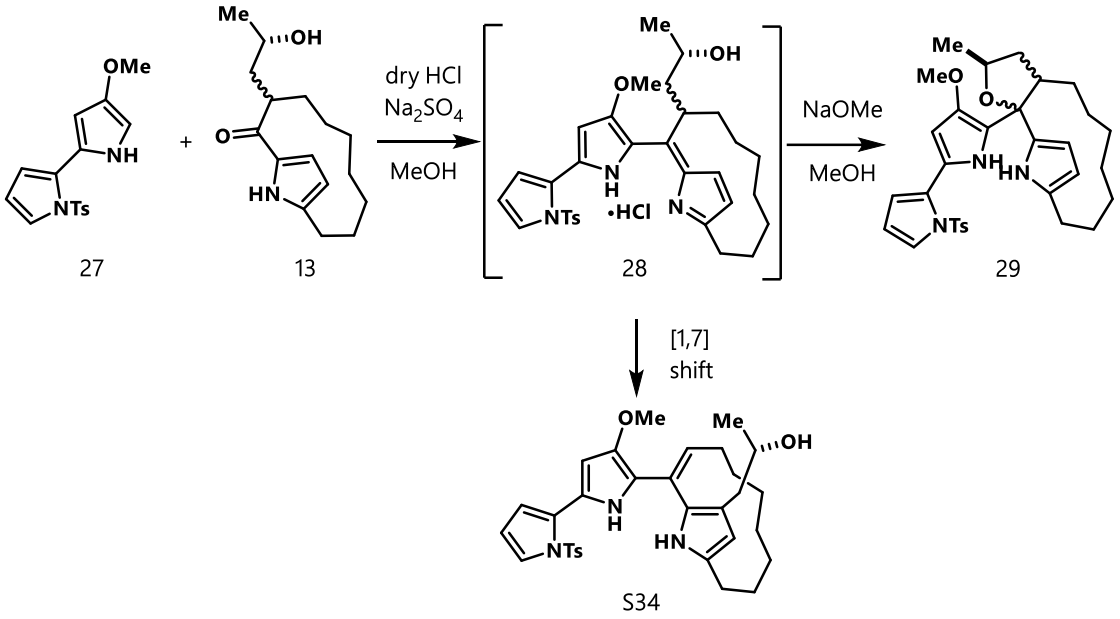


To the mixture of **13a** and **13b** (683 mg, 2.6 mmol, 1.0 eq.) in toluene (26 mL, 0.1 M) and $Na_2SO_4$ (2.6 g) at 0 °C was added HCl (3.9 mL, 1M in MeOH, 1.5 eq), followed by addition of bipyrrole **27** (0.82 g, 2.60 mmol, 1.0 eq) in toluene (20 mL) via syringe pump over 30 min. After addition, the resulting dark red solution was immediately quenched by dropwise addition into a solution of freshly prepared NaOMe (1M in MeOH, 10 mL, 3.85 eq) at 0 °C. The resulting orange solution was added dropwise into ice-water, then extracted with EtOAc (20 mL X 3). The organic layers were combined, washed with brine, dried over $Na_2SO_4$, filtered, and concentrated. The resulting crude product was immediately purified via flash column chromatography on TEA-neutralized silica gel (EtOAc in Hexane: 5%). Concentration resulted in compound **29** as a tan foam containing minor spectroscopic impurities due to oxygen contact. (1.27 g, 87% yield, 1:1 d.r.). These impurities do not affect subsequent reactions performed with this material, but an analytically pure, colorless sample may be isolated via subsequent chromatography, albeit with substantial material loss. The mixture of compounds **29** (unstable when concentrated) was stored

in toluene (0.1M) as a stock solution at -20 °C for later use. If the dark red solution of **28** was left at r.t. for 1h before quenching, it resulted in compound **29** (889 mg, 61% yield, 1:1 dr) as light yellow oil, and compound **S34** (320 mg, 22% yield) as an orange oil.

(25*S*)-22-(4-methoxy-1'-tosyl-1*H*,1'*H*-[2,2'-bipyrrol]-5-yl)-25-methyl-22,23,24,25-tetrahydro-11*H*-1(2,5)-pyrrola-2(2,3)-furanacyclononaphane (**29**)

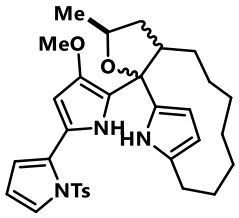


Spectra of this compound are of a colorless sample obtained via the aforementioned secondary purification. $^{1}$H-NMR (500 MHz, $CDCl_3$) δ 8.96 (s, 1H), 8.84 (s, 1H), 8.76 (s, 1H), 8.69 (s, 1H), 7.39 – 7.36 (m, 2H), 7.26 (d, *J* = 3.0 Hz, 2H), 7.25 (d, *J* = 3.0 Hz, 2H), 6.92 (d, *J* = 8.0 Hz, 2H), 6.83 (d, *J* = 8.0 Hz, 2H), 6.23 (t, *J* = 3.3 Hz, 2H), 6.18 (ddd, *J* = 3.3, 1.8, 9.1Hz, 2H), 6.01 (dq, *J* = 3.1, 2.8Hz, 2H), 6.01 (dd, *J* = 3.2, 7.4 Hz, 2H), 5.82 (dt, *J* = 14.8, 2.8 Hz, 2H), 4.45 – 4.38 (m, 1H), 4.20 – 4.14 (m, 1H), 3.83 (s, 3H), 3.8o (s, 3H), 2.87 (q, *J* = 7.5 Hz, 1H), 2.76 (t, *J* = 6.1 Hz, 1H), 2.72-2.51 (m, 4H), 2.28 (s, 3H), 2.24 (s, 3H), 2.22 – 2.16 (m, 1H), 1.88 – 1.83 (m, 1H), 1.79 – 1.72 (m, 1H), 1.69 – 1.58 (m, 2H), 1.57 – 1.42 (m, 6H), 1.39 (d, *J* = 6.2 Hz, 3H), 1.35 (d, *J* = 6.2 Hz, 3H), 1.32 – 0.84 (m, 15H), 0.82 – 0.75 (m, 1H), 0.74 – 0.65 (m, 1H); $^{13}$C-NMR (125 MHz, $CDCl_3$) δ 144.7, 144.6, 141.6, 139.7, 134.7, 134.5, 133.4, 132.2, 131.3 130.9, 129.5, 129.4, 127.60, 127.56, 127.52, 127.4, 123.3, 123.11, 123.08, 121.6, 115.3, 114.9, 114.5, 114.1, 111.3, 111.1, 106.2, 105.3, 105.0, 104.9, 100.0, 99.9, 85.2, 84.5, 75.5, 73.7, 58.82, 58.80, 48.1, 48.0, 42.1, 41.0, 31.6, 31.5, 29.5, 28.2, 27.8, 27.3, 26.8, 26.7, 25.8, 25.5,

25.4, 23.8, 22.7, 21.6, 21.5, 21.3, 14.2, 14.1; HRMS (ESI) calculated for $C_{32}H_{40}N_3O_4S$ [M + H]$^+$: 562.2734, found: 562.2703.

(*S*,*E*)-1-(2-(4-methoxy-1'-tosyl-1*H*,1'*H*-[2,2'-bipyrrol]-5-yl)-11*H*-1(2,5)-pyrrolacyclodecaphan-2-en-13-yl)propan-2-ol (**S34**)

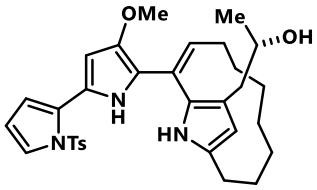


$^1$H-NMR (500 MHz, d6-acetone) δ 9.30 (s, 1H), 9.11 (s, 1H), 7.38 (d, *J* = 8.4 Hz, 2H), 7.32 (dd, *J* = 3.2, 1.9 Hz, 1H), 7.30 (d, *J* = 8.4 Hz, 2H), 6.47 (t, *J* = 8.4 Hz, 1H), 6,26 (m, 2H), 6.08 (s, 1H), 5.79 (d, *J* = 2.8 Hz, 1H), 3.89 (q, *J* = 6.4 Hz, 1H), 3.75 (s, 3H), 2.64 (m, 2H), 2.44 (d, *J* = 7.3 Hz, 1H), 2.42 (d, *J* = 5.9 Hz, 1H), 2.36 (s, 3H), 1.92 (m, 2H), 1.60 (m, 2H), 1.53-1.13 (m, 7H), 1.11 (d, *J* = 6.2 Hz, 3H), 0.61 (m, 1H), 0.54 (m, 1H); $^{13}$C-NMR (125 MHz, d6-acetone) δ 146.1, 146.0, 136.2, 132.9, 130.7, 129.8, 129.2, 129.2, 127.9, 127.4, 127.4, 124.2, 123.9, 119.4, 118.5, 118.3, 117.3, 117.2, 115.2, 112.9, 106.3, 99.9, 99.8, 68.6, 58.1, 37.4, 30.1, 29.0, 28.5, 28.4, 27.7, 27.4, 26.3, 23.6, 21.5; HRMS (ESI) calculated for $C_{32}H_{40}N_3O_4S$ [M + H]$^+$: 562.2734, found: 562.2692.

**Procedure for 'acidic' $MnO_2$ preparation:**

To a solution of $MnSO_4 \cdot H_2O$ (8.45 g, 50 mmol, 5.0 eq.) in DI water (50 mL) cooled in an ice-water bath, a solution of $KMnO_4$ (1.58 g, 10 mmol, 1.0 eq) in DI water (50 mL) was added at a rate such that the reaction was maintained between 5-10 °C. After addition, the mixture was stirred for 1 h (pH ~ 2), then left standing for 12 h. The resulting mixture was filtered, and the filter cake was washed with DI water (100 mL x 3) and acetone (50 mL x 3). The resulting brown powder was stripped with benzene (50 mL x 3) on a rotavapor in a 25 °C water bath, then placed on a high-vac line for 3h, and stored under an atmosphere of Ar.

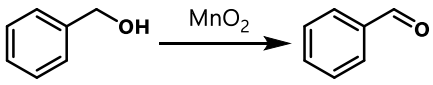


| Eq. of $MnO_2$ | Yield of benzaldehyde | |
|---|---|---|
| | commercial $MnO_2$ | freshly prepared 'acidic' $MnO_2$ |
| 4 | 22 | 0.8 |
| 8 | 39 | 2 |
| 12 | 67 | 2.7 |
| 16 | 71 | 4 |
| 20 | 75 | 5.6 |

**Table 1.5.3**. Relative rates of benzylic oxidation mediated by $MnO_2$ forms.

**General procedure for oxidation of benzyl alcohol with $MnO_2$:**

To a vial with $MnO_2$ solid and a stir bar, was added the solution of benzyl alcohol in $CHCl_3$ (0.1 M, 2 mL). The mixture was stirred at r.t. for 1 h, and then filtered through celite, concentrated on rotavapor (vacuum: 140 mbar) until dry. The yield was determined by $^1$H-NMR using 3,5-dibromobenzadehyde (0.1 mmol) as internal standard.

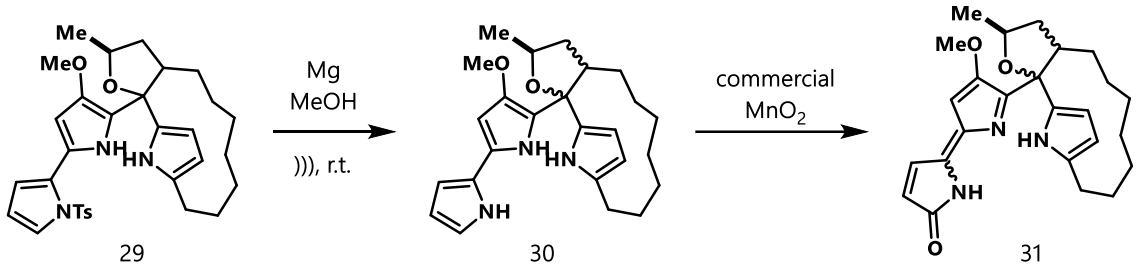


29 30 31

Preparation of **31**:

A dram vial was charged with a toluene stock solution of compound **29** (30 mg, 0.0535 mmol, 1.0 eq.), which was then concentrated and stripped with toluene (1 mL x 2). The resultant oil was then mixed with polished Mg (6.6 mg, 0.275 mmol, 5.0 eq.) under Ar and diluted with MeOH (0.6 mL). The resulting mixture was sonicated at r.t. for 20 min, at which point TLC showed complete conversion. The clear orange solution was transferred into a new vial under Ar and the reaction vial was rinsed with toluene (1 mL) while leaving the unreacted Mg behind. The orange solution was concentrated on a rotavapor to dryness and backfilled with Ar. This process was repeated twice with toluene (1 mL x 2) (after each addition of toluene, the heterogeneous mixture was sonicated to minimize bumping). The residue was taken up in toluene, mixed with celite and filtered through a celite plug into a flame-dried vial under Ar. The plug was rinsed with toluene until the filtrate turned colorless. This provided a solution of **30** in toluene in quantitative yield.

The solution of **30** was added dropwise over 15 min into a vigorously stirred slurry of commercial $MnO_2$ (314 mg, 50 eq) in acetone (1 ml). After addition, the mixture was combined with celite and filtered through a celite plug. The resulting orange solution was concentrated and immediately purified by flash column chromatography (EtOAc/Hexane: 30-40%) to afford compound **31** (11.9 mg, 52% yield) as a mixture of four diastereomers.

4'-methoxy-5'-((25S)-25-methyl-22,23,24,25-tetrahydro-11H-1(2,5)-pyrrola-2(2,3)-furanacyclononaphane-22-yl)-[2,2'-bipyrrolylidene]-5(1H)-one (**31**)

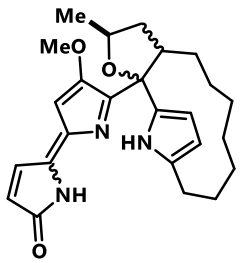


$^1$H-NMR (500 MHz, d6-acetone) δ 10.15 (s, 1H), 10.01 (s, 1H), 9.62 (s, 2H), 8.00 (t, *J* = 5.7 Hz, 2H), 7.81 (d, *J* = 5.6 Hz, 2H), 7.77 (d, *J* = 5.6 Hz, 2H), 7.24 – 7.10 (m, 6H), 6.69 (s, 1H), 6.63 (s,1H), 6.60 (s,1H), 6.57 (s,1H), 6.39 (dd, *J* = 5.7, 9.6 Hz, 2H), 6.36 (d, *J* = 5.7 Hz, 1H), 6.32 (d, *J* = 5.7 Hz, 1H), 5.91 (t, *J* = 2.6 Hz, 1H), 5.88 (t, *J* = 2.7 Hz, 1H), 5.74 – 5.72 (m, 2H), 5.68 – 5.66 (m, 2H), 5.61 (t, *J* = 2.6 Hz, 1H), 5.58 (t, *J* = 2.7 Hz, 1H), 4.42 – 4.38 (m, 2H), 4.27 – 4.25 (m, 1H), 4.20 – 4.16 (m, 1H), 3.81 (s, 3H), 3.80 (s, 3H), 3.74 (s, 3H), 3.72 (s, 3H), 3.28 – 3.24 (m, 2H), 3.05 – 2.95 (m, 2H), 2.70 – 2.57 (m, 8H), 2.55 (t, *J* = 2.2 Hz, 6H). The rest of peaks are not countable due to complexity. HRMS (EI) calculated for $C_{25}H_{31}N_3O_3$ $[M + H]^+$: 422.2438, found: 422.2430.

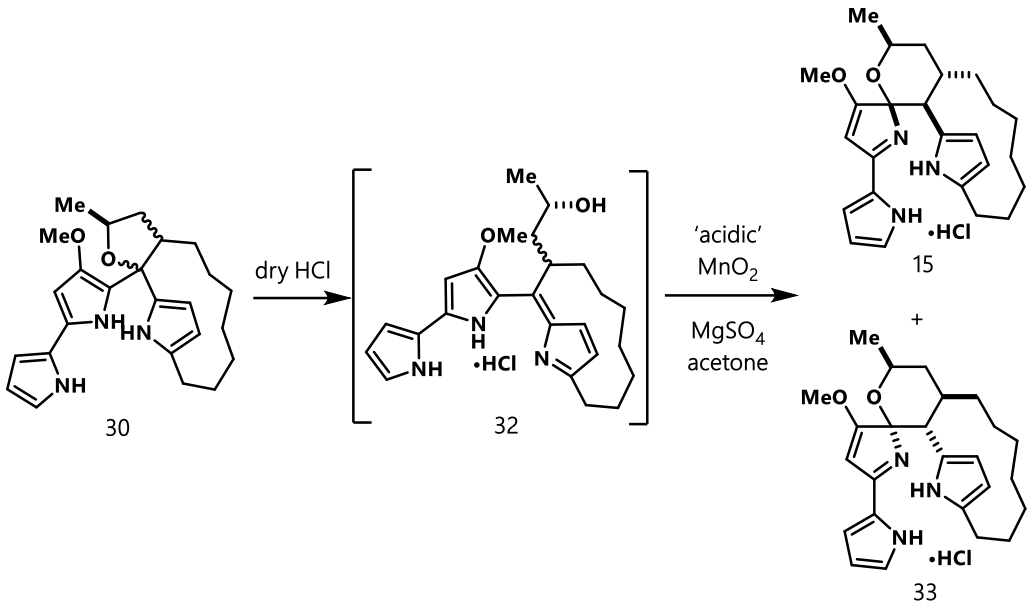


Preparation of **15** and **33**:

A solution of **30** was prepared following the procedure outlined in the preparation of **31**. It was then concentrated to a volume of ~2 mL, then cooled in an ice-water bath for 5 min. Dry HCl solution (0.16 mL, 1M in MeOH, 3.0 eq.) was added and the yellow solution turned dark purple-red immediately. This solution was carefully concentrated without heating on a rotavapor until the pressure reached 20 mbar to remove any MeOH and excess HCl. The vial was placed back into an ice-water bath under Ar and the remaining toluene solution of **32** was diluted with dry acetone to a total volume of 4 mL.

Into each of a set of 4 flame dried dram vials was placed the 'acidic' $MnO_2$ reagent (68 mg, 0.784 mmol) and $MgSO_4$ (30 mg) under argon. To each vial was added dry acetone (0.5 mL). Under vigorous stirring, 1 mL of the dark red solution was added into each vial via syringe pump over 5 min. After addition, the mixture was filtered through a celite plug and rinsed with acetone until the filtrate turned colorless. The yellow filtrate was concentrated, diluted with $CH_3CN$, and purified

by HPLC ($CH_3CN$/water, 0.1% formic acid, Sunfire C18 column, 40-47%, 2-8 min, 20 mL/min). **15** (1.2 mg, 6% yield) and **33** (1.2 mg, 6% yield) were collected.

(2*R*,3'*S*,4'*S*,6'*S*)-3-methoxy-6'-methyl-5-(1*H*-pyrrol-2-yl)spiro[pyrrole-2,2'-1(2,5)-pyrrola-2(3,4)-pyranacyclononaphan]-1-ium chloride (**15**)

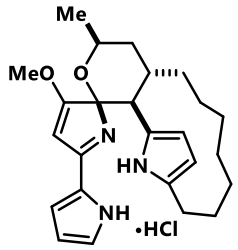


$^1$H-NMR (500 MHz, d6-acetone) δ 13.78 (s, 1H), 12.63 (s, 1H), 10.56 (s, 1H), 7.69 (s, 1H), 7.40 (s, 1H), 6.48 (s, 1H) 6.21 (s, 1H), 5.66 (s, 1H), 5.46 (s, 1H), 4.46 – 4.42 (m, 1H), 4.11 (s, 3H), 2.93 (d, *J* = 12.6 Hz, 1H), 2.85 – 2.80 (m, 1H), 2.45 (d, *J* = 14.2 Hz, 1H), 2.25 (d, *J* = 13.1 Hz, 1H), 1.92 (d, *J* = 11.8 Hz, 1H), 1.73 – 1.61 (m, 4H), 1.47 – 1.25 (m, 12H), 1.08 – 0.73 (m, 7H), 0.60 – 0.50 (m ,1H); $^{13}$C-NMR (125 MHz, d6-acetone) δ 181.5, 165.5, 134.4, 133.9, 126.7, 125.0, 121.8, 114.3, 110.4, 105.5, 97.0, 93.7, 77.2, 71.9, 60.9, 60.5, 47.2, 38.4, 28.9, 28.7, 26.1, 25.5, 25.4, 25.3, 21.5; HRMS (EI) calculated for $C_{25}H_{34}N_3O_2$ $[M + H]^+$: 408.2646, found: 408.2632.

(2*S*,3'*R*,4'*R*,6'*S*)-3-methoxy-6'-methyl-5-(1*H*-pyrrol-2-yl)spiro[pyrrole-2,2'-1(2,5)-pyrrola-2(3,4)-pyranacyclononaphan]-1-ium chloride (**33**)

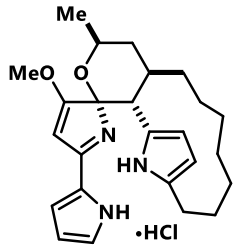


M.P.: 197-198 °C. $^{1}$H-NMR (500 MHz, $CDCl_3$) δ 13.35 (s, 1H), 12.92 (s, 1H), 9.82 (s, 1H), 7.50 – 7.45 (m, 1H), 7.08 – 7.03 (m, 1H), 6.41 (dq, *J* = 2.1, 2.1 Hz, 1H), 5.71 (t, *J* = 2.8 Hz, 1H), 5.57 – 5.54 (m, 2H), 4.26 – 4.18 (m ,1H), 4.05 (s, 3H), 2.93 (d, *J* = 12.6 Hz, 1H), 2.88 – 2.80 (m, 1H), 2.54 (td, *J* = 4.2, 14.6 Hz, 1H), 2.28 (dq, *J* = 5.0, 15.0 Hz, 1H), 2.28 (dq, *J* = 1.8, 13.5 Hz, 1H), 2.09 – 1.98 (m, 2H), 1.92 – 1.82 (m, 1H), 1.54 – 1.48 (m, 1H), 1.47 – 1.39 (m, 1H), 1.26 (d, *J* = 2.1 Hz, 3H), 1.22 (d, *J* = 13.3 Hz, 1H),1.17 – 1.11 (m, 1H), 1.04 – 0.98 (m, 2H), 0.89 – 0.83 (m, 2H), 0.82 – 0.73 (m, 1H), 0.48 – 0.38 (m, 1H); $^{13}$C-NMR (125 MHz, $CDCl_3$) δ 179.4, 164.2, 134.8, 133.4, 125.6, 124.2, 120.9, 113.7, 109.6, 104.4, 97.5, 92.7, 72.7, 60.1, 46.0, 40.5, 33.4, 28.2, 25.0, 24.8, 24.6, 24.5, 21.8; HRMS (EI) calculated for $C_{25}H_{34}N_3O_2$ $[M + H]^+$: 408.2646, found: 408.2618.

(2*R*,3*S*,3'*S*,4'*S*,6'*S*)-3-methoxy-6'-methyl-5-(1*H*-pyrrol-2-yl)-3,4-dihydrospiro[pyrrole-2,2'-1(2,5)-pyrrola-2(3,4)-pyranacyclononaphane], marineosin A (**17**)

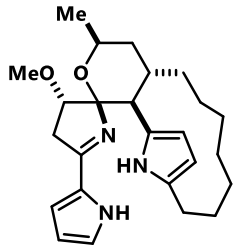


Compound **15** (7.2 mg, 0.0177 mmol) and $Pd/BaSO_4$ (10.2 mg) in EtOAc (1 mL) was stirred vigorously (1500 rpm) under a hydrogen atmosphere (1 atm.) for 16 h. LCMS showed reaction was complete. The mixture was filtered through celite and rinsed with EtOAc. The filtrate was concentrated to afford 6.8 mg crude product, and then purified by PTLC (EtOAc in Hexane, 20%). Pure marineosin A (2.2 mg, 30% yield) was obtained as a colorless oil. $[\alpha]_D$ = +138.7 (c = 0.02, MeOH), lit. –101.7° (c = 0.06, MeOH).[1] $^1$H-NMR (500 MHz, d6-acetone) δ 10.96 (s, 1H), 8.23 (s, 1H), 6.98 (s, 1H), 6.38 (s, 1H), 6.12 (s, 1H), 5.69 (s, 1H), 5.45 (s, 1H), 4.28 – 4.20 (m, 1H), 3.90 – 3.82 (m, 1H), 3.42 (s, 3H), 2.95 – 2.92 (m, 1H), 2.90 – 2.86 (m, 1H), 2.40 – 2.29 (m, 1H), 2.27 – 2.20 (m, 2H), 1.94 – 1.84 (m, 1H), 1.79 (d, *J* = 12.4 Hz, 1H), 1.70 – 1.58 (m, 2H), 1.53 (d, J = 6.6 Hz, 3H), 1.41 – 1.25 (m, 6H), 1.24 – 1.14 (m, 1H), 1.08 – 0.99 (m, 1H), 0.93 – 0.83 (m, 2H), 0.76 – 0.65 (m, 1H), 0.57 – 0.47 (m, 1H); $^{13}$C-NMR (125 MHz, d6-acetone) δ 164.4, 129.9, 129.2, 122.5, 113.5, 110.0, 106.1, 104.7, 90.0, 70.4, 58.5, 45.9, 39.6, 39.1, 32.0, 28.6, 28.1, 25.7, 25.6, 25.5, 22.8; HRMS (EI) calculated for $C_{25}H_{36}N_3O_2$ $[M + H]^+$: 410.2802, found: 410.2791.

The enantiomer of marineosin A was prepared using exactly the same procedures and reagents as marineosin A's, except using (*R*)-propylene oxide for the alkylation.

**Spectral data comparison between natural and synthetic material**

**Table 1.5.4.** Comparison of Marineosin A NMR data in Acetone-D6.

| $^{1}$H-NMR (Natural) | $^{1}$H-NMR (Synthetic) | $^{13}$C-NMR (Natural) | $^{13}$C-NMR (Synthetic) |
|---|---|---|---|
| 10.93 (br s, 1H) | 10.96 (br s, 1H) | 164.4 | 164.4 |
| 8.23 (br s, 1H) | 8.23 (br s, 1H) | 129.9 | 129.9 |
| 6.97 (dd, *J* = 2.5, 1.5 Hz, 1H) | 6.98 (s, 1H) | 129.1 | 129.2 |
| 6.37 (dd, *J* = 2.5, 1.5 Hz, 1H) | 6.38 (s, 1H) | 122.5 | 122.5 |
| 6.11 (dd, *J* = 3.5, 2.5 Hz, 1H) | 6.12 (s, 1H) | 113.5 | 113.5 |
| 5.68 (d, *J* = 3.0 Hz, 1H) | 5.69 (s, 1H) | 110.1 | 110.0 |
| 5.44 (d, *J* = 3.0 Hz, 1H) | 5.45 (s, 1H) | 106.1 | 106.1 |
| 4.23 (m, 1H) | 4.28 – 4.20 (m, 1H) | 104.7 | 104.7 |
| 3.85 (t, *J* = 8.5 Hz, 1H) | 3.90 – 3.82 (m, 1H) | 89.9 | 89.9 |
| 3.40 (s, 3H) | 3.42 (s, 3H) | 70.4 | 70.4 |
| 2.91 (d, *J* = 12.0 Hz, 1H) | 2.95 – 2.92 (m, 1H) | 58.5 | 58.5 |
| 2.88 (dd, *J* = 16.0, 8.5 Hz, 1H) | 2.90 – 2.86 (m, 1H) | 45.9 | 45.9 |
| 2.32 (m, 1H) | 2.40 – 2.29 (m, 1H) | 39.6 | 39.6 |
| 2.23 (m, 2H) | 2.27 – 2.20 (m, 2H) | 39.0 | 39.1 |
| 1.88 (dd, *J* = 16.0, 8.5 Hz, 1H) | 1.94 – 1.84 (m, 1H) | 32.0 | 32.0 |
| 1.77 (m, 1H) | 1.79 (d, *J* = 12.4 Hz, 1H) | 28.6 | 28.6 |
| 1.64 (m, 1H) | 1.70-1.58 (m, 3H) | 28.0 | 28.1 |
| 1.61 (td, *J* = 12.0, 6.5 Hz, 1H) | | 25.7 | 25.7 |
| 1.52 (m, 1H) | | 25.5 | 25.6 |
| 1.51 (d, *J* = 6.5 Hz, 3H) | 1.53 (d, *J* = 6.6 Hz, 3H) | 25.4 | 25.5 |
| 1.37 (m, 1H) | 1.41-1.25 (m, 4H) | 22.8 | 22.8 |
| 1.35 (m, 1H) | | | |
| 1.34 (m, 1H) | | | |
| 1.28 (m, 1H) | | | |
| 1.18 (m, 1H) | 1.24 – 1.14 (m, 1H) | | |
| 1.02 (m, 1H) | 1.08 – 0.99 (m, 1H) | | |
| 0.88 (m, 2H) | 0.93 – 0.83 (m, 2H) | | |
| 0.69 (m, 1H) | 0.76 – 0.65 (m, 1H) | | |
| 0.52 (m, 1H) | 0.57 – 0.47 (m, 1H) | | |

**Crystal Structure Analysis**

Crystals suitable for X-ray analysis were grown by slow diffusion of the samples in EtOAc into Hexane at room temperature. The diffraction data were measured 100K(2) on a Bruker Smart Apex2 CCD-based X-ray diffractometer system equipped with a Mo-Kα radiation (λ = 0.71073 Å). The frames were integrated with the Bruker Saint software package using a narrow-frame integration algorithm. The structure was solved and refined using the Bruker SHELXTL Software Package. All atoms were refined anisotropically, and hydrogen atoms were removed for clarity.

**ORTEP of 23 (50% probability ellipsoids)**

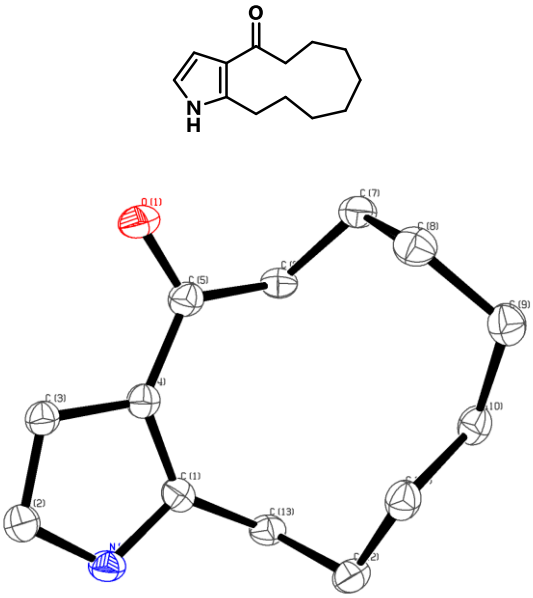

Crystal data and structure refinement for Compound **23**.

| | |
|---|---|
| Identification code | cu_har1703s_a |
| Empirical formula | C13 H19 N O |
| Formula weight | 205.29 |

| | | |
|---|---|---|
| Temperature | 100(2) K | |
| Wavelength | 1.54178 Å | |
| Crystal system | Monoclinic | |
| Space group | $P2_1/n$ | |
| Unit cell dimensions | a = 9.4220(3) Å | a= 90°. |
| | b = 9.3471(3) Å | b= 99.966(2)°. |
| | c = 12.8767(5) Å | g = 90°. |
| Volume | 1116.92(7) $Å^3$ | |
| Z | 4 | |
| Density (calculated) | 1.221 $Mg/m^3$ | |
| Absorption coefficient | 0.594 $mm^{-1}$ | |
| F(000) | 448 | |
| Crystal size | .4 x .3 x .1 $mm^3$ | |
| Theta range for data collection | 5.397 to 69.880°. | |
| Index ranges | -11<=h<=11, -11<=k<=11, -15<=l<=12 | |
| Reflections collected | 8386 | |
| Independent reflections | 2062 [R(int) = 0.0213] | |

| | |
|---|---|
| Completeness to theta = 67.679° | 99.2 % |
| Absorption correction | Semi-empirical from equivalents |
| Max. and min. transmission | 0.75 and 0.68 |
| Refinement method | Full-matrix least-squares on $F^2$ |
| Data / restraints / parameters | 2062 / 0 / 145 |
| Goodness-of-fit on $F^2$ | 1.098 |
| Final R indices [I>2sigma(I)] | R1 = 0.0389, wR2 = 0.0921 |
| R indices (all data) | R1 = 0.0420, wR2 = 0.0934 |
| Extinction coefficient | n/a |
| Largest diff. peak and hole | 0.330 and -0.198 e.$Å^{-3}$ |

**ORTEP of 24 (50% probability ellipsoids)**

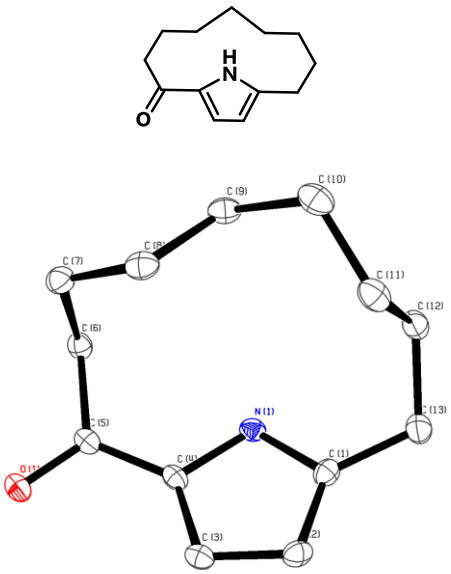


Crystal data and structure refinement for Compound **24**.

| | | |
|---|---|---|
| Identification code | cu_har1702s_a | |
| Empirical formula | C13 H19 N O | |
| Formula weight | 205.29 | |
| Temperature | 0(2) K | |
| Wavelength | 1.54178 Å | |
| Crystal system | Monoclinic | |
| Space group | $P2_1/n$ | |
| Unit cell dimensions | a = 7.7866(3) Å | a= 90°. |
| | b = 15.2172(7) Å | b= 112.279(3)°. |
| | c = 10.1883(5) Å | g = 90°. |

| | |
|---|---|
| Volume | 1117.09(9) $Å^3$ |
| Z | 4 |
| Density (calculated) | 1.221 $Mg/m^3$ |
| Absorption coefficient | 0.594 $mm^{-1}$ |
| F(000) | 448 |
| Crystal size | ? x ? x ? $mm^3$ |
| Theta range for data collection | 5.520 to 69.358°. |
| Index ranges | -8<=h<=9, -18<=k<=15, -11<=l<=11 |
| Reflections collected | 8118 |
| Independent reflections | 2005 [R(int) = 0.0742] |
| Completeness to theta = 67.679° | 98.0 % |
| Refinement method | Full-matrix least-squares on $F^2$ |
| Data / restraints / parameters | 2005 / 0 / 145 |
| Goodness-of-fit on $F^2$ | 0.958 |
| Final R indices [I>2sigma(I)] | R1 = 0.0400, wR2 = 0.0984 |
| R indices (all data) | R1 = 0.0492, wR2 = 0.1006 |
| Extinction coefficient | n/a |

| | |
|---|---|
| Largest diff. peak and hole | 0.218 and -0.229 e.Å$^{-3}$ |

**ORTEP of 25 (50% probability ellipsoids)**

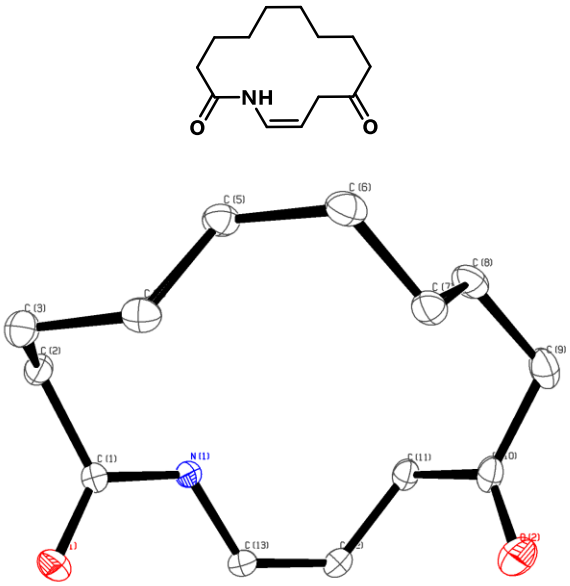


Crystal data and structure refinement for Compound **25**.

| | |
|---|---|
| Identification code | mo_har1704s_a |
| Empirical formula | C13 H21 N O2 |
| Formula weight | 223.31 |
| Temperature | 100(2) K |
| Wavelength | 0.71073 Å |
| Crystal system | Monoclinic |
| Space group | $P2_1/n$ |

| | | |
|---|---|---|
| Unit cell dimensions | a = 9.7653(9) Å | a= 90°. |
| | b = 9.7181(9) Å | b= 98.8330(10)°. |
| | c = 13.3075(12) Å | g = 90°. |
| Volume | 1247.9(2) $Å^3$ | |
| Z | 4 | |
| Density (calculated) | 1.189 $Mg/m^3$ | |
| Absorption coefficient | 0.079 $mm^{-1}$ | |
| F(000) | 488 | |
| Crystal size | 0.400 x 0.300 x 0.200 $mm^3$ | |
| Theta range for data collection | 2.419 to 30.916°. | |
| Index ranges | -13<=h<=13, -13<=k<=13, -18<=l<=19 | |
| Reflections collected | 18951 | |
| Independent reflections | 3718 [R(int) = 0.0224] | |
| Completeness to theta = 25.242° | 100.0 % | |
| Absorption correction | Semi-empirical from equivalents | |
| Max. and min. transmission | 0.75 and 0.70 | |
| Refinement method | Full-matrix least-squares on $F^2$ | |

| | |
|---|---|
| Data / restraints / parameters | 3718 / 0 / 145 |
| Goodness-of-fit on $F^2$ | 1.072 |
| Final R indices [I>2sigma(I)] | R1 = 0.0433, wR2 = 0.1111 |
| R indices (all data) | R1 = 0.0454, wR2 = 0.1133 |
| Extinction coefficient | n/a |
| Largest diff. peak and hole | 0.360 and -0.341 e.$Å^{-3}$ |

**ORTEP of $Cu(NO_3)_2$•[22]$_2$ (50% probability ellipsoids)**

Preparation: To a solution of $Cu(NO_3)_2$ (0.464g, 1.99 mmol) in EtOH (20 mL) at r.t., compound **22** was added. The reaction was then stirred for 40 min. The reaction was then diluted with EtOH and heated until all solids dissolved. The reaction was then allowed to cool to r.t. and then stored in -20 °C for 4-5 hours. The mother liquor was decanted and the green crystals were dried under vacuum.

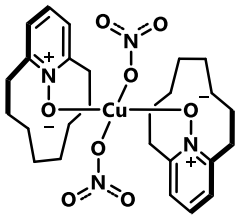

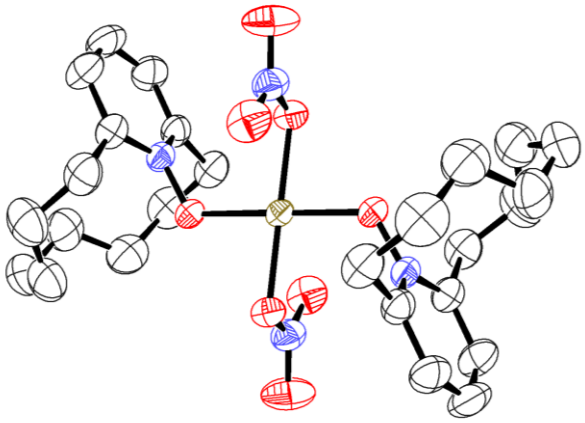

Crystal data and structure refinement for **$Cu(NO_3)_2$•$[22]_2$**.

| | | |
|---|---|---|
| Identification code | $Cu(NO_3)_2$•$[22]_2$ | |
| Empirical formula | C26 H38 Cu N4 O8 | |
| Formula weight | 598.14 | |
| Temperature | 298(2) K | |
| Wavelength | 0.71073 Å | |
| Crystal system | Monoclinic | |
| Space group | $P2_1/c$ | |
| Unit cell dimensions | a = 10.6090(9) Å | a= 90°. |
| | b = 7.8790(6) Å | b= 97.679(2)°. |
| | c = 17.4437(14) Å | g = 90°. |
| Volume | 1445.0(2) $Å^3$ | |

| | |
|---|---|
| Z | 2 |
| Density (calculated) | 1.375 $Mg/m^3$ |
| Absorption coefficient | 0.808 $mm^{-1}$ |
| F(000) | 630 |
| Crystal size | 0.1 x 0.1 x 0.04 $mm^3$ |
| Theta range for data collection | 1.937 to 30.490°. |
| Index ranges | -14<=h<=14, -11<=k<=11, -24<=l<=24 |
| Reflections collected | 23281 |
| Independent reflections | 4275 [R(int) = 0.0311] |
| Completeness to theta = 25.242° | 100.0 % |
| Absorption correction | Semi-empirical from equivalents |
| Max. and min. transmission | 0.74 and 0.67 |
| Refinement method | Full-matrix least-squares on $F^2$ |
| Data / restraints / parameters | 4275 / 0 / 178 |
| Goodness-of-fit on $F^2$ | 1.013 |
| Final R indices [I>2sigma(I)] | R1 = 0.0371, wR2 = 0.0994 |
| R indices (all data) | R1 = 0.0663, wR2 = 0.1119 |

| | |
|---|---|
| Extinction coefficient | n/a |
| Largest diff. peak and hole | 0.647 and -0.316 e.Å$^{-3}$ |

**ORTEP of 33 (50% probability ellipsoids)**

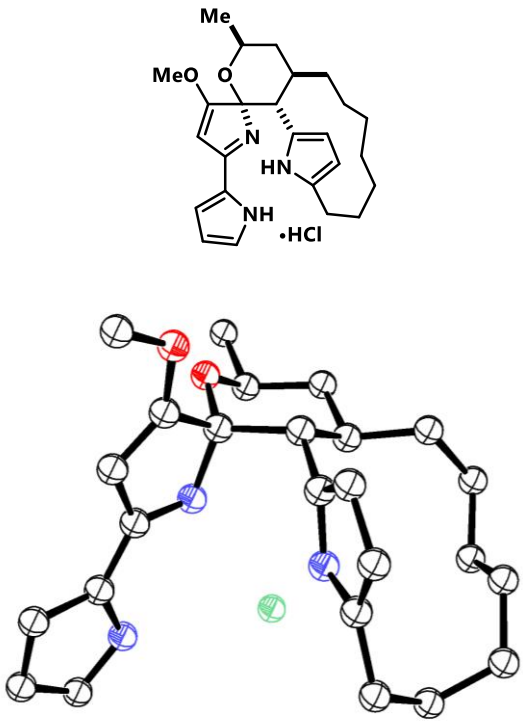


Crystal data and structure refinement for **33**.

| | |
|---|---|
| Identification code | compound **33** |
| Empirical formula | C25 H34 Cl N3 O2 |
| Formula weight | 444.02 |
| Temperature | 100(2) K |
| Wavelength | 1.54178 Å |

| | | |
|---|---|---|
| Crystal system | Monoclinic | |
| Space group | C2 | |
| Unit cell dimensions | a = 33.1593(15) Å | a= 90°. |
| | b = 8.7821(4) Å | b= 129.718(2)°. |
| | c = 23.3882(10) Å | g = 90°. |
| Volume | 5238.9(4) $Å^3$ | |
| Z | 4 | |
| Density (calculated) | 1.180 $Mg/m^3$ | |
| Absorption coefficient | 1.493 $mm^{-1}$ | |
| F(000) | 2004 | |
| Crystal size | 0.4 x 0.1 x 0.1 $mm^3$ | |
| Theta range for data collection | 2.456 to 69.424°. | |
| Index ranges | -37<=h<=39, -10<=k<=9, -28<=l<=28 | |
| Reflections collected | 38002 | |
| Independent reflections | 9489 [R(int) = 0.0573] | |
| Completeness to theta = 67.679° | 98.6 % | |
| Absorption correction | Semi-empirical from equivalents | |

| | |
|---|---|
| Max. and min. transmission | 0.75 and 0.63 |
| Refinement method | Full-matrix least-squares on $F^2$ |
| Data / restraints / parameters | 9489 / 55 / 609 |
| Goodness-of-fit on $F^2$ | 1.048 |
| Final R indices [I>2sigma(I)] | R1 = 0.0460, wR2 = 0.1163 |
| R indices (all data) | R1 = 0.0541, wR2 = 0.1198 |
| Absolute structure parameter | 0.015(8) |
| Extinction coefficient | n/a |
| Largest diff. peak and hole | 0.470 and -0.357 e.$Å^{-3}$ |

## 1.5.2 Supporting Information for Section 1.3

### General Methods

Reagents were purchased from commercial vendors and used as received unless otherwise stated. Tetrahydrofuran (THF) and 1,2-dimethoxy ethane (DME) were passed through a Glass Contour solvent drying system.

Thin-layer chromatography (TLC) was conducted on pre-coated plates (Sorbent Technologies, silica gel 60 PF254, 0.25 mm) and visualized with UV 254 nm. For acid-sensitive compounds, TLC plates were neutralized with TEA/Hexane (1%) before use. Column chromatography was performed on silica gel 60 (SiliCycle, 240−400 mesh). For acid-sensitive compounds, silica gel was premixed with TEA/Hexane (1%) before being loaded into the column. NMR spectra were recorded on Bruker Avance spectrometers ($^{1}$H: 400 $^{13}$C: 100 MHz and $^{1}$H: 600 MHz). Chemical shifts are reported in ppm and referenced to residual internal $CHCl_3$ for $^{1}$H (δ 7.26) and $^{13}$C (δ 77.2) spectra. Deuterated chloroform used in NMR experiments was neutralized prior to sample dissolution via passage through a plug of neutral alumina. UV-Vis spectra were obtained using a Shimadzu UV3101PC UV-Vis-NIR Scanning Spectrophotometer unless otherwise noted. GC/MS analyses were run on an Agilent 7250 Q-TOF GC/MS using an Agilent 19091S-433 HP-5MS capillary column.

Flow photoreactions were carried out using 1/16" ID x 1/8" OD x 1/32" Wall Versilon™ FEP Tubing coiled around an Ace Glass 7858 triple-walled quartz immersion well in either one or three layers. The reaction solution was propelled by a peristaltic pump (Binaca model 1001) through the FEP tubing under irradiation by a Hanovia 450W mercury arc lamp. Time course experiments were

conducted inside of a Rayonet Reactor (Southern New England Ultraviolet Co.) utilizing a 254 nm bulb set unless otherwise stated.

**Experimental Details**

Compound **22** was prepared as outlined in our 2019 publication.[52]

(*Z*)-14-oxa-15-azabicyclo[8.3.2]pentadeca-1(13),10(15),11-triene (**35**)

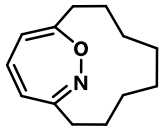


To a 20 ml quartz test tube containing a stir bar was added 21 mg (0.1 mmol) [8]-2,6-pyridinophane *N*-oxide **22**. 5 ml DME then 5 ml water were added and the tube capped with a septum and pierced with a needle. The solution was degassed in a bath sonicator for 5 minutes, after which the tube was suspended in a Rayonet photoreactor equipped with a stir plate and irradiated at 254 nm for 60 minutes. The resulting light-yellow solution was washed with water and the aqueous fraction extracted with EtOAc. The organic layer was dried with $Na_2SO_4$ and concentrated under reduced pressure. 0.5 ml hexanes were added to the residue resulting in precipitation of compounds **24** and **23**. The hexanes were carefully pipetted away and concentrated to afford 12 mg of a light-yellow oil containing ~75% **35** (GC/MS) with **21** as the major contaminant. $^1$H-NMR (600 MHz, $CDCl_3$): δ 5.76 (d, *J*= 4.9 Hz, 1H), 5.58 (d, *J*= 5.5 Hz, 1H), δ 5.55 (t, *J*= 5.2 Hz, 1H), 2.40 (dd, *J*= 6.1, 6.5 Hz, 2H), 2.34 (dd, *J*= 6.0, 6.2 Hz, 2H), 1.76 (m, 2H), 1.55

(m, 2H), 1.45 (m, 4H), 1.34 (m, 4H). $^{13}$C-NMR (100 MHz, $CDCl_3$): δ 160.5, 154.2, 138.1, 116.7, 113.4, 35.2, 34.0, 25.9, 25.0, 24.9, 24.8, 23.9, 22.6. UV-VIS: (0.07 mM THF) $\lambda_{max1}$ = 234 nm, $\lambda_{max2}$ = 288 nm.

(Z)-11-oxa-15-azabicyclo[8.4.1]pentadeca-1(14),10(15),12-triene (**45**)

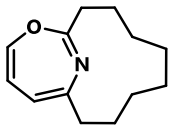


A quartz immersion well enclosing a medium pressure mercury arc lamp and wrapped with FEP tubing was placed in a dewar and cooled to -75 °C with isopropanol and dry ice. The lamp was turned on and allowed to warm up for 15 minutes. A peristaltic pump was then used to drive a solution of **22** (4.1 g, 20 mmol) in anhydrous THF (0.01 M) through the FEP tubing at a rate corresponding to a residence time of 2 minutes. The resulting light yellow solution was concentrated and purified by flash column chromatography using neutralized silica gel (EtOAc in Hexane: 10%) to afford 5 mg of a clear oil containing ~85% **45**. $^{1}$H-NMR (400 MHz, $CDCl_3$): δ 6.58 (d, *J*= 8.0 Hz, 1H), 5.68 (dd, *J*= 8.0, 6.0 Hz, 1H), δ 5.46 (dd, *J*= 5.9, 0.8 Hz, 1H), 2.52 (t, *J*= 6.3 Hz, 2H), 2.31 (t, *J*= 6.2 Hz, 2H), 1.67 (m, 2H), 1.49 (m, 4H), 1.41 (s, 6H). $^{13}$C-NMR (100 MHz, $CDCl_3$): δ 155.5, 154.1, 138.0, 118.4, 112.1, 33.5, 33.4, 24.4, 24.3, 23.3, 22.4, 21.6, 21.4. UV-VIS: (0.07 mM THF) $\lambda_{max1}$ = 238 nm, $\lambda_{max2}$ = 304 nm.

(E)-14-azabicyclo[11.1.0]tetradeca-2,13-dien-4-one (**37**)

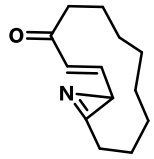


A low temperature flow photolysis was performed using the conditions outlined for preparation of **25**. The concentrated crude product was purified by column chromatography using oven-dried and neutralized silica gel. **6** eluted at 15% EtOAc in Hexanes, giving 12 mg of a light yellow oil. The product's NMR spectra matched those reported by Weber.[2] UV-VIS: (0.01 mM THF) $\lambda_{max1}$ = 238 nm, $\lambda_{max2}$ = 269 nm.

Flow photolysis was carried out using a flow reactor setup as depicted in Figures 1.5.3 and 1.5.4.

**Figure 1.5.3** Flow Reactor Setup. Arrows indicate direction of flow.

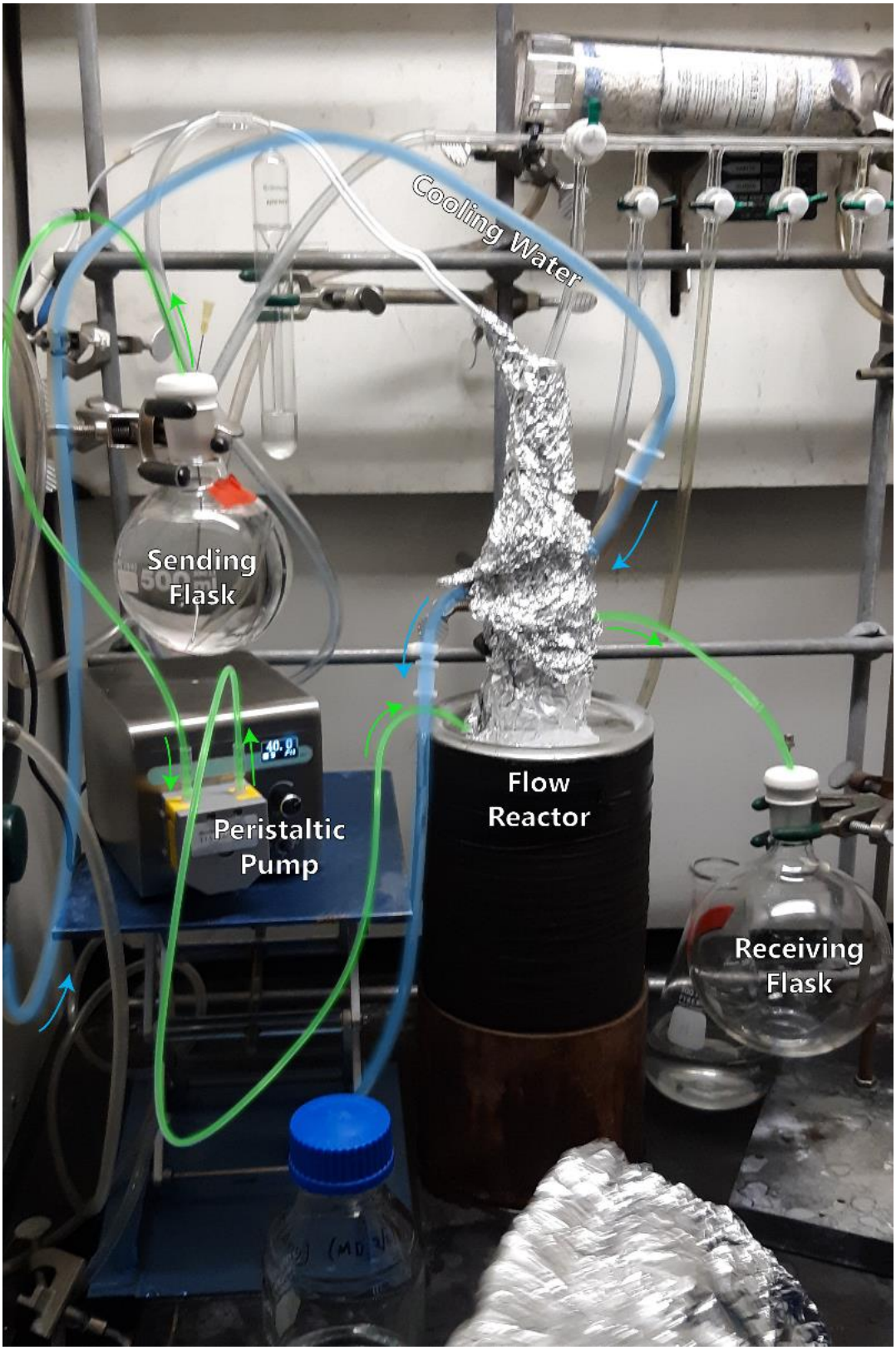

**Figure 1.5.4** Filtered Flow Reactor Setup. Arrows indicate direction of flow.

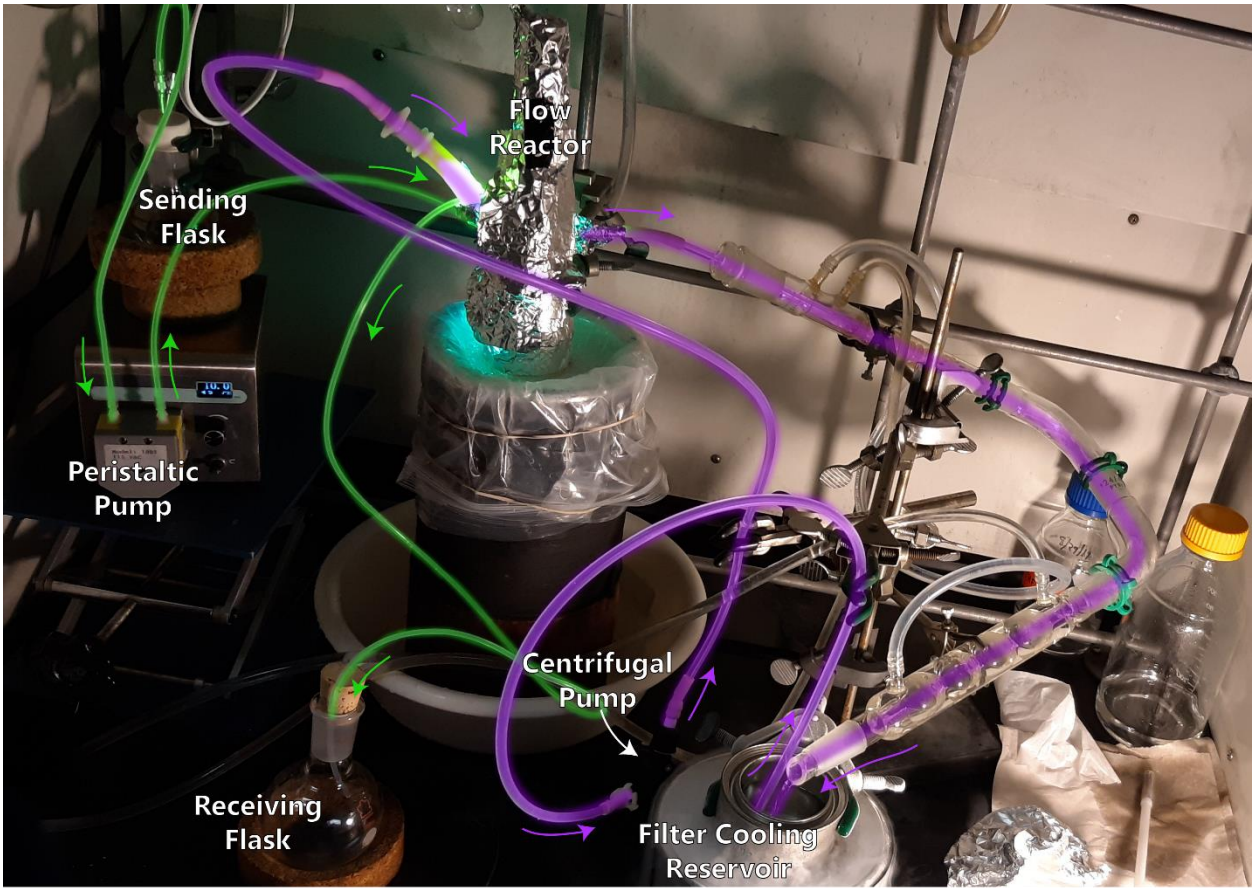


**Time Course Experiments**

General Procedure:

To a 20 ml quartz test tube was added 0.1 mmol **22** and a stir bar. The appropriate solvent was then added and the tube capped with a rubber septum. The septum was pierced with a needle and the vessel was degassed using a bath sonicator for 5 minutes. The tube was then suspended in the center of a Rayonet photoreactor with stirring. The reactor was covered with a light-blocking cloth and powered on. To sample the reaction, the reactor was powered-off, the reaction vessel

was removed and uncapped, and the desired volume of reaction media was removed using a micropipette.

GC/MS Sample Preparation:

To a GC/MS vial containing a low-volume insert was added 50 µl of reaction media, 200 µl of cyclohexane, and 10 µl of a 10 mg/ml cyclohexane solution of [6]-2,6-pyridinophane as an internal standard.

GC/MS Method:

For all samples, oven temperature was held at 70 °C for 1 minute, then ramped up to 300 °C at a rate of 20 °C/min, then held at 300 °C for 4 minutes.

Data Workup:

Peak identity was verified using authentic samples of **22**, **24**, **23**, **25**, and **21** isolated previously by column chromatography.

Peaks of interest for a given sample were integrated manually using Agilent ChemStation software and peak areas were exported as a Microsoft Excel spreadsheet. Spreadsheets of a given time course were then compiled into a single file using Microsoft Excel and peak areas were normalized

with respect to the internal standard's peak area for each time point. The data was then normalized with respect to the largest area observed and plotted. Trend lines are two-period moving averages.

**Figure 1.5.5** GC/MS trace of a flow photolysis reaction from which azirine **37** and 1,3-oxazepine **35** were isolated.

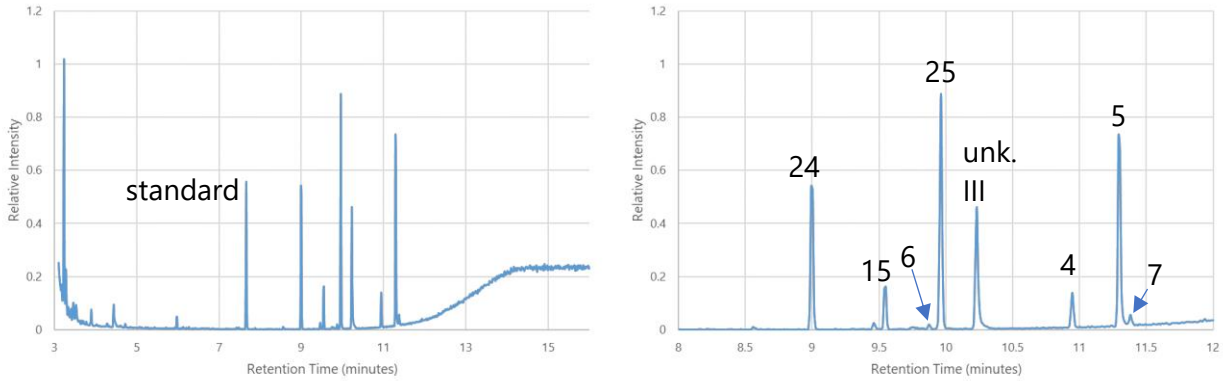


**Figure 1.5.6** Time Course Irradiation of a 0.1 M solution of **11.**

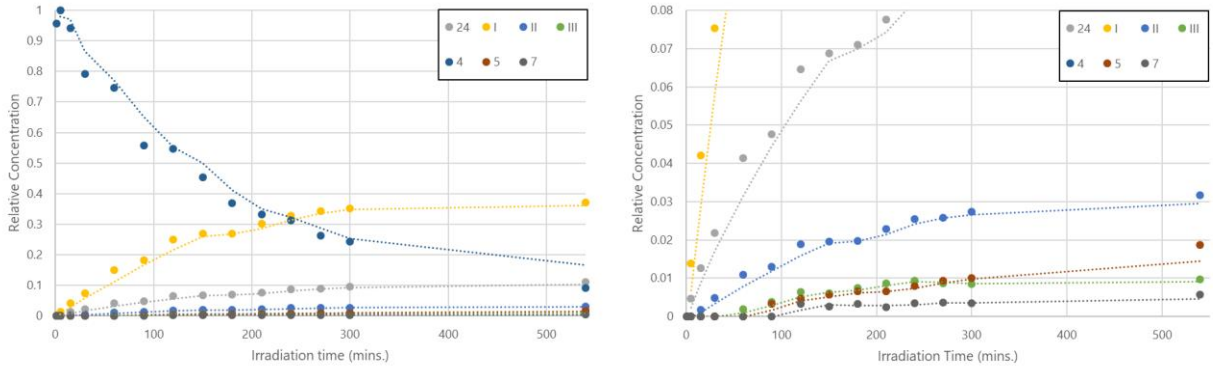

**Figure 1.5.7** Time Course Irradiation of **22** filtered by **44b** (15 mM in 70% aq. glycol).

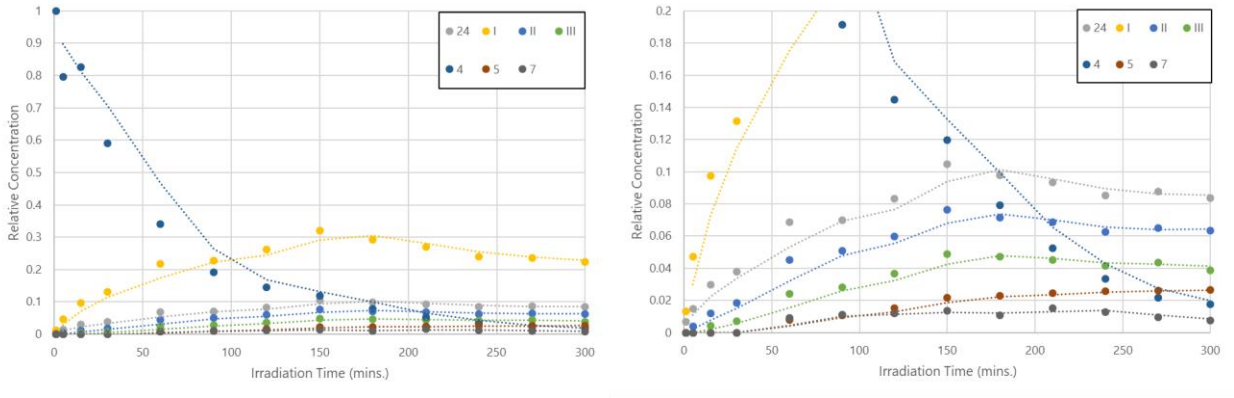


*Filtration was affected by immersion of a stoppered quartz test tube containing the reaction mixture within a larger quartz test tube containing the filter solution. Resultant filtration path length was approximately 1 cm.*

**Figure 1.5.8** Time Course Irradiation of **22** at 312 nm.

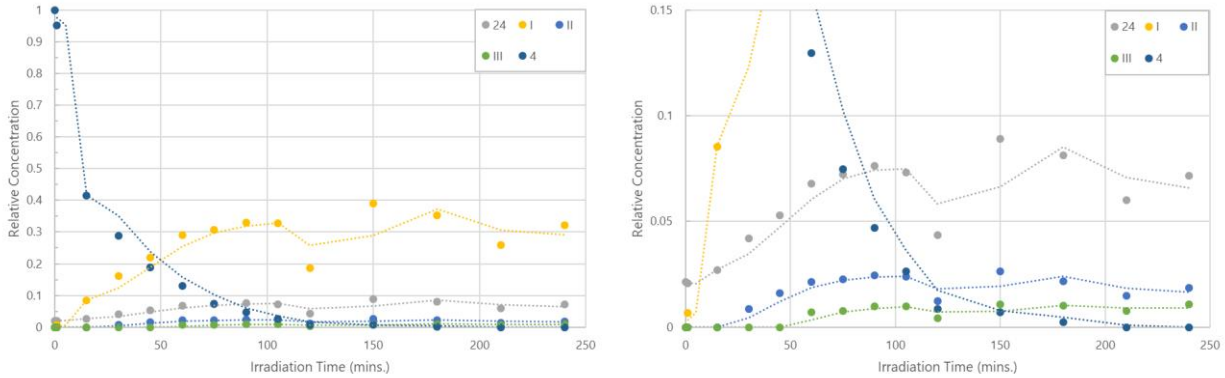

**Figure 1.5.9** Time Course Irradiation of **45** (254 nm, 0.01 M THF).

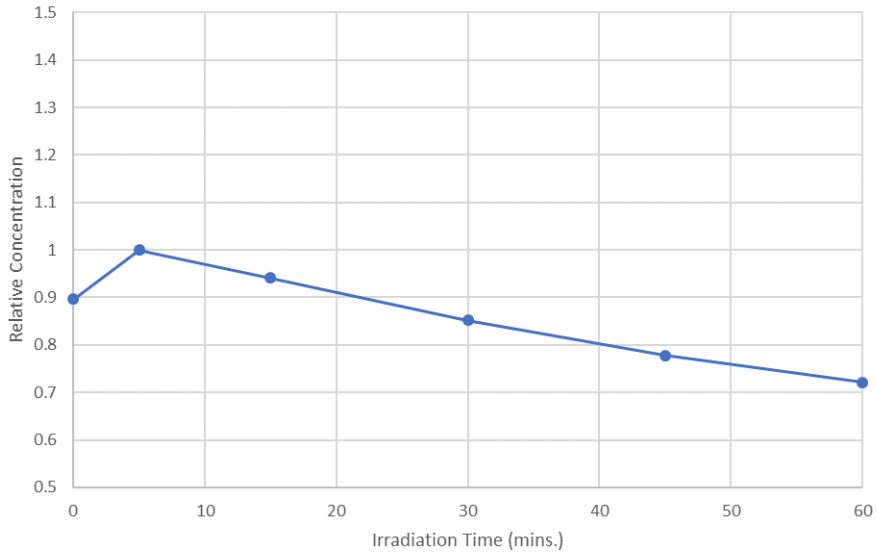


*No products resulting from the photolysis of **45** were detected.*

**Figure 1.5.10** GC/MS chromatograms of **6** before and after hydrolysis on $SiO_2$.

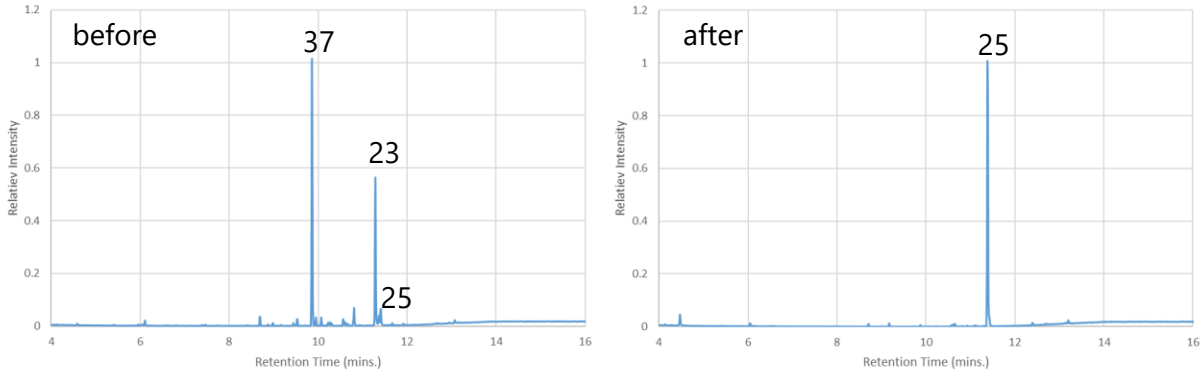

**UV-Vis Spectra**

**Figure 1.5.11** UV-Vis spectrum of **35** (0.07 mM in THF).

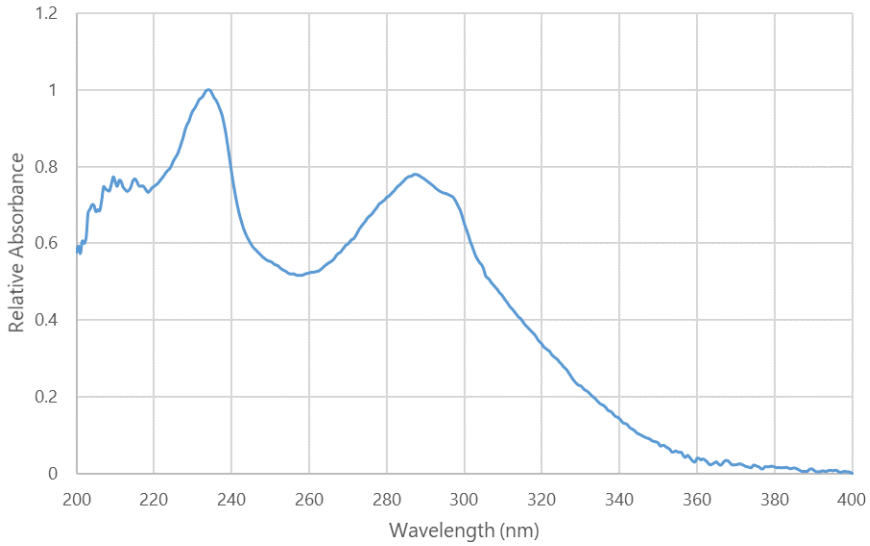


**Figure 1.5.12** UV-Vis spectrum of **45** (0.07 mM in THF).

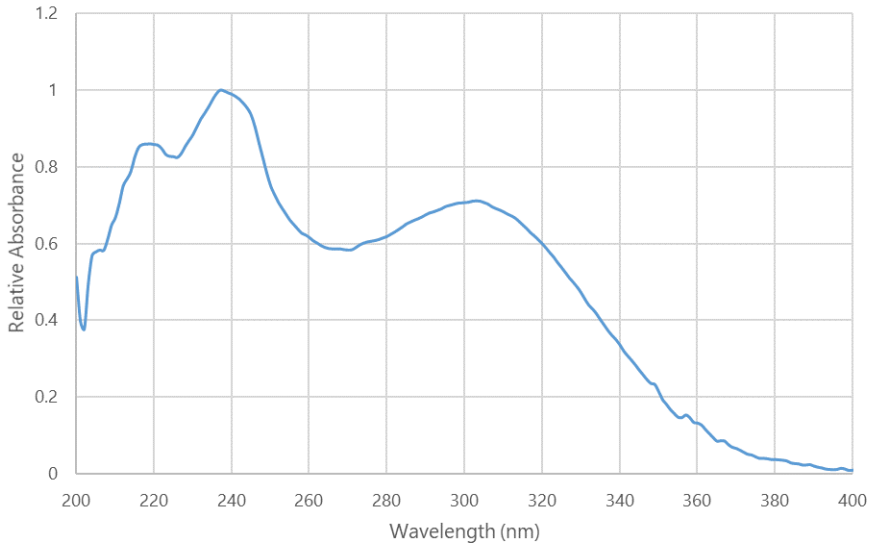

**Figure 1.5.13** UV-Vis spectrum of **37** (0.1 mM in THF).

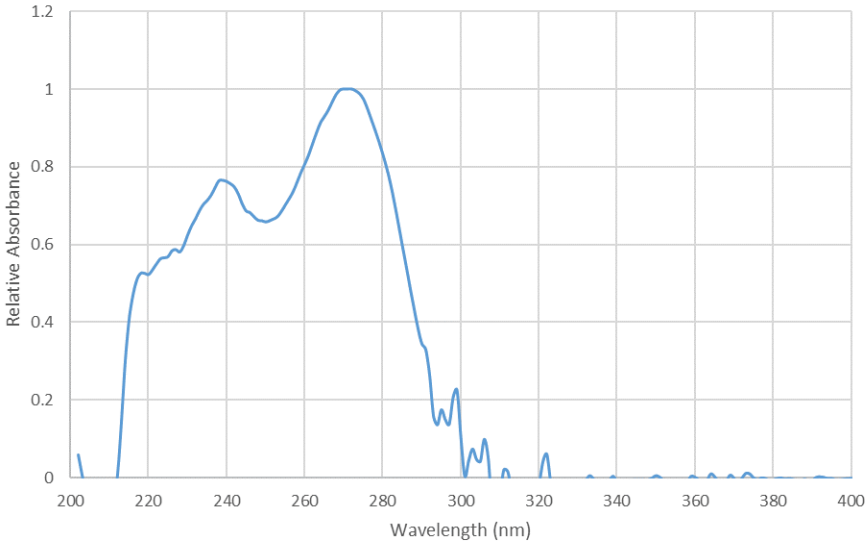


**Figure 1.5.14** UV-Vis spectrum of **22** (0.005 mM in THF).

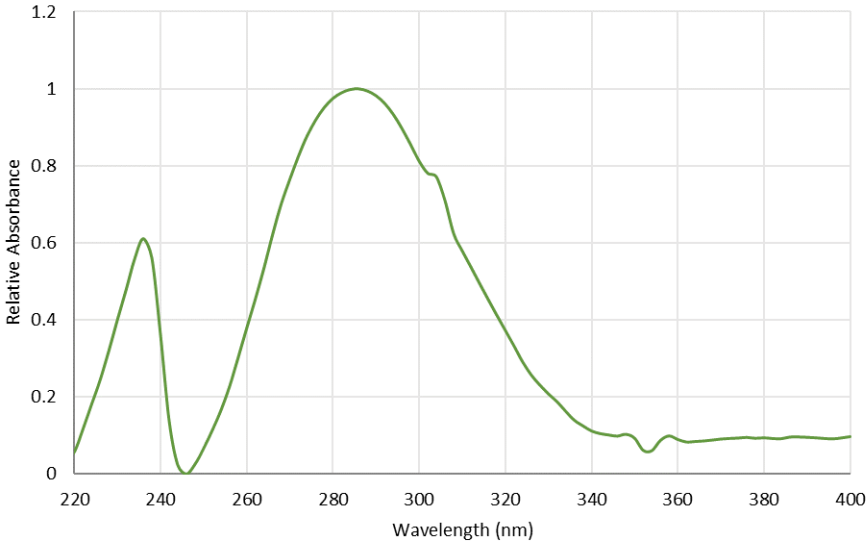

**Figure 1.5.15** UV-Vis spectrum of **24** (0.1 mM in THF).

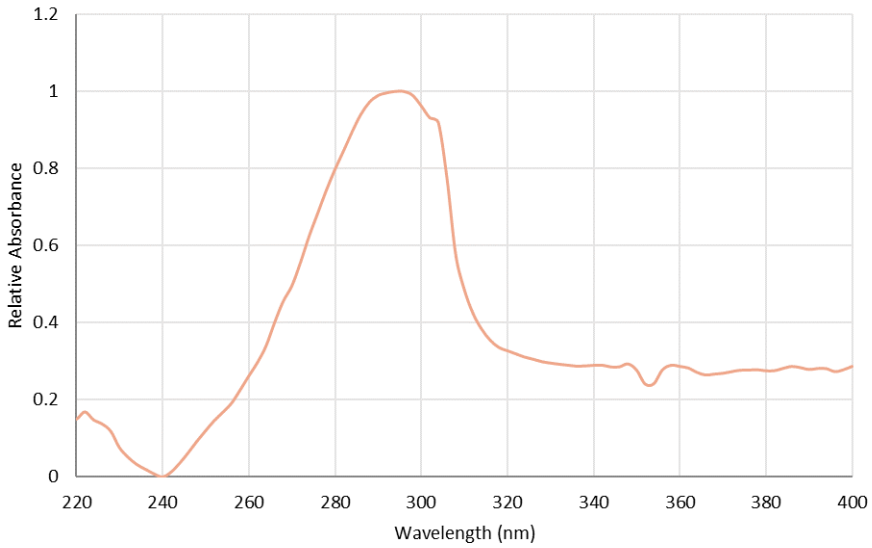


**Figure 1.5.16** UV-Vis of **44b** (15 mM in 70% aqueous glycol) before and after 1 hour of irradiation.

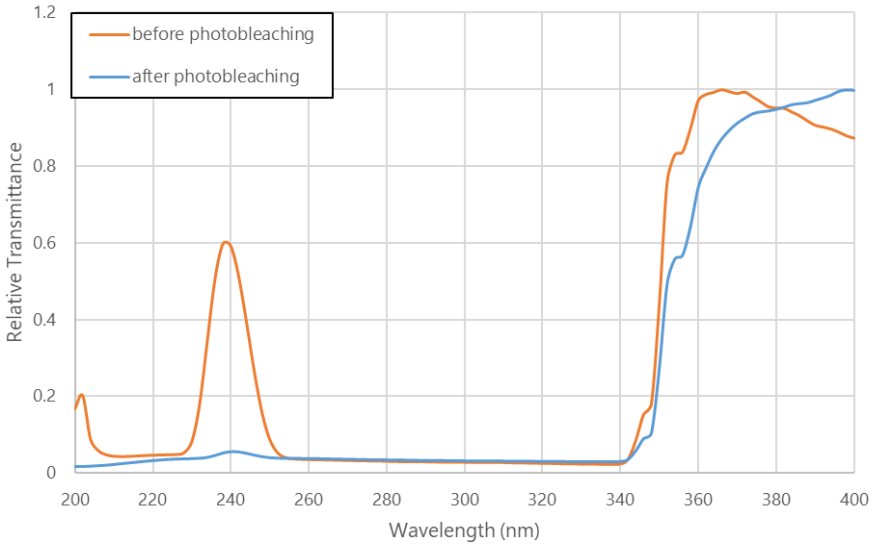

**Figure 1.5.17** UV-Vis spectra of **23b** (15 mM) in glycol solutions of varying aqueous content.

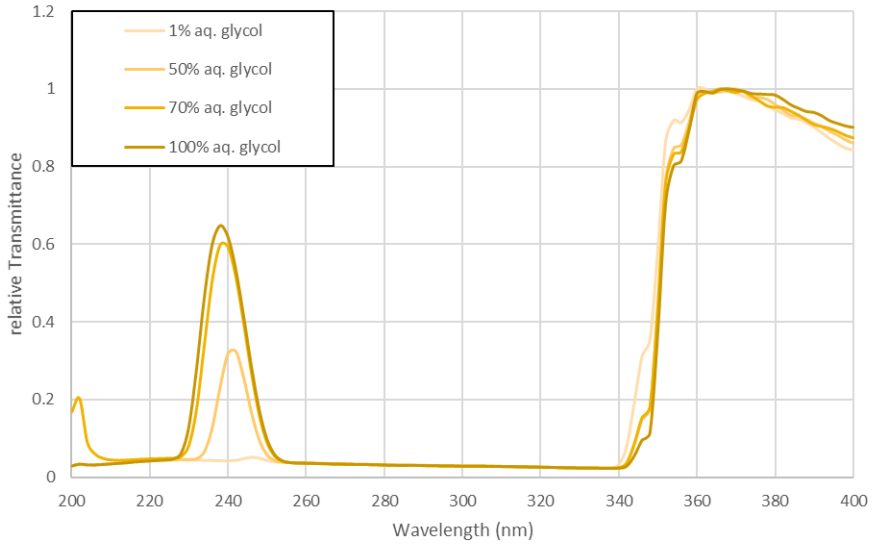


**Figure 1.5.18** UV-Vis spectra of **S1** in various solvents at 60 mM.

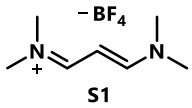


**S1**

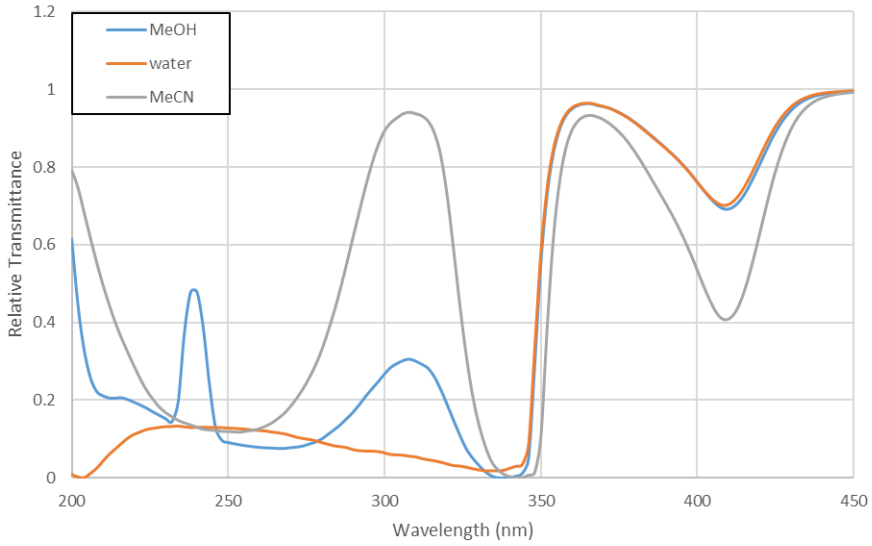


*Spectra in Figure S17 were collected using a JASCO V-770 UV-Vis spectrophotometer.*

### 1.5.3 Supporting Information for Section 1.4

*Computational methods are omitted for conciseness. Please see the original publication for details.*

**General Methods**

Reagents were purchased from commercial vendors and used as received unless otherwise stated. Tetrahydrofuran (THF) and 1,2-dimethoxy ethane (DME) were passed through a Glass Contour solvent drying system.

Thin-layer chromatography (TLC) was conducted on pre-coated plates (Sorbent Technologies, silica gel 60 PF254, 0.25 mm) and visualized with UV 254 nm. For acid-sensitive compounds, TLC plates were neutralized with TEA/Hexane (1%) before use. Column chromatography was performed on silica gel 60 (SiliCycle, 240−400 mesh). For acid-sensitive compounds, silica gel was premixed with TEA/Hexane (1%) before being loaded into the column. NMR spectra were recorded on Bruker Avance spectrometers ($^{1}$H: 400 $^{13}$C: 100 MHz and $^{1}$H: 600 MHz). Chemical shifts are reported in ppm and referenced to residual internal $CHCl_3$ for $^{1}$H (δ 7.26) and $^{13}$C (δ 77.2) spectra. Deuterated chloroform used in NMR experiments was neutralized prior to sample dissolution via passage through a plug of neutral alumina. UV-Vis spectra were obtained using a Shimadzu UV3101PC UV-Vis-NIR Scanning Spectrophotometer unless otherwise noted. GC/MS analyses were run on an Agilent 7250 Q-TOF GC/MS using an Agilent 19091S-433 HP-5MS capillary column.

Photoreactions were conducted inside of a Rayonet Reactor (Southern New England Ultraviolet Co.) utilizing a 254 nm bulb set unless otherwise stated.

**Experimental Details**

(*Z*)-14-oxa-15-azabicyclo[8.3.2]pentadeca-1(13),10(15),11-triene (**35**) was synthesized *via* the same procedure outlined in section 1.5.2.

General procedure for screening non-photochemical rearrangement conditions of **35**:

To a flame-dried 1-dram vial equipped with a magnetic stir bar was added the designated amount of freshly prepared **35** in solvent, followed by the additive. The reaction was stirred at the listed temperature under argon for the listed length of time and analyzed by GC/MS.

GC/MS Sample Preparation:

To a GC/MS vial containing a low-volume insert was added 50 µl of reaction medium, 200 µl of cyclohexane, and 10 µl of 10 mg/ml [6]-2,6-pyridinophane in cyclohexane as an internal standard.

GC/MS Method:

For all samples, oven temperature was held at 70 °C for 1 minute, then ramped up to 300 °C at a rate of 20 °C/min, then held at 300 °C for 4 minutes.

Data Workup:

Peak identity was verified using authentic samples isolated previously by column chromatography. Peaks of interest for a given sample were integrated manually using Agilent ChemStation software.

Chromatograms and peak areas were exported as Microsoft Excel spreadsheets. Chromatograms were normalized to the highest peak and plotted in Microsoft Excel. Peak areas were normalized with respect to the internal standard's peak area for each reaction. Percent conversion was calculated by dividing the peak area of **35** from the reaction in question by the peak area of **35** in the starting material. Percent yield was calculated by dividing the peak area of **37** from the reaction in question by the peak area of **35** in the starting material.

Table 1.4.1 is reproduced below for ease of reference:

| Entry | Additive | Eq. Additive | Solvent | Time (h) | Conversion | Yield of **37** |
|---|---|---|---|---|---|---|
| 1 | $[RhClcod]_2$ | 0.1 | PhMe | 20 | 19% | tr |
| 2 | $RuCl_2cod$ | 0.1 | PhMe | 20 | 29% | tr |
| 3 | $PtCl_2$ | 0.1 | PhMe | 20 | 72% | 5% |
| 4 | $PtCl_2(PhCN)_2$ | 0.1 | $CH_2Cl_2$ | 24 | tr | tr |
| 5 | $PdCl_2(PPh_3)_2$ | 0.1 | $CH_2Cl_2$ | 24 | 23% | tr |
| 6 | $NiCl_2(PPh_3)_2$ | 0.1 | $CH_2Cl_2$ | 20 | 58% | 3% |
| 7 | $PtCl_2$ | 0.2 | PhMe | 18 | 55% | 11% |
| 8 | $PtCl_2$ | 1.0 | PhMe | 21 | 80% | 16% |
| 9 | $PtCl_2$ | 1.0 | $CH_2Cl_2$ | 21 | 52% | 3% |
| 10 | $PtCl_4$ | 1.0 | PhMe | 2 | 100% | 36% |
| 11 | HCl | 0.1 | PhMe | 0.25 | 98% | 6% |
| 12 | $Zn(OTf)_2$ | 0.1 | MeCN | 22 | 96% | 92%[a] |
| 13 | $Zn(OTf)_2$ | 1.0 | MeCN | 17 | 100% | 4% |
| 14 | $Zn(OTf)_2$ | 0.1 | 1:1 DME:$H_2O$ | 17 | 100% | 2% |
| 15 | $Sc(OTf)_3$ | 0.1 | MeCN | 20 | 100% | tr |
| 16 | $In(OTf)_3$ | 0.1 | MeCN | 20 | 100% | tr |
| 17 | $La(OTf)_3$ | 0.1 | MeCN | 21 | 90% | tr |
| 18 | $Yb(OTf)_3$ | 0.1 | MeCN | 21 | 61% | tr |
| 19[b] | $Cu(OTf)_2$ | 0.1 | MeCN | 20 | 100% | 8% |

**Table 1.4.1** Conditions screened for rearrangement of **35**. All reactions were performed at 0.05 mmol scale (0.05 mM) under inert atmosphere unless otherwise noted. Chromatograms are available in the SI. [a]Percent conversion for entry 12 is approximate as the peak corresponding to **37** was atypically broad, potentially due to decomposition during analysis. [b]Experiment was

conducted in two stages. 21 h under standard conditions, followed by 20 h under air. Yields given are after air exposure. See SI for details.

| Compound | Typical Retention Time (minutes) |
|---|---|
| *Reference* | 7.65 |
| **21** | 8.99 |
| **22** | 10.94 |
| **24** | 11.27 |
| **37** | 9.87 |

**Table 1.5.5** Typical retention times of identified products arising from photoirradiation of **35**.

**Figure 1.5.19** Chromatogram of Table 1.4.1 Entry 1-3 Starting Material.

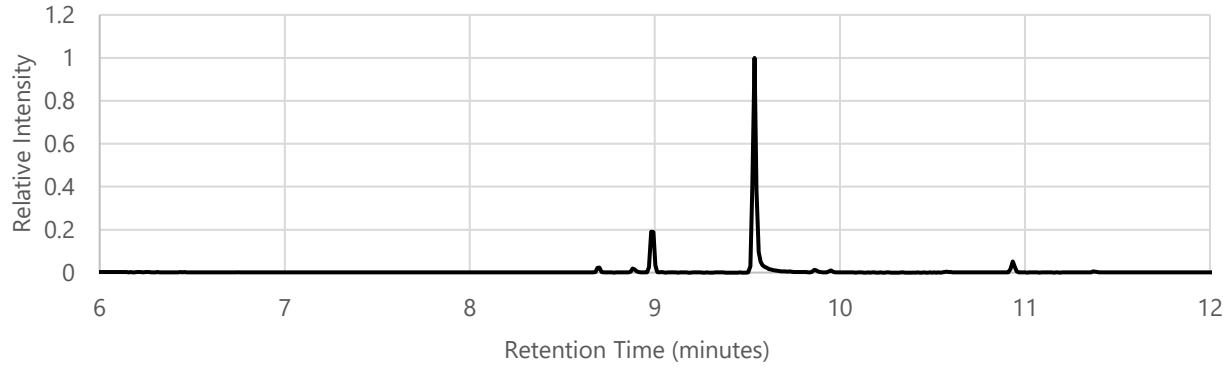


**Figure 1.5.20** Chromatogram of Table 1.4.1 Entry 1-3 Starting Material

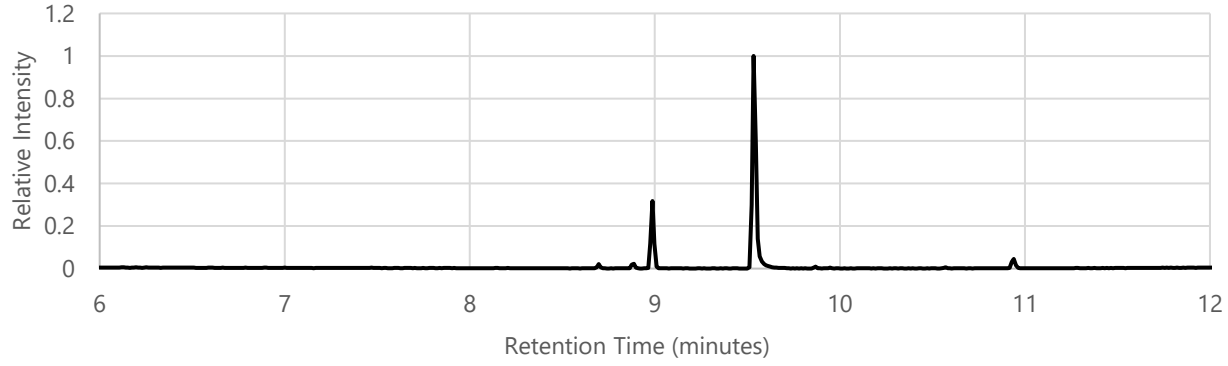


**Figure 1.5.21** Chromatogram of Table 1.4.1 Entry 2.

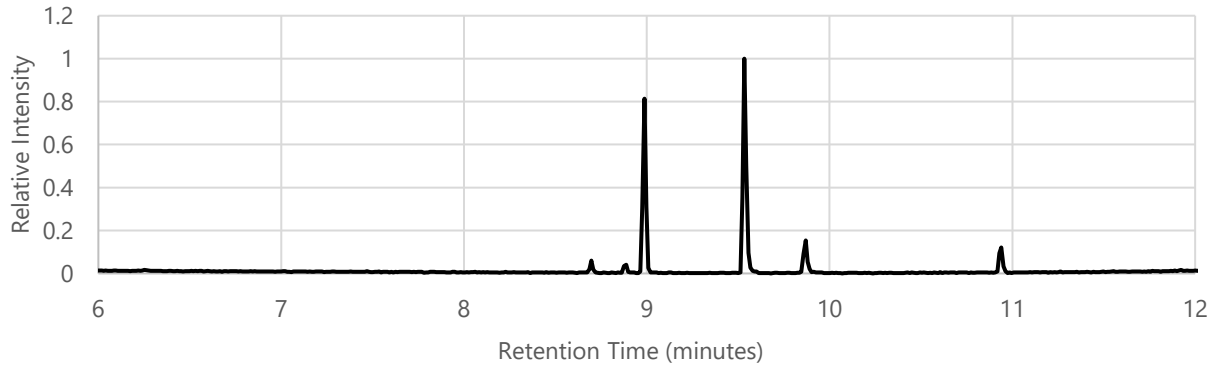

**Figure 1.5.22** Chromatogram of Table 1.4.1 Entry 3.

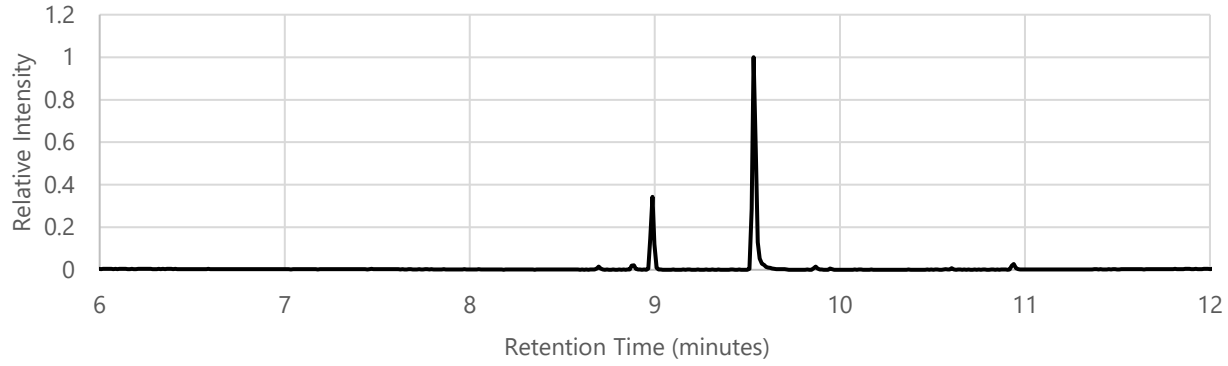


*Peak areas for Figures 1.5.19-22 were normalized with respect to **21** (peak at 8.99').*

**Figure 1.5.23** Chromatogram of Table 1.4.1 Entry 4-6 Starting Material.

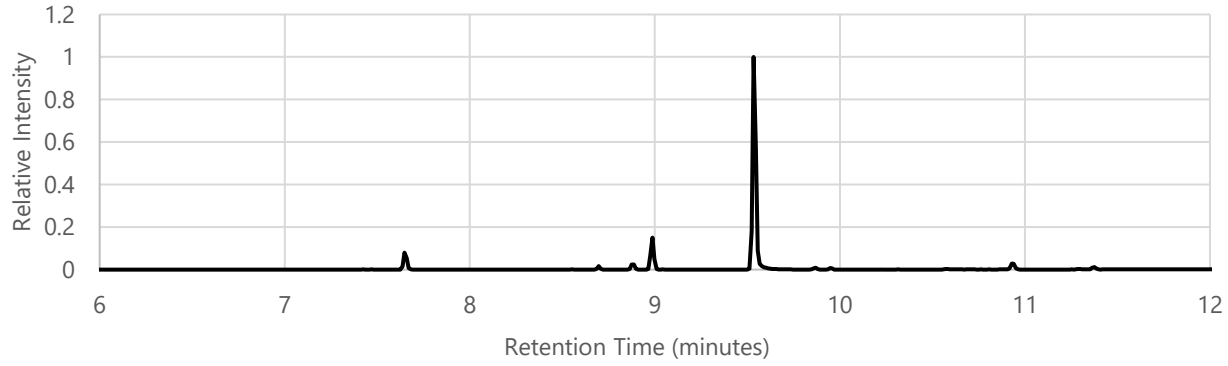


**Figure 1.5.24** Chromatogram of Table 1.4.1 Entry 4.

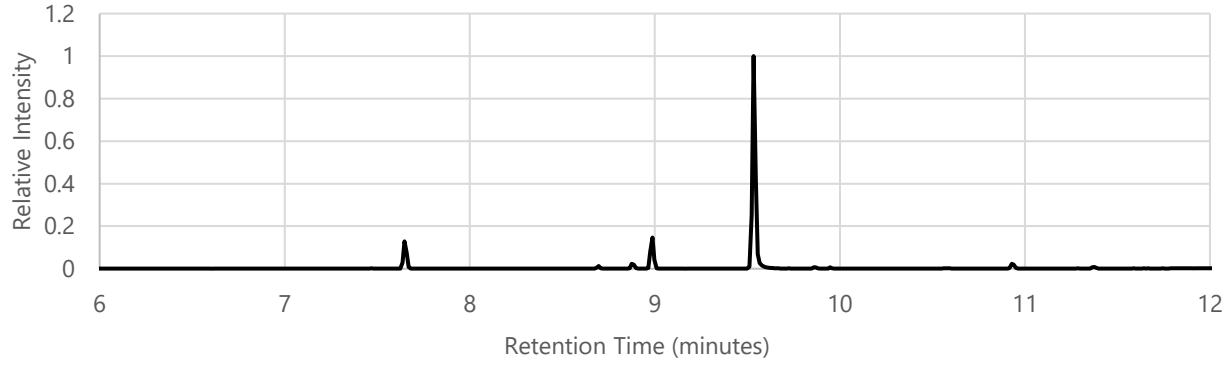

**Figure 1.5.25** Chromatogram of Table 1.4.1 Entry 5.

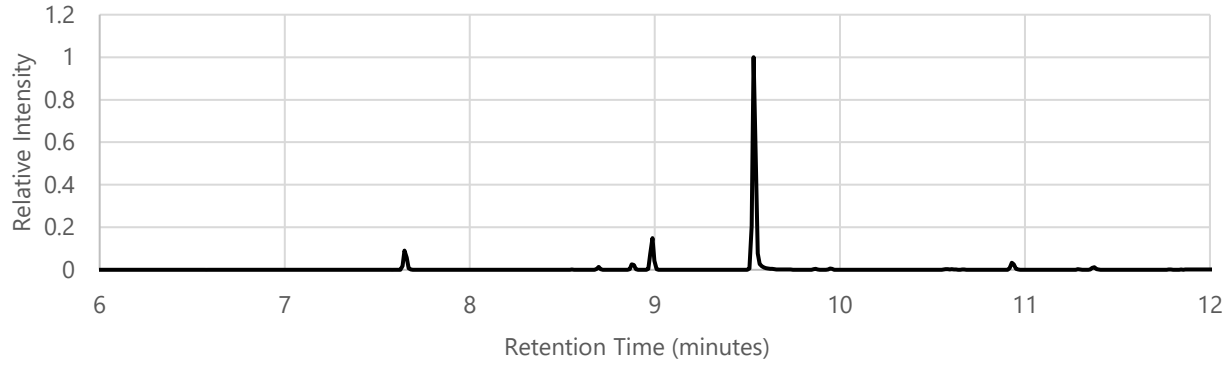


**Figure 1.5.26** Chromatogram of Table 1.4.1 Entry 6.

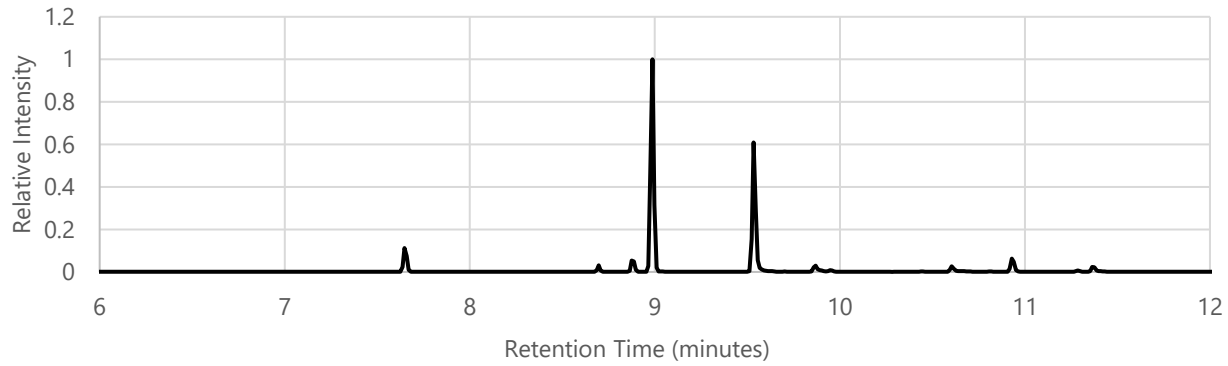


**Figure 1.5.27** Chromatogram of Table 1.4.1 Entry 7-10 Starting Material.

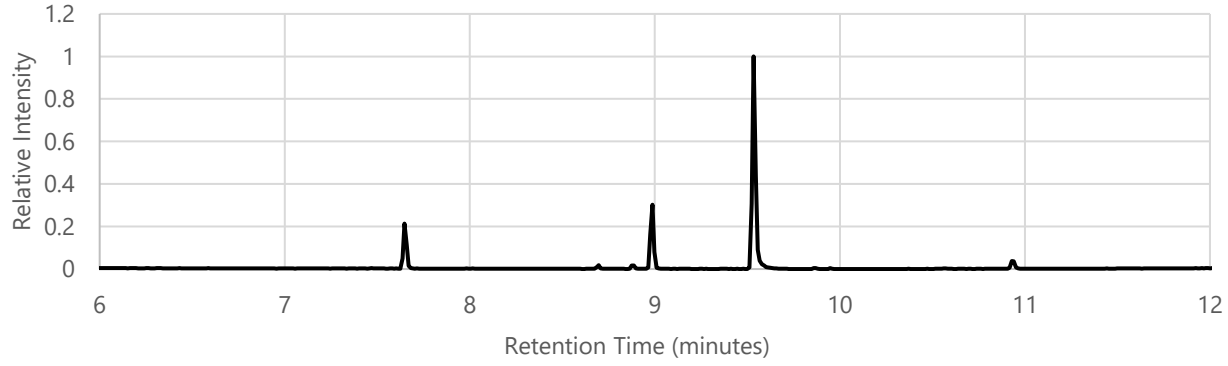

**Figure 1.5.28** Chromatogram of Table 1.4.1 Entry 7.

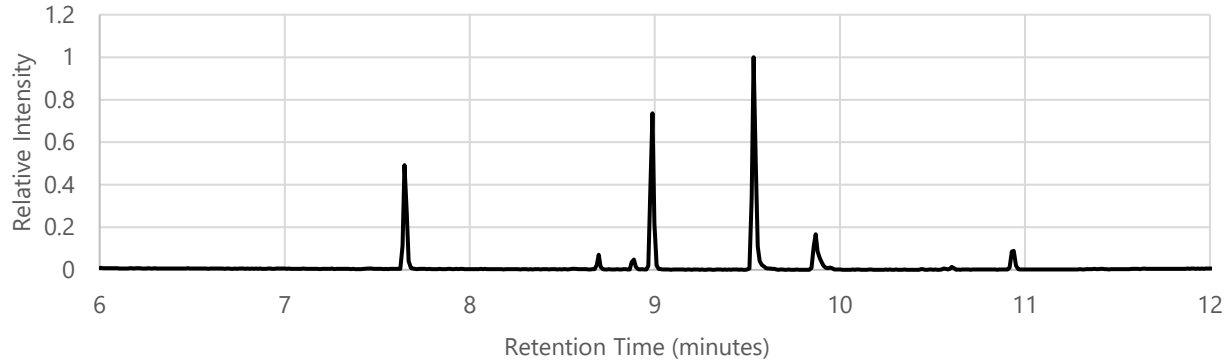


**Figure 1.5.29** Chromatogram of Table 1.4.1 Entry 8.

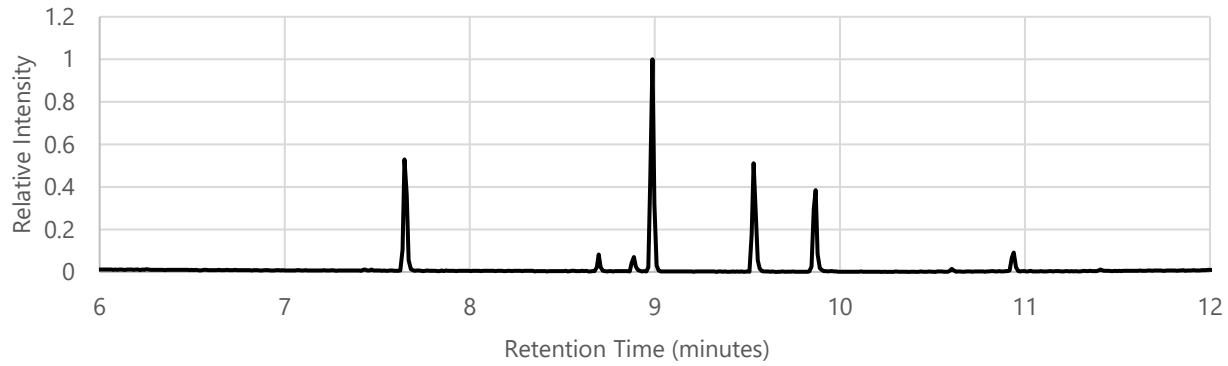


**Figure 1.5.30** Chromatogram of Table 1.4.1 Entry 9.

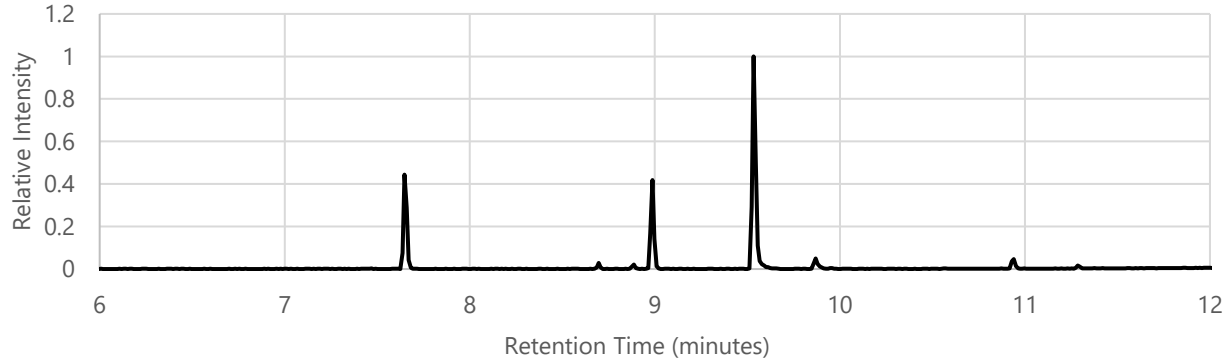

**Figure 1.5.31** Chromatogram of Table 1.4.1 Entry 10.

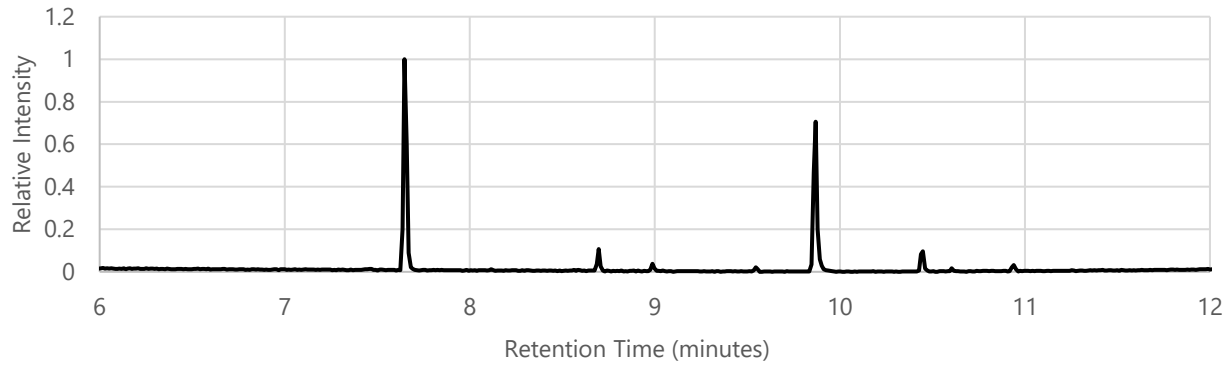


**Figure 1.5.32** Chromatogram of Table 1.4.1 Entry 11-12 Starting Material.

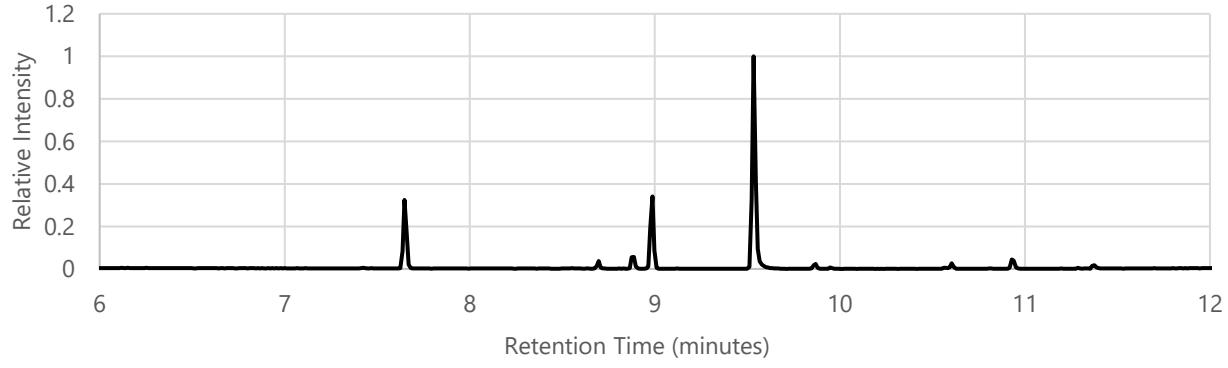


**Figure 1.5.33** Chromatogram of Table 1.4.1 Entry 11.

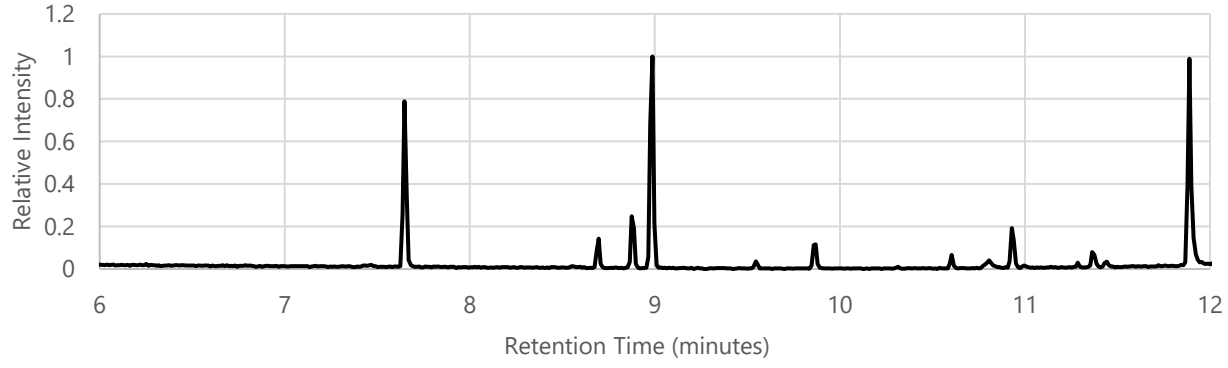

**Figure 1.5.34** Chromatogram of Table 1.4.1 Entry 12.

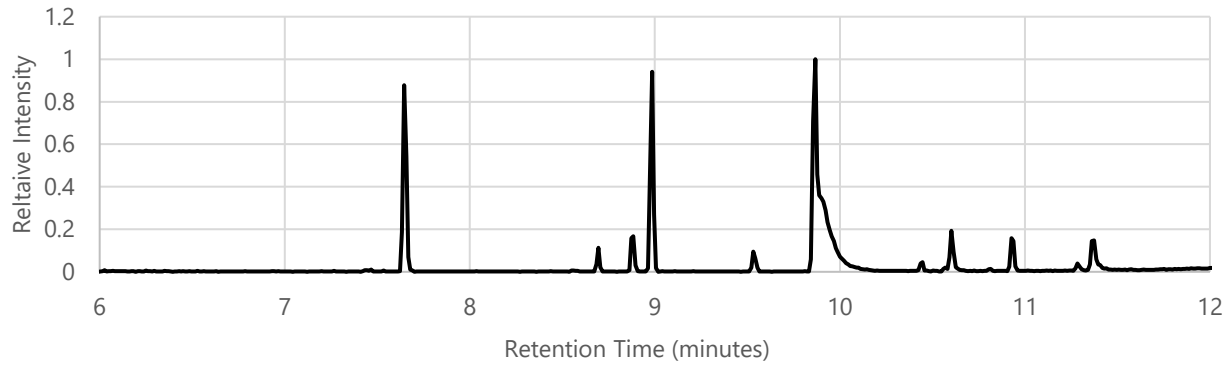


**Figure 1.5.35** Chromatogram of Table 1.4.1 Entry 13-14 Starting Material.

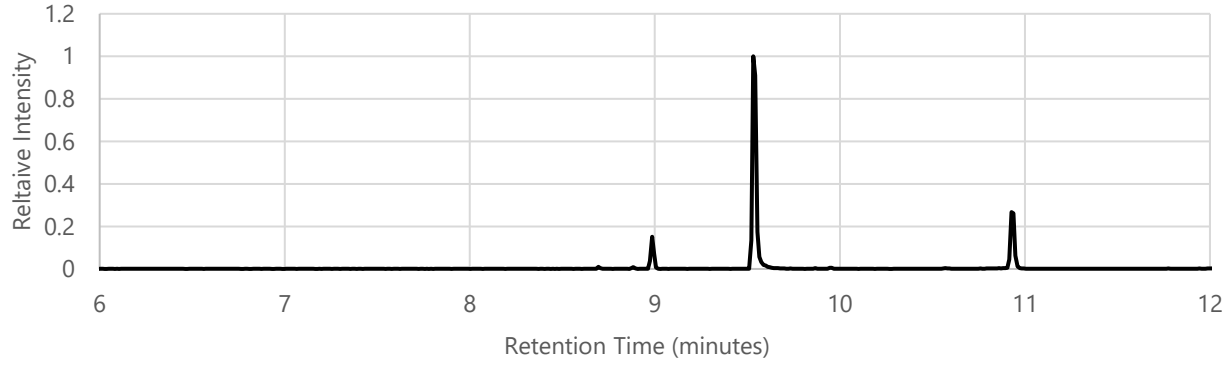


**Figure 1.5.36** Chromatogram of Table 1.4.1 Entry 13.

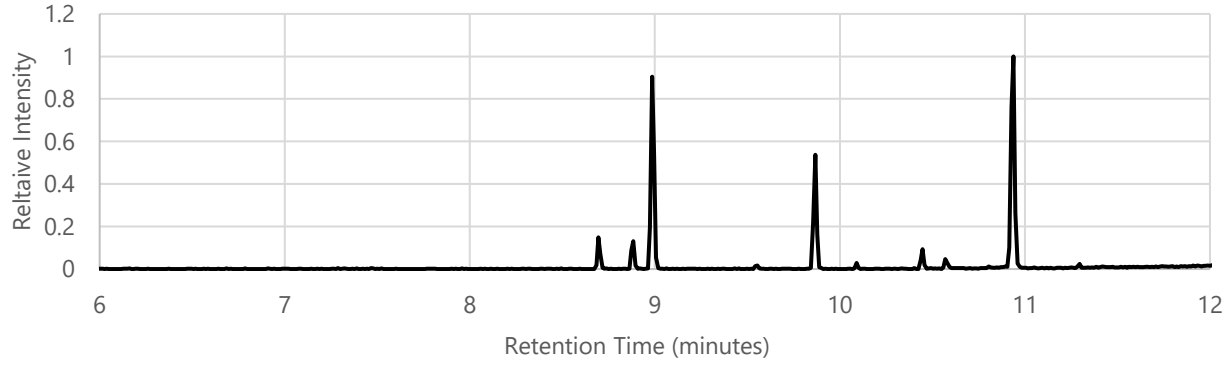

**Figure 1.5.37** Chromatogram of Table 1.4.1 Entry 14.

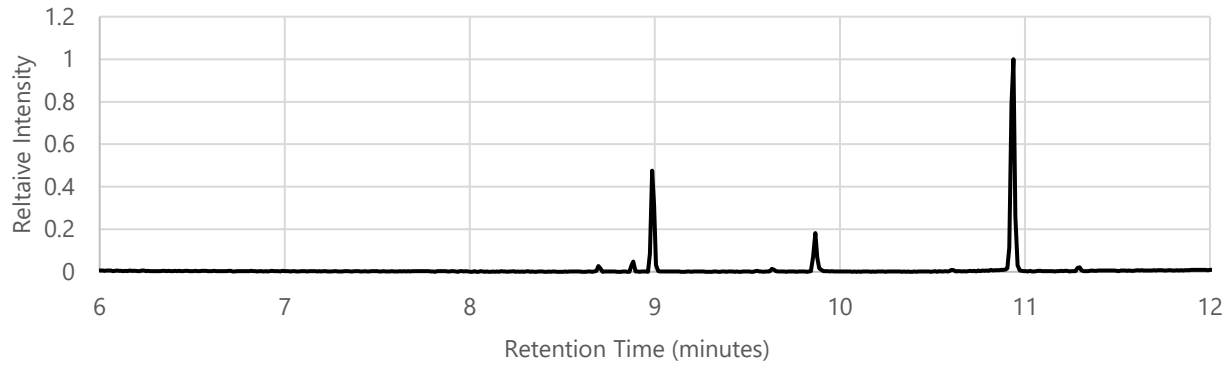


*Peak areas for Figures 1.5.35-37 were normalized with respect to **21** (peak at 8.99').*

**Figure 1.5.38** Chromatogram of Table 1.4.1 Entry 15-16, 19 Starting Material.

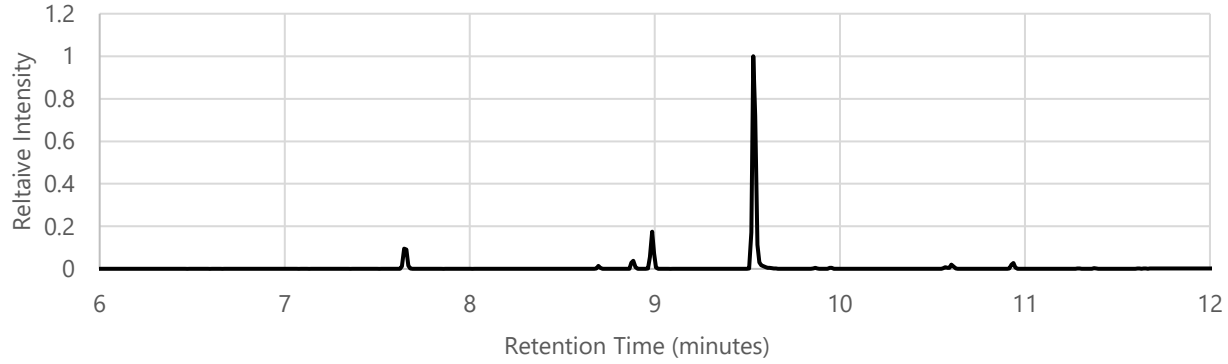


**Figure 1.5.39** Chromatogram of Table 1.4.1 Entry 15.

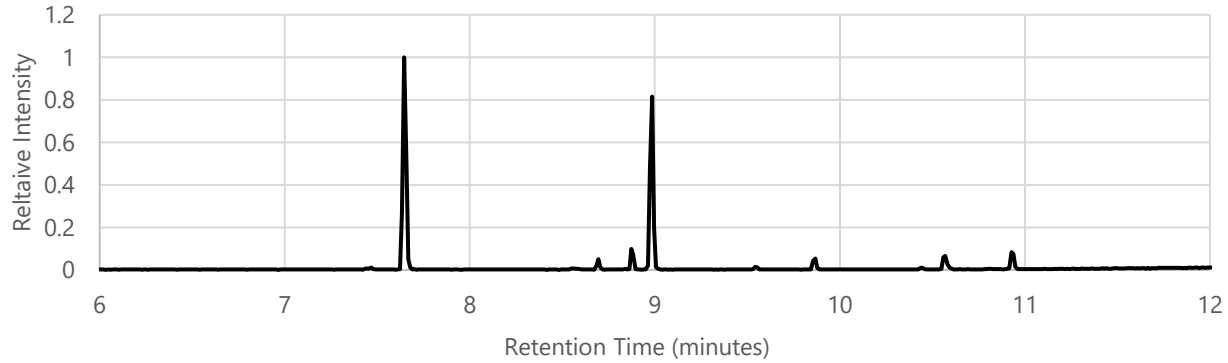

**Figure 1.5.40** Chromatogram of Table 1.4.1 Entry 16.

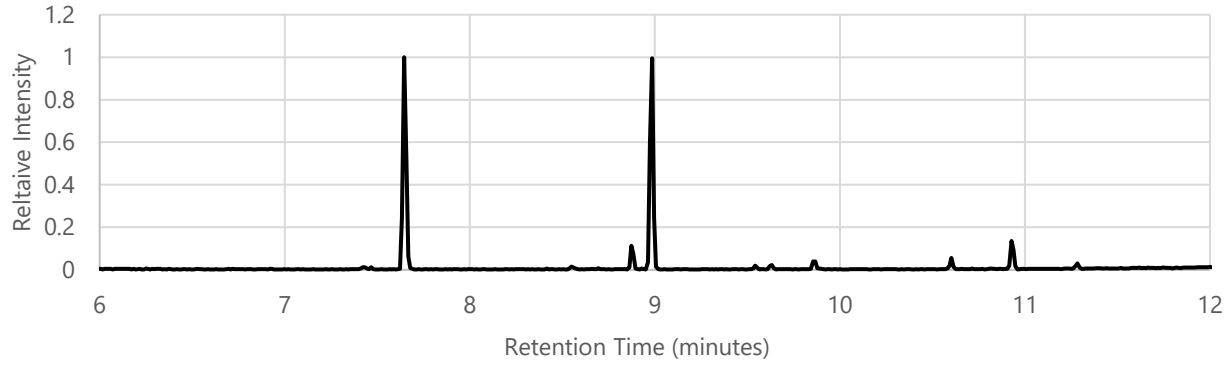


**Figure 1.5.41** Chromatogram of Table 1.4.1 Entry 17-18 Starting Material.

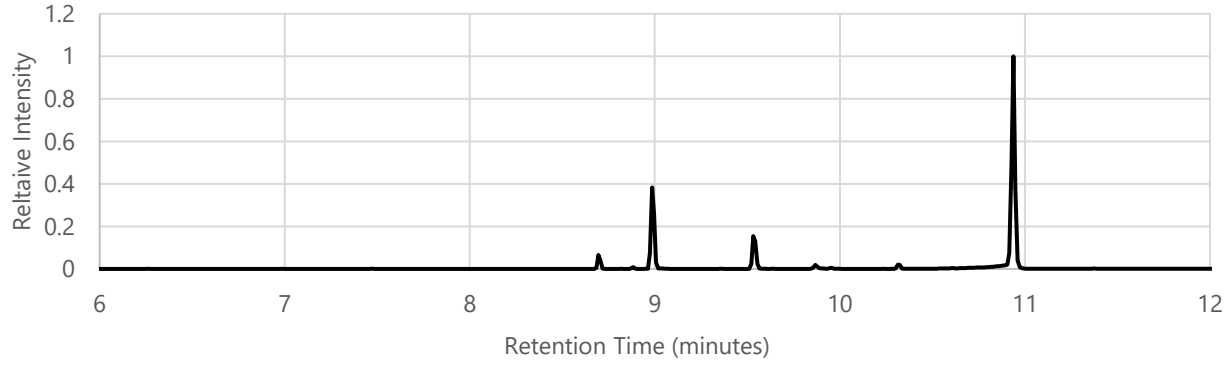


**Figure 1.5.42** Chromatogram of Table 1.4.1 Entry 17.

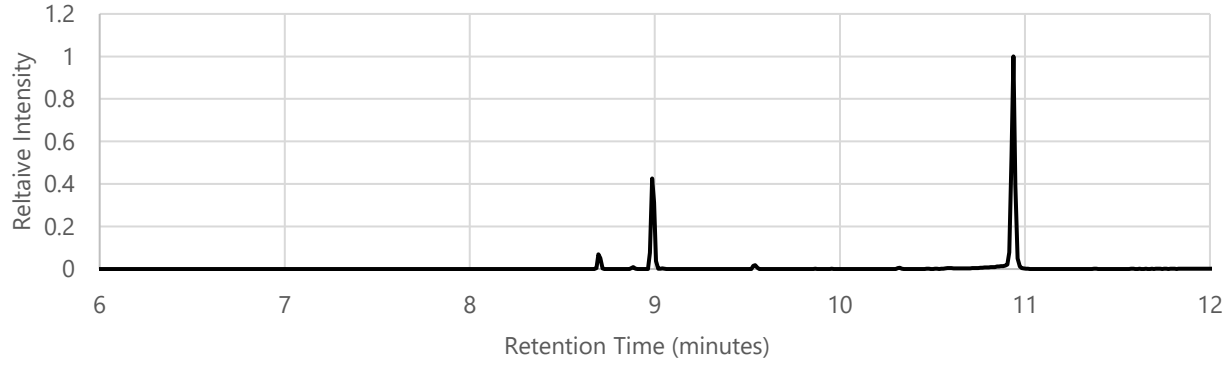

**Figure 1.5.43** Chromatogram of Table 1.4.1 Entry 18.

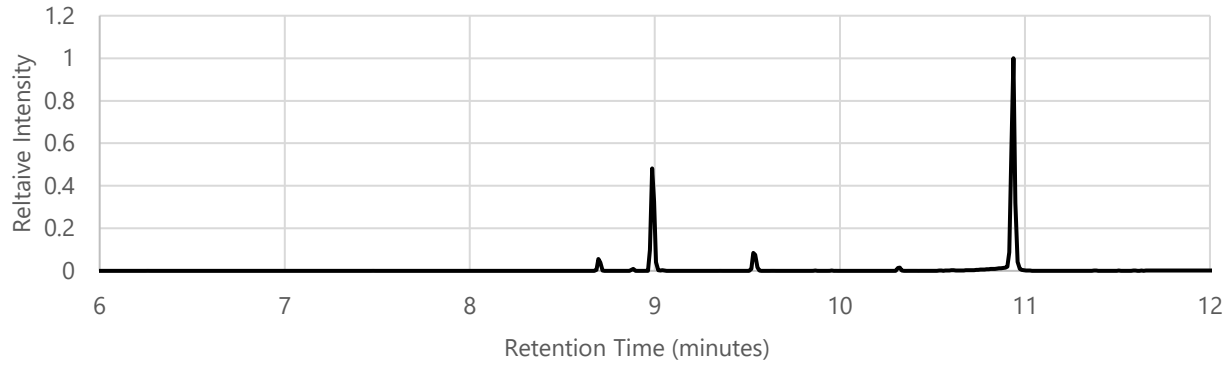


*Peak areas for Figures 1.5.41-43 were normalized with respect to **21** (peak at 8.99').*

**Figure 1.5.44** Chromatogram of Table 1.4.1 Entry 19 21 h under argon.

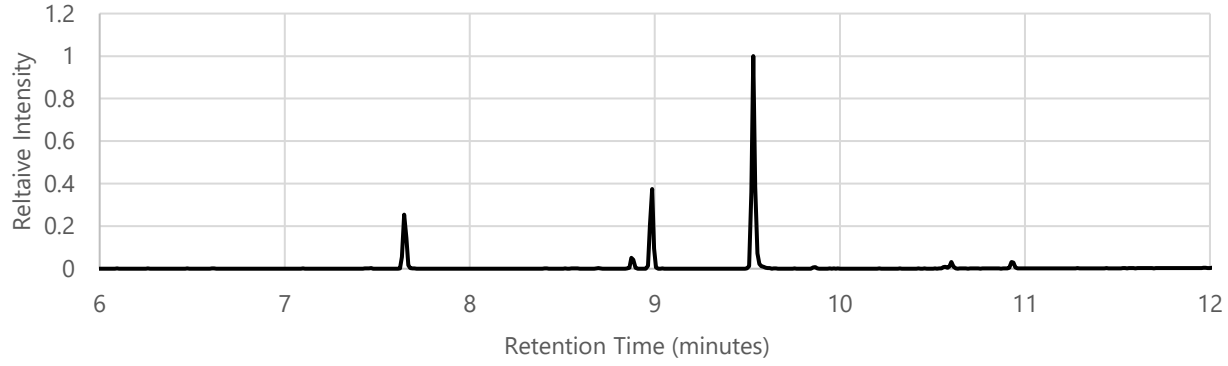


**Figure 1.5.45** Chromatogram of Table 1.4.1 Entry 19 20 h under air.

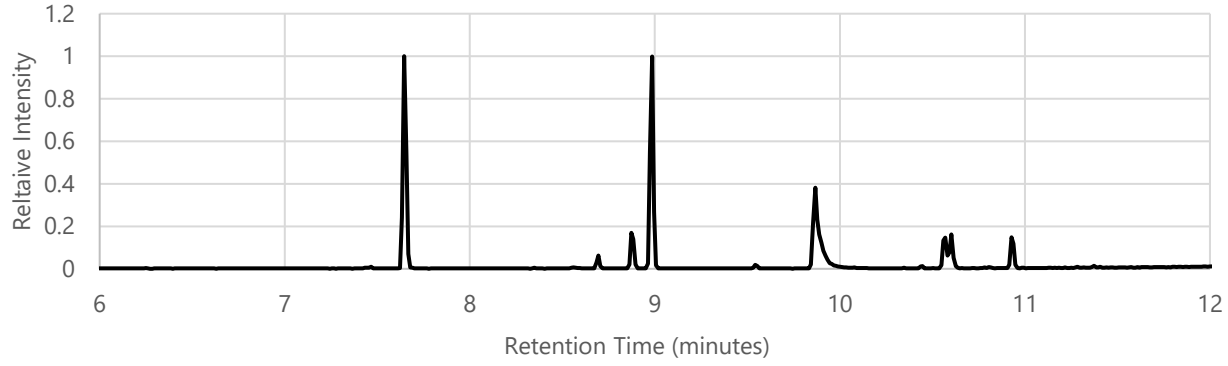

## 1.6 References


1. Spence, G. G.; Taylor, E. C.; Buchardt, O., Photochemical reactions of azoxy compounds, nitrones, and aromatic amine N-oxides. *Chemical Reviews* **1970,** *70* (2), 231-265.
2. Albini, A.; Alpegiani, M., The photochemistry of the N-oxide function. *Chemical Reviews* **1984,** *84* (1), 43-71.
3. Poole, J. S., Recent Advances in the Photochemistry of Heterocyclic N-Oxides and Their Derivatives. In *Heterocyclic N-Oxides*, Larionov, O. V., Ed. Springer International Publishing: Cham, 2017; pp 111-151.
4. Ito, M.; Hata, N., The Ultra-violet Absorption Spectrum of Pyridine N-oxide. *Bulletin of the Chemical Society of Japan* **1955,** *28* (4), 260-263.
5. Hata, N.; Tanaka, I., Chemical Processes Subsequent to n—π* and π—π* Transitions of Pyridine N-oxide and 2-Picoline N-oxide. *The Journal of Chemical Physics* **1962,** *36* (8), 2072-2077.
6. Streith, J.; Sigwalt, C., Contraction d'heterocycles aromatiques par voie photocmique. *Tetrahedron Letters* **1966,** *7* (13), 1347-1350.
7. Splitter, J. S.; Calvin, M., Oxaziridines. I. The Irradiation Products of Several Nitrones1. *The Journal of Organic Chemistry* **1965,** *30* (10), 3427-3436.
8. Bellamy, F.; Martz, P.; Streith, L., An Intriguing Copper Salt Effect upon the Photochemistry of Pyridine-N-oxides. Specific Photoinduced Syntheses of 3-Substituted 2-Formylpyrroles. *Heterocycles* **1975,** *3* (5), 395 - 400.
9. Brüggemann, M.; McDonald, A. I.; Overman, L. E.; Rosen, M. D.; Schwink, L.; Scott, J. P., Total Synthesis of (±)-Didehydrostemofoline (Asparagamine A) and (±)-

Isodidehydrostemofoline. *Journal of the American Chemical Society* **2003,** *125* (50), 15284-15285.

10. Hunter, G. A.; McNab, H.; Withell, K., The Meldrum's Acid Route to Prodigiosin Analogues. *Synthesis* **2010,** *2010* (10), 1707-1711.

11. Boudif, A.; Momenteau, M., A new convergent method for porphyrin synthesis based on a '3 + 1' condensation. *Journal of the Chemical Society, Perkin Transactions 1* **1996,** (11), 1235-1242.

12. Lohse, C.; Hagedorn, L.; Albini, A.; Fasani, E., Photochemistry of pyridine n-oxides. *Tetrahedron* **1988,** *44* (9), 2591-2600.

13. Weber, H.; Rohn, T., 2H-Azirine und 2-(ω-Cyanalkyl)furane als neuartige Photoprodukte aus [n](2,6)Pyridinophan-N-oxiden und ihre Bedeutung für den Reaktionsverlauf. *Chemische Berichte* **1989,** *122* (5), 945-950.

14. Berson, J. A.; Willcott, M. R., New Thermal Rearrangements of Tropilidenes1. *Journal of the American Chemical Society* **1965,** *87* (12), 2751-2752.

15. Furstner, A., Chemistry and biology of roseophilin and the prodigiosin alkaloids: a survey of the last 2500 years. *Angewantde Chemie International Edition* **2003,** *42* (31), 3582-603.

16. Obatoclax at https://clinicaltrials.gov

17. Nguyen, M.; Marcellus, R. C.; Roulston, A.; Watson, M.; Serfass, L.; Murthy Madiraju, S. R.; Goulet, D.; Viallet, J.; Belec, L.; Billot, X.; Acoca, S.; Purisima, E.; Wiegmans, A.; Cluse, L.; Johnstone, R. W.; Beauparlant, P.; Shore, G. C., Small molecule obatoclax (GX15-070) antagonizes MCL-1 and overcomes MCL-1-mediated resistance to apoptosis. *Proceeding of the National Academy of Sciences* **2007,** *104* (49), 19512-7.

18. Hu, D. X.; Withall, D. M.; Challis, G. L.; Thomson, R. J., Structure, Chemical Synthesis, and Biosynthesis of Prodiginine Natural Products. *Chemical Reviews* **2016,** *116* (14), 7818-7853.

19. Collman, J. P.; Chien, A. S.; Eberspacher, T. A.; Brauman, J. I., An Agostic Alternative to the P-450 Rebound Mechanism. *Journal of the American Chemical Society* **1998,** *120* (2), 425-426.

20. Boonlarppradab, C.; Kauffman, C. A.; Jensen, P. R.; Fenical, W., Marineosins A and B, Cytotoxic Spiroaminals from a Marine-Derived Actinomycete. *Organic Letters* **2008,** *10* (24), 5505-5508.

21. Lu, W.; Kancharla, P.; Reynolds, K. A., MarH, a Bifunctional Enzyme Involved in the Condensation and Hydroxylation Steps of the Marineosin Biosynthetic Pathway. *Organic Letters* **2017,** *19* (6), 1298-1301.

22. Salem, S. M.; Kancharla, P.; Florova, G.; Gupta, S.; Lu, W.; Reynolds, K. A., Elucidation of Final Steps of the Marineosins Biosynthetic Pathway through Identification and Characterization of the Corresponding Gene Cluster. *Journal of the American Chemical Society* **2014,** *136* (12), 4565-4574.

23. Sydor, P. K.; Barry, S. M.; Odulate, O. M.; Barona-Gomez, F.; Haynes, S. W.; Corre, C.; Song, L.; Challis, G. L., Regio- and stereodivergent antibiotic oxidative carbocyclizations catalysed by Rieske oxygenase-like enzymes. *Nature Chemistry* **2011,** *3* (5), 388-92.

24. Aldrich, L. N.; Dawson, E. S.; Lindsley, C. W., Evaluation of the biosynthetic proposal for the synthesis of marineosins A and B. *Organic Letters* **2010,** *12* (5), 1048-51.

25. Aldrich, L. N.; Berry, C. B.; Bates, B. S.; Konkol, L. C.; So, M.; Lindsley, C. W., Towards the total synthesis of marineosin A: construction of the macrocyclic pyrrole and an advanced,

functionalized spiroaminal model. *European Journal Of Organic Chemistry* **2013,** *2013* (20), 4215-4218.

26. Cai, X. C.; Wu, X.; Snider, B. B., Synthesis of the spiroiminal moiety of marineosins A and B. *Organic Letters* **2010,** *12* (7), 1600-3.

27. Cai, X.-C.; Snider, B. B., Synthesis of the Spiroiminal Moiety and Approaches to the Synthesis of Marineosins A and B. *Journal of Organic Chemistry* **2013,** *78* (23), 12161-12175.

28. Li, G.; Zhang, X.; Li, Q.; Feng, P.; Shi, Y., A concise approach to the spiroiminal fragment of marineosins. *Organic and Biomolecular Chemitry* **2013,** *11* (18), 2936-8.

29. Xu, B.; Li, G.; Li, J.; Shi, Y., Total synthesis of the proposed structure of marineosin A. *Organic Letters* **2016,** *18* (9), 2028-2031.

30. Weber, H.; Pant, J.; Wunderlich, H., Sterisch gehinderte Pyridiniumsalze, III. Darstellung und Eigenschaften von N-Methyl-[n](2, 6) pyridinophaniumsalzen. *Chemische Berichte* **1985,** *118* (10), 4259-4270.

31. Frederich, J. H.; Matsui, J. K.; Chang, R. O.; Harran, P. G., Substituted 2,2′-bipyrroles and pyrrolylfurans via intermediate isoxazolylpyrroles. *Tetrahedron Letters* **2013,** *54* (21), 2645-2647.

32. Hu, D. X.; Clift, M. D.; Lazarski, K. E.; Thomson, R. J., Enantioselective total synthesis and confirmation of the absolute and relative stereochemistry of streptorubin B. *Journal of the American Chemical Society* **2011,** *133* (6), 1799-1804.

33. Structure 21, and especially 25, were prone to the sigmatropic shift shown below. See SI for details and characterization. Further studies are ongoing. We have not yet found evidence of atropisomerism in the rearrangement products.

34. Battilocchio, C.; Hawkins, J. M.; Ley, S. V., Mild and selective heterogeneous catalytic hydration of nitriles to amides by flowing through manganese dioxide. *Organic Letters* **2014,** *16* (4), 1060-1063.

35. Roy, S. C.; Dutta, P.; Nandy, L. N.; Roy, S. K.; Samuel, P.; Pillai, S. M.; Kaushik, V. K.; Ravindranathan, M., Hydration of 3-cyanopyridine to nicotinamide over MnO2 catalyst. *Applied Catalysis A: General* **2005,** *290* (1), 175-180.

36. $[\alpha]^{25}_{D}$ reported for natural marineosin A was −101.7° (c 0.06, MeOH), whereas we observed $[\alpha]^{25}_{D}$ = + 138.7° (c 0.02, MeOH) for 10. Notably, $[\alpha]^{25}_{D}$ reported for marineosin B was +143.5° (c 0.09, MeOH), close to our value. Reynolds et al. firmly established marineosin A is biosynthesized from a C23-S precursor.[18] Absolute stereochemistry at C23 in our synthesis derives from (S)-propylene oxide (98% ee) and was confirmed in the X-ray structure of 26. We postulate natural marineosin A is dextrorotatory, identical to synthetic 10. [α] values for marineosins A and B were likely interchanged in ref. 17. Professor Fenical informed us his samples of natural marineosins have decomposed. We therefore synthesized the antipode of **17** from (R)-propylene oxide. The biological properties of both enantiomers will be examined.

37. Becke, A. D., Density-functional thermochemistry. III. The role of exact exchange. *Journal of Chemical Physics* **1993,** *58*, 5648-5652.

38. Lee, C.; Yang, W.; Parr, R. G., Development of the Colle-Salvetti correlation-energy formula into a functional of the electron density. *Physical Review B Condensed Matter* **1988,** *37* (2), 785-789.

39. Stephens, P. J.; Devlin, F. J.; Chabalowski, C. F.; Frisch, M. J., Ab Initio Calculation of Vibrational Absorption and Circular Dichroism Spectra Using Density Functional Force Fields. *The Journal of Physical Chemistry* **1994,** *98* (45), 11623-11627.

40. Vosko, S. H.; Wilk, L.; Nusair, M., Accurate spin-dependent electron liquid correlation energies for local spin density calculations: a critical analysis. *Canadian Journal of Physics* **1980,** *58* (8), 1200-1211.

41. Zhao, Y.; Truhlar, D. G., The M06 suite of density functionals for main group thermochemistry, thermochemical kinetics, noncovalent interactions, excited states, and transition elements: two new functionals and systematic testing of four M06-class functionals and 12 other functionals. *Theoretical Chemistry Accounts* **2008,** *120* (1), 215-241.

42. Macrae, C. F.; Sovago, I.; Cottrell, S. J.; Galek, P. T. A.; McCabe, P.; Pidcock, E.; Platings, M.; Shields, G. P.; Stevens, J. S.; Towler, M.; Wood, P. A., Mercury 4.0: from visualization to analysis, design and prediction. *Journal of Applied Crystallography* **2020,** *53* (1), 226-235.

43. Padwa, A.; Smolanoff, J.; Tremper, A., Intramolecular photochemical and thermal cyclization reactions of 2-vinyl substituted 2H-azirines. *Tetrahedron Letters* **1974,** *15* (1), 29-32.

44. Padwa, A.; Smolanoff, J.; Tremper, A., Photochemical transformations of small ring heterocyclic systems. LXV. Intramolecular cycloaddition reactions of vinyl-substituted 2H-azirines. *Journal of the American Chemical Society* **1975,** *97* (16), 4682-4691.

45. Padwa, A., Azirine photochemistry. *Accounts of Chemical Research* **1976,** *9* (10), 371-378.

46. *UV Atlas of Organic Compounds*. Springer Science+Business Media: New York, 1967; Vol. III, p. 183.

47. Arnold, Z.; Dvořák, D.; Havránek, M., Convenient Preparation of 1,3-Bis(dimethylamino)trimethinium Perchlorate, Tetrafluoroborate and Hexafluorophosphate. *Collection of Czechoslovak Chemhemical Communications* **1996,** *61* (11), 1637-1641.

48. Yamada, S.; Kaneko, C., Studies on the n-oxides of π-deficient n-heteroaromatics—XXX11Part XXIX. C. Kaneko, M. Yamamori, A. Yamamoto and R. Hayashi, Tetrahedron Letters 2799 (1978). This paper also forms Part VII of Studies on the Oxazepine Derivatives—VI: C. Kaneko, S. Kawai and M. Somei, Chemistry Letters submitted.: Photochemistry of acridine 10-oxides (2):2 synthesis and reaction of dibenz[c,f]-1,2-oxazepines. *Tetrahedron* **1979,** *35* (10), 1273-1278.

49. Kurihara, T.; Nasu, K.; Mizuhara, Y.; Hayashi, K., Reaction of 3-[3-(2-Nitrophenyl)-2-propenylidene]-2, 4-pentanedione with Hydroxylamine Hydrochloride. Formation of a 2-Chloromethyleneindolin-3-one. *Chemical & Pharmaceutical Bulletin* **1982,** *30* (8), 2742-2746.

50. Bellamy, F.; Streith, J., The Photochemistry of Aromatic N-Oxides. A Crystal Review. *Heterocycles* **1976,** *4* (8), 1391-1447.

51. Ishikawa, M.; Kaneko, C.; Yokoe, I.; Yamada, S., Photolysis of 2,6-dicyanopyridine 1-oxides. *Tetrahedron* **1969,** *25* (2), 295-300.

52. For previous syntheses of 1,3-oxazepines, see: (a) Kumagai, T.; Sawaura, M.; Kabuto, C.; Mukai, T., Organic photochemistry. 66. Photochemical reaction of 2-oxa-3-

azabicyclo[3.2.0]hepta-3,6-diene derivatives. *Nippon Kagaku Kaishi* **1984**, *1*, 158-164. (b) Kobayashi, T.; Nitta, M., The Reaction of (Z)-2-(3-Oxo-1-propenyl)-2H-azirine Derivative with Molybdenum Carbonyl Complexes. *Bulletin of the Chemical Society of Japan* **1985**, *58* (3), 1057-1058. (c) Kurita, J.; Iwata, K.; Tsuchiya, T., Synthesis of the first examples of fully unsaturated monocyclic 1,4-oxazepines. *Journal of the Chemical Society, Chemical Communications* **1986**, (15), 1188-1189.

53. Scaiano has postulated deoxygenation of pyridine N-oxide can occur via N-O homolysis to afford atomic oxygen. See Bucher, G.; Scaiano, J. C., Laser Flash Photolysis of Pyridine N-Oxide: Kinetic Studies of Atomic Oxygen [O(3P)] in Solution. *The Journal of Physical Chemistry* **1994**, *98* (48), 12471-12473.

54. Shimbayashi, T.; Sasakura, K.; Eguchi, A.; Okamoto, K.; Ohe, K., Recent Progress on Cyclic Nitrenoid Precursors in Transition-Metal-Catalyzed Nitrene-Transfer Reactions. *Chemistry – A European Journal* **2019,** *25* (13), 3156-3180.

# Chapter Two

*Characterization of Prodiginine–MicroRNA Interactions.*

## 2.1 Introduction.

MicroRNAs (miRNAs) are short, non-coding RNAs which play a significant role in post-transcriptional regulation of gene expression. The miRNA gene is transcribed to produce primary miRNA (pri-miRNA), which is cleaved within the nucleus by Drosha/DGCR8 to yield pre-miRNA (Figure 2.1.1). Nuclear export followed by cleavage of pre-miRNA by DICER affords a miR duplex, one strand of which is incorporated into a miR-induced silencing complex (miRISC). Binding of miRISC to its target mRNA results in translational suppression and/or mRNA degradation.[1] Dysregulation of miRNA expression is linked to human carcinogenesis;[2] counteracting these tumorigenic alterations inhibits cancer growth in vitro and in vivo.[3-5] This, and the propensity of pri- and pre-miRNAs to adopt discrete tertiary structures suggests they could be targeted by small molecule therapeutics. Of known oncogenic miRNAs, miR-21 figures prominently.[6-7] It is upregulated in many human cancers[8] and its knock-down induces apoptosis in multiple cancer cell lines.[9-15]

With miR-21 shown to be a desirable therapeutic target, there have been several studies aimed at identifying small molecules capable of inhibiting its production. One of the first small molecules identified to inhibit miR-21 maturation was streptomycin.[16] It was found to bind pre-miR-21 with moderate affinity and prevent processing by DICER. Though this was a substantial discovery at the time, the practicality of using aminoglycosides to therapeutically target miRNA is questionable due to their well-characterized side effects and predisposition to bind a multitude

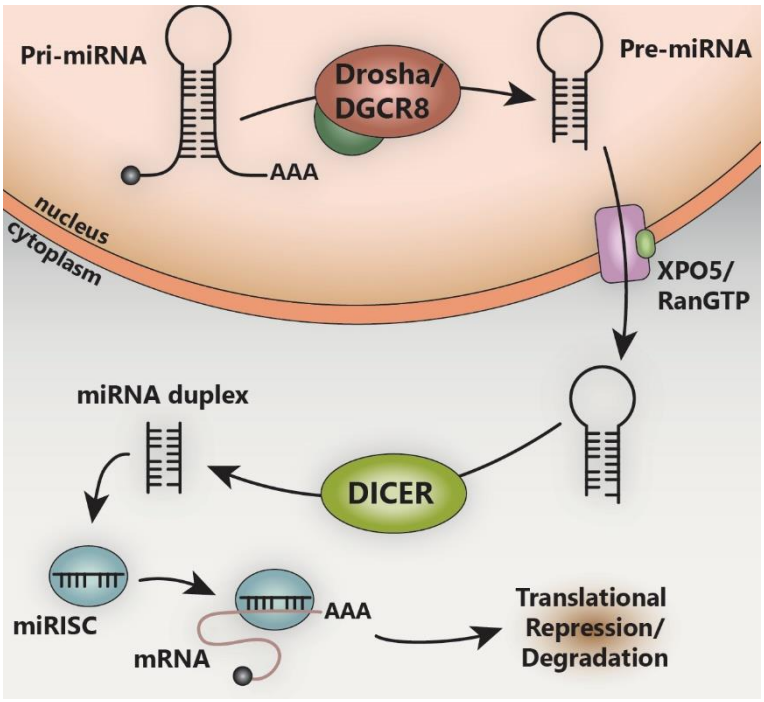


**Figure 2.1.1** miRNA negatively regulates protein expression in eukaryotes.

of RNA types.[17] Using small molecule microarrays, Connelly et al. found dibromocarbazole **1** (Figure 2.1.2) to bind pre-miR-21 within its DICER recognition site and inhibit its processing.[18] Analogs of **1** were screened, but binding affinity could not be increased; alterations to the carbazole moiety were not tolerated. Additionally, compounds of nearly identical structure were found to enhance neuron formation in the hippocampus of adult mice,[19] indicating development of **1** as a selective pre-miR-21 binder is likely to be impractical. An arginine-rich cyclic peptide (cyclo(RVRTRGKRRIRRpP)) has also been shown to bind to pre-miR-21 ($K_d$ = 200 nm).[20] For each of these three molecules, binding affinity was lost when the adenine 29 bulge (Figure 2.2.1a) was removed.

O'Keefe and coworkers at the NCI recently identified prodiginines butylcycloheptyl prodigiosin (**2**), prodigiosin (**3**), and obatoclax (**4**, Figure 2.1.2) as having high affinity for pre-miR-

21 ($K_d$ = 410, 160, and 9 nM, respectively) via a direct-binding assay using intrinsic fluorescence.[21] Obatoclax is one of the strongest pre-miR-21 binding small molecules discovered to-date. Moreover, **2** was found to prevent processing of pre-miR-21 by DICER *in vitro*. When cancer cells were treated with 50 nM **2**, miR-21 expression was decreased, upregulation of miR-21 target genes was detected, and a cytostatic effect was observed. We saw this as an appealing entry point into the rapidly growing field of RNA-targeting small molecules, as the Harran lab has extensive experience synthesizing prodiginine compounds.[22-23] To pursue the study of prodiginine–pre-miRNA interactions, we began a collaboration with Prof. Feng Guo of the UCLA Molecular Biology Institute, an expert in miRNA structural biology. Prof. Guo has developed a powerful technology wherein an RNA fragment is fused to a riboswitch-derived scaffold (YdaO, a c-di-AMP riboswitch) which can be readily crystallized.[24] The appended RNA is positioned within a large lattice cavity, allowing it to adopt a conformation representative of its solution structure. This technique has achieved resolutions of 2.7-3.0 Å, which is sufficient to allow us to observe the interaction between a small molecule and its miRNA target.

This project resides at the interface of organic chemistry and molecular biology, and is comprised of two interdependent goals:

1) Obtain a prodiginine-RNA co-crystal structure using YdaO scaffold-directed crystallography or another crystallographic technique.

2) Develop the prodiginine scaffold as a potent and selective pre-miR-21-targeting agent.

The following sections detail the progress made towards these goals during the latter part of my graduate career.

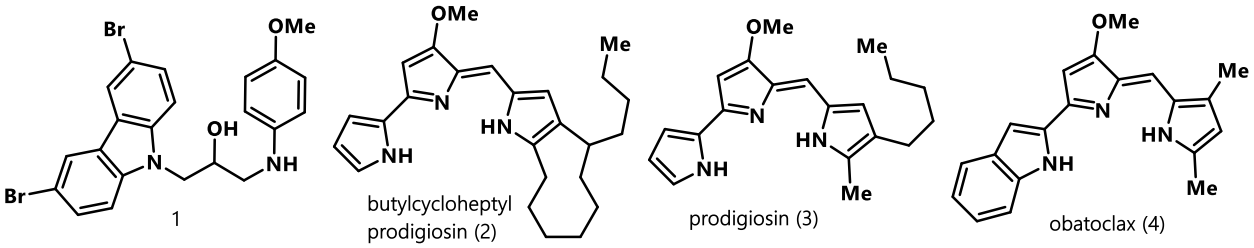


**Figure 2.1.2** Small molecule binders of pre-miR-21.

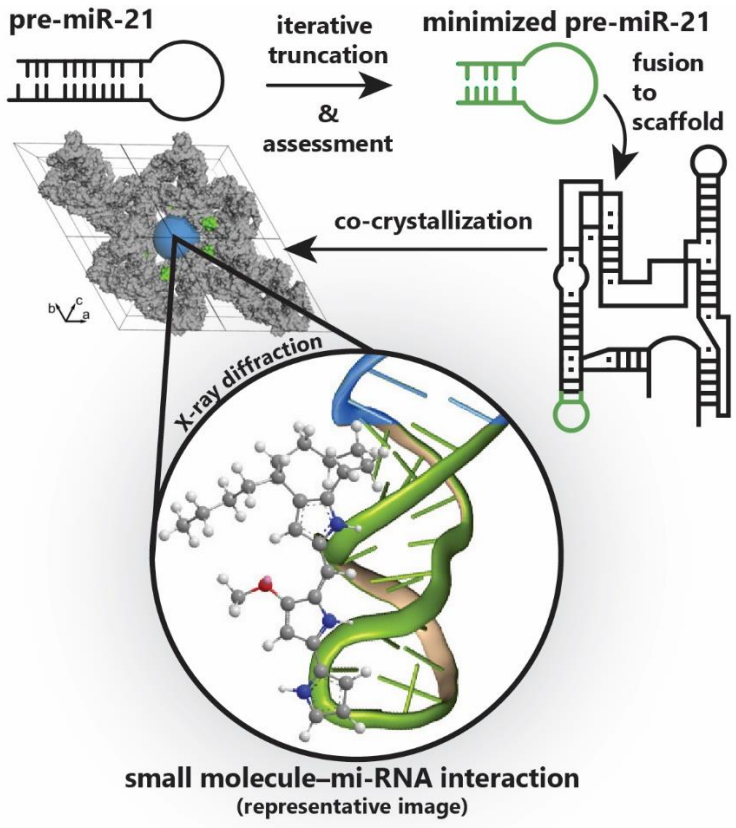


**Figure 2.1.3** Approach to a general method for small-molecule–RNA co-crystallization.

## 2.2 Characterizing the Interaction of Pre-miR-21 and Prodiginine Compounds.

I began by recapitulating O'Keefe's direct-binding assay wherein, upon binding to the target RNA, the prodiginine's fluorescence yield is increased *via* disruption of non-radiative decay pathways. A $K_d$ can then be determined by fitting a non-linear function to fluorescence data collected over a range of analyte concentrations. I used an RNA construct (pri-miR-21 63-mer; 63-mer; **I**, Figure 2.2.1) produced through *in vitro* transcription (IVT) as an analog of the pre-miR-21

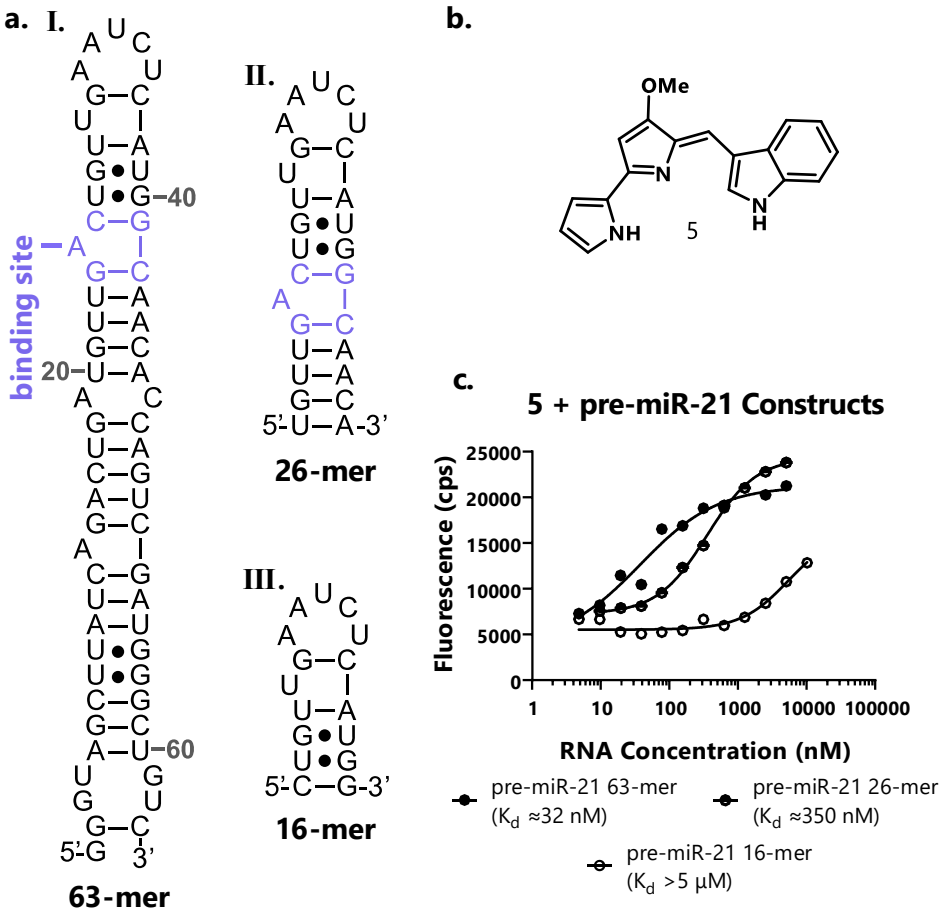


**Figure 2.2.1 a**. Pre-miR-21 63-mer **I** and truncated constructs **II** and **III**. **b**. **5** is one of the strongest known binders of pre-miR-21. **c**. Binding curves of **5** with pre-miR-21 constructs. Data is one replicate and $K_d$ values should be taken as approximate. $K_d$ values were calculated using GraphPad Prism 9.3.1 (sigmoidal, 4PL).

hairpin produced *in vivo*. Measuring the change in fluorescence of obatoclax mesylate (**4**) upon its titration into a 10 nM solution of 63-mer gave a $K_d$ which agreed with that published by O'Keefe.

Testing an initial set of easily-accessed analogs (compounds **5**, **9**, and **10**. See section 2.5) revealed **5** as the strongest binder and it was selected as our lead for further biochemical characterization. This assay was designed to conserve RNA by using repeatedly adding small molecule to a single RNA sample. While successful in this regard, the methodology suffered from a marked decrease in fluorescence signal strength over time. This effect was strong enough that I could not be confident that equilibrium was established between the RNA's bound and unbound states. The decay in signal strength likely results from aggregation of the prodiginines; aqueous, buffered solutions of **4** produced a pink precipitate after standing for 60 minutes (see Figure 2.6.1). To counteract this, I chose to instead vary the RNA concentration while keeping the concentration of **5** low. Although this method consumed larger quantities of RNA, the fluorescence signal was stable and accurate $K_d$ values could be calculated.

With a reliable assay established, I designed experiments to determine the location of pre-miR-21's prodiginine binding site. Truncated constructs 26-mer (**II**) and 16-mer (**III**) were evaluated for binding activity. **II** was bound by **5**, though with somewhat reduced affinity, and **III** displayed an affinity of greater than 5 μM. These experiments indicated that the residues differing between the 16- and 26-mer constructs were necessary for binding. Notably, this region contains the same A-bulge crucial to other small molecule binding interactions.[18,20] These data gave us enough confidence to proceed with further studies.

## 2.3 Synthesis and Attempted Crystallization of YdaO Constructs Bearing a Prodiginine Binding Site.

With the prodiginine binding site of pre-miR-21 identified, the next goal was to design and synthesize YdaO scaffolds bearing the receptor. The P2 hairpin was chosen as a starting point as it had been proven amenable to engineering in previous work performed by Guo lab.[24] The same work had determined P2 could be replaced by up to nine residues. Based on this constraint, I designed three initial constructs (**IV**-**VI**, Figure 2.3.1b). The first incorporated a bare-minimum 5-residue binding site and $GA_3$ loop, while the second and third included an additional base-pair, either apical or basal to the binding motif. I synthesized these constructs using mutagenic PCR amplification of the wild-type YdaO template followed by *in vitro* transcription and purification. Gratifyingly, **5** strongly bound scaffold **V** and did not bind to WT YdaO RNA, indicating that the grafted pre-miR-21 fragment is sufficient for binding and the fusion faithfully recapitulates the prodiginine binding site (Figure 2.3.2).

Using crystallization conditions established in prior work,[24] I screened the new constructs for crystallinity with and without **5** present. One major challenge was maintaining solubility of **5** under the optimal YdaO crystallization conditions. Prodiginines are weakly basic ($pK_a$ ~7.4)[25] and are most soluble in acidic buffers. The YdaO crystallization conditions are slightly alkaline (pH 7.4) and do not solubilize **5** well. To accommodate the small molecule, I opted to add 1% DMSO or 1%-15% 1-methyl-1,4-pentanediol (MPD) to the crystallization slution. Despite numerous attempts, these P2 constructs failed to produce crystals in the presence of **5** or on their own.

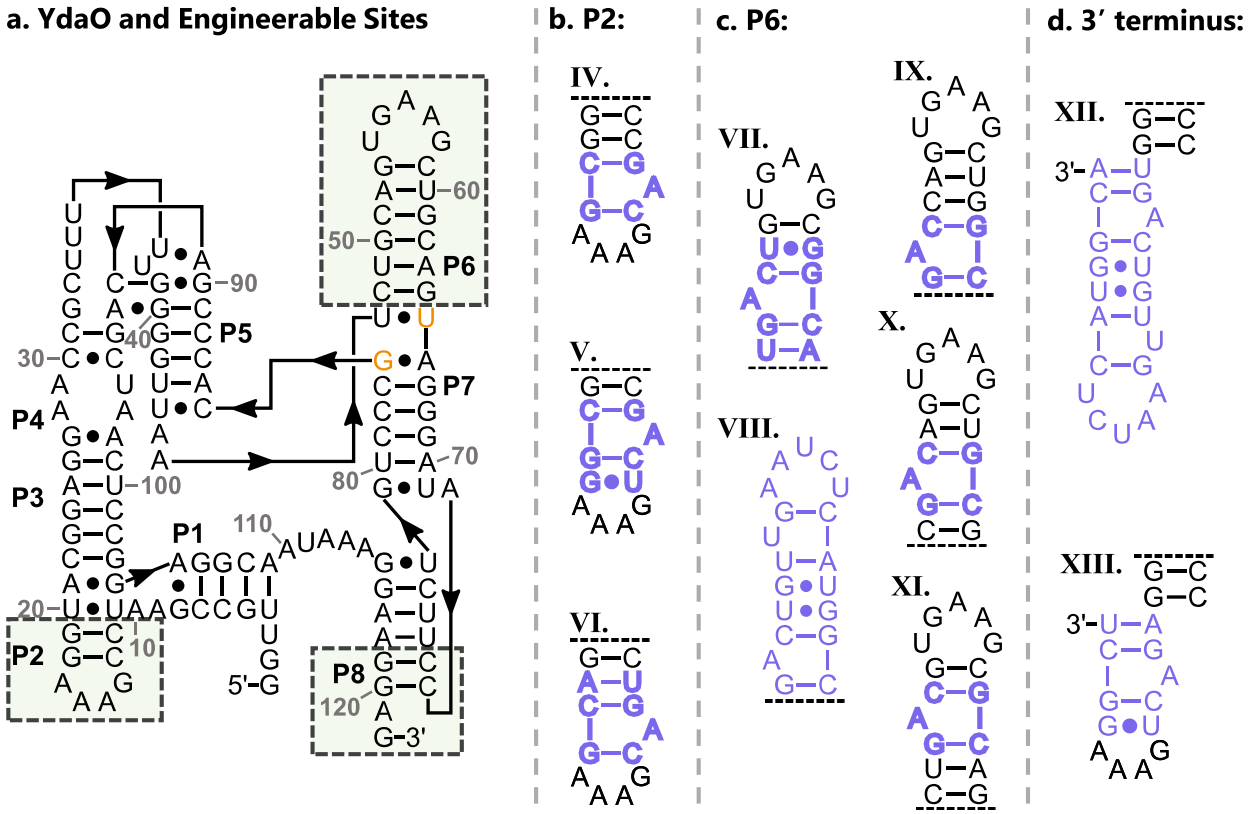


**Figure 2.3.1** Schematic depiction of YdaO indicating engineerable sites and specific constructs synthesized.

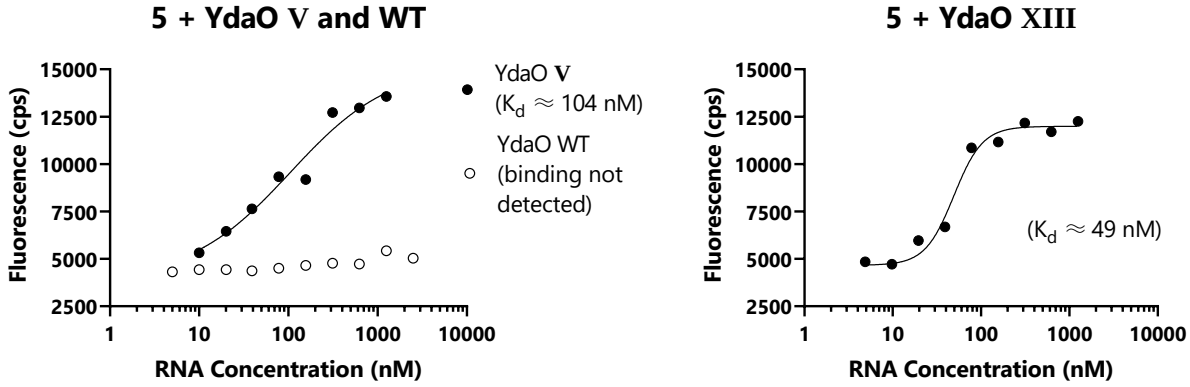


**Figure 2.3.2** Binding curves of **5** with YdaO constructs. Data is one replicate and $K_d$ values should be taken as approximate. $K_d$ values were calculated using GraphPad Prism 9.3.1 (sigmoidal, 4PL).

Another set of constructs I developed engaged YdaO's P6 hairpin. Prior unpublished work in the Guo lab had discovered (using *in crystallo* selection methodology[26]) a crystallizable YdaO bearing two mutations (U65A, G84U, Figure 2.3.1a, orange residues) which changed the angle of P6 and disengaged the hairpin from neighboring molecules within the crystal lattice. Because P6 was no longer crucial for crystal formation, I postulated that larger pieces of RNA could be grafted to this site. Initial attempts to synthesize constructs **VII** and **VIII** using overlap-extension PCR failed to produce an IVT template of useable purity. Instead, I designed several more-conservative constructs (**IX**-**XI**, Figure 2.3.1b) and prepared the RNA from commercially synthesized DNA templates. These scaffolds were screened for crystallization in a 96-well hanging drop format using the optimized conditions (see SI), but did not form crystals.

Finally, I designed a third set of constructs bearing a hairpin appended to the 3′ end (**XII** and **XIII** Figure 2.3.1c). I considered this design feasible as the unpaired 3′ residues in WT YdaO dangle into the large lattice cavity and could theoretically accommodate large pieces of RNA without disrupting crucial lattice contacts. These constructs were based on a reliably crystalline YdaO construct bearing the apical loop of pre-miR-378a at P2 and were produced using mutagenic PCR followed by IVT. As with the preceding constructs, these did not produce any crystals. While unfortunate, the lack of crystal formation across the above constructs is not entirely surprising; Guo lab's previous work indicated a crystallization-rate of ~20%. Future attempts to crystallize YdaO bearing a small molecule binding site are likely to succeed if a large number of constructs can be generated.

## 2.4 Additional Prodiginine-RNA Co-Crystallization Constructs.

In addition to YdaO scaffolds, I designed several other types of small molecule co-crystallization constructs. The first is pictured in Figure 2.4.1a (**XIV**). Two RNA strands are annealed together to produce pre-miR-21's prodiginine binding site with a 5'-UA overhang on either strand. These overhangs can base pair, allowing tessellation of the RNA duplex and thus facilitating crystal growth. This technique has been used previously with good success.[27] I purchased the two RNA strands, annealed them, and set up a sparse-matrix crystallization screen containing either equi- or super-stoichiometric **5**. This construct formed crystalline needles across many wells, but gave best results at 475 μM in 40 mM cacodylate buffer pH 7.0 containing 12 mM spermine, 80 mM NaCl, 1.9 mM **5**, 2.5% DMSO, and 30% MPD. I then designed constructs **XV** and **XVI** bearing an additional G-C pair at either the top or bottom of the duplex with the aim of stabilizing the duplex. **XV** has produced small plates and is being optimized to produce larger crystals.

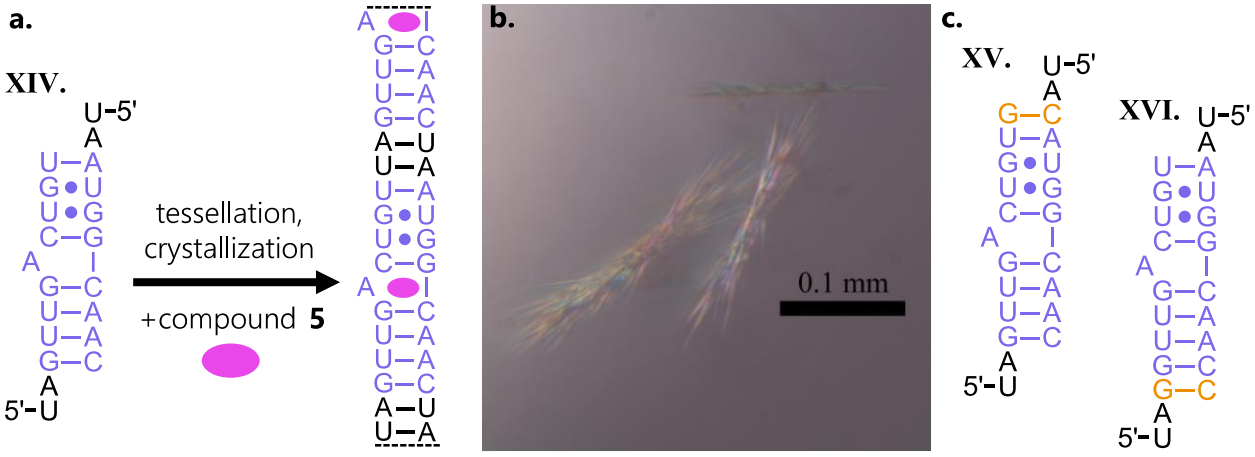


**Figure 2.4.1** a. Original tessellating construct design. b. Image of needles produced from construct **XIV**. **c**. Constructs derived from **XIV**.

## 2.5 Exploring the Structure-Affinity Relationship in Prodiginine–RNA Interactions.

Obatoclax is one of the strongest small molecule binders of pre-miR-21 known. This compound was originally developed as an anti-cancer agent, but failed in a phase II clinical trial due to off-target toxicity. Off-target pathways include copper-mediated production of reactive oxygen species[28] and membrane depolarization via anion transport.[29-30] These pathways likely arise from two properties of the prodiginine skeleton: 1. Freebase prodiginines readily coordinate metal cations, becoming redox-active after doing so (Figure 2.5.1a).[28, 31-32] 2. Protonated prodiginines are membrane-permeable and readily bind chloride,[33] bicarbonate,[30] methylsulfonate,[34] and diethyl phosphate anions (Figure 2.5.1a, c). It is therefore critical to balance the scaffold's ion-binding properties during structure-affinity optimization, given that it is likely an electrostatic attraction between the protonated prodiginine scaffold and the miRNA's phosphodiester backbone constitutes a driving force for binding (Figure 2.5.1b).

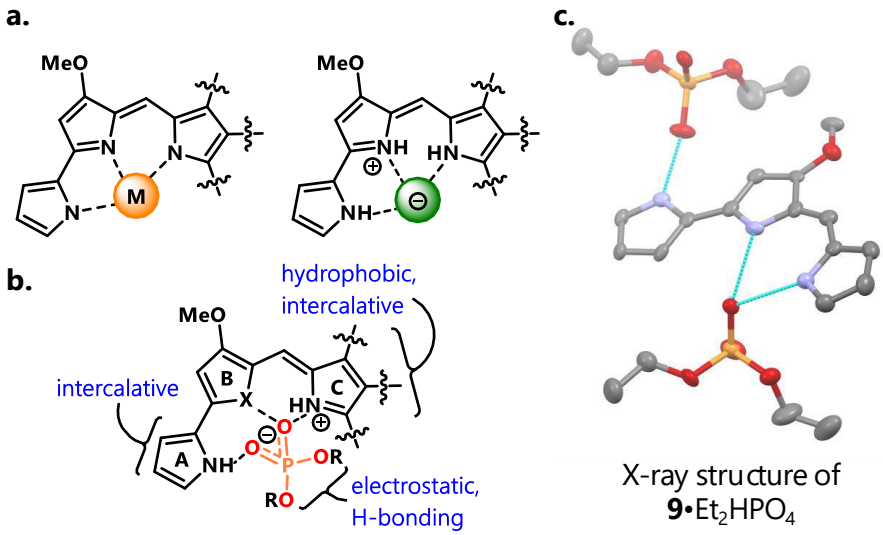


**Figure 2.5.1 a**. Binding modes of prodiginines to metal cations and anions. **b**. Postulated binding mode of prodiginines to RNA. **c**. Crystal structure of **9**•$Et_2HPO_4$. Atoms are displayed as 50% probability thermal ellipsoids.

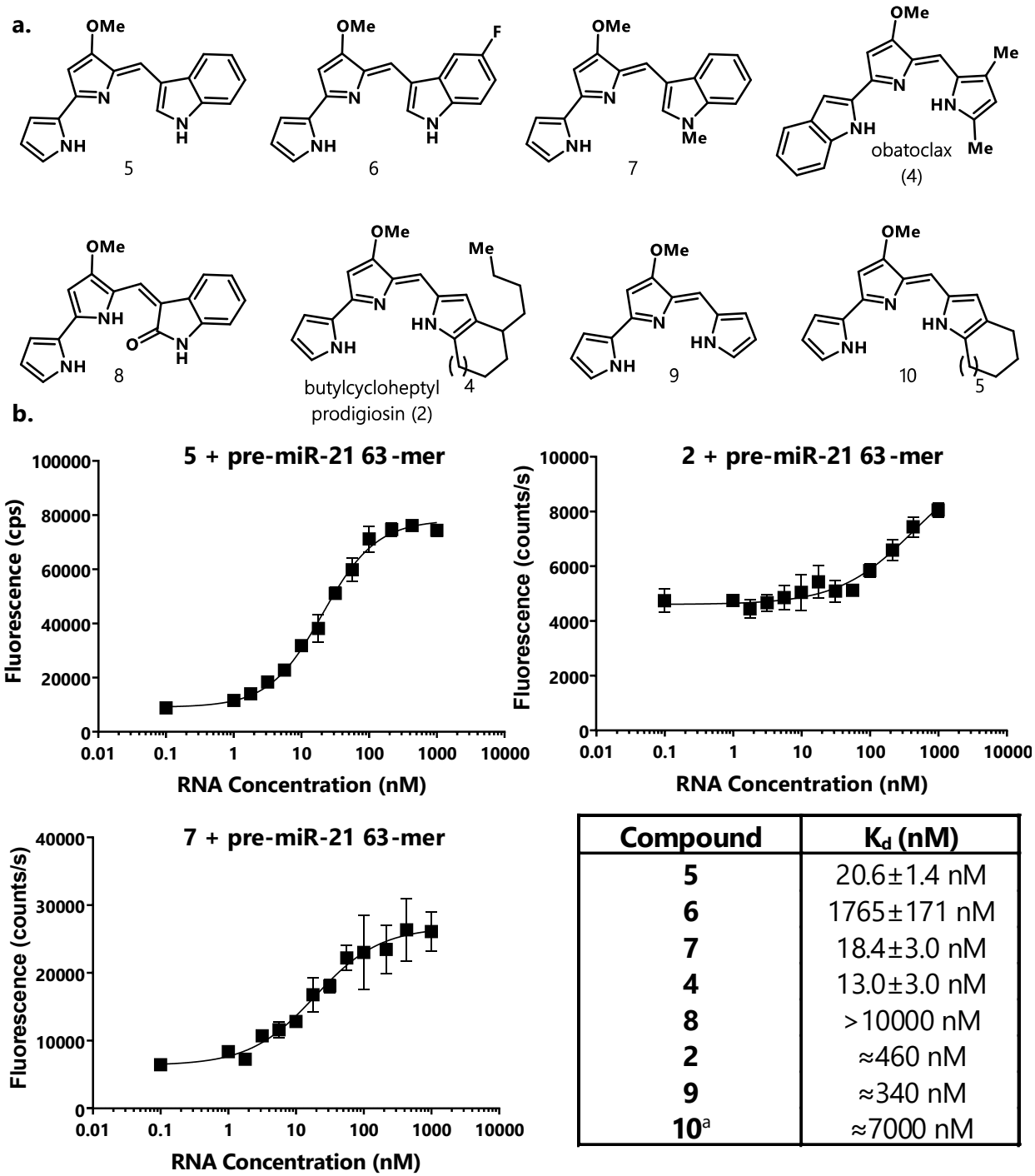


| Compound | $K_d$ (nM) |
|---|---|
| **5** | 20.6±1.4 nM |
| **6** | 1765±171 nM |
| **7** | 18.4±3.0 nM |
| **4** | 13.0±3.0 nM |
| **8** | >10000 nM |
| **2** | ≈460 nM |
| **9** | ≈340 nM |
| **10**[a] | ≈7000 nM |

**Figure 2.5.2 a**. Small molecules assayed for binding to pre-miR-21 63-mer. **b**. Binding curves for **5**, **2**, and **7** and tabulated $K_d$ values for all molecules in panel **a**. [a] $K_d$ derived from a single replicate. All others are three independent replicates; error bars indicate one standard deviation.

Maintaining or increasing ionizability may be key to optimizing the scaffold, though it is not straightforward to do so while preventing metal binding and transmembrane anion shuttling. Analogs wherein X=O (2.5.1b) could prevent $Cu^{2+}$ chelation,[31] but would reduce the compound's basicity. An alternative strategy would be to disrupt the scaffold's dipyrrin motif through altering connectivity on the C ring. **5** is an example of such a compound and has strong affinity for pre-miR-21 63-mer nearly identical to that of obatoclax. This compound and the others listed in Figure 2.5.2 were assayed using the procedure outline in section 2.2. Compounds **6** and **8** were also assayed using a modified procedure where small molecule concentration was varied and new solutions were produced for each measurement. This minimized the likelihood of small molecule aggregation.

Interestingly, fluorinating the indole's 5 position (**6**) drastically reduced binding affinity, while *N*-methylation reduced affinity only slightly (**7**). Weakly basic oxindole **8**'s affinity could not be measured, suggesting that the scaffold's cationic nature is indeed important. Butylcycloheptyl prodigiosin's (**2**) affinity reflected the previously reported value,[21] and the bare prodiginine scaffold **9** bound with similar affinity. Increasing the alkyl bulk on ring C is detrimental, as demonstrated by **10**. From these examples it is clear that the binding affinity is very sensitive to C-ring substitution and that the substrate may be participating in pi-stacking interactions. Further analysis of the structure-affinity relationship will require a larger variety of prodiginine analogs. An interesting route to explore would be to replace ring A with non-coordinating arenes. This would disrupt Cu-binding activity[35] but preserve the basic dipyrrin motif. Synthesis of these compounds should be straightforward using established procedures.[36]

## 2.6 Supporting Information

### General Methods

Unless otherwise specified, all manipulations of biochemical reagents were carried out using sterile technique in a nuclease-free environment. All water used to prepare solutions was twice deionized and all solutions were sterilized by passage through a 0.22 μM PES filtration membrane prior to use. Reagents (including fine chemicals, synthetic oligonucleotides, and recombinant proteins) were purchased from commercial vendors and used as received. PCR was performed using Phusion DNA polymerase (New England Biolabs) under the manufacturer's recommended conditions and cycle count. Anion-exchange chromatography was performed using an ÄKTA Prime chromatography system equipped with a HI-Trap Q anion exchange column. Preparative tube-gel electrophoresis was performed using a Biorad 491 Tube Gel Apparatus (4% denaturing polyacrylamide) and an ÄKTA chromatography system. All small molecules were stored at -20 °C at 10 mM in DMSO. Dilutions were freshly prepared and discarded immediately after use.

Tetrahydrofuran (THF) and 1,2-dimethoxy ethane (DME) were passed through a Glass Contour solvent drying system. Thin-layer chromatography (TLC) was conducted on pre-coated plates (Sorbent Technologies, silica gel 60 PF254, 0.25 mm) and visualized with UV 254 nm. For acid-sensitive compounds, TLC plates were neutralized with TEA/Hexane (1%) before use. Column chromatography was performed on silica gel 60 (SiliCycle, 240−400 mesh) or neutral aluminum oxide (Sigma-Aldrich, 40-160 μm, Brockmann I). For acid-sensitive compounds, silica gel was premixed with TEA/Hexane (1%) before being loaded into the column. NMR spectra were

recorded on a Bruker Avance spectrometer $^{1}H$: 500 $^{13}C$: 126 MHz. Chemical shifts are reported in ppm and referenced to residual internal solvents: $CHCl_3$ $^{1}H$ (δ 7.26), $^{13}C$ (δ 77.2); acetone $^{1}H$ (δ 2.05), $^{13}C$ (δ 29.8); acetic acid $^{1}H$ (δ 2.08), $^{13}C$ (δ 177.2). Deuterated chloroform used in NMR experiments was neutralized prior to sample dissolution via passage through a plug of neutral alumina. UV-Vis spectra were obtained using a Shimadzu UV3101PC UV-Vis-NIR Scanning Spectrophotometer. Fluorescence measurements were conducted using a Jobin Yvon Horiba FluoroMax-3 fluorimeter. UV-Vis and Fluorescence data were exported as text files and worked-up in OriginPro 9.1. Non-linear regression fits used to determine $K_d$ values were calculated using GraphPad Prism 9.3.1. Crystal structures were rendered in Mercury 2022.1.

**General Procedure for *In vitro* Transcription**

Transcription reactions contained ~400 µg (45 nM) DNA template, 40 mM Tris pH 7.5, 25 mM $MgCl_2$, 4 mM DTT, 2 mM spermidine, 0.7 mg T7 RNA polymerase, and 3 mM each NTP in a total volume of 5 mL. The reaction was incubated at 37°C for 2-3 hours. Reactions were ethanol precipitated and purified using tube-gel electrophoresis. Fractions containing the RNA product were concentrated in an Amicon Ultra-15 centrifugal filter unit with 30-kDa molecular weight cutoff. RNA was buffer-exchanged three times into 10 mM NaHEPES pH 7.0 and concentrated to ~50 µL final volume.

**Analytical Polyacrylamide Gel Electrophoresis**

For native gel electrophoresis, RNA was mixed with a 2X loading dye containing 40 mM Tris pH 7.0, 50 mM KCl, 5 mM $MgCl_2$, 20% (v/v) glycerol, and xylene cyanol, and analyzed on a 10% polyacrylamide gel with 1x Tris-borate buffer containing 90 mM Tris base, 90 mM boric acid, and 2 mM EDTA. The gel was stained with Sybr Green II and imaged on a Fotodyne, 2MPix monochrome Analyst® Express system.

Denaturing gel electrophoresis was performed as above using a denaturing 2X loading dye containing 0.5x Tris-borate buffer, 10 M urea, and xylene cyanol, and was analyzed on a 10% polyacrylamide gel containing urea with 1x Tris-borate as running buffer.

**YdaO Transcription Template Synthesis**

Transcription templates for YdaO constructs **I**, **II**, and **III** were produced using a two-round PCR sequence. First-round products from a 50-µL PCR reaction were purified by 2% agarose gel electrophoresis and second-round products from a 2-mL PCR reaction were purified *via* anion-exchange chromatography. Both rounds used the same reverse primer bearing 2′-*O*-methylation on the two 5′ residues to reduce un-templated nucleotide addition by T7 RNA polymerase.[37] In the first round, a forward primer containing residues corresponding to the desired P2 mutant was used to amplify a WT YdaO template. The second round used a common forward primer to introduce a complete T7 promoter sequence and EcoRI cut site. Bolded residues indicate WT YdaO, underlined residues indicate an engineered P2 hairpin, and italic residues indicate the T7 promoter sequence. "m_" indicates a 2′-*O*-methylated residue.

Common reverse primer:

5′- m**C**m**UCCTTCCTTTATTGCCTCC**-3′

Round 1 forward primers:

5′-*ACTATA**GG***TTGCCGAATCCGACGAAAGC**GGTACGGAGGAACCGCTTTTTG**-3′ (construct **I**)

5′-*ACTATA**GG***TTGCCGAATCGACTGAAAGGC**GTACGGAGGAACCGCTTTTTG**-3′ (construct **II**)

5′-*ACTATA**GG***TTGCCGAATCTGACGAAAGCA**GTACGGAGGAACCGCTTTTTG**-3′ (construct **III**)

Round 2 forward primer:

5′-GCAGAATTC*TAATACGACTCACTATA**GG***TTGCCGAATC-3′

Transcription templates for YdaO constructs **IV**, **V**, and **VI** were purchased as gene blocks and PCR-amplified using common forward and reverse primers. The products were purified using anion-exchange chromatography.

Common reverse primer:

5′- m**C**m**UCCTTCCTTTATTGCCTCC**-3′

Common forward primer:

5′-*TAATACGACTCACTATA**GG***-3′

Transcription templates for YdaO constructs **X** and **XI** were produced using a two-round PCR sequence. First-round products were purified by 2% agarose gel electrophoresis and second-round products were purified *via* anion-exchange chromatography. Both rounds used the same forward primer. The starting template was a YdaO template containing a T7 promoter sequence and a P2 hairpin replaced by the apical loop of pri-miR-378a (5′-CCTAGAA-3′). The first round used a reverse primer containing the desired hairpin attached to the 3′ end of YdaO. The second round used a shorter version of the first-round reverse primer bearing 2′-*O*-methylation on the two 5′ residues. Bolded residues indicate WT YdaO, underlined residues indicate an engineered 3′ hairpin, and italic residues indicate the T7 promoter sequence. "m_" indicates a 2′-*O*-methylated residue.

Round 1 reverse primers:

5′- AGCCTTTCGGTCT**CCTTCCTTTATTGCCTCC**-3′ (construct **X**)

5′- AGCCATGAGATTCAACAGTCT**CCTTCCTTTATTGCCTCC**-3′ (construct **XI**)

Round 2 reverse primers:

5′-mAmGCCTTTCGGTCT**CCTTC**-3′ (construct **X**)

5′-mAmGCCATGAGATTCAACAG-3′ (construct **XI**)

Common forward primer:

5′-*TAATACGACTCACTATA**GG***-3′

**RNA Crystallization Screening Conditions**

YdaO Scaffolds:

A solution containing 0.15-0.3 mM RNA, 1 mM c-di-AMP, 100 mM KCl, 10 mM $MgCl_2$, and 20 mM NaHEPES pH 7.4 was heated to 90°C for 1 min, snap cooled on ice, and equilibrated for 15 min at 37°C immediately prior to crystallization. If a small molecule was included, it was added at the start of equilibration. Screening was conducted in 96-well plates with 300 nL hanging drops. Well solutions were a matrix of 1.5-2.1 M $(NH_4)_2SO_4$ (0.05 M increments) and 0.2-0.3 M $Li_2SO_4$ (0.0125 M increments) in 100 mM NaHEPES pH 7.4.

Other RNA constructs:

A solution containing 0.15-0.5 mM RNA in 10 mM NaHEPES pH 7.0 was heated to 90 °C for 1 minute then plunged into ice. The small molecule was added and the solution was allowed to incubate at room temperature for 15 minutes. Screens were performed in a 96-well plate using the commercial NATRIX sparse-matrix screen (Hampton Research).

**Fluorescence Binding Measurements**

All fluorescence emission data was collected at 560 nm with excitation at 515 nm. All binding experiments were conducted in 10 mM NaHEPES pH 7.0.

Titration of RNA into small molecule solutions (for compounds with $K_d$ < 1000 nM):

10x RNA stock solutions in 10 mM NaHEPES pH 7.0 were prepared according to Table 2.6.1 and were heated to 90 °C for 2 minutes then plunged into ice. 1x RNA solutions containing 10 nM small molecule in 10 mM NaHEPES pH 7.0 were prepared individually and incubated for 1 minute at room temperature immediately before measurement. For measurements involving a YdaO scaffold, the RNA was folded according to the procedure given in the crystallization screening experimental. Experiments were performed in triplicate unless otherwise specified.

| 10x Stock Solution (nM) | 1x Experimental Solution (nM) |
|---|---|
| 10000 | 1000 |
| 4310 | 431 |
| 2150 | 215 |
| 1000 | 100 |
| 562 | 56.2 |
| 316 | 31.6 |
| 178 | 17.8 |
| 100 | 10 |
| 56 | 5.6 |
| 32 | 3.2 |
| 18 | 1.8 |
| 10 | 1 |
| 1 | 0.1 |

**Table 2.6.1**

Titration of small molecules into RNA solutions (for compounds with $K_d$ > 1000 nM):

10x small molecule stock solutions in DMSO were prepared according to Table 2.6.2. 1x small molecule solutions containing 10 nM snap-cooled RNA in 10 mM NaHEPES pH 7.0 were prepared individually and were incubated for 1 minute at room temperature immediately before measurement. Experiments were performed in triplicate unless otherwise specified.

| 10x Stock Solution (nM) | 1x Experimental Solution (nM) |
|---|---|
| 100000 | 10000 |
| 43100 | 4310 |
| 21500 | 2150 |
| 10000 | 1000 |
| 5620 | 56.20 |
| 3160 | 31.60 |
| 1780 | 17.80 |
| 1000 | 100 |
| 560 | 5.60 |
| 320 | 3.20 |
| 180 | 1.80 |
| 100 | 10 |
| 10 | 1 |

**Table 2.6.2**

To determine $K_d$ values, the triplicate fluorescence data was normalized to [0, 1] then fitted with a non-linear regression (sigmoidal, 4PL; Y=Bottom+(Top-Bottom)/(1+($K_d$/X)^HillSlope)). Error bars indicate standard error of the mean for three independent replicates and $K_d$ error is given as one standard deviation.

To assess the stability of obatoclax's (**4**) fluorescence signal, a 10 nM solution of pre-miR-21 63-mer was treated with 430 nM **4** and fluorescence readings were taken every 2 minutes.

**Figure 2.6.1** Time course of fluorescence of **4** complexed to pre-miR-21 63-mer.

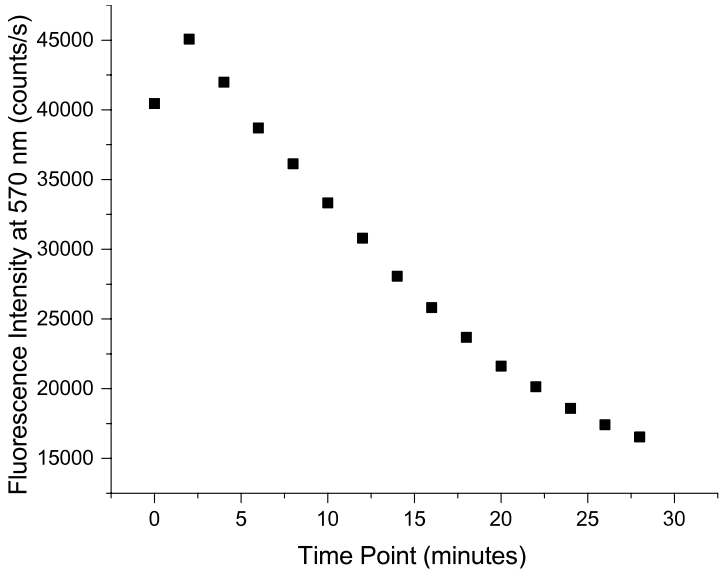


**Figure 2.6.2** Binding Curve of **5** and pre-miR-21 63-mer.

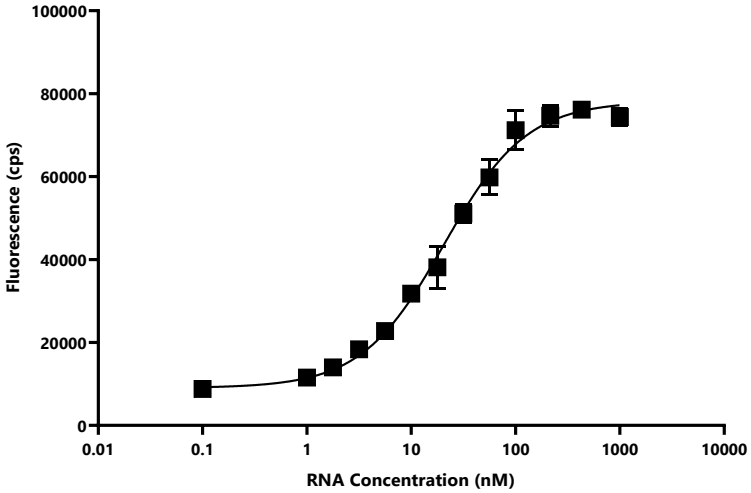


| Goodness of Fit | |
|---|---|
| Degrees of Freedom | 38 |
| R squared | 0.6713 |
| Sum of Squares | 1979803 |
| Sy.x | 228.3 |

$K_d$=20.6±1.4 nM

**Figure 2.6.3** Binding Curve of **6** and pre-miR-21 63-mer.

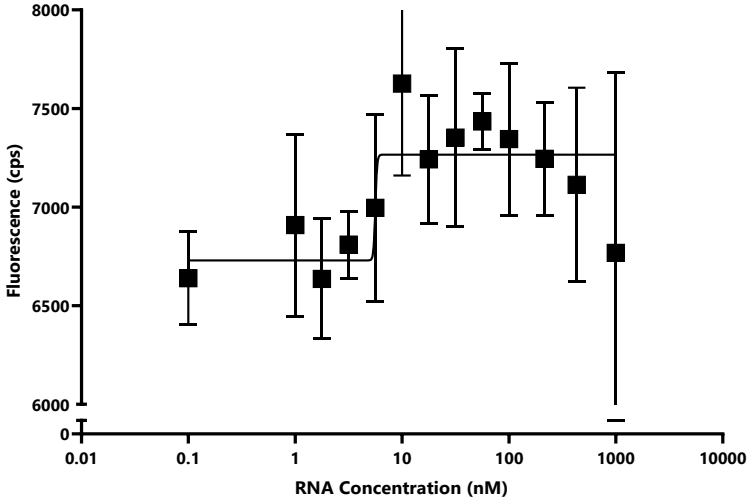


| Goodness of Fit | |
|---|---|
| Degrees of Freedom | 38 |
| R squared | 0.2901 |
| Sum of Squares | 6518900 |
| Sy.x | 414.2 |

Binding not detected

**Figure 2.6.4** Binding Curve of **6** and pre-miR-21 63-mer (variable small molecule concentration).

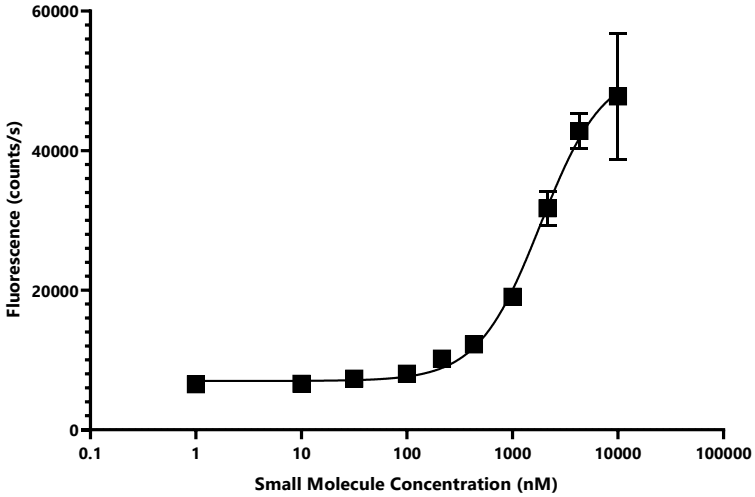


| Goodness of Fit | |
|---|---|
| Degrees of Freedom | 29 |
| R squared | 0.9716 |
| Sum of Squares | 210416797 |
| Sy.x | 2694 |

$K_d$=1765±171 nM

**Figure 2.6.5** Binding Curve of **7** and pre-miR-21 63-mer.

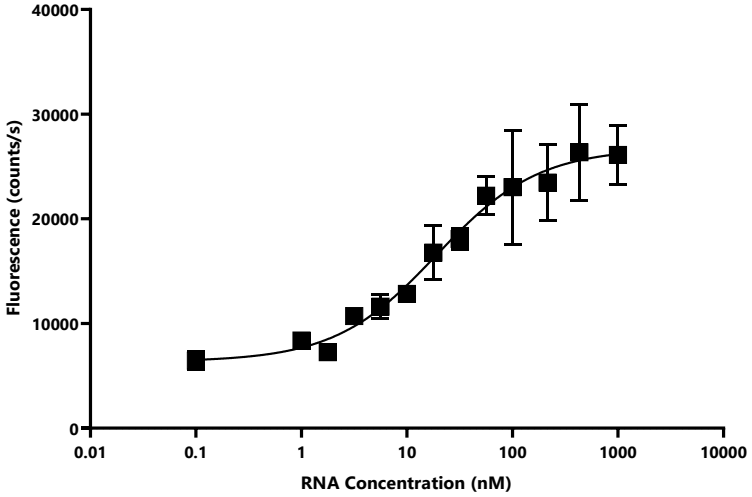


| Goodness of Fit | |
|---|---|
| Degrees of Freedom | 38 |
| R squared | 0.9174 |
| Sum of Squares | 196190018 |
| Sy.x | 2272 |

$K_d$=18.4±3.0 nM

**Figure 2.6.6** Binding Curve of **4** and pre-miR-21 63-mer.

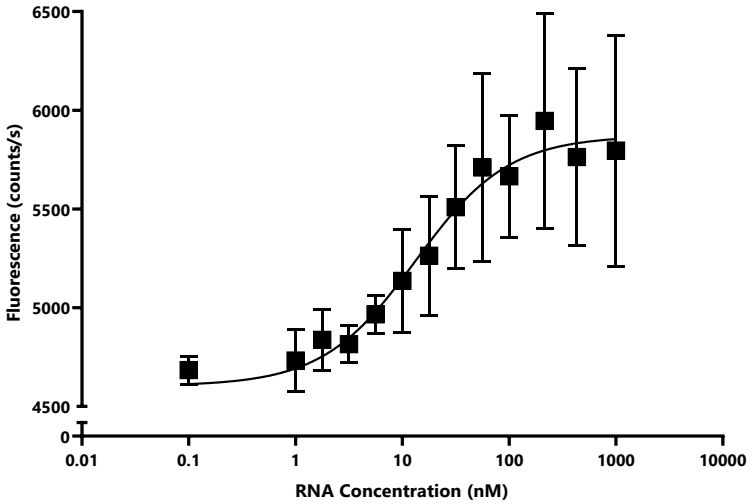


| Goodness of Fit | |
|---|---|
| Degrees of Freedom | 38 |
| R squared | 0.7398 |
| Sum of Squares | 3229734 |
| Sy.x | 291.5 |

$K_d$=13.0±3.0 nM

**Figure 2.6.7** Binding Curve of **8** and pre-miR-21 63-mer.

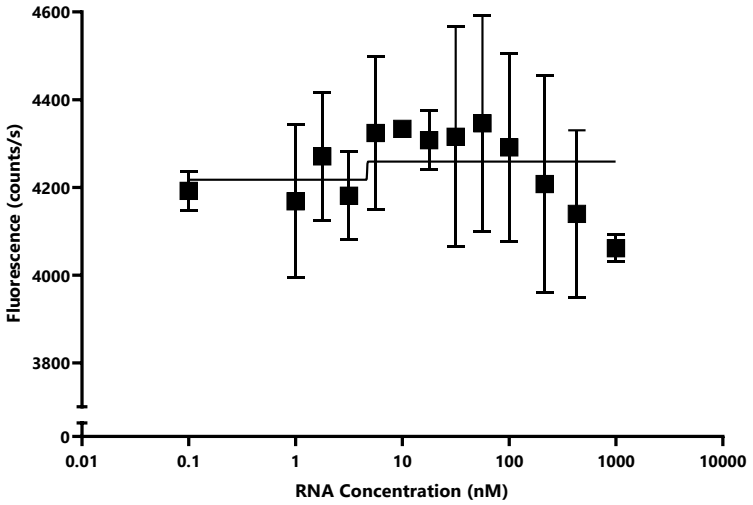


| Goodness of Fit | |
|---|---|
| Degrees of Freedom | 38 |
| R squared | 0.02086 |
| Sum of Squares | 1000002 |
| Sy.x | 162.2 |

Binding not detected

**Figure 2.6.8** Binding Curve of **8** and pre-miR-21 63-mer (variable small molecule concentration).

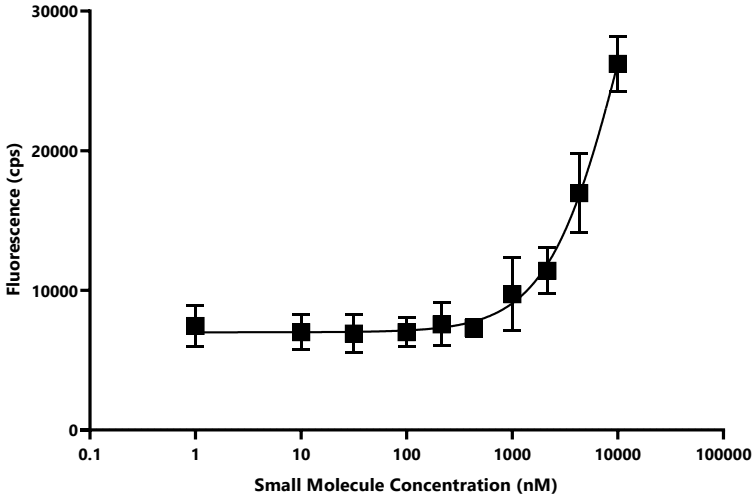


| Goodness of Fit | |
|---|---|
| Degrees of Freedom | 29 |
| R squared | 0.9399 |
| Sum of Squares | 70712881 |
| Sy.x | 1562 |

$K_d$ > 10000 nM

**Figure 2.6.9** Binding Curve of **2** and pre-miR-21 63-mer.

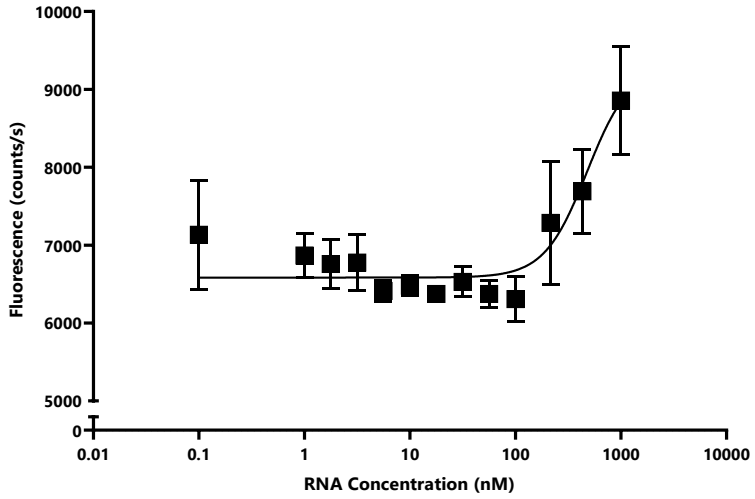


| Goodness of Fit | |
|---|---|
| Degrees of Freedom | 38 |
| R squared | 0.6879 |
| Sum of Squares | 7588961 |
| Sy.x | 446.9 |

$K_d \approx 460$ nM

**Figure 2.6.10** Binding Curve of **9** and pre-miR-21 63-mer.

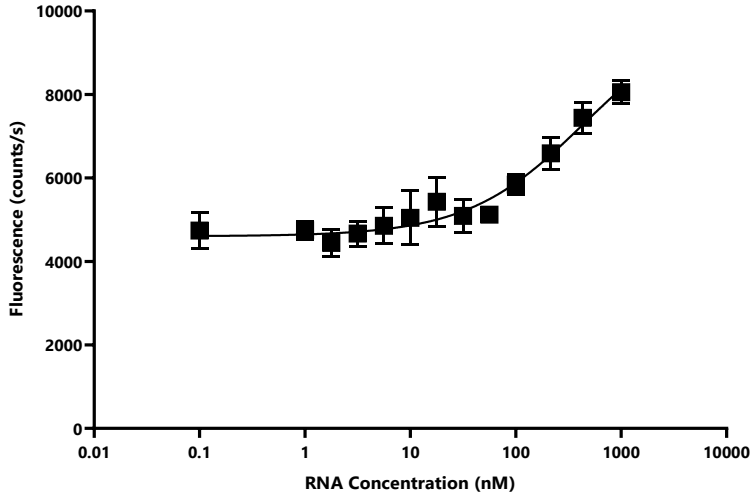


| Goodness of Fit | |
|---|---|
| Degrees of Freedom | 38 |
| R squared | 0.8951 |
| Sum of Squares | 5701120 |
| Sy.x | 387.3 |

$K_d \approx 339$ nM

**Figure 2.6.11** Binding Curve of **10** and pre-miR-21 63-mer (variable small molecule concentration).

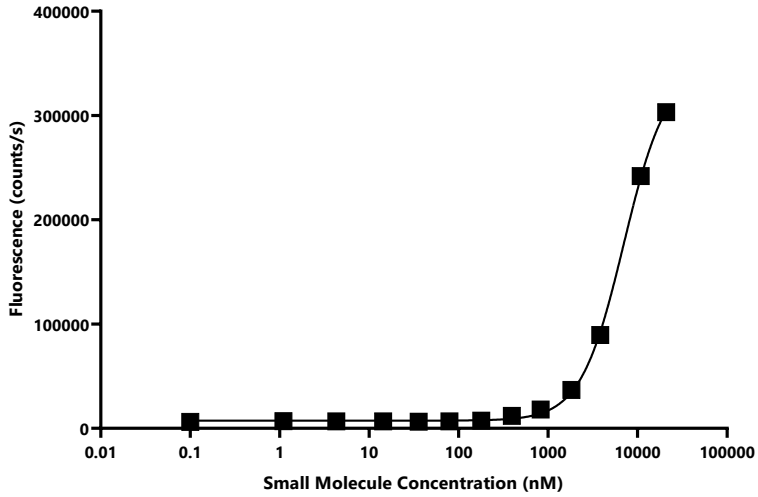


| Goodness of Fit | |
|---|---|
| Degrees of Freedom | 10 |
| R squared | 0.9996 |
| Sum of Squares | 45643109 |
| Sy.x | 2136 |

$K_d \approx 7000$ nM

These data are a single replicate.

**Small Molecule Synthesis**

General synthesis for compounds **5**-**7**:

To 4-methoxy-1H,1'H-[2,2'-bipyrrole]-5-carbaldehyde (1 eq.) and the corresponding indole (2 eq.) in anhydrous THF was added 1.5 eq. of HCl in THF which resulted in a gradual color change from tan to fuchsia. Once the reaction was complete as determined by TLC monitoring, the crude mixture quenched with aqueous sodium bicarbonate, extracted three times with EtOAc, dried over $Na_2SO_4$, and concentrated under reduced pressure. The resulting dark film was taken up in $CHCl_3$ and purified by two stages of gravity chromatography on neutral alumina, eluting with 40% MeCN in $CHCl_3$.

General synthesis for compounds **8**-**10**:

To the corresponding aldehyde (1 eq.) in anhydrous methanol was added freshly prepared 4'-methoxy-1-tosyl-1H,1'H-2,2'-bipyrrole (1 eq.) in anhydrous methanol dropwise over 30 minutes. As soon as the first drop had been dispensed, 1M HCl in MeOH (1.5 eq.) was added in one portion. This caused a rapid color change from light yellow/tan to vivid fuchsia. Once the reaction was complete as determined by TLC monitoring, the crude mixture quenched with aqueous sodium bicarbonate, extracted three times with EtOAc, dried over $Na_2SO_4$, and concentrated under reduced pressure. The crude material was purified by flash column chromatography in silica gel, with the product eluting at 20% EtOAc in hexanes.

To the tosyl-protected prodiginine in MeOH was added 20 eq. of KOH. Once the reaction was complete as determined by TLC monitoring, the crude mixture quenched with aqueous $NH_4Cl$, extracted three times with EtOAc, dried over $Na_2SO_4$, and concentrated under reduced pressure. The resulting dark film was taken up in $CHCl_3$ and purified by two stages of gravity chromatography on neutral alumina, eluting with 40% MeCN in $CHCl_3$.

Experimental details specific to each compound's synthesis are included in the corresponding characterization data.

All prodiginines were formulated as the mesylate salt to increase aqueous solubility. This was accomplished by dissolving the small molecule in THF and adding 1 eq. MsOH in MeOH. For all compounds this caused a color change from yellow/orange to deep fuchsia. The resulting solution was concentrated under reduced pressure and diluted to 10 mM in DMSO. 4-methoxy-1H,1'H-[2,2'-bipyrrole]-5-carbaldehyde, 4'-methoxy-1-tosyl-1H,1'H-2,2'-bipyrrole, and **1** were

prepared according to the published procedures.[36, 38] 1,4,5,6,7,8,9,10,11,12-decahydrocycloundeca[*b*]pyrrole-2-carbaldehyde was prepared by Mr. Morris Dweck.

(*Z*)-3-((4'-methoxy-1*H*,5'*H*-[2,2'-bipyrrol]-5'-ylidene)methyl)-1*H*-indole (**5**)

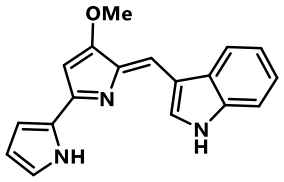


| | |
|---|---|
| Indole: | 1*H*-indole (0.11 mmol) |
| Yield: | 87% (26 mg) |

$^{1}$H NMR (500 MHz, Acetone) δ 9.08 (s, 1H), 8.00 (s, 1H), 7.47 (s, 1H), 7.33 (s, 1H), 7.19 (s, 2H), 7.04 (s, 1H), 6.83 (s, 1H), 6.23 (d, *J* = 14.3 Hz, 2H), 3.98 (s, 3H). $^{13}$C NMR (126 MHz, Acetone) δ 169.46, 137.56, 133.99, 128.71, 123.51, 121.89, 119.54, 118.40, 113.26, 112.95, 111.16, 96.23, 59.07. $C_{18}H_{16}N_3O^+$ $[M+H]^+$: 290.1288, found: 290.1306

(*Z*)-5-fluoro-3-((4'-methoxy-1*H*,5'*H*-[2,2'-bipyrrol]-5'-ylidene)methyl)-1*H*-indole (**6**)

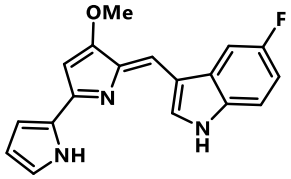


| | |
|---|---|
| Indole: | 5-fluoro-1*H*-indole (0.52 mmol) |
| Yield: | |

$^{1}$H NMR (500 MHz, Acetic) δ 9.36 (s, 1H), 7.62 (s, 1H), 7.56 – 7.51 (m, 2H), 7.44 (s, 1H), 7.29 (d, *J* = 2.7 Hz, 1H), 7.06 (td, *J* = 9.2, 2.5 Hz, 1H), 6.48 (s, 1H), 6.45 (dd, *J* = 4.0, 2.4 Hz, 1H), 4.13 (s, 2H). $^{13}$C NMR (126 MHz, Acetic) δ 167.58, 160.55, 158.67, 152.48, 136.37, 133.00, 129.64, 128.70, 126.79,

121.39, 121.01, 119.81, 114.05, 112.74, 112.08, 110.13, 103.71, 94.60, 59.04. HRMS (ESI) calculated for $C_{18}H_{15}FN_3O^+$ $[M+H]^+$: 308.1194, found: 308.1216

(*Z*)-3-((4'-methoxy-1*H*,5'*H*-[2,2'-bipyrrol]-5'-ylidene)methyl)-1-methyl-1*H*-indole (**7**)

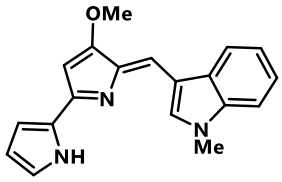


| Indole: | 1-methyl-1H-indole (0.52 mmol) |
|---|---|
| Yield: | |

$^1$H NMR (500 MHz, Acetic) δ 9.36 (s, 1H), 7.87 (d, *J* = 7.8 Hz, 1H), 7.69 (s, 1H), 7.51 (d, *J* = 7.9 Hz, 1H), 7.44 (s, 1H), 7.36 (dq, *J* = 14.3, 7.2 Hz, 2H), 7.26 (s, 1H), 6.46 (s, 2H), 4.12 (s, 3H), 4.00 (s, 3H). $^{13}$C NMR (126 MHz, Acetic) δ 167.29, 151.67, 138.71, 137.71, 129.18, 128.34, 126.26, 123.97, 122.77, 121.46, 120.33, 119.87, 118.34, 112.57, 110.93, 109.36, 94.38, 58.91, 33.29. HRMS (ESI) calculated for $C_{19}H_{18}N_3O^+$ $[M+H]^+$: 304.1444, found: 304.1490

(*Z*)-3-((4-methoxy-1'-tosyl-1*H*,1'*H*-[2,2'-bipyrrol]-5-yl)methylene)indolin-2-one (**S1**)

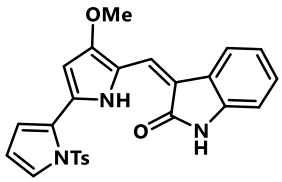


| Aldehyde: | 2-oxoindoline-3-carbaldehyde (0.25 mmol) |
|---|---|
| Yield: | 41 mg, 36% |

$^1$H NMR (500 MHz, $CDCl_3$) δ 12.99 (s, 1H), 8.64 (s, 1H), 7.52 (s, 1H), 7.52 – 7.48 (m, 2H), 7.43 (d, *J* = 7.3 Hz, 2H), 7.11 (d, *J* = 8.5 Hz, 3H), 7.04 (t, *J* = 7.6 Hz, 1H), 6.82 (d, *J* = 7.6 Hz, 1H), 6.58 – 6.53 (m,

1H), 6.39 – 6.34 (m, 1H), 6.28 (dd, *J* = 2.7, 1.2 Hz, 1H), 3.94 (s, 3H), 2.26 (s, 3H). $^{13}$C NMR (126 MHz, $CDCl_3$) δ 170.71, 160.65, 157.52, 144.72, 142.10, 138.23, 135.33, 129.70, 129.50, 128.67, 127.24, 127.22, 126.29, 123.13, 122.24, 121.93, 118.11, 113.75, 112.16, 109.17, 108.13, 97.91, 63.11, 58.13, 21.47. HRMS (ESI) calculated for $C_{25}H_{22}N_3O_4S^+$ $[M+H]^+$: 460.1326, found: 460.1331

(*Z*)-3-((4-methoxy-1*H*,1'*H*-[2,2'-bipyrrol]-5-yl)methylene)indolin-2-one (**8**)

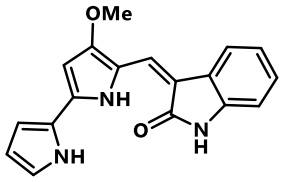


| Yield: | 7 mg, 50% |
|---|---|

$^1$H NMR (500 MHz, Acetone) δ 13.79 (s, 1H), 10.75 (s, 1H), 9.74 (s, 1H), 7.53 (d, *J* = 7.5 Hz, 1H), 7.49 (s, 1H), 7.07 (td, *J* = 7.6, 1.2 Hz, 1H), 6.99 (dd, *J* = 7.5, 1.1 Hz, 1H), 6.97 (dd, *J* = 2.9, 1.2 Hz, 1H), 6.95 (d, *J* = 7.6 Hz, 1H), 6.62 (tt, *J* = 2.4, 1.4 Hz, 1H), 6.37 (d, *J* = 2.7 Hz, 1H), 6.27 (dt, *J* = 3.5, 2.3 Hz, 1H), 3.94 (s, 3H). $^{13}$C NMR (126 MHz, Acetone) δ 170.70, 157.83, 138.83, 132.43, 127.63, 125.82, 125.63, 121.98, 121.53, 120.62, 118.20, 117.98, 110.94, 110.79, 110.17, 107.83, 91.91, 58.61. HRMS (ESI) calculated for $C_{18}H_{16}N_3O_2^+$ $[M+H]^+$: 306.1237, found: 306.1245

(*Z*)-5'-((1*H*-pyrrol-2-yl)methylene)-4'-methoxy-1-tosyl-1*H*,5'*H*-2,2'-bipyrrole (**S2**)

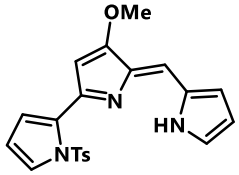

| | |
|---|---|
| Aldehyde: | 1*H*-pyrrole-2-carbaldehyde (1.0 mmol) |
| Yield: | 87% (341 mg) |

$^{1}$H NMR (500 MHz, $CDCl_3$) δ 7.69 (dd, *J* = 3.4, 1.8 Hz, 1H), 7.56 (d, *J* = 8.4 Hz, 2H), 7.21 (s, 1H), 7.10 (d, *J* = 8.4 Hz, 2H), 6.88 (s, 1H), 6.75 (dd, *J* = 3.6, 1.8 Hz, 1H), 6.64 (d, *J* = 3.7 Hz, 1H), 6.37 (t, *J* = 3.5 Hz, 1H), 6.32 – 6.26 (m, 1H), 5.71 (s, 1H), 3.80 (s, 3H), 2.30 (s, 3H). $^{13}$C NMR (126 MHz, $CDCl_3$) δ 167.34, 157.13, 144.80, 141.76, 135.64, 131.29, 130.41, 129.52, 128.54, 127.33, 126.59, 119.78, 118.72, 118.17, 111.45, 110.76, 97.21, 58.33, 45.78, 21.60. HRMS (ESI) calculated for $C_{21}H_{20}N_3O_3S^+$ $[M+H]^+$: 394.1220, found: 394.1257

(*Z*)-5'-((1*H*-pyrrol-2-yl)methylene)-4'-methoxy-1*H*,5'*H*-2,2'-bipyrrole (**9**)

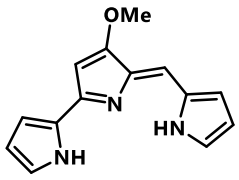


| | |
|---|---|
| Yield: | 73% (24 mg) |

$^{1}$H NMR (500 MHz, Acetic) δ 7.51 – 7.48 (m, 1H), 7.45 – 7.42 (m, 1H), 7.26 (dd, *J* = 4.0, 1.4 Hz, 1H), 7.22 (s, 1H), 7.09 (d, *J* = 4.1 Hz, 1H), 6.48 (dd, *J* = 4.0, 2.4 Hz, 1H), 6.46 (dd, *J* = 4.1, 2.3 Hz, 1H), 6.44 (s, 1H), 4.09 (s, 3H). $^{13}$C NMR (126 MHz, Acetic) δ 167.95, 152.09, 131.56, 129.68, 126.85, 125.08, 124.61, 121.63, 120.19, 116.36, 113.27, 112.67, 94.27, 58.93. HRMS (ESI) calculated for $C_{14}H_{14}N_3O^+$ $[M+H]^+$: 240.1131, found: 240.1163

(*Z*)-2-((4'-methoxy-1-tosyl-1*H*,5'*H*-[2,2'-bipyrrol]-5'-ylidene)methyl)-1,4,5,6,7,8,9,10,11,12-decahydrocycloundeca[*b*]pyrrole (**S3**)

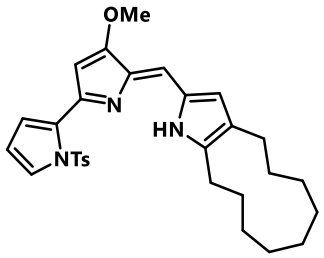


| | |
|---|---|
| Aldehyde: | 1,4,5,6,7,8,9,10,11,12-decahydrocycloundeca[b]pyrrole-2-carbaldehyde (0.35 mmol) |

HRMS (ESI) calculated for $C_{30}H_{36}N_3O_3S^+$ $[M+H]^+$: 518.2472, found: 518.2460

**S3** was taken forward to the next step without purification.

(*Z*)-2-((4'-methoxy-1*H*,5'*H*-[2,2'-bipyrrol]-5'-ylidene)methyl)-1,4,5,6,7,8,9,10,11,12-decahydrocycloundeca[*b*]pyrrole (**10**)

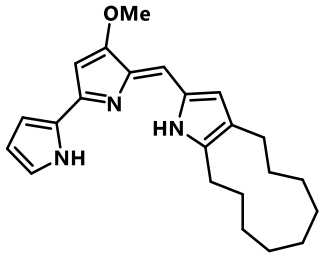


| | |
|---|---|
| Yield: | 60% (13 mg) |

$^1$H NMR (500 MHz, $CDCl_3$) δ 6.84 (s, 1H), 6.82 (s, 1H), 6.69 (s, 1H), 6.40 (s, 1H), 6.22 (s, 1H), 6.00 (s, 1H), 3.95 (s, 3H), 2.52 (t, *J* = 5.0 Hz, 2H), 2.49 – 2.43 (m, 2H), 1.65 (s, 2H), 1.55 (s, 2H), 1.23 (s, 6H), 1.13 (d, *J* = 6.1 Hz, 1H), 1.05 (d, *J* = 6.7 Hz, 2H), 0.99 (d, *J* = 6.6 Hz, 1H). $^{13}$C NMR (126 MHz, $CDCl_3$)

δ 128.59, 115.68, 110.41, 94.87, 77.28, 77.03, 76.77, 62.55, 58.41, 52.20, 47.90, 29.72, 28.30, 28.26, 27.16, 26.84, 25.76, 24.78, 24.56, 24.26, 23.15, 22.61, 20.06, 19.21, 14.22. HRMS (ESI) calculated for $C_{23}H_{30}N_3O^+$ $[M+H]^+$: 364.2383, found: 364.2428

**UV-Vis and Fluorescence Emission Spectra**

Spectra were collected in 10 mM NaHEPES pH 7.0 at the indicated concentration. Fluorescence emission spectra were collected at the maximum absorbance wavelength from the corresponding UV-Vis spectrum.

**Figure 2.6.12** UV-Vis (100 μM) and fluorescence emission (100 μM) spectra for compound **5**.

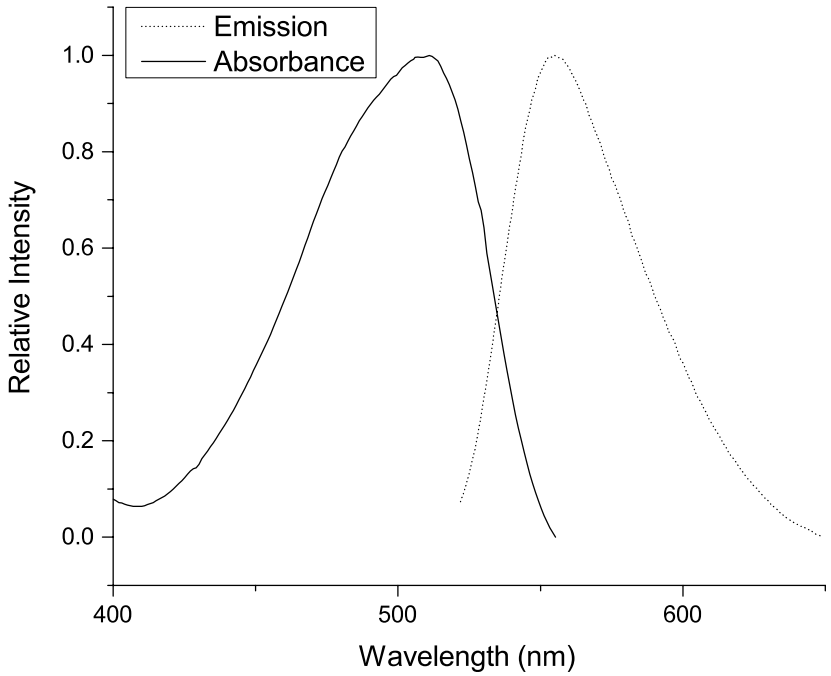

**Figure 2.6.13** UV-Vis (50 μM) and fluorescence emission (50 μM) spectra for compound **6**.

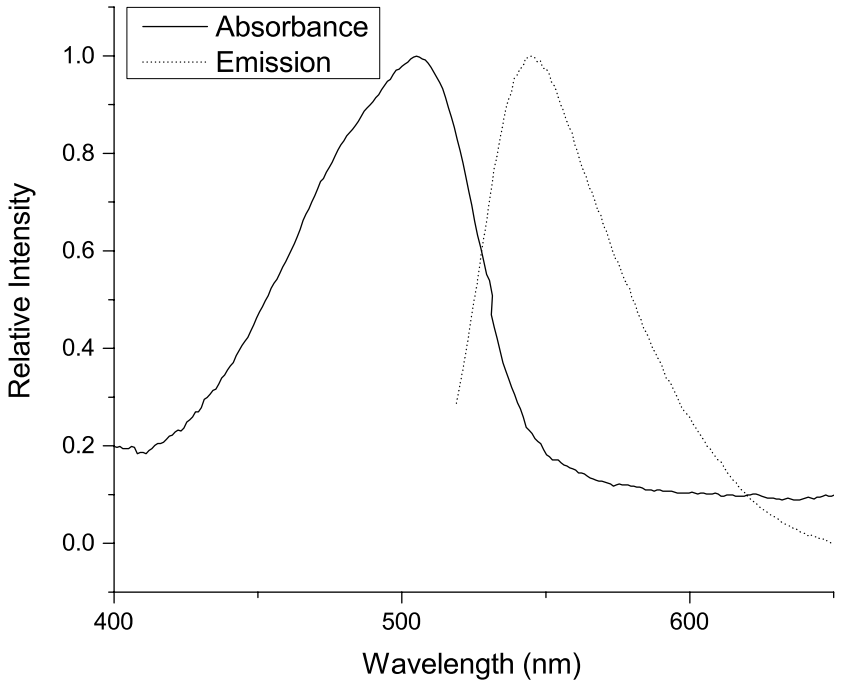


**Figure 2.6.14** UV-Vis (50 μM) and fluorescence emission (50 μM) spectra for compound **7**.

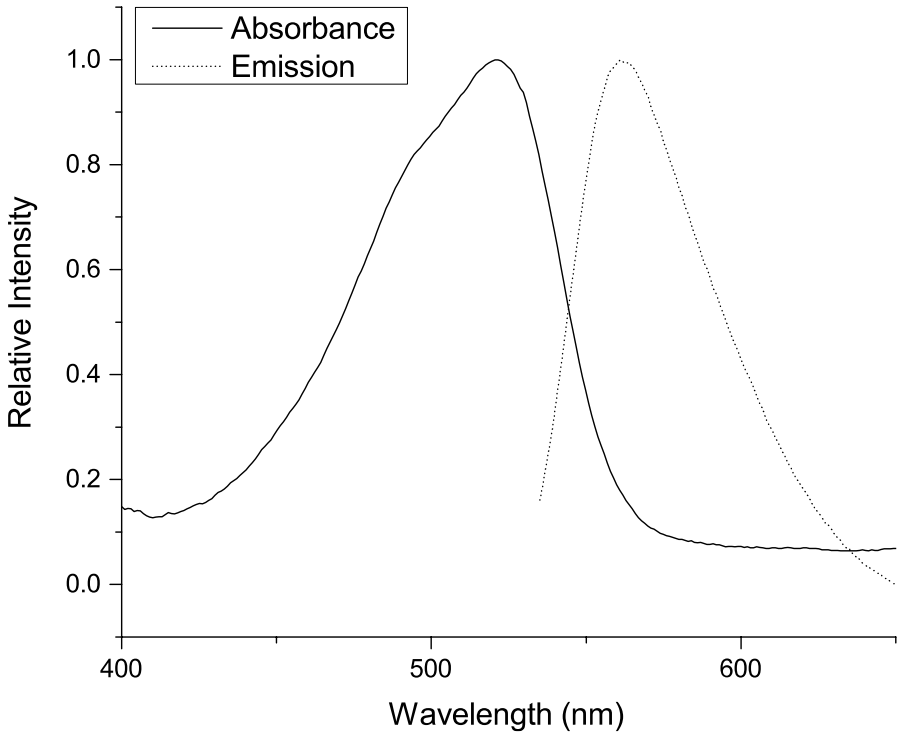

**Figure 2.6.15** UV-Vis (50 μM) and fluorescence emission (50 μM) spectra for compound **8**.

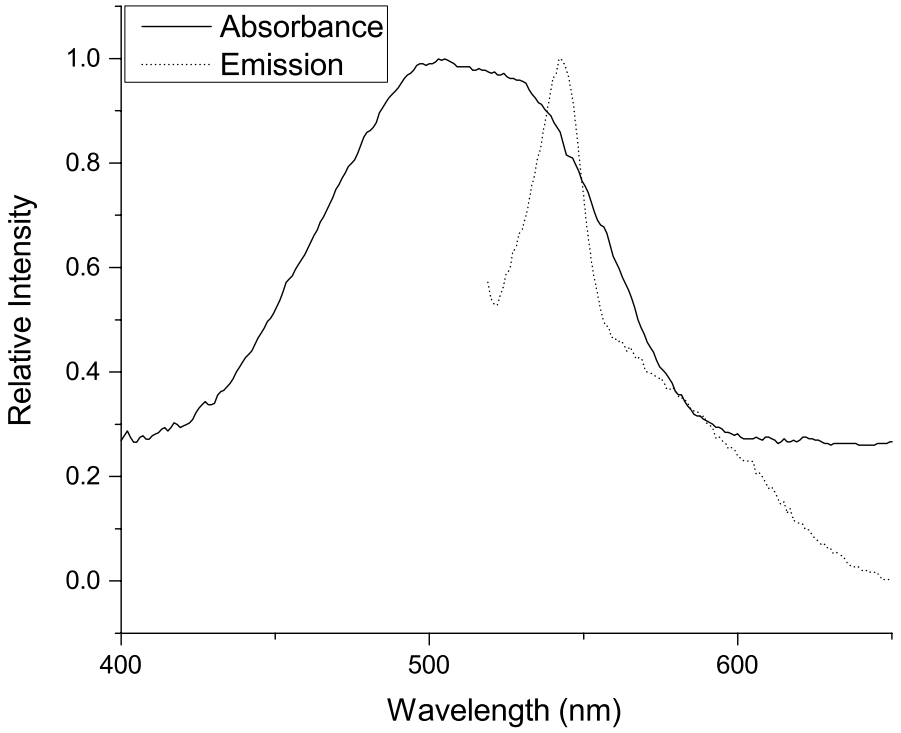


**Figure 2.6.16** UV-Vis (50 μM) and fluorescence emission (50 μM) spectra for compound **9**.

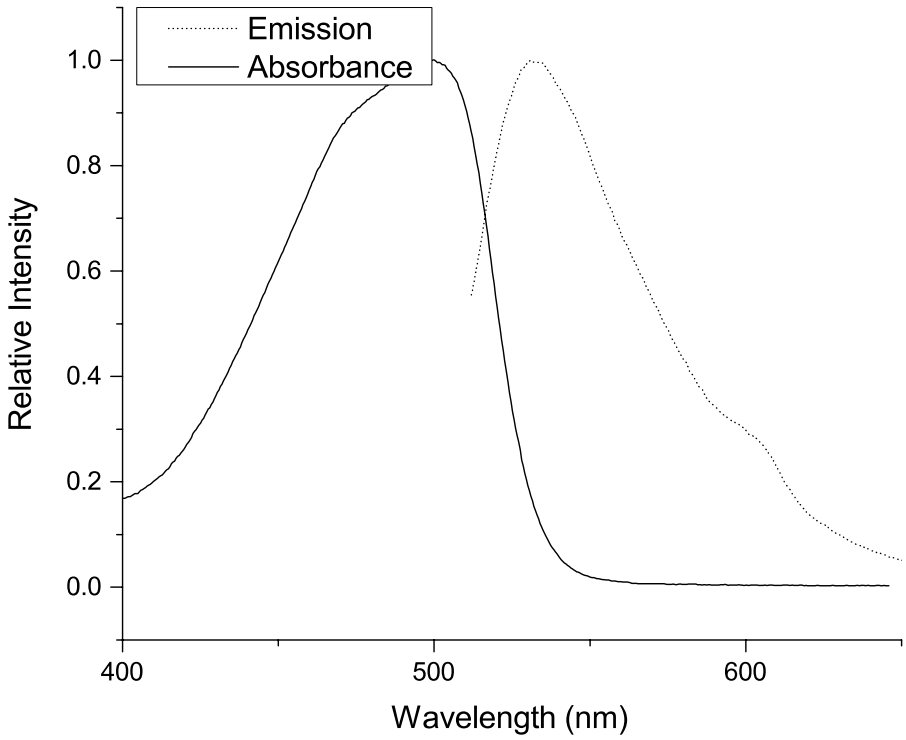

**Figure 2.6.17** UV-Vis (100 μM) and fluorescence emission (100 μM) spectra for compound **10**.

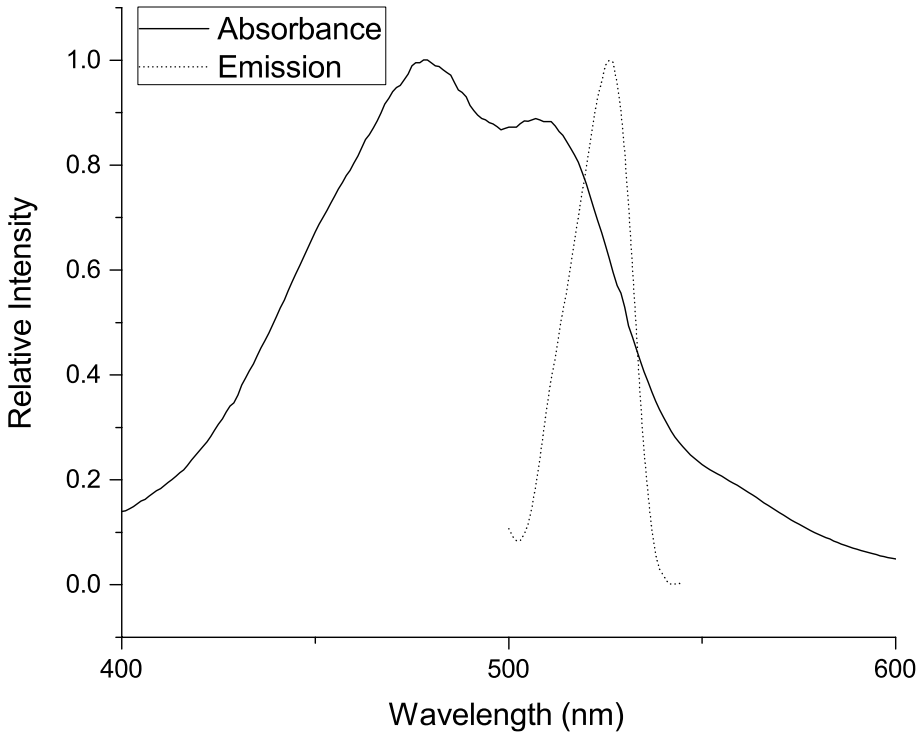

**Figure 2.6.18** $^{1}$H NMR Spectrum (500 MHz, Acetone-$D_6$) for compound **5**.

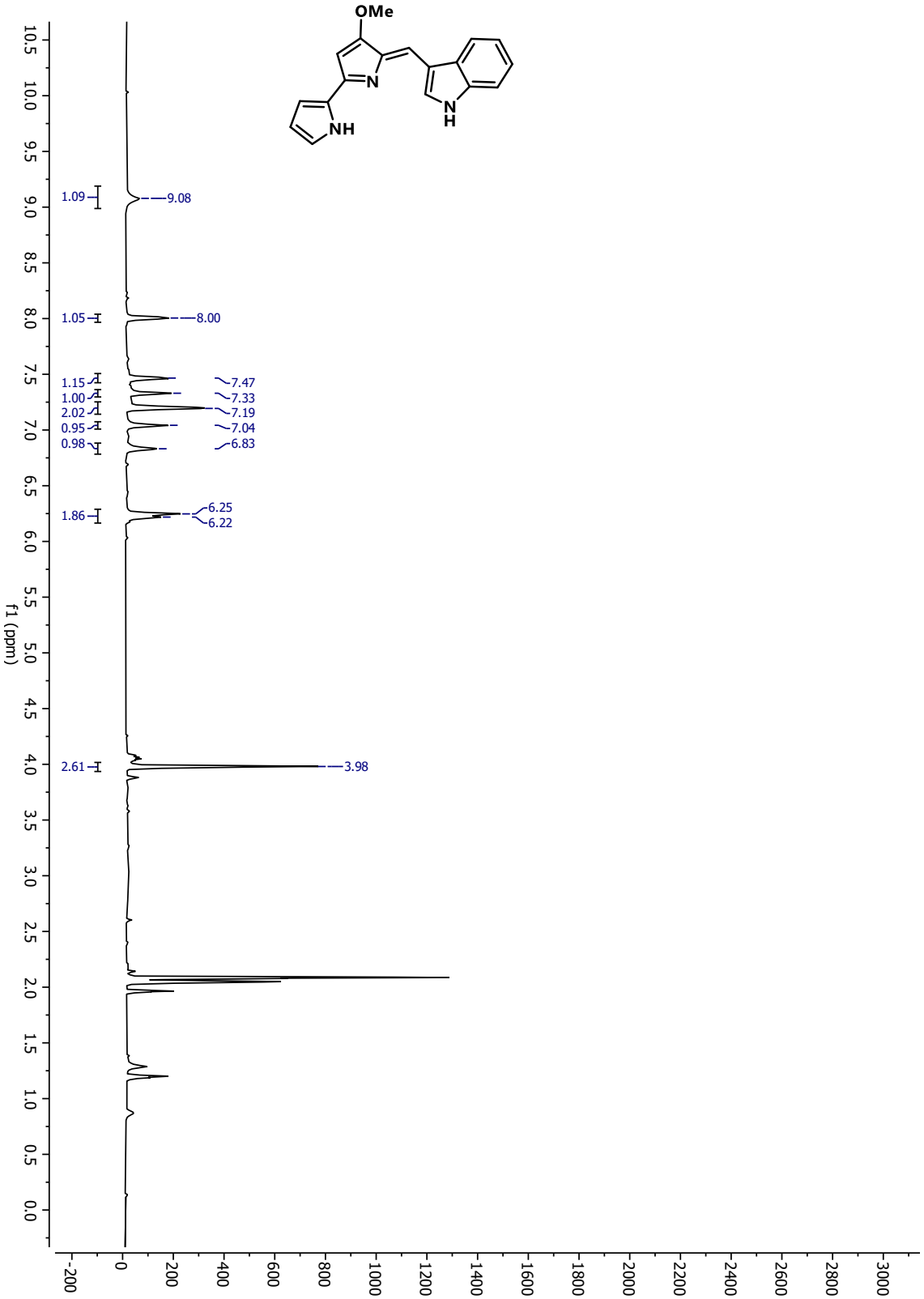

**Figure 2.6.19** $^{13}C$ NMR Spectrum (126 MHz, Acetone-$D_6$) for compound **5**.

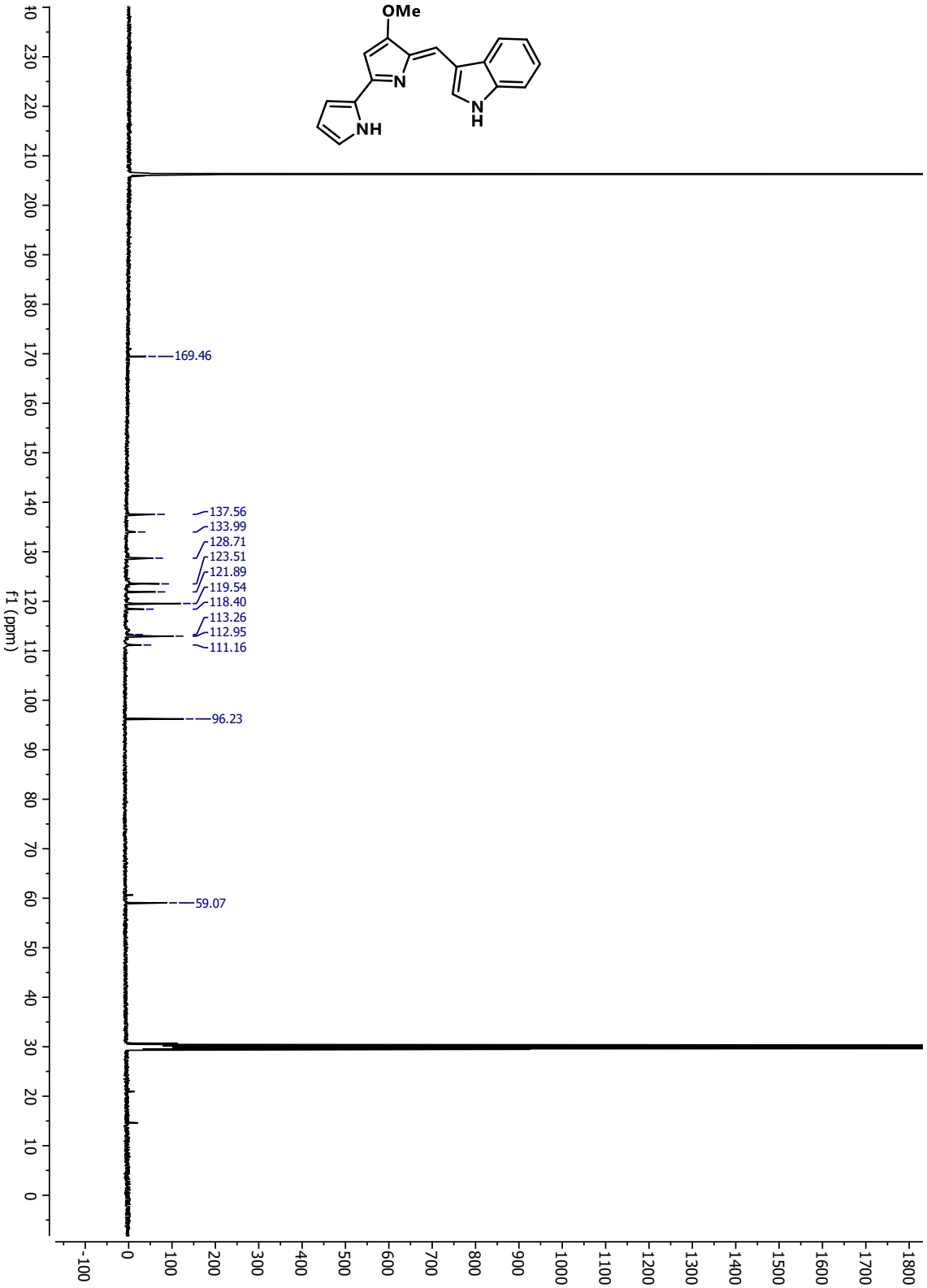

**Figure 2.6.20** $^{1}$H NMR Spectrum (500 MHz, Acetic Acid-$D_4$) for compound **6**.

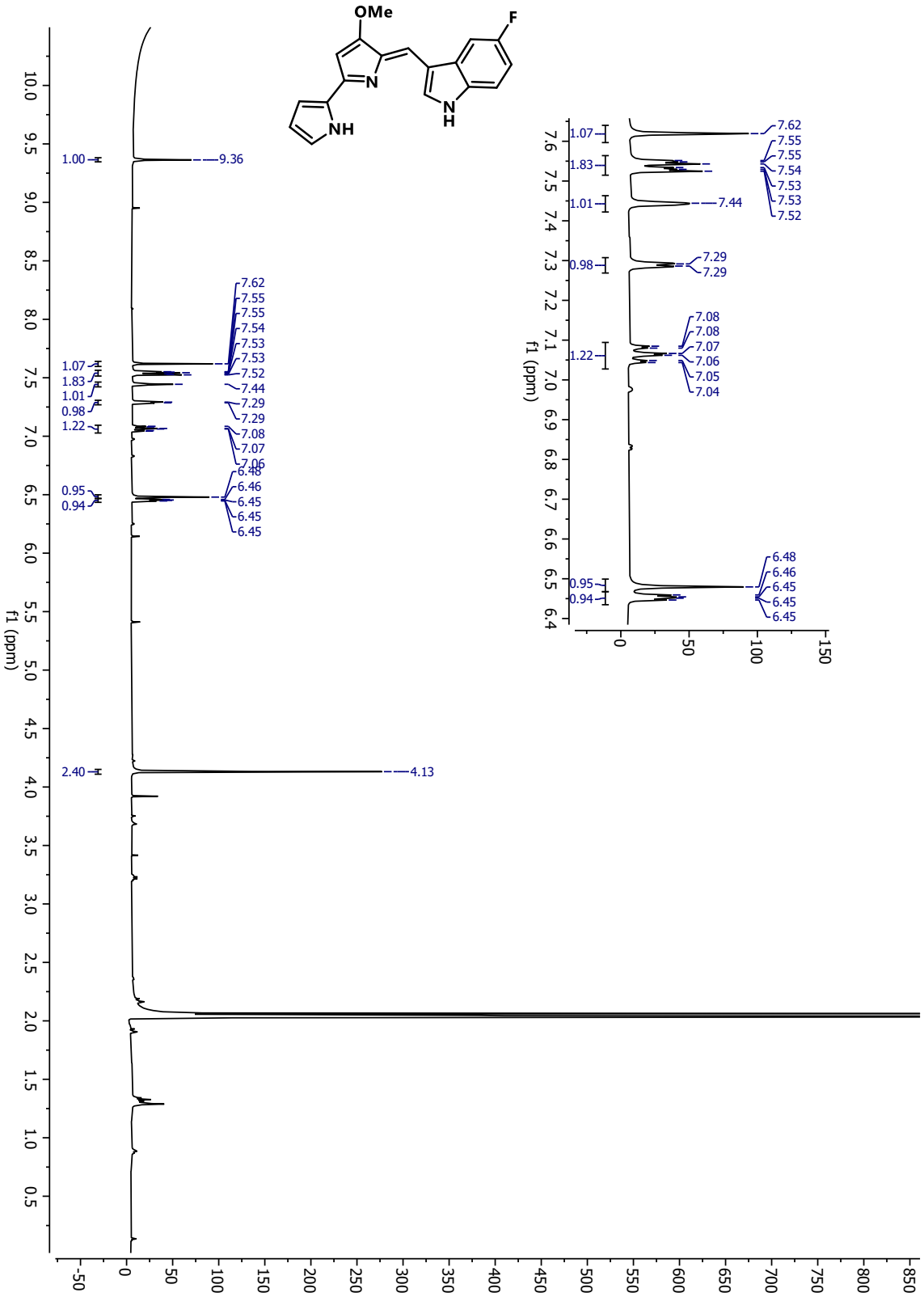

**Figure 2.6.21** $^{13}C$ NMR Spectrum (126 MHz, Acetic Acid-$D_4$) for compound **6**.

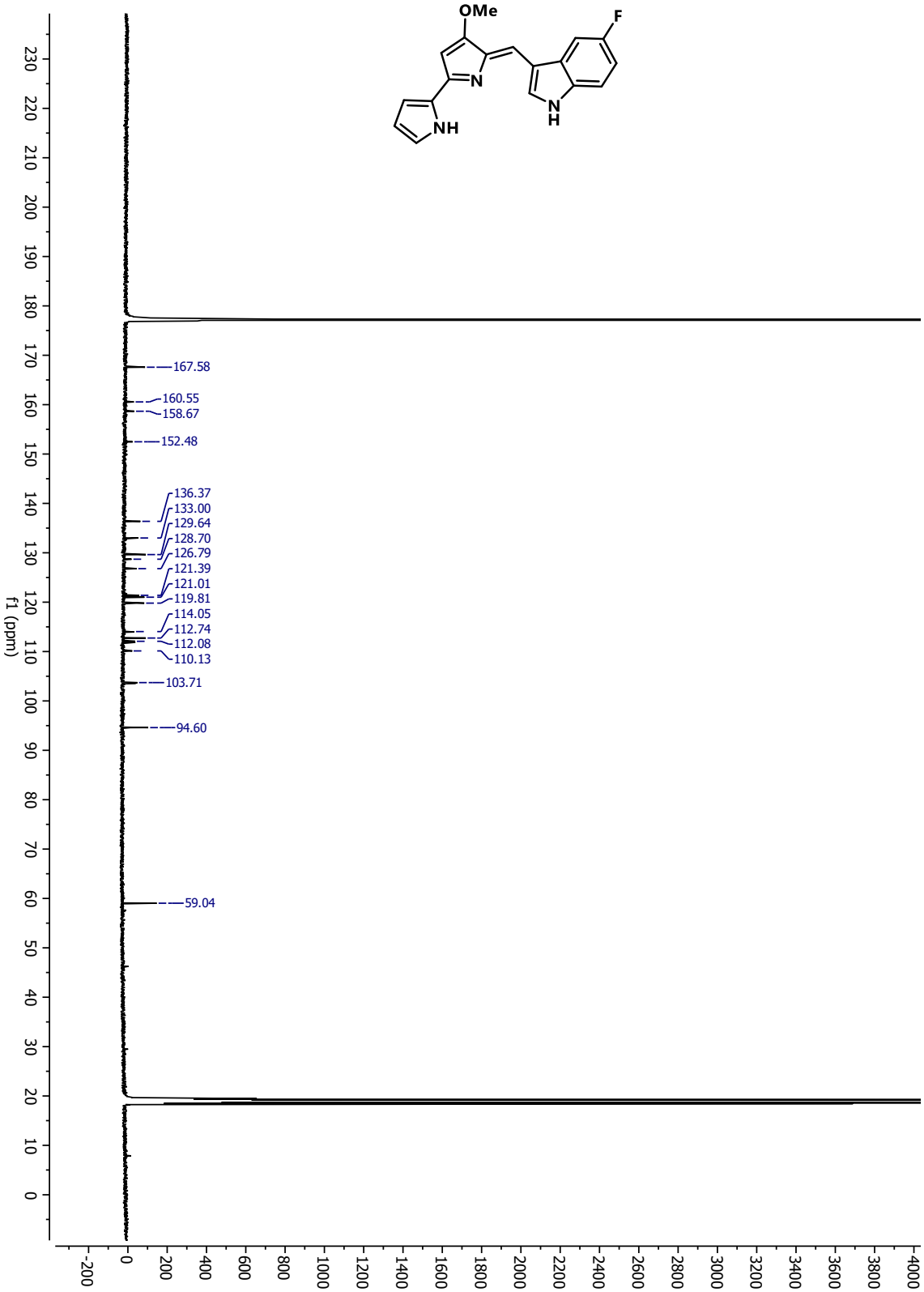

**Figure 2.6.22** $^{1}$H NMR Spectrum (500 MHz, Acetic Acid-$D_4$) for compound **7**.

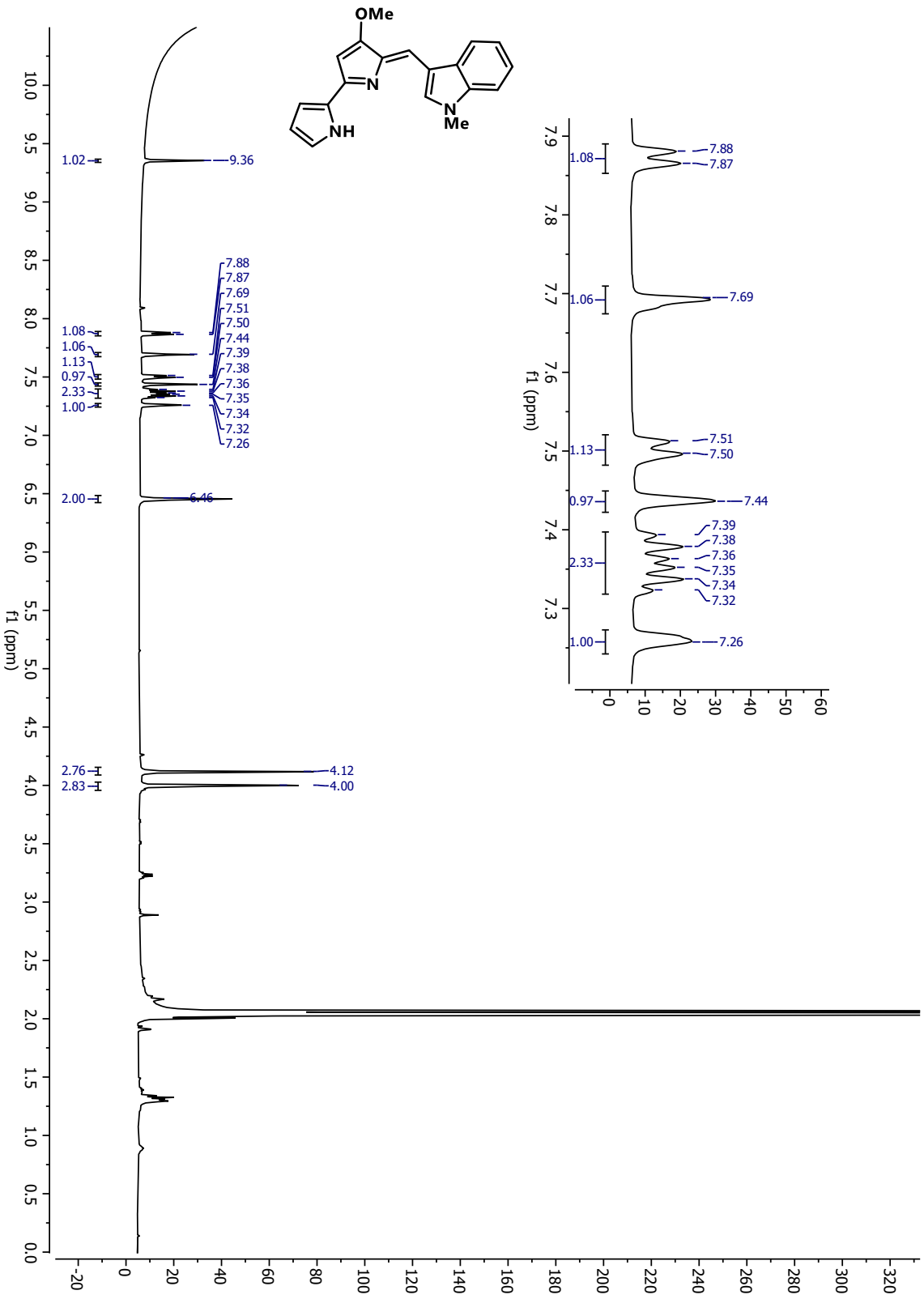

**Figure 2.6.23** $^{13}C$ NMR Spectrum (126 MHz, Acetic Acid-$D_4$) for compound **7**.

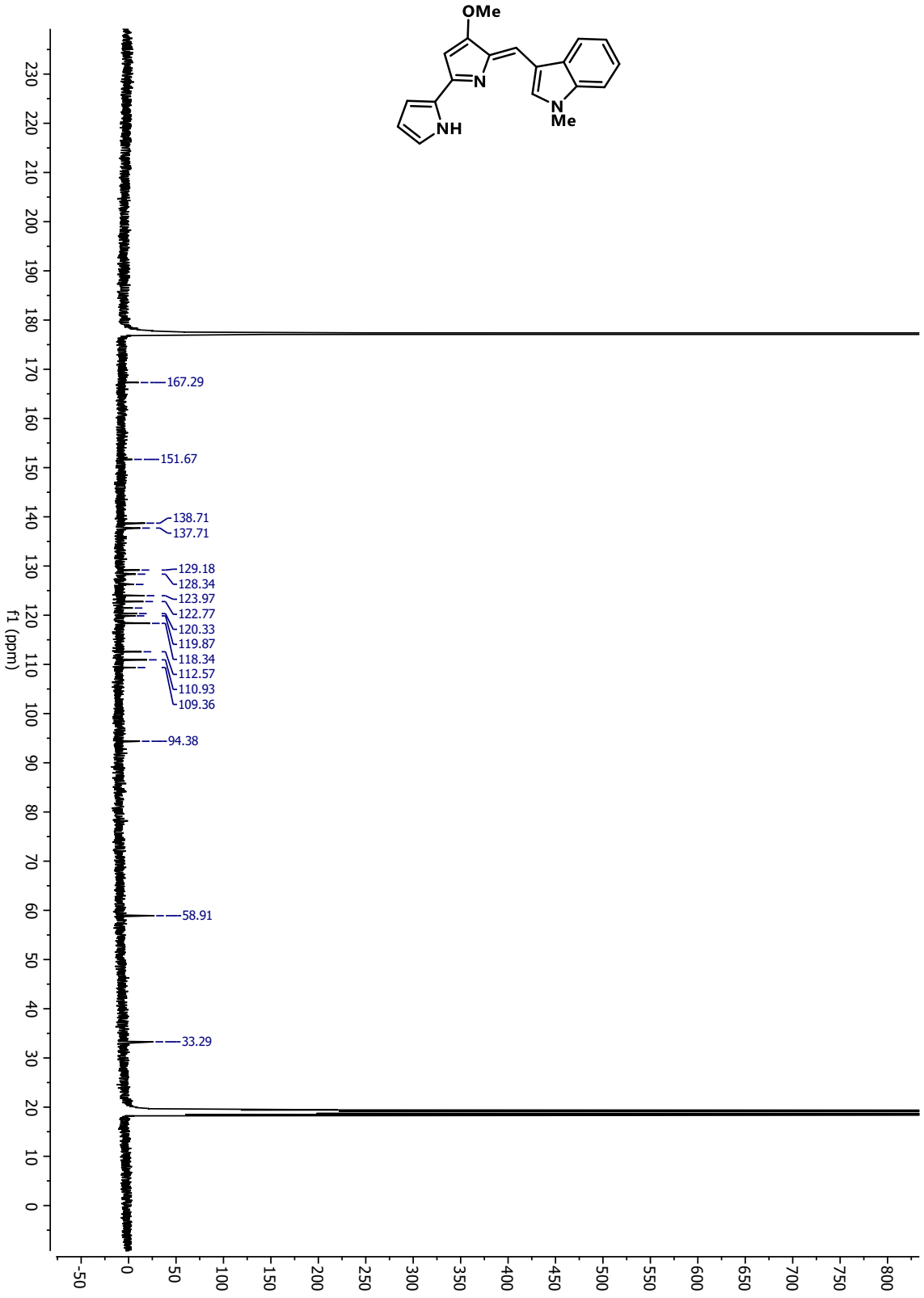

**Figure 2.6.24** $^{1}$H NMR Spectrum (500 MHz, Chloroform-D) for compound **S1**.

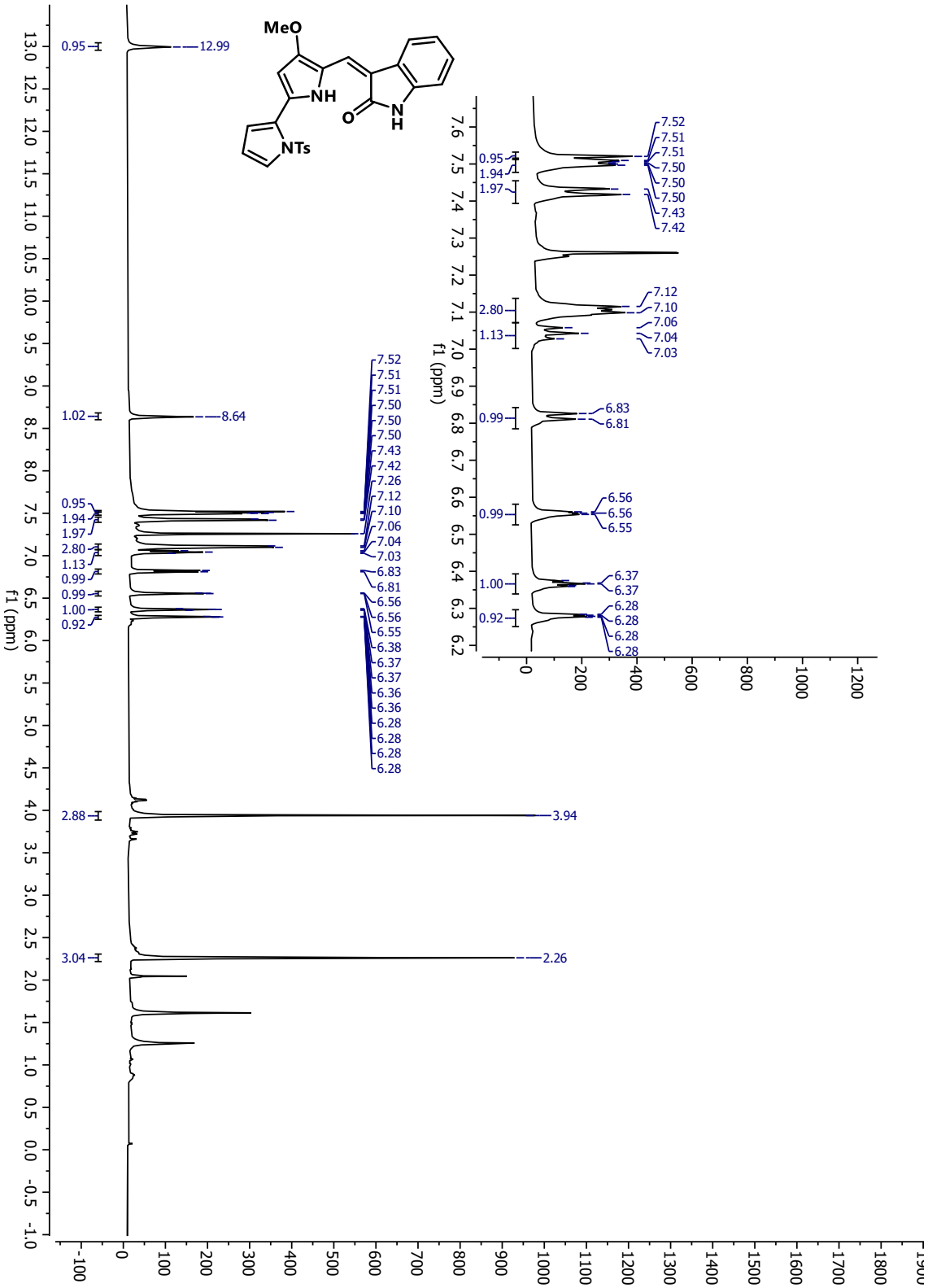

**Figure 2.6.25** $^{13}$C NMR Spectrum (126 MHz, Chloroform-D) for compound **S1**.

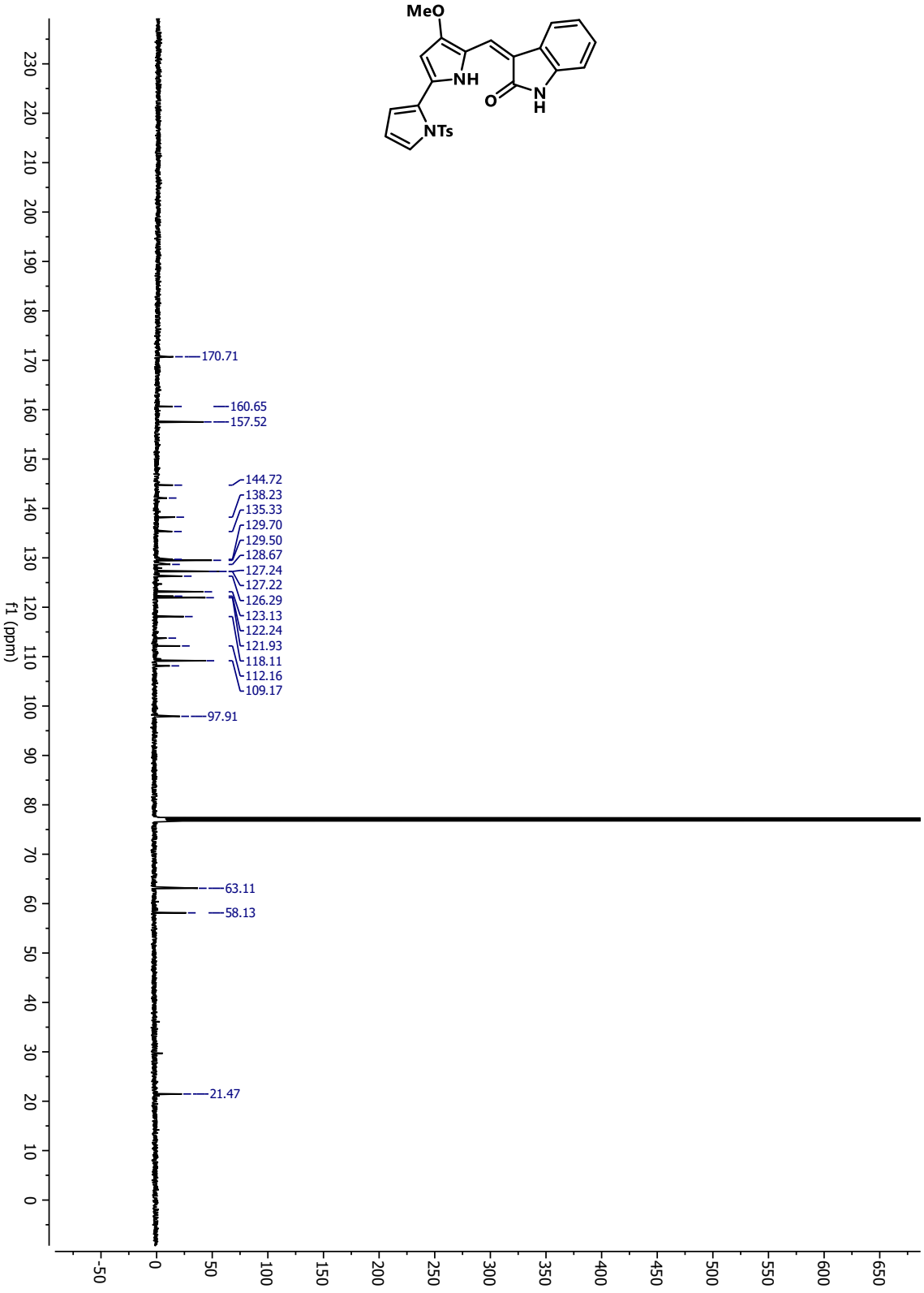

**Figure 2.6.26** $^{1}$H NMR Spectrum (500 MHz, Acetone-$D_6$) for compound **8**.

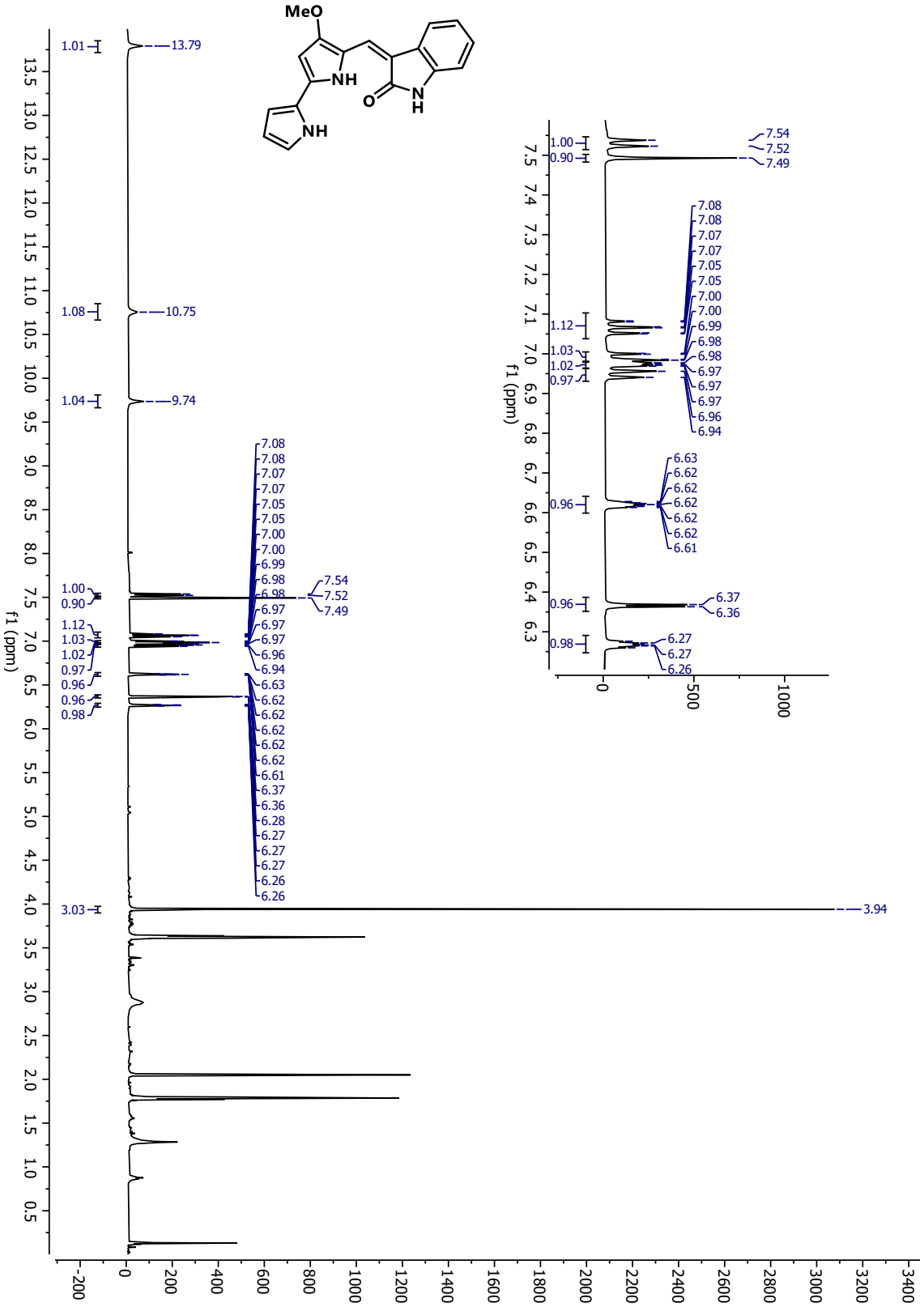

**Figure 2.6.27** $^{13}C$ NMR Spectrum (126 MHz, Acetone-$D_6$) for compound **8**.

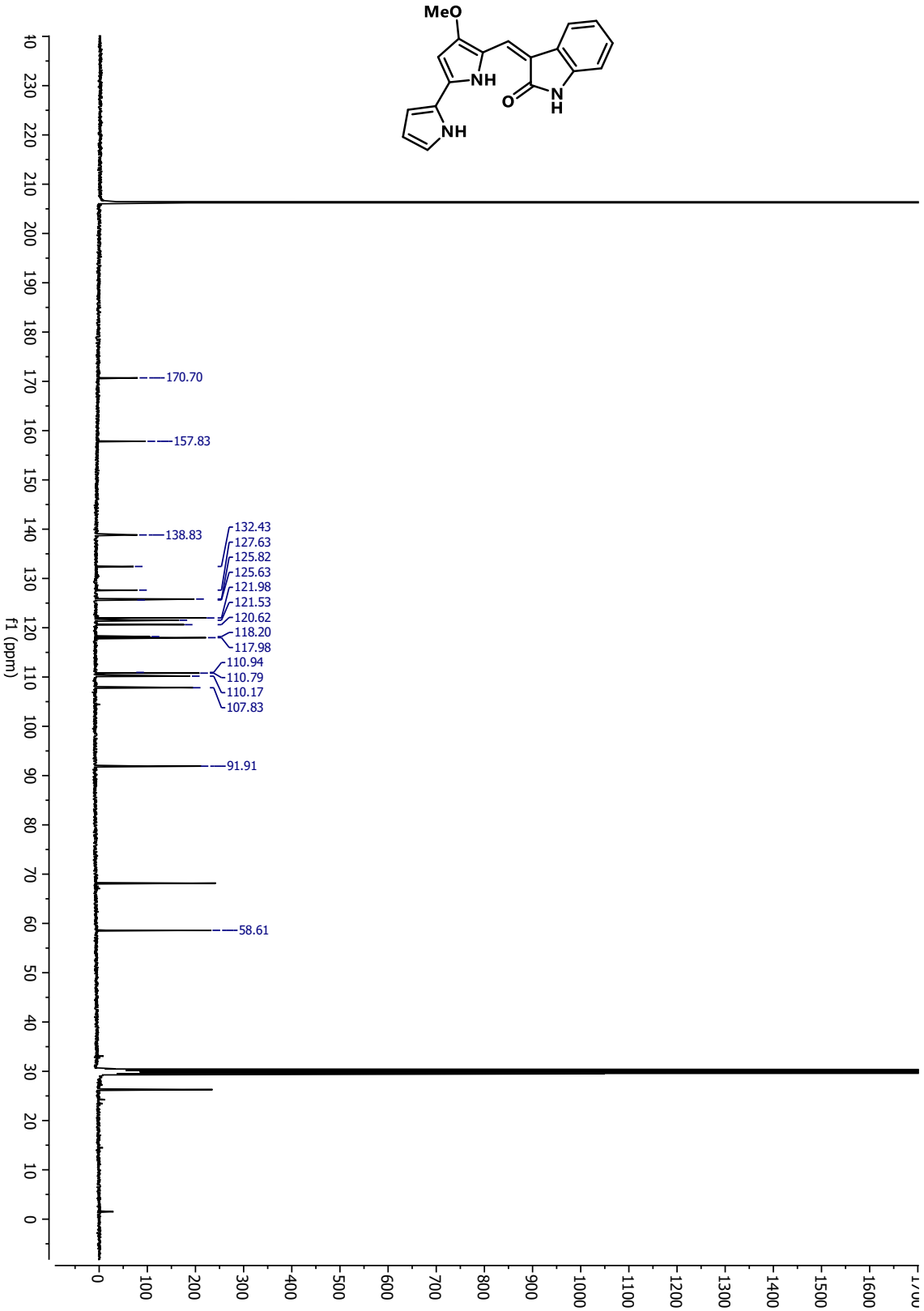

**Figure 2.6.28** $^{1}$H NMR Spectrum (500 MHz, Chloroform-D) for compound **S2**.

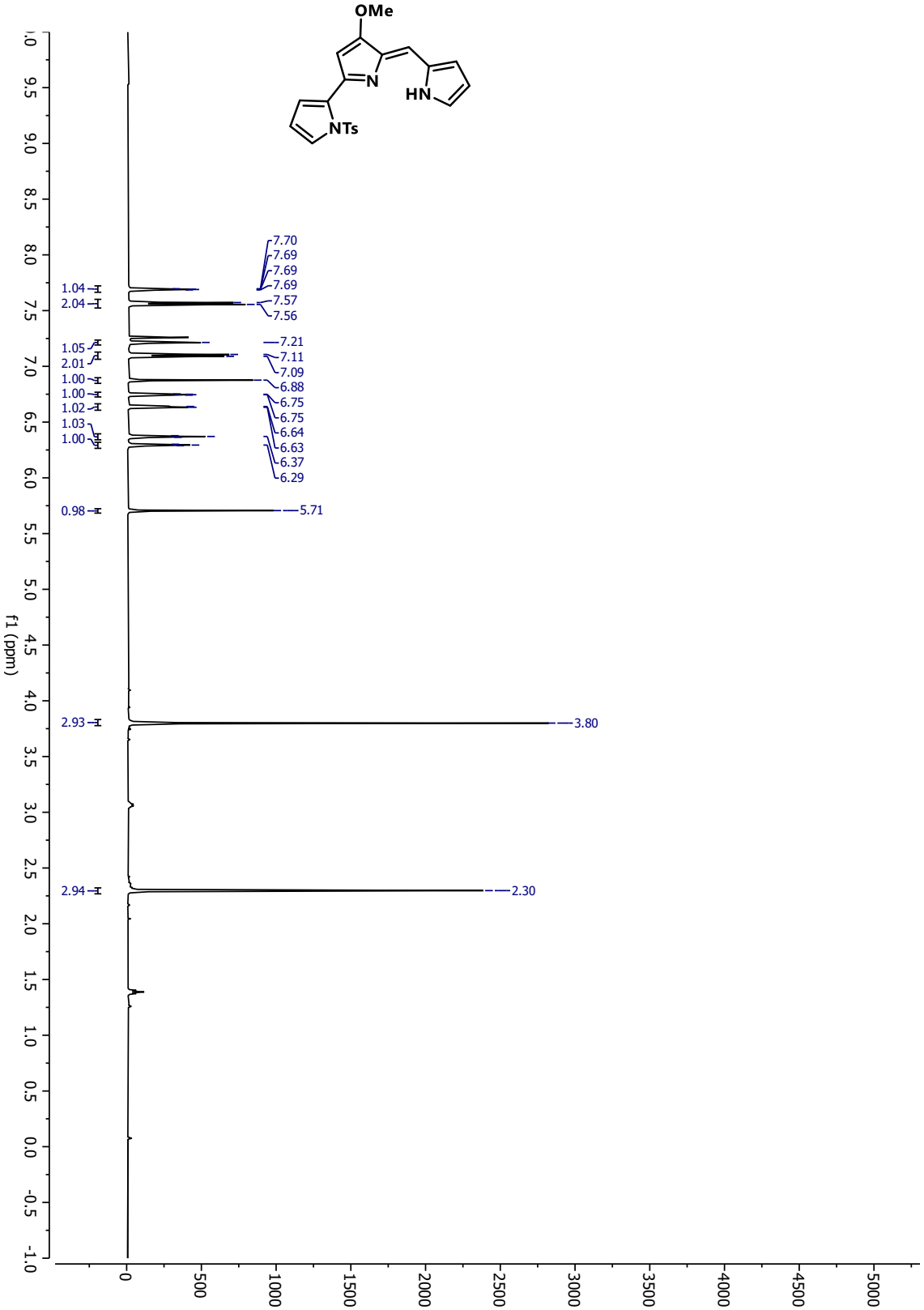

**Figure 2.6.29** APT NMR Spectrum (126 MHz, Chloroform-D) for compound **S2**.

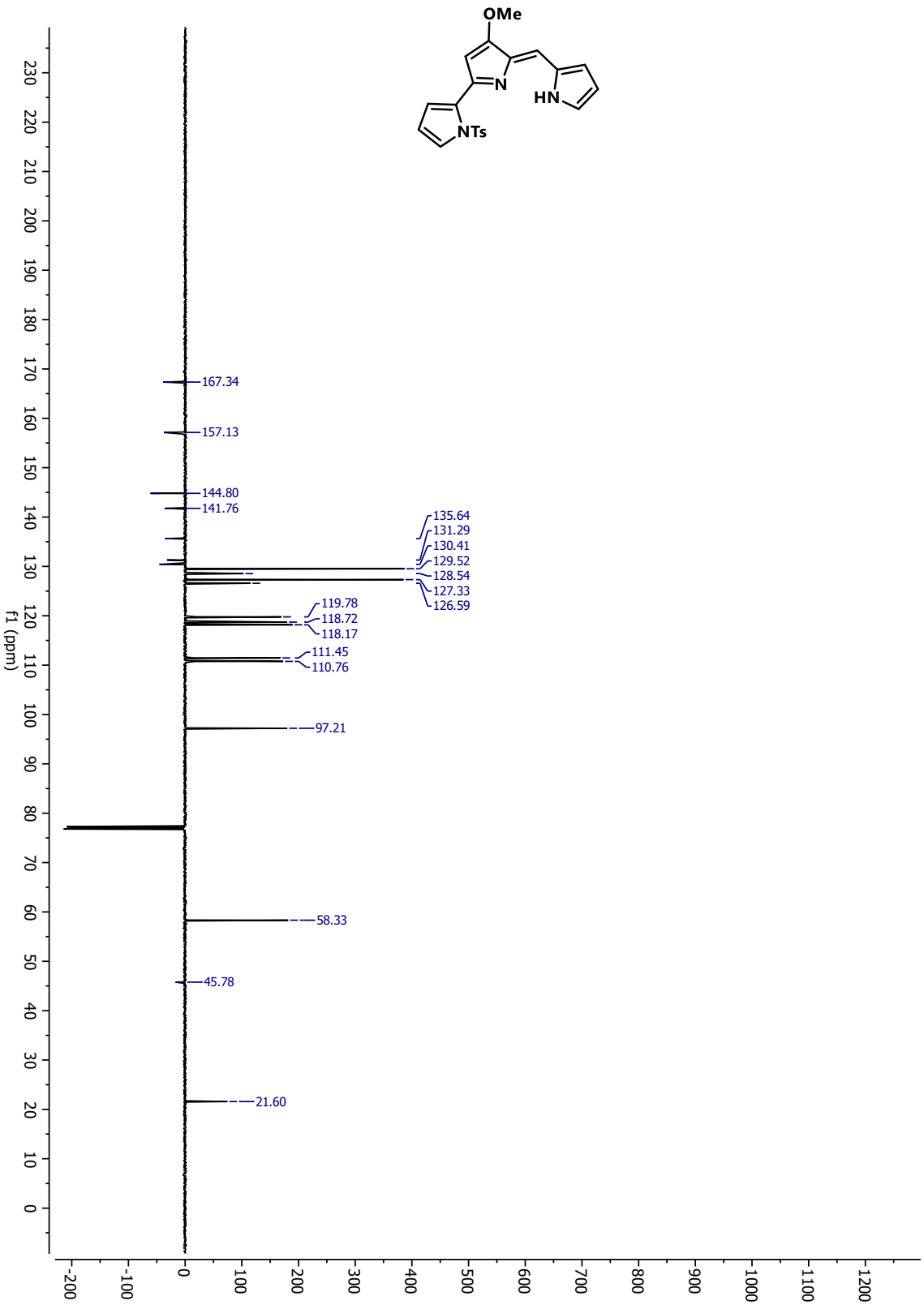

**Figure 2.6.30** $^{1}$H NMR Spectrum (500 MHz, Acetic Acid-$D_4$) for compound **9**.

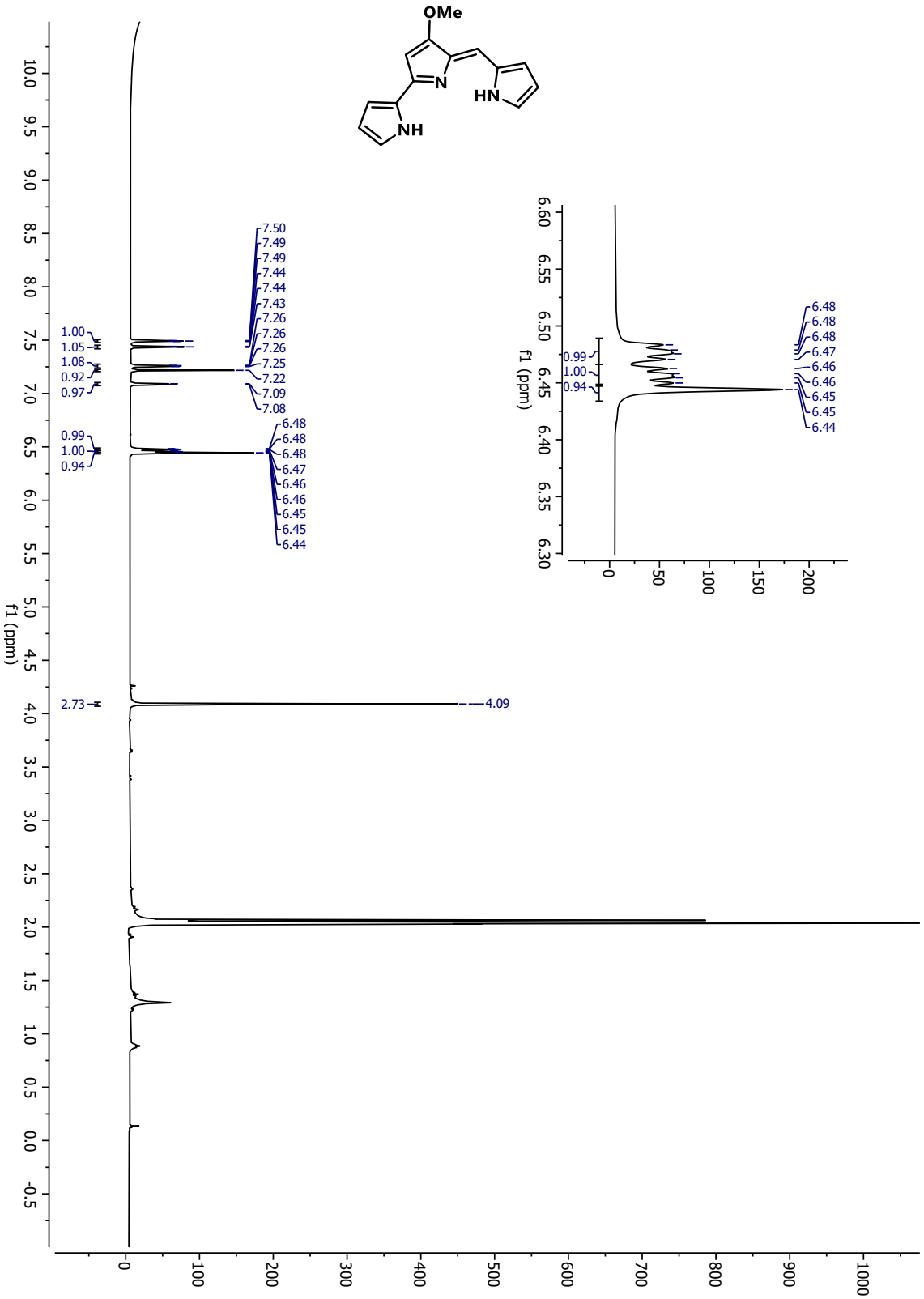

**Figure 2.6.31** $^{13}C$ NMR Spectrum (126 MHz, Acetic Acid-$D_4$) for compound **9**.

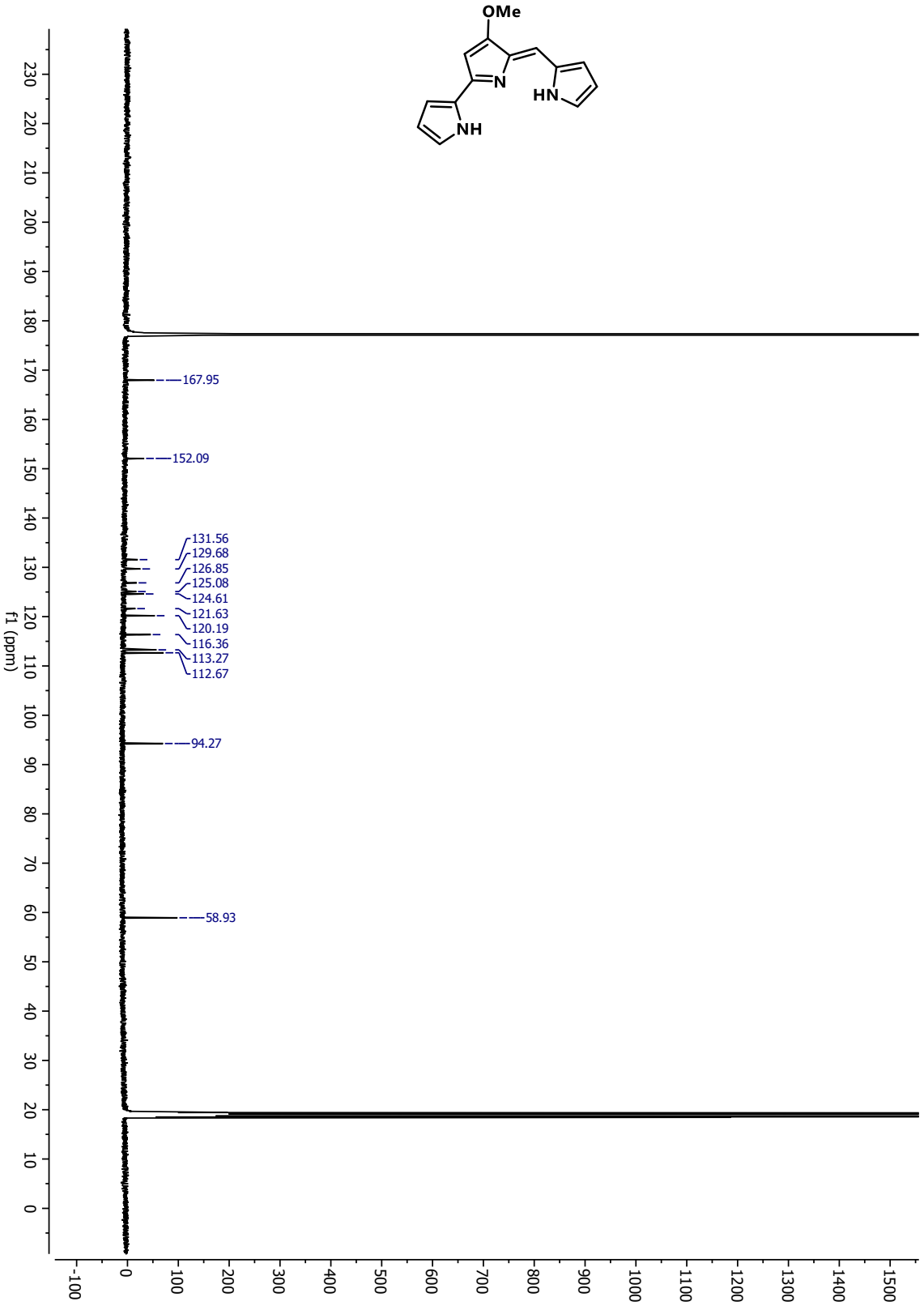

**Figure 2.6.32** $^{1}$H NMR Spectrum (500 MHz, Chloroform-D) for compound **10**.

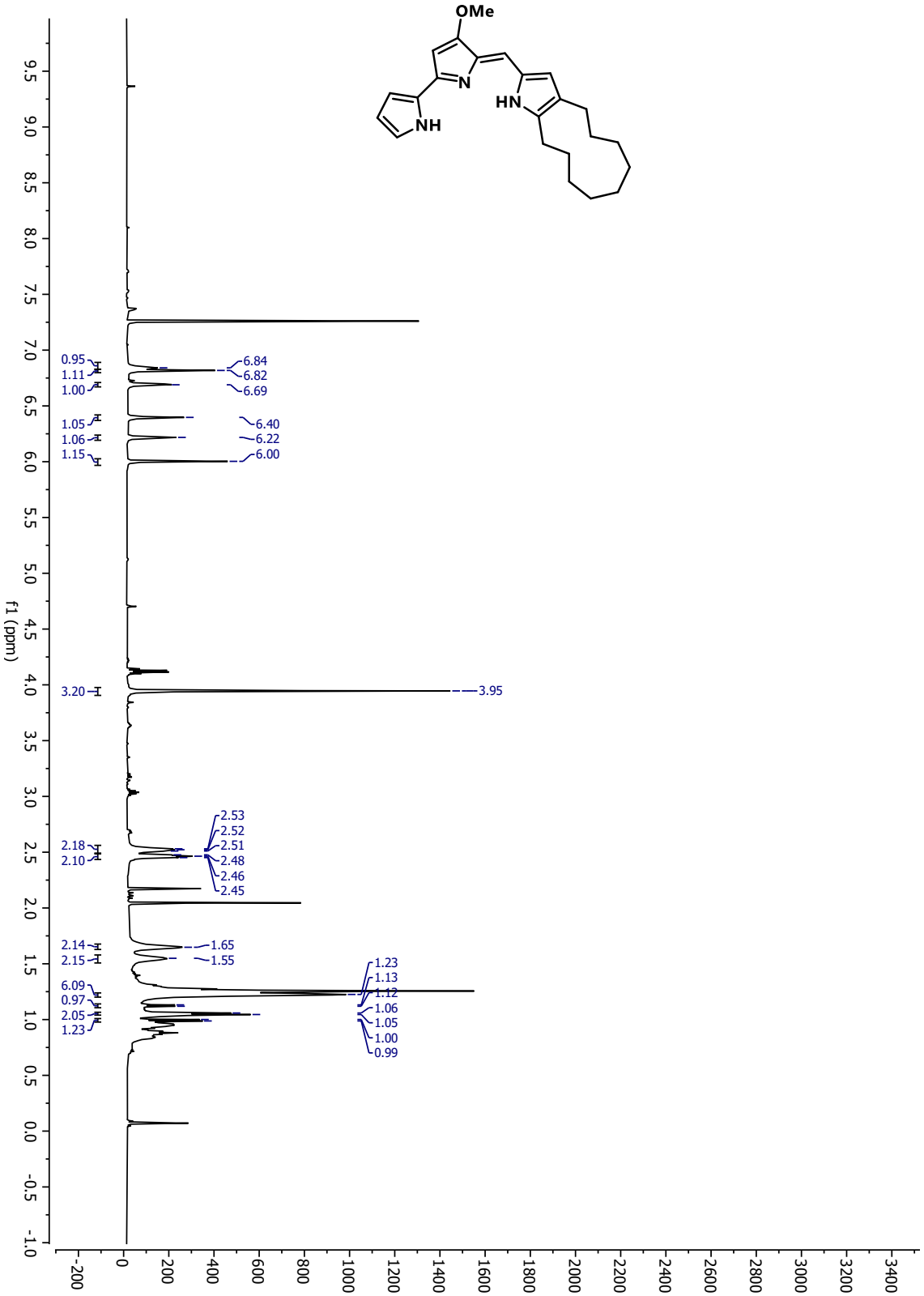

**Figure 2.6.33** APT NMR Spectrum (126 MHz, Chloroform-D) for compound **10**.

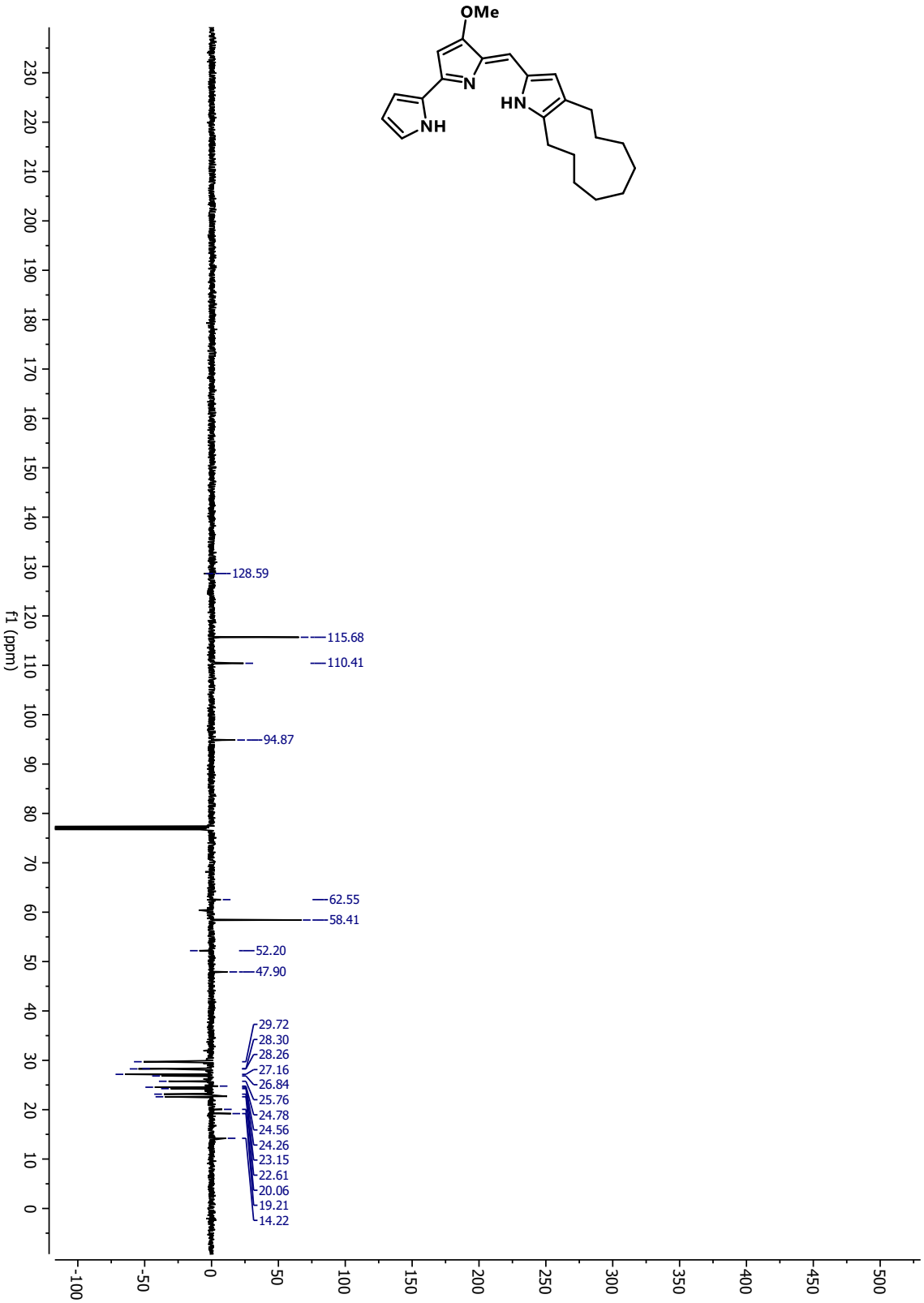

**Crystallographic Data**

Crystals of **9**•$Et_2HPO_4$ were produced by slow evaporation of an EtOAc solution of **9** containing an excess of diethyl phosphoric acid. The crystals obtained were of low quality, but atom connectivity could still be determined. The data was not of sufficient quality to be uploaded to the CCDC and the corresponding .cif is available upon request.

**Figure 2.6.34** Crystal structure of **9**•$Et_2HPO_4$. Atoms are displayed as 50% probability thermal ellipsoids.

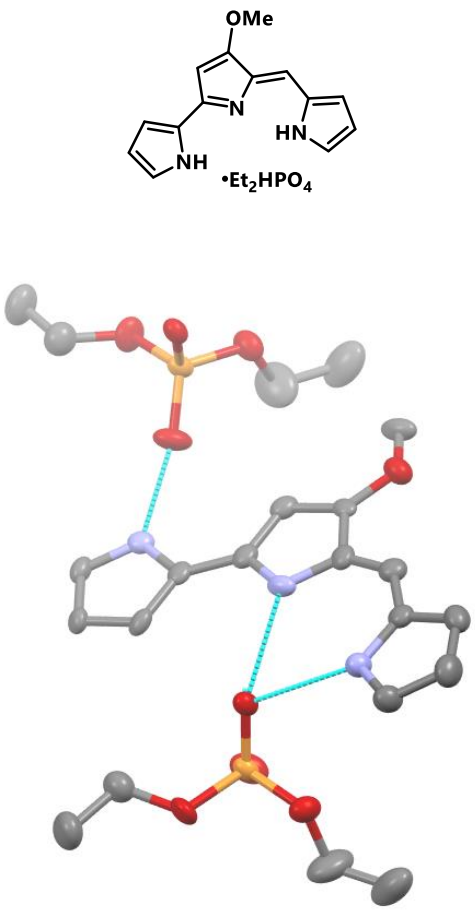

## 2.7 References


1. O'Brien, J.; Hayder, H.; Zayed, Y.; Peng, C., Overview of MicroRNA Biogenesis, Mechanisms of Actions, and Circulation. *Front Endocrinol (Lausanne)* **2018,** *9*, 402.
2. Peng, Y.; Croce, C. M., The role of MicroRNAs in human cancer. *Signal Transduction Targeted Therapeutics* **2016,** *1*, 15004.
3. Medina, P. P.; Nolde, M.; Slack, F. J., OncomiR addiction in an in vivo model of microRNA-21-induced pre-B-cell lymphoma. *Nature* **2010,** *467* (7311), 86-90.
4. Ji, W.; Sun, B.; Su, C., Targeting MicroRNAs in Cancer Gene Therapy. *Genes (Basel)* **2017,** *8* (1), 21.
5. Shah, M. Y.; Ferrajoli, A.; Sood, A. K.; Lopez-Berestein, G.; Calin, G. A., microRNA Therapeutics in Cancer - An Emerging Concept. *EBioMedicine* **2016,** *12*, 34-42.
6. Li, S.; Liang, Z.; Xu, L.; Zou, F., MicroRNA-21: a ubiquitously expressed pro-survival factor in cancer and other diseases. *Molecular and Cellular Biochemistry* **2012,** *360* (1-2), 147-58.
7. Jazbutyte, V.; Thum, T., MicroRNA-21: from cancer to cardiovascular disease. *Current Drug Targets* **2010,** *11* (8), 926-35.
8. Volinia, S.; Calin, G. A.; Liu, C. G.; Ambs, S.; Cimmino, A.; Petrocca, F.; Visone, R.; Iorio, M.; Roldo, C.; Ferracin, M.; Prueitt, R. L.; Yanaihara, N.; Lanza, G.; Scarpa, A.; Vecchione, A.; Negrini, M.; Harris, C. C.; Croce, C. M., A microRNA expression signature of human solid tumors defines cancer gene targets. *Proceeding of the National Academy of Sciences* **2006,** *103* (7), 2257-61.
9. Seike, M.; Goto, A.; Okano, T.; Bowman, E. D.; Schetter, A. J.; Horikawa, I.; Mathe, E. A.; Jen, J.; Yang, P.; Sugimura, H.; Gemma, A.; Kudoh, S.; Croce, C. M.; Harris, C. C., MiR-21 is an

EGFR-regulated anti-apoptotic factor in lung cancer in never-smokers. *Proceedings of the National Academy of Sciences* **2009,** *106* (29), 12085-12090.

10. Chan, J. A.; Krichevsky, A. M.; Kosik, K. S., MicroRNA-21 is an antiapoptotic factor in human glioblastoma cells. *Cancer Research* **2005,** *65* (14), 6029-33.

11. Zhou, X.; Ren, Y.; Moore, L.; Mei, M.; You, Y.; Xu, P.; Wang, B.; Wang, G.; Jia, Z.; Pu, P.; Zhang, W.; Kang, C., Downregulation of miR-21 inhibits EGFR pathway and suppresses the growth of human glioblastoma cells independent of PTEN status. *Laboratory Investigation* **2010,** *90* (2), 144-55.

12. Gabriely, G.; Wurdinger, T.; Kesari, S.; Esau, C. C.; Burchard, J.; Linsley, P. S.; Krichevsky, A. M., MicroRNA 21 promotes glioma invasion by targeting matrix metalloproteinase regulators. *Molecular and Cellular Biology* **2008,** *28* (17), 5369-80.

13. Si, M. L.; Zhu, S.; Wu, H.; Lu, Z.; Wu, F.; Mo, Y. Y., miR-21-mediated tumor growth. *Oncogene* **2007,** *26* (19), 2799-803.

14. Meng, F.; Henson, R.; Wehbe-Janek, H.; Ghoshal, K.; Jacob, S. T.; Patel, T., MicroRNA-21 regulates expression of the PTEN tumor suppressor gene in human hepatocellular cancer. *Gastroenterology* **2007,** *133* (2), 647-58.

15. Wagenaar, T. R.; Zabludoff, S.; Ahn, S. M.; Allerson, C.; Arlt, H.; Baffa, R.; Cao, H.; Davis, S.; Garcia-Echeverria, C.; Gaur, R.; Huang, S. M.; Jiang, L.; Kim, D.; Metz-Weidmann, C.; Pavlicek, A.; Pollard, J.; Reeves, J.; Rocnik, J. L.; Scheidler, S.; Shi, C.; Sun, F.; Tolstykh, T.; Weber, W.; Winter, C.; Yu, E.; Yu, Q.; Zheng, G.; Wiederschain, D., Anti-miR-21 Suppresses Hepatocellular Carcinoma Growth via Broad Transcriptional Network Deregulation. *Molecular Cancer Research* **2015,** *13* (6), 1009-21.

16. Bose, D.; Jayaraj, G.; Suryawanshi, H.; Agarwala, P.; Pore, S. K.; Banerjee, R.; Maiti, S., The Tuberculosis Drug Streptomycin as a Potential Cancer Therapeutic: Inhibition of miR-21 Function by Directly Targeting Its Precursor. *Angewantde Chemie International Edition* **2012,** *51* (4), 1019-1023.

17. Thomas, J. R.; Hergenrother, P. J., Targeting RNA with Small Molecules. *Chemical Reviews* **2008,** *108* (4), 1171-1224.

18. Connelly, C. M.; Boer, R. E.; Moon, M. H.; Gareiss, P.; Schneekloth, J. S., Discovery of Inhibitors of MicroRNA-21 Processing Using Small Molecule Microarrays. *American Chemical Society Chemical Biology* **2017,** *12* (2), 435-443.

19. Pieper, A. A.; Xie, S.; Capota, E.; Estill, S. J.; Zhong, J.; Long, J. M.; Becker, G. L.; Huntington, P.; Goldman, S. E.; Shen, C. H.; Capota, M.; Britt, J. K.; Kotti, T.; Ure, K.; Brat, D. J.; Williams, N. S.; MacMillan, K. S.; Naidoo, J.; Melito, L.; Hsieh, J.; De Brabander, J.; Ready, J. M.; McKnight, S. L., Discovery of a proneurogenic, neuroprotective chemical. *Cell* **2010,** *142* (1), 39-51.

20. Shortridge, M. D.; Walker, M. J.; Pavelitz, T.; Chen, Y.; Yang, W.; Varani, G., A Macrocyclic Peptide Ligand Binds the Oncogenic MicroRNA-21 Precursor and Suppresses Dicer Processing. *American Chemical Society Chemical Biology* **2017,** *12* (6), 1611-1620.

21. Matarlo, J. S.; Krumpe, L. R. H.; Heinz, W. F.; Oh, D.; Shenoy, S. R.; Thomas, C. L.; Goncharova, E. I.; Lockett, S. J.; O'Keefe, B. R., The Natural Product Butylcycloheptyl Prodiginine Binds Pre-miR-21, Inhibits Dicer-Mediated Processing of Pre-miR-21, and Blocks Cellular Proliferation. *Cell Chemical Biology* **2019**, *26*, (8), 1133-1142.

22. Frederich, J. H.; Harran, P. G., Modular access to complex prodiginines: total synthesis of (+)-roseophilin via its 2-azafulvene prototropisomer. *Journal of the American Chemical Society* **2013,** *135* (10), 3788-91.

23. Feng, Z.; Allred, T. K.; Hurlow, E. E.; Harran, P. G., Anomalous Chromophore Disruption Enables an Eight-Step Synthesis and Stereochemical Reassignment of (+)-Marineosin A. *Journal of the American Chemical Society* **2019,** *141* (6), 2274-2278.

24. Shoffner, G. M.; Peng, Z.; Guo, F., Structures of microRNA-precursor apical junctions and loops reveal non-canonical base pairs important for processing. *bioRxiv* **2020**, 2020.05.05.078014.

25. Harashima, K.; Tsuchida, N.; Tanaka, T.; Nagatsu, J., Prodigiosin-25 C. *Agricultural and Biological Chemistry* **1967,** *31* (4), 481-489.

26. Shoffner, G. M.; Wang, R.; Podell, E.; Cech, T. R.; Guo, F., In Crystallo Selection to Establish New RNA Crystal Contacts. *Structure* **2018,** *26* (9), 1275-1283.e3.

27. Pujari, N.; Saundh, S. L.; Acquah, F. A.; Mooers, B. H.; Ferré-D'Amaré, A. R.; Leung, A. K.-W., Engineering crystal packing in RNA structures I: past and future strategies for engineering RNA packing in crystals. *Crystals* **2021,** *11* (8), 952.

28. Su, J.-C.; Chang, J.-H.; Huang, J.-W.; Chen, P. P. Y.; Chen, K.-F.; Tseng, P.-H.; Shiau, C.-W., Copper–obatoclax derivative complexes mediate DNA cleavage and exhibit anti-cancer effects in hepatocellular carcinoma. *Chemico-Biological Interactions* **2015,** *228*, 108-113.

29. Díaz de Greñu, B.; Iglesias Hernández, P.; Espona, M.; Quiñonero, D.; Light, M. E.; Torroba, T.; Pérez-Tomás, R.; Quesada, R., Synthetic prodiginine obatoclax (GX15-070) and related

analogues: anion binding, transmembrane transport, and cytotoxicity properties. *Chemistry* **2011,** *17* (50), 14074-83.

30. Davis, J. T.; Gale, P. A.; Okunola, O. A.; Prados, P.; Iglesias-Sanchez, J. C.; Torroba, T.; Quesada, R., Using small molecules to facilitate exchange of bicarbonate and chloride anions across liposomal membranes. *Nature Chemistry* **2009,** *1* (2), 138-44.

31. Fürstner, A.; Grabowski, E. J., Studies on DNA cleavage by cytotoxic pyrrole alkaloids reveal the distinctly different behavior of roseophilin and prodigiosin derivatives. *Chembiochem* **2001,** *2* (9), 706-9.

32. Park, G.; Tomlinson, J. T.; Melvin, M. S.; Wright, M. W.; Day, C. S.; Manderville, R. A., Zinc and Copper Complexes of Prodigiosin: Implications for Copper-Mediated Double-Strand DNA Cleavage. *Organic Letters* **2003,** *5* (2), 113-116.

33. Jenkins, S.; Incarvito, C. D.; Parr, J.; Wasserman, H. H., Structural studies of C-ring substituted unnatural analogues of prodigiosin. *CrystEngComm* **2009,** *11* (2), 242-245.

34. Rizzo, V.; Morelli, A.; Pinciroli, V.; Sciangula, D.; D'Alessio, R., Equilibrium and Kinetics of Rotamer Interconversion in Immunosuppressant Prodigiosin Derivatives in Solution. *Journal of Pharmaceutical Sciences* **1999,** *88* (1), 73-78.

35. Melvin, M. S.; Calcutt, M. W.; Noftle, R. E.; Manderville, R. A., Influence of the a-ring on the redox and nuclease properties of the prodigiosins: importance of the bipyrrole moiety in oxidative DNA cleavage. *Chemical Research in Toxicology* **2002,** *15* (5), 742-8.

36. Frederich, J. H.; Matsui, J. K.; Chang, R. O.; Harran, P. G., Substituted 2,2′-bipyrroles and pyrrolylfurans via intermediate isoxazolylpyrroles. *Tetrahedron Letters* **2013,** *54* (21), 2645-2647.

37. Kao, C.; Zheng, M.; Rüdisser, S., A simple and efficient method to reduce nontemplated nucleotide addition at the 3′ terminus of RNAs transcribed by T7 RNA polymerase. *RNA* **1999,** *5* (9), 1268-1272.

38. Dairi, K.; Tripathy, S.; Attardo, G.; Lavallée, J.-F., Two-step synthesis of the bipyrrole precursor of prodigiosins. *Tetrahedron letters* **2006,** *47* (15), 2605-2606.